Data-Driven, Mechanistic and Hybrid Modelling for Statistical Fault Detection and Diagnosis in Chemical Processes

by:

Shallon Stubbs

A Thesis submitted in partial fulfilment of the requirements for the degree of Doctor of Philosophy

School of Chemical Engineering and Advanced Materials
Newcastle University
United Kingdom

November, 2011

Abstract

Research and applications of multivariate statistical process monitoring and fault diagnostic techniques for performance monitoring of continuous and batch processes continue to be a very active area of research. Investigations into new statistical and mathematical methods and there applicability to chemical process modelling and performance monitoring is ongoing. Successive researchers have proposed new techniques and models to address the identified limitations and shortcomings of previously applied linear statistical methods such as principal component analysis and partial least squares. This thesis contributes to this volume of research and investigation into alternative approaches and their suitability for continuous and batch process applications. In particular, the thesis proposes a modified canonical variate analysis state space model based monitoring scheme and compares the proposed scheme with several existing statistical process monitoring approaches using a common benchmark simulator – Tennessee Eastman benchmark process. A hybrid data driven and mechanistic model based process monitoring approach is also investigated. The proposed hybrid scheme gives more specific considerations to the implementation and application of the technique for dynamic systems with existing control structures. A non-mechanistic hybrid approach involving the combination of nonlinear and linear data based statistical models to create a pseudo time-variant model for monitoring of large complex plants is also proposed. The hybrid schemes are shown to provide distinct advantages in terms of improved fault detection and reliability. The demonstration of the hybrid schemes were carried out on two separate simulated processes: a CSTR with recycle through a heat exchanger and a CHEMCAD simulated distillation column. Finally, a batch process monitoring schemed based on a proposed implementation of interval partial least squares (IPLS) technique is demonstrated using a benchmark simulated fed-batch penicillin production process. The IPLS strategy employs data unfolding methods and a proposed algorithm for segmentation of the batch duration into optimal intervals to give a unique implementation of a Multiway-IPLS model. Application results show that the proposed method gives better model prediction and monitoring performance than the conventional IPLS approach.

Acknowledgement

I would like to first express my deepest appreciation for the supervision and guidance offered by my academic supervisors Dr. Jie Zhang and Professor Julian Morris. Their patience and accommodation was instrumental to arriving at this point and as done much for my character development.

I would like to acknowledge my sponsors, BP International Ltd and the Engineering and Physical Science Research Council (EPSRC) and express my gratitude for being made a recipient of the Dorothy Hodgkin’s Postgraduate Award. Also a special thank you note to my industrial supervisors and liaisons, Dr. Zaid Rawi and Dr. Ian Alleyne.

Finally, a big thank you to my parents, brothers, and sisters who have all been very encouraging and supportive over the last four years, love you all.

Table of Contents

Abstract i

Acknowledgement... ii

Publications vivi

List of Figures vii

List of Tables..x

List of Acronyms and Abbreviations..……………………………………………xi

Chapter 1 : Introduction 1

1.1 Background and Motivation..1

1.2 Aims and Objective 4

1.3 Thesis Contribution 5

1.4 Thesis Outline 6

Chapter 2 : Review of Linear Multivariate Statistical Monitoring Techniques.......................9

2.1 Introduction 9

2.2 Principal Component Analysis..11

2.3 Partial Least Squares 17

2.4 Monitoring Metrics: *Hotelling's* T^2 and Q Statistics..20

2.5 Multiblock and Multiway PCA/PLS methods and Interval PLS (IPLS) 27

2.5.1 Multiblock Partial Least Squares 27

2.5.2 Multiway PLS and PCA...28

2.5.3 Interval Partial Least Squares...30

2.6 Dynamic PCA and PLS...31

2.7 Summary 33

Chapter 3 : Review of Subspace, Non-linear and Hybrid Modelling Techniques.................34

3.1 Introduction 34

3.2 Canonical Variate Analysis and State Space Approach.......................................35

3.2.1 Canonical Variate Analysis..36

3.2.2 State Space Modelling..38

3.2.3 State Vector Derivation...39

3.2.4 Stochastic estimation of the state space matrices...42

3.3 N4SID and MOESP 44

3.4 Model order selection and past and future vector lag sizing....................................51

3.4.1 Akaike Information Criterion...52

3.4.2 Normalized Residual Sum of Squares....................54
3.4.3 Multiple correlation coefficient....................54
3.4.4 The Overall F-Test of the loss function 55
3.4.5 The Final prediction error criterion....................56
3.4.6 The Bayesian Information Criterion 56
3.4.7 The Law of Iterated Logarithms Criterion 57
3.5 Nonlinear Extension to PCA and PLS 57
3.5.1 Nonlinear PCA (NLPCA) 58
3.5.2 Non-linear Projection to latent spaces (NLPLS)....................61
3.5.3 Non-Linear Canonical Correlation Analysis (NLCCA)....................63
3.6 Hybrid Data Driven/ Mechanistic Model based Approaches....................64
3.7 Summary 68
Chapter 4 : A Simplified CVA State Space Modelling Approach for Process-Monitoring Specific Applications 70
4.1 Introduction 70
4.2 The CVA State Space Modified Approach 72
4.2.1 The Proposed Representation and Redefining of the Past Vector 72
4.2.2 Simplification of the State Matrices Derivation....................74
4.3 State matrix sizing and other modelling considerations....................78
4.4 Simulation 1: Evaluating the Proposed CVA SS model Accuracy and Predictive Capabilities....................85
4.5 Simulation 2: Fault Detection Capabilities Based on TE Simulator....................88
4.5.1 The Tennessee Eastman Process 88
4.5.2 Fault Monitoring Statistics and Results 93
4.6. Conclusions 99
Chapter 5 : Hybrid Model Based Approach to Process-Monitoring....................101
5.1 Introduction 101
5.2 The Plant, Model, and Fault Simulator 103
5.2.1 CSTR Plant Simulator....................103
5.2.2 The CSTR Simulator with Model Plant Mismatch 106
5.3. Exploring Data Driven and Hybrid Model based Approaches 109
5.4 Performance Comparison of Mechanistic and Hybrid Fault Detection Monitoring Schemes....................121
5.4.1 The Fault Simulations 121
5.4.2 Fault Detection 125

5.5 Distillation column, hybrid model, and disturbance overview 134
5.6 Hybrid Model Development and Fault Detection Scheme 137
5.7 Impact Analysis and Detection of Simulated Disturbances 140
5.7.1 Feed Temperature Change 140
5.7.2 Feed Composition Change 142
5.7.3 Change in Feed Flow Rate 144
5.7.4 Combine fault Detection 145
5.8 Conclusions 147
Chapter 6 : Batch Process Monitoring Using Multi-way and Interval PLS methods 149
6.1 Introduction 149
6.2. Combining Data Unfolding and Interval Splicing Techniques 151
6.2.1 Three-dimensional data unfolding 151
6.2.2 A binary dividing search algorithm approach for subdivision length selection..153
6.3 Fed-batch penicillin simulator prediction and fault monitoring...............................160
6.3.1 Fed-batch Penicillin Production Process Simulator Overview 160
6.3.2 Prediction and Process Monitoring 163
6.4 Prediction and Monitoring Results...167
6.4.1 Predictive Model Performance of MiPLS Approach 167
6.4.2 Process Monitoring Performance 169
6.5 Conclusion...173
Chapter 7 : Conclusions and Suggestions for Further Works..174
7.1 Conclusions 174
7.2 Suggestions for Further Works 177
Appendix A 180
Appendix B 191
References ………………………………………………………………………….. 194

Publications

Stubbs, S., J. Zhang, and J. Morris (2009), Fault detection of dynamic processes using a simplified monitoring-specific CVA state space approach, *19th European Symposium on Computer Aided Process Engineering* – ESCAPE19, Krakow, Poland.

Stubbs, S., J. Zhang, and J, Morris (2010), A Revised State Space Modelling Approach and Improved Fault Detection Using Combined Index Monitoring for Dynamic Processes, *9th International Symposium on Dynamics and Control of Process Systems* - DYCOPS, Leuven, Belgium.

Stubbs, S., J. Zhang, and J. Morris (2011), Fault detection of dynamic processes using a simplified monitoring-specific CVA state space approach, *Journal of Computers and Chemical Engineering.* (Accepted subject to minor revisions)

Stubbs, S., J. Zhang, and J. Morris (2011), Multiway Interval Partial Least Squares and a Novel Algorithm for Optimal Interval Splicing*, Journal of Chemometrics and Intelligent Laboratory Systems*. (Review Pending)

List of Figures

Figure 2.1 Decomposition of the data matrix X into a collection of scores and loadings ……………………………………………………………………………15
Figure 2.2 Example plot of an SPE and T^2 Monitoring on three different data sets of historical data collected during different periods of process operation. (Stubbs, 2007)........24
Figure 2.3 SPE contribution chart of a PCA model developed for monitoring of catalyst production plant (Excerpt from MSc. Thesis – Stubbs, 2007)..26
Figure 2.4 Time-mode Unfolding 28
Figure 2.5 Batch-mode Unfolding 29
Figure 2.6 Variable-Mode Unfolding 29
Figure 2.7 Unfolding of site level (batch) data. (Cherry and Qin., 2006)..........................30
Figure 3.1 Comparing the subspace development algorithm stage of N4SID, MOESP, and CVA………… 45
Figure 3.2 The polygonal line algorithm 60
Figure 3.3 Architecture of neural network used to implement NLCCA. Hsieh (2001)......63
Figure 3.4 Model based PCA 65
Figure 3.5 Super-model based PCA...67
Figure 4.1 a) 3-D plot of model error vs. state vector and lag window sizes; b) Equivalent 2-D family of plots for different lag size L - MSE versus state vector dimension. 80
Figure 4.2 Plots of the AIC, BIC, LILC criteria dissected in terms of model complexity term and model fitness term 84
Figure 4.3 Autocorrelation plots of the output residuals ABG state space model 86
Figure 4.4 Autocorrelation plots of the output residuals ABCDG state space model. 87
Figure 4.5 Reconstruction of outputs for both CVA State Space models..........................87
Figure 4.6 Histogram plot of the output residual distribution for both CVA SS models...88
Figure 4.7 Diagram of the Tennessee Eastman process simulator under Lyman and Georgakis control scheme. (Lyman and Georgakis, 1995) 89
Figure 4.8 AIC and NRSS computation for the monitoring-specific SS models (ABG) spanning lag size from 1 to 5 and state order from 10 to 50. 91
Figure 4.9 BIC and LLIC computation for the monitoring-specific SS models (ABG) spanning lag size from 1 to 5 and state order from 10 to 50. 92
Figure 4.10. Fault detection delay time comparison of the 5 monitoring statistics across the 2 CVA state space models. Missing bars indicate zero detection delay time, negative bars indicate false alarm condition and full length bars indicate failed/missed detections. 95
Figure 4.11 Detection of fault No. 15 using ABG and ABCDG state space models 96
Figure 4.12 Fault detection performance of the Hotelling's T^2 statistics on the output residuals (ABG model)...97
Figure 5.1. Continuous Stirred Tank Reactor CSTR with recycle loop via Heat Exchanger HTX………...104
Figure 5.2 Plant vs Mechanistic Model Outputs for different size plant-model mismatch error…………...108
Figure 5.3 Mismatch index plot monitoring for four different level of plant-model mismatch……. 109

Figure 5.4 Mechanistic Model-Plant interfacing options along with compensation data driven model (a) Traditional Mechanistic Model-Plant interface (b) Proposed mechanistic-plant interface. 110
Figure 5.5 Plant-model offset in controller output (manipulated variables) due to mechanistic model implementation approach of Figure 5.7(a). 111
Figure 5.6 Data-based compensation model employing delayed feedback output of the plant and mechanistic model 113
Figure 5.7 Mechanistic (left pane) versus PLS1 hybrid (right pane) one-step ahead prediction of plant measured variables. Mechanistic implementation of Figure 5.4(a) employed…… 115
Figure 5.8 Mechanistic (left pane) vs PLS1 hybrid (right pane) prediction of plant measured variables. Mechanistic implementation of Figure 5.4(b) employed. 116
Figure 5.9 NRSE plots per output for hybrid model alternatives....119
Figure 5.10 NN Hybrid model HM2 and uncompensated mechanistic model normal probability plot on residuals 119
Figure 5.11 Simulated perturbations of CSTR input variables with additive noise....120
Figure 5.12. Plant overview showing unit operation faults F_p and sensor faults F_s within and outside the process control loop. 121
Figure 5.13 (a) Incipient fault - Product Stream Pipe Blockage (b) Incipient faults – Cool-water (CW) valve sticking....123
Figure 5.14 Fault Detection Performance of Mechanistic Model (non-hybrid approach) using a Q statistics monitoring index. 126
Figure 5.15 (a) The impact of the heat exchanger fouling fault on the measured process variables and mechanistic model output (b) The gradual decline in the magnitude of the squared residual after the fault is initiated. 127
Figure 5.16 Heat exchanger fouling fault impact and detection via hybrid mechanistic – data driven model 128
Figure 5.17 Fault detection monitoring using Q statistic applied to the residuals of the 4 different hybrid model variants. 129
Figure 5.18 Detection of recycle pipe blockage fault using Q, T^2 and combine index monitoring statistics on the hybrid HM3 model. 130
Figure 5.19 Detection of reactor level sensor drift using Q, T^2, and combine index statistics on the hybrid HM3 model. 131
Figure 5.20 Fault Magnitudes at the point of detection for the Q-statistics of the four hybrid models.133
Figure 5.21 Dynamic Distillation Column with feed composition and condition switch implementation....135
Figure 5.22 Hybrid data driven model architecture comprising an ANN and an OLS model. One network is developed for each output variable. 138
Figure 5.23 Complete multi-network hybrid data driven model base monitoring scheme ……………… 139
Figure 5.24 Training data profile of some of the process variable measurements used as input and output of the hybrid data driven base process performance monitoring scheme .140
Figure 5.25 Impact of feed temperature change on distillate stream (a) flow rate plot (b) temperature plot. 141
Figure 5.26 Detection of feed temperature disturbance using T2 and Q statistics....142

Figure 5.27 Impact of feed composition change on composition of top product. 142
Figure 5.28 Impact of feed composition change on distillate stream (a) flow rate plot (b) temperature plot. 143
Figure 5.29 PCA based T2 and Q Statistics detection of composition disturbance. 144
Figure 5.30 (a) Impact of feed flow disturbance based on the distillate steam flow rate (b) Detection of the feed flow rate disturbance using T^2 and Q statistics. 145
Figure 5.31 Distillate stream process variable profiles before and after feed flow-rate and temperature change (a) Temperature (b) Mass flow-rate. 146
Figure 5.32 T^2 detection of simultaneous fault conditions – (i) temperature and flow rate change (ii) Temperature and composition change. 147
Figure 6.1 a) Time Unfolding b) Batch-mode Unfolding..........152
Figure 6.2 Batch-wise interval segmented unfolding of data set..........153
Figure 6.3 Flowchart of binary interval splitting algorithm 154
Figure 6.4 Illustrative example of binary division algorithm for interval splitting..........155
Figure 6.5 Plot of predicted response versus actual response through different stages of the interval splitting algorithm for case 1 with S_{min} = 15. 160
Figure 6.6 Flow sheet of Penicillin Cultivation Process 161
Figure 6.7 PLS2 and PLS1 implementation of a) Predictive model b) Fault monitoring model………..........163
Figure 6.8 Plot comparing prediction of Penicillin and Biomass concentration using online measurements a) Standard PLS model b) proposed MiPLS model 168
Figure 6.9 Plot of root-mean square error RMSE reduction with discovery of the intervals 168
Figure 6.10 Impact of a 50% step decrease in substrate feed rate (Fault #2) on a) Biomass concentration b) Penicillin Concentration..........169
Figure 6.11 Detection of sudden faults 1 through to 3 using T^2 and *SPE* statistics 170
Figure 6.12 Detection of incipient faults 1 and 2 using Hotelling's T^2 statistics 171
Figure 6.13 Detection of incipient Fault # 2 using T^2 statistics a) Fault initiated at t = 50h b) Fault initiated at t = 100h c) Fault initiated at t = 200h 172
Figure A.1 Canonical Variate Analysis (CVA) state space script layout ………..… 181
Figure A.2 CSTR plant-model mismatch coding chart ……………………………… 182
Figure A.3 Code chart outline of binary dividing segment length search algorithm… 183
Figure B.1 Interpretation of the orthogonal projection in the j-dimensional space (j = 2 in this case) ……………………………………………………………………..192
Figure B.2 Interpretation of the oblique projection in the j-dimensional space (j = 2 in this case) ……………………………………………………………………..193

List of Tables

Table 2.1 NIPALS Algorithm for PCA 13

Table 2.2 The Bootstrap PLS Algorithm 19

Table 3.1 Interpretation of three different subspace algorithms in a unifying framework .51

Table 4.1 Computational complexity (FLOPs) of proposed and traditional CVA methods 78

Table 4.2 A list of model size selection criteria 82

Table 4.3 List of simulated disturbances and faults 90

Table 4.4 Detection delay times of proposed CVA model with previously reported results. 94

Table 4.5 Fault detection performance comparison of CVA versus DICA and SSICA 99

Table 5.1 CSTR Plant and Model Simulator Constants....106

Table 5.2 Model Mismatch Case: Plant vs Model Constants Employed 107

Table 5.3 Simulated Process Variables – Input/Output Classification 112

Table 5.4 Process variables prediction MSE given as a percentage of the steady state process variable mean values 117

Table 5.5 Summary of the Hybrid Mechanistic–Data Driven Modelling Schemes Investigated... 118

Table 5.6 Simulated Fault Summary....124

Table 5.7 Fault detection delay times for all hybrid models 132

Table 5.7 Feed composition and flow rate changes used in simulation 136

Table 5.8 Process variable measurements used as inputs and outputs of Hybrid Data Driven Model. 137

Table 6.1 Simulation Results Evaluating the Capability and Accuracy of Proposed Interval Division Algorithm 159

Table 6.2 Initial Conditions and Set-points used by Penicillin Simulator 162

Table 6.3 Summary of Fault Scenarios in Simulated Penicillin Cultivation Process 162

Table 6.4 Specifications of the iPLS models used to Implement Process Monitoring Strategy....164

Table 6.5 Bootstrap PLS algorithm Integrated Within Variable Selection Algorithm 166

Table 6.6 Predictive Model Description for Penicillin and Biomas Concentration 167

List of Abbreviations and Acronyms

Symbol	**Description**
ABCDG	5 Matrices State Space Representation
ABG	3 Matrices State Space Representation
AIC	Akaike Information Criterion
ANN	Artificial Neural Network
BIC	Bayesian Information Criterion
BR	Balanced Realisation
BTPLS	Box-Tidwell transformation based partial least squares
CA	Correspondence Analysis
CCA	Canonical Correlation Analysis
CCR	Canonical Correlation Regression
cov	Covariance
CSTR	Continuous Stirred Tank Reactor
CUSUM	Cumulative Sum (Statistic Monitoring Chart)
CVA	Canonical Variate Analysis
CW	Cool Water
DICA	Dynamic Independent Component Analysis
DPCA	Dynamic Principal Component Analysis
DPLS	Dynamic Partial Least Squares
EWMA	Exponentially Weighted Moving Average (Statistic Monitoring Chart)
FLOPS	Floating point operations
FPE	Final Prediction Error (criterion)
FTIR	mid-infrared spectrum
GA	Genetic Algorithm
GSVD	Generalized Single Value Decomposition
HANN	Hybrid Artificial Neural Network
IID	Identically Identically Distributed
iPLS	Interval Partial Least Squares
LILC	Law of Iterative Logarithms Criterion
MBPLS	Multiblock Partial Least Squares
MIMO	Multiple Input Multiple Output
MiPLS	Multi-way Interval Partial Least Squares
MOESP	Multiple Output Error State Space
MPLS	Multiway Partial Least Squares
MSE	Mean Squared Error
MSPC	Multivariate Statistical Process Control

N4SID	Numerical Algorithms for Subspace State Space System Identification
NIPALS	Non-linear Iterative Partial Least Square
NIR	Near infrared spectrum
NLCCA	Non-linear canonical correlation analysis
NLPLCA	Non-linear Principal Component Analysis
NLPLS	Non-linear Partial Least Squares
NN	Neural Network
NRSS	Normalized Residual Sum Squares
OLS	Ordinary Least Squares
OVF	Overall F-test of the loss function (criterion)
PCA	Principal Component Analysis
PENSIM	Fed-batch Penicillin Fermentation Simulator (Birol, et al., 2002)
PLS	Partial Least Squares
PLS1	Single-Block PLS
PLS2	Two-Block PLS
PLSR	Partial Least Squares Regression
QPLS	Quadratic Partial Least Squares
RMSE	Root Mean Square Error
SPC	Statistical Process Control
SPE	Square Prediction Error or Q Statistics
SS	State Space
SSICA	State Space Independent Component Analysis
SVD	Single Value Decomposition
TE	Tennessee Eastman (Simulator)
TSS	Total Sum of Squares

Chapter 1 : Introduction

1.1 Background and Motivation

Two separate advances, one in sensing technology and data acquisition system and the other in process modelling software has revolutionized the chemical process industry in aspects ranging from plant design, implementation, monitoring and controls. The control strategies have become more complex and more model-based strategies are being explored as the drive to be more efficient, globally competitive and environmentally friendly continues to impose upon production facilities tighter safety and product quality operating constraints. Engineers, plant managers, and operators are becoming increasingly aware of the unlocked potential of the volume of measurement data that is sampled and stored in computer archives. With more complex plants and operating constraints, more efforts are being utilized to extract as much information and understanding from the process data gathered by the various plant sensors. The ultimate objective is that such acquired knowledge and insight into the plant dynamics can be translated into improved plant performance monitoring and control schemes.

There is also the growing curiosity about extracting more usefulness from chemical process modelling software beyond plant design or feasibility and pinch analysis evaluation. To that end advances in chemical modelling software continue to seek to provide more user-friendly development environment for more robust and accurate dynamic models that can be employed as engines in model-based control systems or for the purposes of online process monitoring and quality variable prediction.

Given the nature and complexity of many industrial continuous and batch mode process operations, in terms of non-linearity, dynamics and time varying characteristics, development of reliable long-term multi-step-ahead prediction and robust process performance monitoring systems poses a significant challenge. Plant measurement data quite commonly does not hold true to the assumptions of stationarity and normality. The transition from univariate statistical process monitoring to multivariate statistical process control (MSPC) was advanced as a more effective process monitoring solution that would be able to detect fault conditions only detectable within the cross-correlation structure of the process variables (Morris and Martin, 1998). However, in addition to the cross-correlation structure that such data exhibit, the process variables tend to also exhibit significant auto correlation structure which non-dynamic statistical process models fail to account for. Techniques in existence such as those based on principal component analysis (PCA) and partial least squares (PLS) only account for the linear cross-correlation in the data set. Consequently, researchers have sought to improve these methods to compensate for specific short-comings linked to the restrictive assumptions upon which these techniques were founded.

Variants to PCA and PLS such as dynamic PCA (DPCA) (Ku, et al. 1995; Russell, et al. 2000), and dynamic PLS (DPLS) (Chen and Liu 2002), have been proposed to tackle fault detection monitoring for both continuous and batch dynamic processes. Kernel based PCA (KPCA) (Scholkopf et al., 1998) and PLS (KPLS) , along with a number of different implementation of non-linear variants – Nonlinear PCA (NLPCA) (Dong and McAvoy, 1996a) and PLS (NLPLS) (Wolds et al., 1987; Baffi et al., 1997; Wilson et al., 1997), have been proposed to tackle non-linear process monitoring and product quality prediction. Likewise, extensive research have been carried out into the development of subspace and state space modelling for process monitoring and prediction, notably the use of canonical variate analysis (CVA) state space modelling approach have been explored and compared with several non-dynamic approaches (Russell et al., 2000; Simoglou et al., 1999a). These methods have demonstrated capabilities for accurate prediction for dynamic processes, however, research is on-going in this area to see how such models can be more effectively implemented for applications relating to process performance monitoring.

The developments of simple process faults often propagate into complex faults due to process feed recycle loops and control system feedback. The control system may also conceal the development of the fault depending upon the nature of the fault and its impact on the process. Developing better understand of the impact such control loops have on the detection and development of faults is one avenue by which existing fault monitoring schemes could be enhanced. It is the author's view that in deriving and developing better statistical models for monitoring, not only the statistical nature of the process data but also other aspects specific to the design and operation of industrial processes should be taken into consideration. Such work will hopefully help resolve some of the conflict that sometimes appears to exist between process controls and process monitoring systems. Process control and predictive modelling should be able to co-exist with statistical process monitoring, each providing support and coordinating with the other.

The statistical data based models for monitoring is significantly more prevalent than mechanistic first principle models because of the time, process knowledge and overall cost involved in developing robust and reliable mechanistic models, particular for large plants characterized by complex and non-linear dynamics. The main advantage that the mechanistic model approach may provide over data driven models is the ability to incorporate process knowledge into the model design. With the models being based upon actual chemistry and design parameters of the process, it may prove more effective in capturing the relevant process dynamics and non-linear features characterizing the operation of plant, thus enabling more reliable and robust model for process monitoring application. Reported advances in software development packages, particularly in the area of dynamic online models, have made such endeavours more feasible. However, the question of whether it is possible to produce robust and sufficiently reliable model based on limited process information and or imprecise data with uncertainty is the more pertinent issue that also needs to be taken into consideration.

The two approaches have contrasting strengths and weaknesses which should be weighed against each in order for one method to be declared better than the other. Case in point, if the mechanistic fault monitoring approach is capable of yielding better detection and diagnostic improvements over a statistical data driven method, is the improvements significant enough to warrant the additional effort in developing such models? Or perhaps one may want to consider whether the fusion of the two approaches could be orchestrated to complement each other and yield a superior hybrid process monitoring scheme.

Mcpherson (2007) explored several hybrid schemes in her doctoral research thesis, the schemes analysed used PCA, CVA, NLPCA, autoregressive with exogenous input (ARX) time series model combined with mechanistic models of a batch process to monitor several different types of simulated faults. The analysis, however, does not include the application of hybrid approaches involving the merger of different statistical data driven methods or the comparative performance of pure data driven or pure mechanistic approaches for process performance monitoring.

1.2 Aims and Objective

The main goal of this research is to provide novel statistical modelling solutions and or enhancements to existing methods that will improve the reliability, speed of fault detection, and scope of application for model based process monitoring and fault diagnostics systems. More specifically, the following objectives will be sought to be achieved:

i) Discovering statistical methods and design methodologies for improving dynamic modelling approaches. The success of any proposed method to be evaluated via comparative analysis with pre-existing approaches.

ii) Development of hybrid approaches involving the combination of mechanistic (first principle models) and statistical linear and or non-linear data driven methods. Specific consideration will be given to implementation, the impact of mechanistic model-plant mismatches on the performances of such system, the choice of data based model and performance improvement over traditional non-hybrid data driven approaches.

iii) Development of hybrid data based models employing both linear and non-linear statistical data driven methods for applications where the cost of development of a mechanistic model is prohibitive or the chemistry and dynamics of the system are not well defined.

iv) Improving predictive modelling and fault monitoring of batch processes characterized by nonlinearity and significant inter-batch variation.

1.3 Thesis Contribution

The thesis contributes both investigatory research expanding upon evaluation and analysis carried out by previous researchers and also proposes several novel approaches to fault detection model development and detection monitoring metrics for both continuous and batch process performance monitoring. The key contributions are summarized as follows:

- An amendment to the traditional canonical variate analysis state space model development process is proposed that leads to a simpler monitoring scheme. The model's simplification is demonstrated via the reduction in the model parameterization dimensions and the computationally simpler algorithms required for parametric estimation. The fault detection performance capabilities of the proposed model is compared with several other traditional statistical models such as PCA, DPCA, correspondence analysis (CA), and the Larimore's CVA state space model implementation. The results indicate that the fault detection performance of the proposed model is not compromised by the simplification achieved.

- A central aim of this research was to investigate the employment of hybrid modelling architecture for process performance monitoring endeavours. The hybrid schemes investigated in this thesis involved mechanistic (first principle) models and data driven statistical models as well as combining statistical data driven approaches of different types. To justify the need for the proposed hybrid approaches or the role of the data based compensation model, the fault detection and process performance monitoring hybrid schemes were evaluated and compared against an approach based on a mechanistic based only system. A non-mechanistic hybrid scheme implementation combining an ordinary least squares (OLS) and neural network based model is proposed and evaluated as a solution to large scale plant monitoring applications characterized by nonlinear variability due to operating point fluctuations.

- Finally, multi-way data unfolding method was combined with interval partial least squares (iPLS) to provide an improved linear approximation model of a highly non-linear batch penicillin production process. An algorithm for deriving the optimal lengths of the intervals to be employed was developed by the author and demonstrated to give very consistent results. Multiway interval partial least squares (MiPLS) models were developed for both quality variable prediction and fault detection.

1.4 Thesis Outline

The remaining part of the thesis is organised as follows. Chapter 2 summarizes and provides succinct description of some of the linear multivariate statistical process monitoring approaches that have been reported in the literature. The review spans a wide range of research commencing with an overview of PCA and PLS. The coverage will expand to the several extensions of these methods, namely multi-way and multi-block PCA and PLS, and a more recent evolution in PLS modelling – interval partial least squares.

Chapter 3 extends the literature review focusing on dynamic and non-linear extension to the linear statistical models introduced in Chapter 2. The coverage will include DPCA and DPLS, and other subspace projection methods will also be discussed such as CVA state space models and so forth. With regards to the nonlinear models, the chapter will review nonlinear principal component analysis (NLPCA) and nonlinear partial least squares (NLPLS) along with a dynamic nonlinear canonical correlation analysis (CCA) approach. The chapter also gives an overview of several hybrid mechanistic – data driven model approaches that have been previously proposed in literature.

.

Chapter 4 presents the author's investigation into CVA state space modelling for dynamic process monitoring and modelling. A variant to the traditional CVA state space model is presented and both the proposed and traditional CVA state space modelling approach were dissected revealing the significant gains in computational simplicity achieved via use of a simpler state space representation and estimation algorithms employed by the proposed model. The performance results of the models will be evaluated on the Tennessee Eastman process simulator and compared against other statistical projection techniques such as (D)PCA and correspondence analysis CA. Results obtain from a second case study based upon process monitoring of a distillation column model will also be reported.

In Chapter 5, several hybrid modelling schemes for process monitoring are proposed and analyzed. For the proposed mechanistic-data driven hybrid scheme specific consideration are given to the implementation and monitoring of process plants under close-loop controls. The chapter explores implementation issues with regards to defining the interface between the mechanistic model and the actual plant. The impact of model plant mismatches is also explored and the capabilities of the data based model to compensate for such. The fault detection and monitoring performance of several proposed hybrid architectures are analyzed. The hybrid model based performance monitoring schemes were evaluated using a continuous stirred tank reactor CSTR – heat exchanger recycle loop simulator which has been employed in previous research work (Zhang, 2006; Zhang, et al., 1996). An alternative hybrid scheme based on combining a nonlinear and linear statistical data base model is also proposed as a means of developing a pseudo time-variant model for a distillation column process simulator.

The results reported in the chapter demonstrate the feasibility of both proposed hybrid schemes. More specifically it provides evidence that both the prediction and fault detection performance of a mechanistic model-based monitoring scheme can be enhanced by compensating the model with a data-driven model.

In Chapter 6 the focus is shifted to addressing quality variable prediction and performance monitoring of non-linear batch processes using a monitoring strategy that merges both three dimensional data unfolding techniques proposed by Wold et al. 1987 with an emerging partial least squares modelling technique referred to as interval partial least squares iPLS. The multiway iPLS (MiPLS) model development employs a novel algorithm, described in the chapter, for partitioning of the intervals used by the model. The MiPLS model's quality variable prediction and overall batch monitoring performance is demonstrated to be superior to the standard PLS model-based approach. The well-known penicillin fermentation simulator developed and enhance by researchers out of Illinois Institute of Technology (Birol, et al. 2002) was employed for evaluating the predictive and process monitoring capable of the proposed model.

Chapter 7 closes with a summary overview on the various statistical and mechanistic model-based approaches explored in the research, highlighting the main conclusions from key results obtained. The scope of potential future research in the area is also discussed.

Chapter 2 : Review of Linear Multivariate Statistical Monitoring Techniques

2.1 Introduction

The major limitation of traditional univariate statistical process control (SPC) for process performance monitoring, as pointed out by Martin et al. (1996) , is the independent basis by which each process variable is monitored to identify developing faults. The detection and diagnosis of malfunctions may in such case be impaired by this limitation. Firstly, due to the fact that the select monitored variables are not necessarily independent and hence faults due to multivariate correlated occurrences may go undetected. And secondly, in the case of large complex plant set up, the large number of sensor measurement sampled on a 24 hour basis can easily overwhelm such an approach. Multivariate SPC (MSPC) is an extension of univariate SPC where the correlation between process quality variables and process variables are taken into consideration.

MSPC methods unlike its univariate counterpart are capable of detecting malfunctions that are due to correlated events and events that are not detected readily by magnitude deviations in independently monitored quality variables. MSPC is based mainly on projection methods that seeks to extract the correlation in variability among a set of simultaneously measured process variables and or to quantify the extent to which such variability and correlation structure may be linked to observable trends in one or more process quality variables. The two most common projection methods are PCA and PLS (MacGregor et al., 1991) .

PCA is a data dimension reduction technique that exploits the correlations among the vast amounts of plant measurement data collected (Jolliffe, 2002; Wold, et al., 1987). It is inherently static as the projection and directional information with respect to the variability in the data at any given time is only dependent upon the current samples and does not take into account the possible influence of past samples on the current observation (Russell, et al., 2000).

Projection to latent structures or partial least squares seeks to simultaneously reduce the dimensional space of the process measurement variables and process quality variables. The method is employed in product quality prediction as PLS extracts a set of latent variables that not only account for the variability in the process variables but are also most correlated to the variability in the product quality variables.

During the reign of univariate SPC, the univariate monitoring of process quality variables would involve the use of univariate statistical charts, such as CUSUM (cumulative sum) plots, EWMA (exponentially weighted moving average) charts and Shewhart charts (MacGregor and Kourti, 1995). These charts evaluate the performance of the process by comparing them against derived control limits determined from measurements taken when the process was known to be conforming to the product specification limits. Similarly an essential component to MSPC is the development of multivariate control charts to detect disturbances and fault conditions as they may arise. Multivariate project techniques employ the same philosophy as that for univariate or multivariate shewharts charts (MacGregor and Kourti, 1995). The multivariate Hotelling's T^2 chart and the square prediction error (SPE) or Q-Statistics chart is generated based upon of a subset of the latent vectors used in defining the model. The main understanding and justification of the use of such chart for monitoring can be found in Kresta et al. (1991b). The mathematics behind such charts is described in greater detail in later subsections. Other proposed multivariate control charts include Multivariate CUSUM charts (Healy, 1987), multivariate EWMA charts (Lowry et al., 1991).

Recent researches have been directed at addressing and compensating for specific-shortcomings linked to the restrictive assumptions upon which techniques such as PCA and PLS is based. That is, the assumption that the data samples exhibit minimal auto and cross-correlation. Several variants to the standard PCA and PLS approach have been proposed in the literature and will be addressed in this and the following chapter.

The remainder of this chapter is as follows. Section 2.2 describe the projection method of PCA, the NIPALS PCA algorithm, and theory behind identifying the reduce subspace for data dimension reduction. Section 2.3 reviews both the single and two block PLS methods, the various proposed PLS algorithms and discussion on their suitability for process monitoring applications. Section 2.4 looks the two most well-known monitoring statistics – Hotelling's T^2 and Q statistics and discusses their application to process monitoring. Section 2.5 reviews the PLS and PCA variants that have been reported in the literature which are particularly applicable to batch processes such as Multi-way and Multi-block PLS and PCA methods. Section 2.6 reviews the dynamic extension to the standard PCA and PLS method. Section 2.7 closes the chapter with a summary overview of the literature reviewed.

2.2 Principal Component Analysis

Principal component analysis (PCA) is a mathematical linear orthogonal transformation technique that exploits the correlation existing among measured process variables in order to reduce the dimensionality of the measurements. The principal component score vectors are linear weighted sum of the original process variables. The weights associated with the process variables for a given score/principal component computation defines the principal component score vector and are alternately referred to as the loadings for the principal component. The loadings are derived from the eigenvectors of the covariance matrix and as such the resulting scores are themselves uncorrelated and hence a significantly reduce number of scores can be used to represent the majority of the variability in the measurement variables provided that the process variables exhibit a high degree of correlation.

PCA was first introduced by Karl Pearson in 1991 but did not really catch on in use and popularity until advances in computing and electronics facilitated such (Jolliffe, 2002). The methods of deriving the principal component using eigenvector decomposition or single value decomposition (SVD) were considered computationally intensive at the time of its inception. The method has will be shown in the following analysis is both scale and noise sensitive.

If **A** is an $n \times n$ matrix and **u** is $n \times 1$ vector such that:

$$\mathbf{A}\boldsymbol{u_i} = \boldsymbol{\lambda_i l_i} \tag{2.1}$$

where $\boldsymbol{l}_i$ is an eigenvector of the matrix **A** and the scalar quantity λ_i is the associated eigenvalue.

If the matrix **A** represents the covariance matrix of the process variables:

$$\mathbf{A} = \mathbf{cov}(\boldsymbol{X}, \boldsymbol{X}) \tag{2.2}$$

where **X** is an $n \times m$ matrix of n samples of m process variables, then the eigenvalues can be shown to be equal to the variances of the scores. If **X** is autoscaled, that is, each process variable is mean-centred and scaled by their respective standard deviation then the matrix **A** represents the correlation matrix and in such a case the relative size of the eignenvalue may therefore be used to indicate the significance or dominance of the principal component vector in the representation of the process variability. The correlation matrix **A** can be approximated by the sample covariance matrix:

$$\mathbf{A} = \left(\frac{\mathbf{1}}{\boldsymbol{n}-\mathbf{1}}\right)\mathbf{X}^{\mathbf{T}}\mathbf{X} \tag{2.3}$$

The Non-linear Iterative Partial Least Square (NIPALS) algorithm (Wold, et al. 1987), is one methods of decomposing and extracting the loadings and scores or obtaining the eigenvectors of the matrix **X**. The method is outlined in Table 2.1 and was first develop for PCA but have since been incorporated and applied to other statistical modelling methods. Alternatively, the principal components can be derived from the single value decomposition of the autoscaled data matrix **X** which gives:

$$\mathbf{svd}(\mathbf{X}) = \mathbf{V\Sigma L^T} \tag{2.4}$$

where $\mathbf{V}^{\mathrm{T}}\mathbf{V} = \mathbf{I}_{\mathrm{n}}$ and $\mathbf{LL}^{\mathrm{T}} = \mathbf{I}_{\mathrm{m}}$ and Σ is a $n \times m$ matrix of singular values σ_i, where $\sigma_i \neq 0$ for $i = 1,2, ..$ m and $\sigma_i = 0$ for i = m + 1, …,n.

The singular values are the standard deviations of the principal component scores and are hence related to the square root of the eigenvalues of the correlation matrix **A** since:

$$\boldsymbol{X}^T\boldsymbol{X} = (\boldsymbol{L}\Sigma\boldsymbol{V}^T)\boldsymbol{V}\Sigma\mathbf{L}^{\mathrm{T}}$$

$$\boldsymbol{X}^T\boldsymbol{X} = \boldsymbol{L}\Sigma I_n\Sigma\boldsymbol{L}^{\mathrm{T}}$$

Post-multiplying both sides by $\boldsymbol{L}$**:**

$$\boldsymbol{AL} = \boldsymbol{L}\boldsymbol{\Sigma}^2\mathbf{I_m}$$

Considering the above equation in relation to Eq. (2.1), the right-hand size matrix $\boldsymbol{L}$ and diagonal matrix of singular values **Σ** maps unto the full set of eigenvectors and eigenvalues:

$$\boldsymbol{L} = [\boldsymbol{l}_1, \boldsymbol{l}_2, \ldots.., \boldsymbol{l}_{\mathrm{m}}] \text{ and } \boldsymbol{\Sigma}^2 = \mathbf{diag}(\boldsymbol{\lambda}_{1,}\ \boldsymbol{\lambda}_2, \ldots\ldots, \boldsymbol{\lambda}_{\mathbf{m}}) \qquad (2.5)$$

Table 2.1 NIPALS Algorithm for PCA

0	Set t = to a column in X; set E_0 = X; set threshold (e.g. $\tau = 0.001$) for convergence check; *i* = 1.
1	Project X onto ***t*** to find the corresponding loading ***l***: $\boldsymbol{l}_i = \boldsymbol{E}_{i-1}^T\boldsymbol{t}_i/(\boldsymbol{t}_i^T\boldsymbol{t}_i)$
2	Normalize the loading vector ***l*** to unit length: $\boldsymbol{l}_i = \boldsymbol{l}_i/\sqrt{\boldsymbol{l}_i^T\boldsymbol{l}_i}$
3	Project X onto ***l*** to find the corresponding score vector ***t***: $\boldsymbol{t}_i = \boldsymbol{E}_{i-1}^T\boldsymbol{l}_i/(\boldsymbol{l}_i^T\boldsymbol{l}_i)$
4	Check for convergence: If the difference between the eigenvalues $\sigma_{new} = \boldsymbol{t}_i^T\boldsymbol{t}_i$ in the current iteration is > $\tau * \sigma_{old}$ then return to step 1 else move to step 5.
5	Prepare for next loadings and score vector extraction: *i* = *i* + 1; $\boldsymbol{E}_i = E_{i-1} - \boldsymbol{t}_i\boldsymbol{l}_i^T$

The scores may be interpreted as the projection or mapping of the original sample measurements unto the subspace spanned by the subset of the *p* selected uncorrelated principal component vectors. Eq.(2.7) describes the linear variable transformation carried out on the *m* process variables collected at the *i*th sample instance to compute the score projection onto the *j*th principal component:

$$t_{ij} = l_{1j}x_{i1} + l_{2j}x_{i2} + l_{3j}x_{i3}.........+ l_{mj}x_{im} \tag{2.6}$$

The principal component vector loading l_{kj} is the coefficient associated with the *kth* process variable and the *jth* principal component while x_{ik}, is the *ith* sampled measurement of the *kth* process variables. The principal component scores computation of *n* samples using a subset of *p* principal component loadings is represented in matrix form via Eq.(2.8) or diagrammatically in Figure 2.1.

$$\begin{bmatrix} t_{11} & t_{12} & . & . & t_{1p} \\ t_{21} & t_{22} & . & . & t_{2p} \\ . & . & & & . \\ . & . & & & . \\ . & . & & & . \\ . & . & & & . \\ t_{n1} & t_{n2} & . & . & t_{np} \end{bmatrix} = \begin{bmatrix} x_{11} & x_{12} & . & . & x_{1m} \\ x_{21} & x_{22} & & & x_{2m} \\ & & & & . \\ & & & & . \\ & & & & . \\ & & & & . \\ x_{n1} & x_{n2} & & & x_{nm} \end{bmatrix} \begin{bmatrix} l_{11} & l_{12} & .... & l_{1p} \\ l_{21} & l_{22} & .... & l_{2p} \\ & & & \\ & & & \\ l_{m1} & l_{m2} & .... & l_{mp} \end{bmatrix} \tag{2.7}$$

The principal component loadings (L_p = [$\boldsymbol{l_1}$ $\boldsymbol{l_2}$ **.......** $\boldsymbol{l_p}$]) are of unit length and are orthogonal as such, if the full set or subset of principal component are used, the loading matrix pre-multiplied by its transpose would give a *p* x *p* identity matrix:

$$L_p^T L_p = I_p \tag{2.8}$$

where *p* <= *m*. Note post-multiplication does not result in an identity matrix as will be shown later.

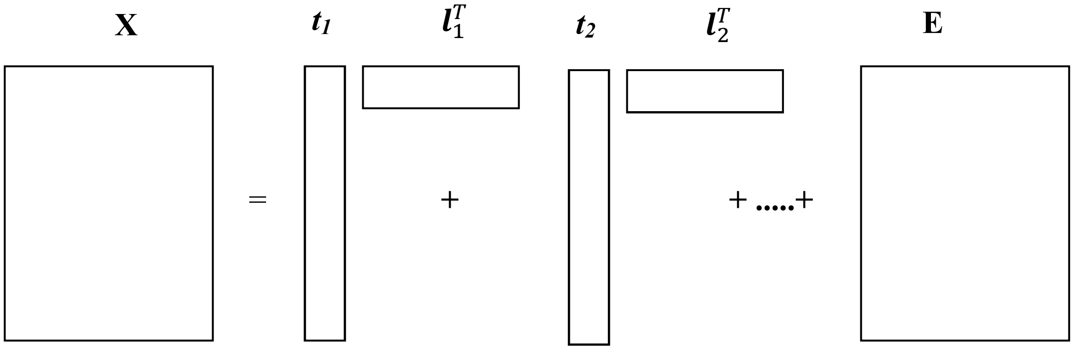

Figure 2.1 Decomposition of the data matrix X into a collection of scores and loadings

The reconstruction based upon the reduce dimension subspace of principal component loadings and computed scores is given by:

$$\hat{X} = T_p L_p^T \tag{2.9}$$

The choice of the subspace dimension ($p < m$) usually incorporates the most significant principal components. The common justification provided is that, the choice separates the full dimension of principal components into two subspace with $\boldsymbol{L}_\text{p}$ subspace accounting for the structured variability present in the measurement and the other subspace made up of the higher order principal components accounting mostly for the unstructured noise present in the measurements (MacGregor and Kourti, 1995).

Since $\boldsymbol{T_p} = \boldsymbol{XL_p}$ then:

$$\hat{\boldsymbol{X}} = \boldsymbol{X}\boldsymbol{L}_p\boldsymbol{L}_p^T = \boldsymbol{X}\boldsymbol{P}_m \tag{2.10}$$

where $\boldsymbol{P}_m$ is an $m \times m$ matrix but not necessarily an identity matrix.

In fact $\boldsymbol{P}_m$ only computes into a perfect identity matrix when the full complement or the number of components equal to the rank order of the matrix is included in the PCA model.

Consider the residual matrix representing the difference between the actual measurements and the reconstructed estimates based upon the PCA model, it can be proven that the residuals are actually a function of the higher-order principal components not included in the PCA model:

$$\widetilde{\boldsymbol{X}} = X - \hat{X} = \boldsymbol{X}(\boldsymbol{I}_m - \boldsymbol{P}_m) \tag{2.11}$$

Now by expressing the identity matrix $\boldsymbol{I}_m$ using its two constituent parts as defined by those principal components included in the PCA model $\boldsymbol{L}_p$ and those not used $\boldsymbol{L}_{\text{m-p}}$:

$$\begin{aligned} I_m &= \left[\boldsymbol{L}_p \; \boldsymbol{L}_{m-p}\right]\begin{bmatrix} \boldsymbol{L}_p^T \\ \boldsymbol{L}_{m-p}^T \end{bmatrix} \\ &= \left[\boldsymbol{L}_p\boldsymbol{L}_p^T + \boldsymbol{L}_{m-p}\boldsymbol{L}_{m-p}^T\right] \\ &= \left[\boldsymbol{P}_m + \boldsymbol{L}_r\boldsymbol{L}_r^T\right] \end{aligned} \tag{2.12}$$

It, therefore, follows from Eq.(2.12) that residual matrix can be equivalently expressed as:

$$\widetilde{\boldsymbol{X}} = \boldsymbol{X}\boldsymbol{L}_r\boldsymbol{L}_r^T = \boldsymbol{X}\boldsymbol{R}_m \tag{2.13}$$

where $\mathbf{L}_\text{r}$ is used to replace $\boldsymbol{L}_{\text{m-p}}$ and represents the subset of higher order principal components.

From Eq.(2.14) it is clear that the residuals simply accounts for the reconstruction of **X** based upon the higher order principal components left out of the subspace model defined by $\boldsymbol{L}_\text{p}$. The subspace transformation matrix defined by $\boldsymbol{P}_\text{m}$ and $\boldsymbol{R}_\text{m}$ have complementary values, that is, the non-main diagonal elements are of the same magnitude but opposite in sign and the main diagonals elements are given by $\alpha_{\text{ri}} = 1 - \alpha_{\text{pi}}$ where α_{ri} and α_{pi} are the *i*th diagonal element of the matrix $\boldsymbol{R}_\text{m}$ and $\boldsymbol{P}_\text{m}$ respectively. This naturally follows since:

$$\boldsymbol{P}_\text{m} + \boldsymbol{R}_\text{m} = \boldsymbol{I}_\text{m} \tag{2.14}$$

and this will later also provide an explanation as to why the Hotelling's T^2 statistics on the scores projection and the square prediction error Q statistics on the residual matrix tends to give complimentary detection, that is, a fault detected by one statistics may fail to be detected by the other.

2.3 Partial Least Squares

Let us consider that the product quality variable measurements are stored in the n x s output matrix $\mathbf{Y}$ and the process variable measurements in the $n \times m$ input matrix **X**. There are two types of PLS algorithm, PLS1 for the case of a univariate quality variable (s = 1) and two block PLS (PLS2) for the multivariate output matrix **Y** (s > 1). However, PLS2 have come under much criticism from the statistics community. A number of publications, including (Breiman and Friedman, 1997; Frank and Friedman, 1993; Garthwaite, 1994) expressed opinions that PLS2 performs worse than other regression methods. Extensive simulation studies conducted by Breiman and Friedman (1997), comparing univariate and multivariate regression methods, including PLS1, PLS2, OLS, ridge regression, and other biased regressions methods found that PLS1 outperformed PLS2 and was competitive with other univariate biased regression methods. It was therefore advised that building multiple PLS1 models for each process quality variable maybe a better strategy than employing PLS2 for multivariate regression modelling.

The projection to latent structures or partial least squares is a method of projecting the combine data set unto a low-dimensional space defined by a set of latent vectors ($\mathbf{t}_1$, $\mathbf{t}_2$, ...,$\mathbf{t}_A$) as follows:

$$\mathbf{X} = \mathbf{T}\mathbf{P}^T + \mathbf{E}$$

$$\mathbf{Y} = \mathbf{U}\mathbf{Q}^T + \mathbf{F} \qquad (2.15)$$

where $\mathbf{T}$ = [$\mathbf{t}_1$, $\mathbf{t}_2$, ...,$\mathbf{t}_A$] is the score matrix, $\mathbf{P}$ = [$\boldsymbol{p}_1$, $\boldsymbol{p}_2$, ..., $\boldsymbol{p}_A$] is the loading matrix for **X,** likewise $\mathbf{U}$ = [$\mathbf{u}_1$, $\mathbf{u}_2$, ...,$\mathbf{u}_A$] is the score matrix, and $\mathbf{Q}$ = [$\boldsymbol{q}_1$, $\boldsymbol{q}_2$, ...$\boldsymbol{q}_A$] is the loading matrix for **Y**. **E** and **F** are the modelling residual of **X** and **Y** respectively. The objective of PLS is to find the set of the latent vectors or of **X** and **Y** that are most highly correlated and which also accounts for the greatest variability in the **X** and **Y** space. Thus the projection method not only identifies those vectors that reduce the dimensionality of **X** but the vectors that are also most predictive of the process quality variables in the **Y** matrix (Wise and Gallagher, 1996).

In accordance with the previously stated objective, the PLS algorithm seeks to find the solution to the following problem:

$$\begin{aligned} &\max \quad \boldsymbol{w}_i^T \mathbf{X}_i^T \mathbf{Y}_i \boldsymbol{q}_i \\ &s.t \quad \|\boldsymbol{w}_i\| = 1 \; and \; \|\boldsymbol{q}_i\| = 1 \end{aligned} \tag{2.16}$$

where $\boldsymbol{w}_i$ represent the factor weighting vectors of **X** and $\boldsymbol{q}_i$ the same for **Y** (refer to Eq. (2.17)).

$$\begin{aligned} &\boldsymbol{t}_i = \boldsymbol{X}\boldsymbol{w}_i \\ &\boldsymbol{u}_i = \boldsymbol{Y}\boldsymbol{q}_i \end{aligned} \tag{2.17}$$

The equations of Eq. (2.17) are referred to as the outer relations for the **X** and **Y** blocks. An inner linear equation is defined that regresses the vector $\boldsymbol{u}_i$ unto $\boldsymbol{t}_i$, taken pair by pair:

$$\boldsymbol{u}_i = \boldsymbol{t}_i b_i + \varepsilon \tag{2.18}$$

where b_i is a scalar representing the *ith* regression coefficient term. This particular step is only applicable for PLS2 regression modelling along with those other steps highlighted in gray in Table 2.2, according to Malthouse (1995).

As new pairs of latent vectors are generated, **X** and **Y** are independently and linearly regressed unto their respective latent vectors with the residuals being used in place of the **X** and **Y** blocks on successive regressions:

$$\mathbf{E}_i = \boldsymbol{t}_i \boldsymbol{p}_i^T + E_{i+1} \qquad \text{and} \quad \mathbf{F}_i = \boldsymbol{u}_i \boldsymbol{q}_i^T + F_i \tag{2.19}$$

The initial residues $\mathbf{E}_1 = \mathbf{X}$ and $\mathbf{F}_1 = \mathbf{Y}$ and successive residues are therefore given by:

$$E_{i+1} = X - \sum_{i=1}^{k} T_i p_i \quad \text{and} \quad F_{i+1} = Y - \sum_{i=1}^{k} U_i q_i \tag{2.20}$$

Table 2.2 The Bootstrap PLS Algorithm

0	Mean center and scale **X** and **Y**; set $\mathbf{E}_0 = \mathbf{X}$ and $\mathbf{F}_0 = \mathbf{Y}$ and $k = 1$.
1	Set $\boldsymbol{u}_{\text{k}}$ to the first column of $\boldsymbol{F}_{\text{k-1}}$
2	$\boldsymbol{w}_k = \boldsymbol{E}_{k-1}^T \boldsymbol{u}_k / (\boldsymbol{u}_k^T \boldsymbol{u}_k)$
3	scale $\boldsymbol{w}_{\text{k}}$ to unit length: $\boldsymbol{w}_k = \boldsymbol{w}_k / \Vert \boldsymbol{w}_k \Vert$
4	$\boldsymbol{t}_k = \boldsymbol{E}_{k-1} \boldsymbol{w}_k$
5	$\boldsymbol{q}_k = \boldsymbol{F}_{k-1}^T \boldsymbol{t}_k / (\boldsymbol{t}_k^T \boldsymbol{t}_k)$
6	scale $\boldsymbol{q}_{\text{k}}$ to unit length: $\boldsymbol{q}_k = \boldsymbol{q}_k / \Vert \boldsymbol{q}_k \Vert$
7	$\widetilde{\boldsymbol{u}}_k = \boldsymbol{F}_{k-1}^T \boldsymbol{q}_k / (\boldsymbol{q}_k^T \boldsymbol{q}_k)$
8	Check for convergence. set $\boldsymbol{u}_k = \widetilde{\boldsymbol{u}}_k$
9	If converges go to step 10 else return to step 2
10	$\boldsymbol{E}_{\text{k-1}}$ loadings: $\boldsymbol{p}_k = \boldsymbol{E}_{k-1}^T \boldsymbol{t}_k / (\boldsymbol{t}_k^T \boldsymbol{t}_k)$
11	Regress $\boldsymbol{u}_{\text{k}}$ unto $\boldsymbol{t}_{\text{k}}$: $b_k = \boldsymbol{u}_k^T \boldsymbol{t}_k / (\boldsymbol{t}_k^T \boldsymbol{t}_k)$
12	Compute Residuals: $\boldsymbol{E}_k = \boldsymbol{E}_k - \boldsymbol{t}_k \boldsymbol{p}_k^T$ and $\boldsymbol{F}_k = \boldsymbol{F}_k - b_k \boldsymbol{t}_k \boldsymbol{p}_k^T$
13	Apply cross-validation to determine whether to generate additional latent structure, if required then increment k and return to step 1.

Alternatively the latent variables could be derived by working on the sample covariance matrix $(\mathbf{X}^{\mathrm{T}}\mathbf{Y})(\mathbf{X}^{\mathrm{T}}\mathbf{Y})^{\mathrm{T}}$. In the version of the PLS method presented by Höskuldsson (1988), the first PLS latent variable $\boldsymbol{t}_1 = \mathbf{X}\boldsymbol{w}_1$ is that linear combination of the **X** variable block that minimizes the covariance between it and the **Y** space. As such, the first PLS loading vector $\boldsymbol{w}_1$ is the first eigenvector of the sample covariance matrix $\mathbf{X}^{\mathbf{T}}\mathbf{Y}\mathbf{Y}^{\mathbf{T}}\mathbf{X}$**.** However, for large ill-conditioned data set it is best to derive the latent variables sequentially as described previously using a version of the NIPALS Algorithm adapted specifically of PLS2 modelling (Geladi and Kowalski, 1986). The sequential approach also facilitates extending the linear PLS to non-linear PLS by training neural networks to derive latent variables as non-linear functions of the independent variables **X**. A generally accepted version of the NIPALS algorithm adopted for PLS modelling, Bootstrap PLS (Zhao, et al. 2006), is provided in Table 2.2.

If we define the following $\mathbf{R} = [\boldsymbol{r}_1, \boldsymbol{r}_2, \ldots\ldots, \boldsymbol{r}_A]$ as:

$$\boldsymbol{r}_1 = \boldsymbol{w}_1$$

$$\boldsymbol{r}_i = \prod\left(\mathbf{I}_m - \boldsymbol{w}_j \boldsymbol{p}_j^T\right)\boldsymbol{w}_i, \quad i > 1 \tag{2.21}$$

Then the scores matrix **T** can be computed directly from the original **X** matrix without deflation and the final model can be expressed in closed form multiple regression type prediction model (Dejong, 1993; Li, et al., 2010):

$$\mathbf{T} = \mathbf{XR} \tag{2.22}$$

$$\begin{aligned} \mathbf{Y} &= \mathbf{X}\boldsymbol{B}_{PLS} + \mathbf{F} \\ \boldsymbol{B}_{PLS} &= \mathbf{RQ}^T \end{aligned} \tag{2.23}$$

P, **R**, and **W** have the following relationship:

$$\mathbf{R} = \mathbf{W}(\mathbf{P}^T\mathbf{W})^{-1} \tag{2.24}$$

$$\mathbf{R}^{\boldsymbol{T}}\mathbf{P} = \mathbf{P}^{\boldsymbol{T}}\mathbf{R} = \mathbf{W}^{\boldsymbol{T}}\mathbf{W} = \mathbf{I}_{\boldsymbol{A}} \tag{2.25}$$

Li, et al. (2010) compared the suitability of two other proposed PLS algorithms – Weight-deflated PLS (WPLS) (Helland, 1998) and SIMPLS (Dejong, 1993) with the standard (established) PLS algorithm described earlier and documented in Table 2.2. The paper concluded based upon geometric analysis of the algorithms and simulation performance results that the standard PLS algorithm was best suited for applications involving fault detection monitoring.

2.4 Monitoring Metrics: *Hotelling's T^2* and *Q* Statistics

The Hotelling's T^2 and squared prediction error (SPE) or Q-statistics monitoring plots and contribution charts are quite effective multivariate control charts which can be employed in distinguishing between the good-nominal operating plant conditions versus an abnormal plant condition (MacGregor and Kourti, 1995). The T^2 plots and *SPE* (*Q*) statistics are interlinked in that they are both dependent upon the number of principal components (latent variables in the case of PLS) chosen for inclusion.

$$\boldsymbol{t_j} = \mathbf{x}_{\boldsymbol{new}}\boldsymbol{l_j} \tag{2.26}$$

where $\boldsymbol{t_j}$ is the scores/principal component, $\boldsymbol{l_j}$ is the *jth* loading vector or latent variables (in the case of PLS), and $\mathbf{x}_{new}$ is the 1 × m row vector of new measurements on the process variables. Note that there is a score vector evaluated per loading vector and represents the projection of the variance in the original measurement variables onto that particular principal component axis.

The T^2 plot is a measure of the deviation of the squared scores scaled by the eigenvalues (variance of the scores) obtained from the PCA model developed using normal operation (NOP) data. Eq. (2.27) evaluates the overall squared score values at the *ith* sample instance by summing together the square of the *A* scores value representing the projection of the m process variables unto the *A* dominant principal component vectors.

$$T_i^2 = \sum_{j=1}^{A} \frac{\boldsymbol{t}_{ij}^2}{\lambda_j} \tag{2.27}$$

Alternatively, the *Hotelling's* T^2 statistics on the scores can be expressed using matrix notation:

$$T^2 = \mathbf{X}\boldsymbol{L_p}\boldsymbol{\Sigma}^{-2}\boldsymbol{L}_{\boldsymbol{p}}^{T}\mathbf{X}^{T} \tag{2.28}$$

PLS has been used in multivariate monitoring of process is pretty much identical ways to PCA based monitoring (Kresta, et al., 1991a). In the case of PLS, similar T^2 statistics have been proposed for monitoring using the latent vectors of **X** that can be conveniently be extracted using Eq. (2.22), the Hotelling's T^2 statistics is then similarly calculated using:

$$\boldsymbol{t} = \mathbf{x}_{\text{new}}\mathbf{R}$$

$$T^2 = \boldsymbol{t}_{\boldsymbol{new}}^{\boldsymbol{T}}\boldsymbol{\Lambda}^{-\mathbf{1}}\boldsymbol{t}_{\boldsymbol{new}} \tag{2.29}$$

where $\boldsymbol{\Lambda} = \frac{1}{n-1}\mathbf{T}^T\mathbf{T}$ is the sample covariance matrix of the scores.

In general, SPE or Q statistics plot is based upon evaluating the summation of the square difference or squared residuals between actual process variable measurements and that of the reconstructed estimates of the said:

$$SPE = \sum_{i=1}^{m} (x_{new,i} - \hat{x}_{new,i})^2$$
$$\text{where } \hat{X}_{new} = T_{A,new} P_A^T \tag{2.30}$$

In the case of PCA the estimation $\widehat{\mathbf{X}}$ can be derived using Eq. (2.9) or (2.10) and the residuals $\widetilde{\mathbf{X}} = \mathbf{X} - \widehat{\mathbf{X}}$ can be alternatively computed directly from $\mathbf{X}$ using Eq. (2.13). Consequently, the PCA Q statistics can also be interpreted in terms of the lower-order principal components. If the first p of the total m principal components are chosen the $\boldsymbol{Q}$ (SPE) statistics maybe expressed in terms a dot product operation followed by a summation along the rows of the matrix to give a single column vector and this can be shown to be mathematically equivalent to the following matrix operation:

$$\boldsymbol{Q} = \mathbf{x}\boldsymbol{R}_m\boldsymbol{R}_m^T\mathbf{x}^T \tag{2.31}$$

where $\mathbf{x} = [\mathbf{x}_{i1}\ \mathbf{x}_{i2} \ldots \mathbf{x}_{im}]$ is a 1 × m row vector representing ith sample instance within the data matrix $\mathbf{X}$. Eq.(2.32) is simplified to:

$$Q = \mathbf{x}\boldsymbol{L}_r\boldsymbol{L}_r^T\mathbf{x}^T \tag{2.32}$$

Since $\boldsymbol{R}_m\boldsymbol{R}_m^T = \boldsymbol{L}_r\boldsymbol{L}_r^T(\boldsymbol{L}_r\boldsymbol{L}_r^T) = \boldsymbol{L}_r\boldsymbol{I}_r\boldsymbol{L}_r^T$

Applying a Q statistics to the PLS type model is achieved by evaluating the summation of the squared of the residuals on the quality variables $\boldsymbol{Q} = \left\|\widetilde{\boldsymbol{Y}}\right\|^2$ where $\widetilde{\mathbf{Y}} = \mathbf{Y} - \widehat{\mathbf{Y}}$**.** The most convenient means of deriving the predictions $\widehat{\mathbf{Y}}$ of the quality variables is via the closed form regression equation given as Eq. (2.23). However, such is only possible if the quality variable measurements are available online.

The confidence bounds on the scores, *SPE* and T^2 plot are the equivalent of control limits defined for univariate control charts. They are used to aid in the detection of the *m*-dimensional process departure from the nominal in-control process operation. The Hotelling's T^2 distribution as the statistic *(n – 1)mF/(n – m)*, where *F* has a central F-distribution. The confidence bound on such a distribution is therefore given by

$$T_0^2 > \frac{(n-1)mF_{m,n-m,\alpha}}{n(n-m)} \tag{2.33}$$

where there is a 100α % (5% if α = 0.05) chance that a detected departure is a false alarm (Martin, et al., 1996).

Jackson and Mudkulhor (1979) proposed a transformation that could be used to transform the Q statistics or SPE of the residuals of a principal component analysis model to a standard normal distribution of zero mean and unit variance:

$$C = \theta_1 \left[\frac{(Q/\theta_1)^{h_0} - \left[\{\theta_2 h_0 (h_0 - 1)/\theta_1^2\} + 1\right]}{\sqrt{2\theta_2 h_0^2}} \right] \tag{2.34}$$

where $h_0 = 1 - \frac{2\theta_1\theta_2}{3\theta_3}$ and $\theta_j = \sum_{i=q+1}^{p} \left(\sqrt{\lambda_i}\right)^j, \quad for\ j = 1,2,3$

The control limit of the *Q* statistics can then be mapped to the normal variate value c_α which encapsulates an area under the distribution of 95% or 99% (α = 0.95 or α = 0.99). Rearrangement of Eq. (2.34) would then give:

$$q_\alpha = \theta_1 \left(c_\alpha \sqrt{2\theta_2 h_0^2} + \left[\{\theta_2 h_0 (h_0 - 1)/\theta_1^2\} + 1\right] \right)^{(1/h_0)} \tag{2.35}$$

Figure 2.2 provides an example illustration of the application of the T^2 and *Q* statistics monitoring. The application is an excerpt taken from results documented by the author in a previous MSc. dissertation (Stubbs, 2007).

Yue and Qin (2001) proposed a combined index as a convenient alternative for merging the information from both the T^2 and *SPE* into a single value for process monitoring. The combined index is defined as the summation of the *SPE* and T^2 weighted against their respective control limits:

$$\varphi = \frac{SPE}{\delta^2} + \frac{T^2}{\tau^2} = \mathbf{X}^T \Phi \mathbf{X} \tag{2.36}$$

where

$$\Phi = \frac{P_{m-k} P_{m-k}^T}{\delta^2} + \frac{P_k S_k P_k^T}{\tau^2} \tag{2.37}$$

The control limits of the combined index are determined based upon similar assumptions that the observations **X** is multivariate normal and hence follows or approximates an *F* distribution.

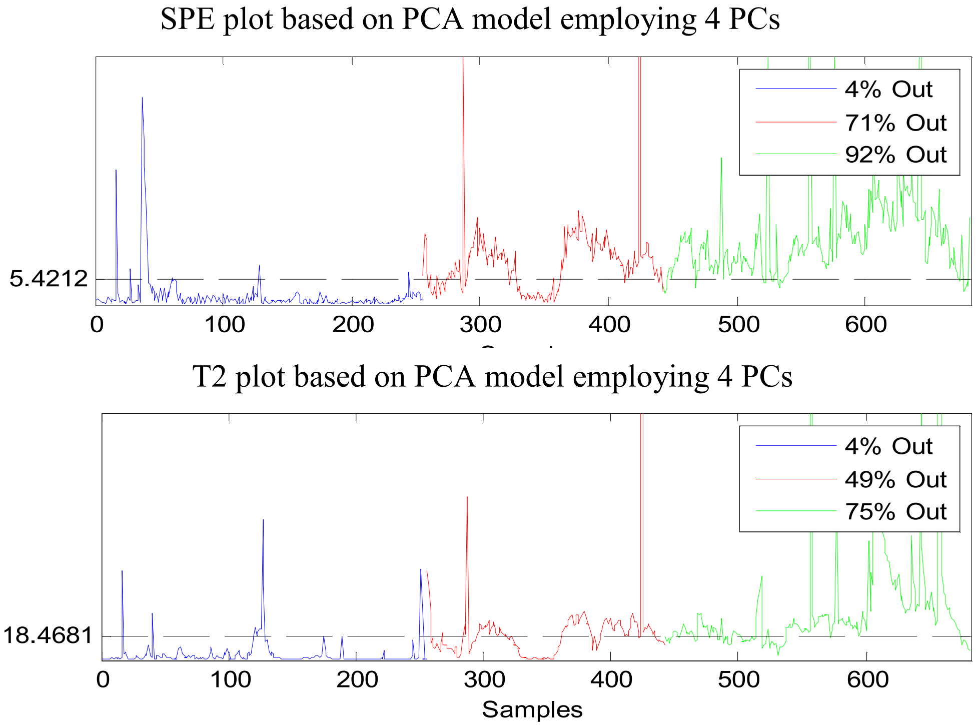

Figure 2.2 Example plot of an SPE and T^2 Monitoring on three different data sets of historical data collected during different periods of process operation. (Stubbs, 2007)

There are two types of contribution plots, one affiliated with the scores/principal components and the other affiliated with the *SPE*. The contribution plot in general looks at each process variable contribution to the overall *SPE* or T^2 value for a specific sample instance or over a range of samples. Typically a contribution plot is a bar chart, good technical references with regards to the application and implementation of such charts can be found in Macgregor and Kourti (1995) and Miller et al. (1995).

An *SPE* contribution plot maybe computed, for instance, by considering the individual squared prediction error associated with each of the process variable estimates using the PCA model of the process. Likewise, a T^2 contribution plot maybe computed along a given principal component vector by measuring the variables weighted contribution to the calculated final value of the score. Since a principal component represents a linear weighted some of the individual process variables then the value of the score is dependent upon both the measured process variable at a given instance and the loading associated with the variable for that particular principal component. Figure 2.3 compares the SPE contribution plot profile of a process under normal operation versus abnormal faulty operation. In this particular example the contribution plot reveals that variable # 1 is the key variable that contributes to deviation of the SPE plot based upon the time sample slice windows over which the contribution chart are generated and compared.

The T^2 and Q statistics can be and have been applied to other multivariate statistical methods other than PCA, such as CVA state space monitoring. However, the parametric equations as applied to the Q statistics of the PCA based monitoring (Eq. 2.38) is not directly applicable to the residuals of the state or output matrix seeing that the transformation equation would have to possibly factor in the number of states used, the singular values of the Hankel matrix, and possibly the state space representation employed. An in depth review of CVA state space modelling is presented in the following chapter.

In any event, these parametric methods rely on the assumption that the sample data are serially independent, that is, independently identically distributed (IID). Given the nature of process data, dynamics, and sampling rates, the serially independent sample constraint is more often not the case. Alternative non-parametric approaches have been proposed in the literature. A common technique is the use of bootstrapping to estimate the percentiles of the underlying empirical distribution, (Buhlmann, 1995; DiCiccio and Efron, 1996; Liu and Tang, 1996). A hybrid approach was proposed by Martin and Morris (1996) that utilized both kernel density estimation and bootstrapping. Whilst other researchers (Liu, et al., 2004; Simoglou, et al., 2002) have opted to compute control limits based on the empirical reference distribution (ERD) (Willemain and Runger, 1996).

Both the T^2 and Q statistics given by Equation (2.28), (2.29) and (2.32) can be shown to be reducible to a weighted sum of the variance and covariance between the variables based upon the dominant principal components selected. The weightings are fixed and the detection of a given fault by a statistics is therefore largely dependent on the distribution of the weightings and the process variables impacted by the fault:

$$\emptyset = a_{11}\mathbf{x}_{i1}^{\mathbf{2}} + \ldots + a_{mm}\mathbf{x}_{\mathrm{im}}^{\mathbf{2}} + a_{12}\mathbf{x}_{i1}\mathbf{x}_{i2} + a_{13}\mathbf{x}_{i1}\mathbf{x}_{i3} + \cdots + a_{jk}\mathbf{x}_{\mathrm{ij}}\mathbf{x}_{ik} \tag{2.38}$$

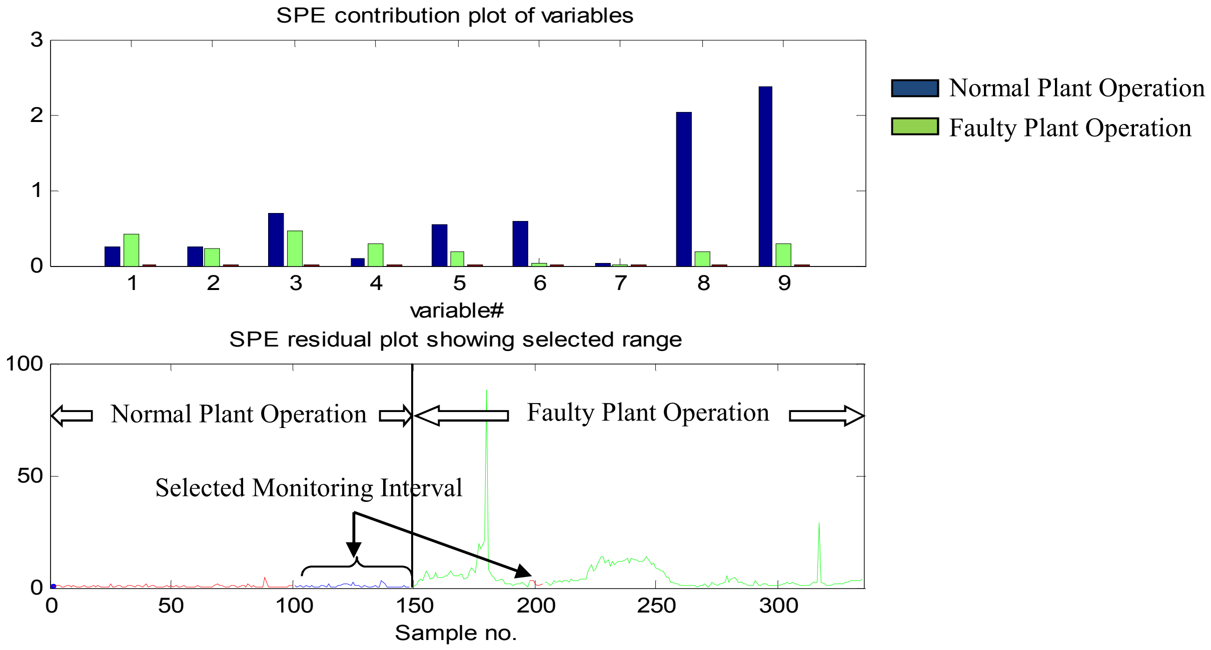

Figure 2.3 SPE contribution chart of a PCA model developed for monitoring of catalyst production plant (Excerpt from MSc. Thesis – Stubbs, 2007)

2.5 Multiblock and Multiway PCA/PLS methods and Interval PLS (IPLS)

Multi-block PLS (MBPLS) and multi-way PCA are yet another variant to PCA and PLS intended at adapting the methods to better suit batch processes with time dependencies and those processes involving a very large number of variables.

2.5.1 Multiblock Partial Least Squares

In MBPLS approach, large sets of process variables (X) are divided in to smaller meaningful sub-blocks, for instance each block may be associated with a specific section of the plant or a specific process unit. From this multivariate control charts for the important subsection of the plant and the entire plant can be constructed.

In the Multiblock PLS approach the sub-blocks are weighted in such a way that they are most predictive of Y thus the monitoring space is determined by the combined model and not by separate models for each block. Details of the theory and algorithm for the implementation of MBPLS are documented in the works of Wangen and Kowalski (1989) and more recently by Westerthuis and Coenegracht (1997). These two algorithms are different in the sense that the early publication proposed deflates the **X** and **Y** blocks using the block scores while the more recent publications have endorsed deflation by way of the super-scores. It turns out that the latter approach leads to superior predictive performance equivalent to that which would have been obtained using the unfolded matrix and application of the traditional PLS method (Lopes, et al. 2002). In an application of MBLS to an industrial pharmaceutical process, Lopes et al. (2002) modelled the production of an active pharmaceutical ingredient by fermentation. The observations gathered over thirty batch runs where separated into four data blocks of manipulated and quality variables for incolium production stage and the API production fermentation stage.

2.5.2 Multiway PLS and PCA

Multiway partial least squares is an extension of PLS to deal with data in three dimension arrays. By three dimensions we refer to variables sampled over a fix time duration collected across several batches (repeat runs of the same process). The multiway technique of transforming a three dimensional data set into a two dimensional representation was first introduced and applied to PCA and PLS by Wold et al. (1987), and was followed up by several other key publications (Nomikos and MacGregor, 1995; Kosanovich, et al., 1994). Since then there have been many publications on the applications of MPCA, MPLS, and their variants such as batch dynamic PCA and PLS (Chen and Liu, 2002; Hu and Yuan, 2008). The MPLS is essentially the equivalent of PLS applied to the unfolded three dimension data set **X** ($\boldsymbol{I} \times \boldsymbol{J} \times \boldsymbol{K}$) where $\boldsymbol{I}$ is the number of batches $\boldsymbol{J}$ is the number of variables and $\boldsymbol{K}$ represents the number of measurement sample for the duration of the batch run. As shown in Figures 2.4 to 2.6 the data can be unfolded in one of three different modes: i) Time ii) Batch and iii) Variable.

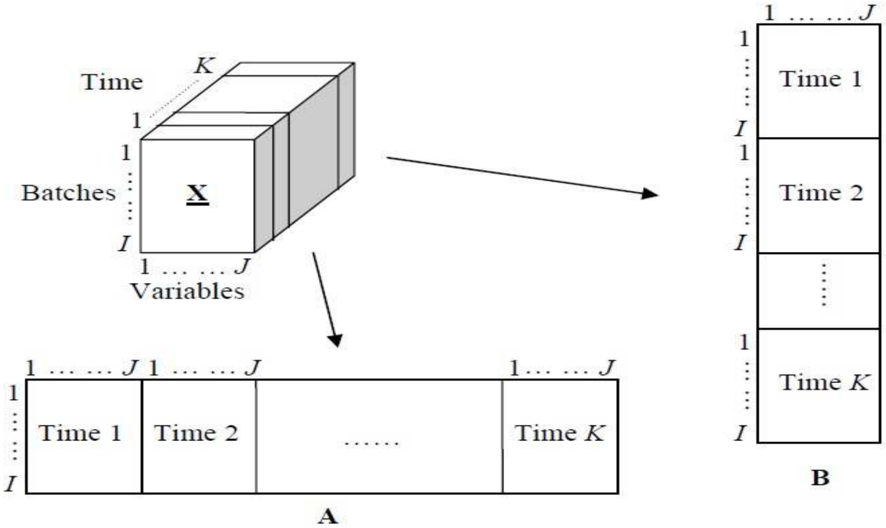

Figure 2.4 Time-mode Unfolding

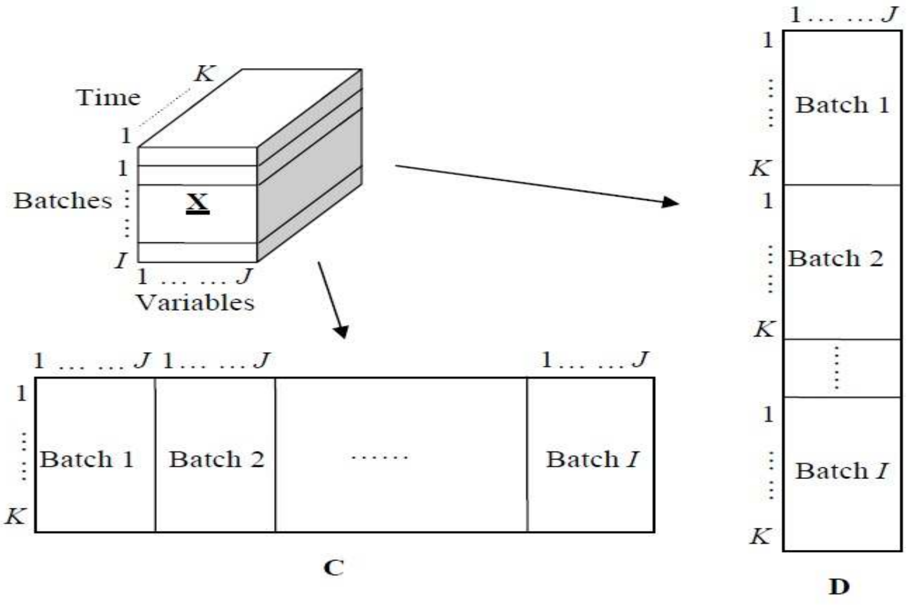

Figure 2.5 Batch-mode Unfolding

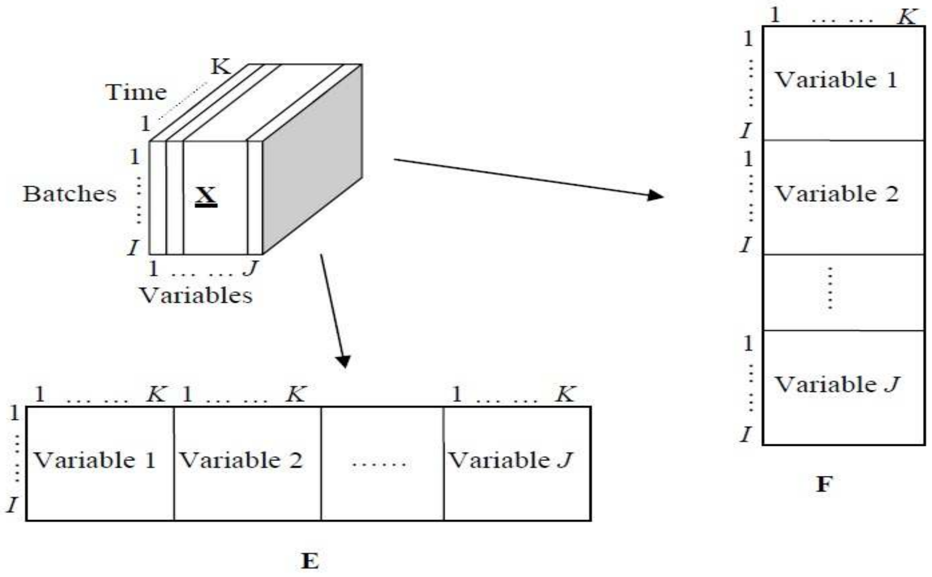

Figure 2.6 Variable-Mode Unfolding

Each of the three general unfolding categories carries two alternatives making the total number of two-dimensional structure representations equal to six. However, due to the equivalence of some of the unfolded structure, the number of unique 2-dimensional data set structure reduces to three. For instance, A and E are essential the same with the columns ordered differently. Likewise, B and D are also of the same dimension (***KI*** × ***J***), in this case the ordering of the rows are different.

In multi-way PCA unfolding of a three-way array is first performed to transform the matrix into a two dimensional array and then standard PCA is applied. Figure 2.7 illustrates an application of MPCA in the monitoring of a semiconductor manufacturing process by Cherry and Qin (2006).

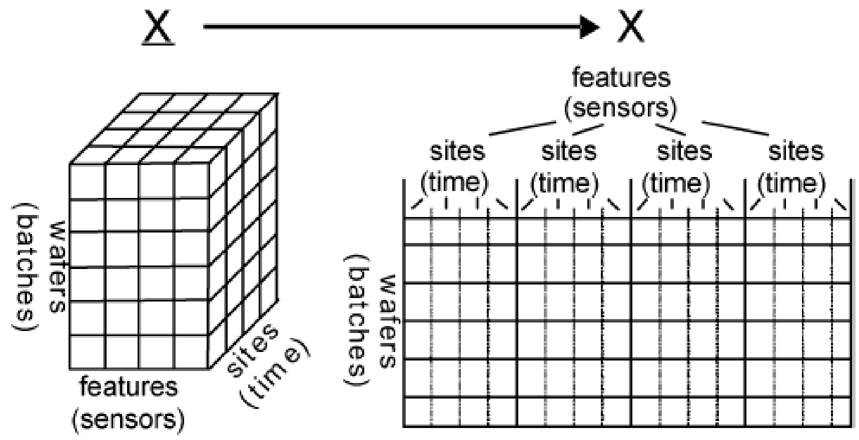

Figure 2.7 Unfolding of site level (batch) data. (Cherry and Qin., 2006)

2.5.3 Interval Partial Least Squares

In recent years the method of interval partial least squares (iPLS) have been applied successfully to the monitoring and prediction of quality variables using the mid-infrared (FTIR) and near-infrared (NIR) spectrum. The technique has been reported in applications ranging from pharmaceutical medicinal explorations - measuring the content of flavone an active ingredient in a rare medicinal plant called snow lotus (Chen, et al. 2010), determination of total polyphenols content in green tea (Chen, et al. 2008), and for simultaneous active substance detection in pharmaceutical formulations (Silva, et al. 2009), to the detection of quality parameters in biodiesel/diesel blends (Ferrao, et al. 2011) and the detection of contaminants in lubricating oil (Borin and Poppi, 2005). The principle of this method involves splitting a spectrum or batch duration into several equidistance sub-intervals or regions and then developing PLS algorithm for each sub-interval using a select number of latent variables. This iPLS approach will be employed and applied to the batch-wise unfolded data set to produce Multiway iPLS (MiPLS) monitoring and predictive models in Chapter 6.

2.6 Dynamic PCA and PLS

The PCA model is limited to capturing only the static underlying correlation and cross-covariance structure between the process variables. This is a direct result of the scores or latent variables being based only on the current time samples of all the process variables as shown in Eq. (2.6). In a dynamic system the current state or values of the process outputs (variables) are also dependent upon the past values. Therefore, a representative model would be required not only to capture the linear relation between the variables at the current time t but also the serial correlation (autocorrelation), the relationship between $\mathbf{X}(t)$ and previous instances - $\mathbf{X}(t\text{-}1)$, $\mathbf{X}(t-2)$, and so forth. PCA can be extended to dynamic system by carrying out a matrix expansion of the original data matrix with time-shifted duplicated vectors. By appropriate selection of the number of lags l to be included - $\mathbf{X}(t-l)$, both the static and dynamic relationship between the variables can be accounted for.

$$\mathbf{X_d} = [\mathbf{X}(k)\ \mathbf{X}(k\text{-}1)\ \ldots\ldots \mathbf{X}(k\text{-}l)] \tag{2.39}$$

One of the earlier publications describing the extension of PCA to dynamic multivariate statistical monitoring was by Ku, et al. (1995) in which the theoretical basis and justification of the approach was presented. More recently Liu, et al. (2004) look at the application of DPCA to enhance chunk monitoring of an industrialized fluidized-bed reactor and explored several methods of selecting the number of lags l to be used. The additional task of identifying the number of lag terms to be used in the dynamic model is a major drawback associated with the dynamic model extension of PCA and will also apply in the case of dynamic partial least squares

(DPLS) and CVA. The selection process becomes an even more challenging task when the dynamic expansion is to be carried out on a variable-dependent basis. There is also the risk of the dynamic matrix given by Eq. (2.40) being ill-conditioned due to strong serial correlation in the measurement data.

As it relates to DPLS there are few different approaches to incorporating the time-shifted data variables. This can be applied only on the **X** block as carry out by Ricker (1988), both orthogonal decomposition and PLS decomposition was applied to the $\mathbf{X_d}$ matrix to improve the conditioning of the matrix and subsequent the estimation of regression parameters. Alternatively dynamic expansion of both the **X** and **Y** block can be carried out as done by Qin and McAvoy (1993) to reflect an autoregressive moving average (ARMA) time series mathematical model. In a later publication dynamic PLS was combined with a neural network approach to develop a non-linear finite impulse response FIR model (Qin and McAvoy, 1996). The ARMA time series model includes past values of the response (output) variables as part of the dynamic expansion of the **X** block unlike the FIR model:

$$\mathbf{X_d} = \left[\mathbf{X}(k), \quad \mathbf{X}(k-1), \cdots \quad \mathbf{X}(k-l_x), \ \mathbf{y}(k-1), \quad \mathbf{y}(k-2) \ldots, \ \mathbf{y}(k-l_y)\right] \tag{2.40}$$

where l_x is the number of lags on the input and l_y is the number of lags on the outputs. Lakshminarayanan, et al. (1997) chose to build a dynamic regression model to define the inner relation between the time-shifted scores of the X and Y blocks without expansion of the original variable block with time-shifted process variables.

The major drawback of these dynamic projection methods is the increased numerical computation involving a much larger data set with the time-shifted variable duplications added on. A limited number of the published applications have actually explored defining variable specific lags as different process variables will have different dynamics. Simoglou, et al. (1999a) applied such an approach in the development of a DPLS and CVA statistical model of a binary distillation column.

2.7 Summary

Multivariate statistical process controls is an extension of univariate SPC that has proven to be a more effective statistical approach to process monitoring because it accounts for both the variance and covariance structure in a data set. PCA and PLS are the two corner stone projection methods of MSPC from which several offshoots have emerged. These offshoots have emerged out of necessity to address issues relating to improve modelling and monitoring of dynamic, nonlinear processes, and batch processes.

In the case of dynamic processes – DPCA and DPLS have been proposed as extensions to to PCA and PLS respectively. For batch processes Multi-way and Multi-block PLS and PCA have evolved to more effectively capture the correlation structure across the batches and sub block of process variables of different types.

Finally, the literature review touched on the two most common monitoring statistics – Hotelling's T^2 square and Q statistics. The review presented on some of the equations that been proposed for computing the control limit of these statistics

Chapter 3 : Review of Subspace, Non-linear and Hybrid Modelling Techniques

3.1 Introduction

Subspace system identification is a very popular system identification method that has been around since the early eighties. The popularity is owed to the advantages that the modelling technique and algorithm offers over other methods. In particularly, they are non-iterative, and robust as they employ primarily numerically stable mathematical methods of linear algebra. They are well suited to modelling multiple-input multiple output systems providing reliable state space model alternatives to polynomial based models and models based on instrumental variable method (Borjas and Garcia, 2010).

State Space modelling is a class of subspace modelling that seeks to model, monitor and/or control the process by successive approximation of the memory or states of the process. Approximation of the states of the process may be carried out in a number of different ways: PLS, numerical algorithms for state space subspace system identification (N4SID); balanced realisation (BR) and canonical correlation regression CCR. Comparisons with CVA against these alternatives have been carried out (Juricek, et al. 2005; Negiz and Cinar, 1997b; Simoglou, et al., 1999a) and they have all concluded that CVA outperforms the other methods in terms of model stability and parsimony. Several methods used for identifying the dimension of the subspace model in terms of the number of lags, states and other modelling parameters have been applied in the literature and will be reviewed in this chapter.

One can usually assume that the process behaves fairly linear within the region of its operating conditions, however when this is not the case application of linear PCA and PLS methods may generate erroneous results and lead to misleading interpretation (Dong and McAvoy, 1996b). Several nonlinear extensions to PCA and PLS proposed in the literature will be particularly applicable to processes whose variability are characterized by significant nonlinearity. Other approaches to quantifying and effectively model nonlinear process dynamics have applied hybrid models combining mechanistic and data driven statistical models (Lee, et al. 2005; Oliveira 2004; Peres, et al. 2001; Psichogios and Ungar, 1992).

This chapter will review three subspace algorithms. Section 3.2 will review an algorithm proposed by Larimore (Larimore, 1983; Larimore, 1990) which employs the mathematics of principal angles and directions to identify a canonical correlation structure upon which the subspace model predictive capabilities are based. In section 3.3 two other algorithms are explored in less detail – MOESP proposed by Verhaegen (1994) and stands for Multiple Output Error State Space, and N4SID by Van Overschee and De Moor (1994). N4SID stands for 'numerical algorithms for subspace state space system identification'. Section 3.4 provides an overview of several model selection criterion and procedures that have been applied in the literature. Section 3.5 discusses several nonlinear extensions to linear projections and dynamic subspace methods covered in this and the previous chapter. Section 3.6 revisits several hybrid models that have been applied in the literature for prediction and process monitoring applications. Section 3.7 provides a summary overview of the modelling approaches reviewed in the chapter.

3.2 Canonical Variate Analysis and State Space Approach

Canonical Correlation Analysis (CCA) was first introduced by Hotelling sometime between 1933 and 1936 based on the accounts of Negiz and Cinar (1997b). It was later applied to linear dynamic system modelling and Markovian state space system identification by Akaike, see

(Akaike, 1974a; Akaike, 1974b; Akaike, 1975). Further theoretical analysis, improvements and generalization of Akaike's canonical correlation method was later made by Larimore (Larimore 1996; Larimore 1983; Larimore 1990). In particular, Larimore applied CCA as the statistical basis of the well know Canonical Variate Analysis subspace system identification method. One of the earliest direct application to the modelling of chemical process was published by Schaper, et al. (1994). The paper evaluated the modelling approach using a simulated chemical process that accounted for the impact of measurement and process noise, nonlinear dynamics, among other practical issues associated with such processes. It was also applied to the modelling of a pilot-scaled distillation column.

3.2.1 Canonical Variate Analysis

The main idea behind canonical variate analysis or canonical correlation analysis (as it is more generally know) is to extract the relationship between two sets of variables **X** and **Y** by finding corresponding sets of linear combinations of the original data sets (the canonical variates **U** and **V**):

$$\mathbf{U} = \mathbf{XJ}$$

$$\mathbf{V} = \mathbf{YL} \tag{3.1}$$

The choice of transformation matrix **J** and **L** is towards maximising the correlation between the canonical variates:

$$\text{Maximise } \frac{\mathbf{J}^{\mathrm{T}}\mathbf{R}_{\mathrm{xy}}\,\mathbf{L}}{\sqrt{\mathbf{J}^{\mathrm{T}}\mathbf{R}_{\mathrm{xx}}\,\mathbf{J}}\sqrt{\mathbf{L}^{\mathrm{T}}\mathbf{R}_{\mathrm{yy}}\,\mathbf{L}}} \tag{3.2}$$

where $\mathbf{R}_{\mathrm{xx}} = E(\mathbf{X}^{\mathrm{T}}\mathbf{X})$, $\mathbf{R}_{\mathrm{yy}} = E(\mathbf{Y}^{\mathrm{T}}\mathbf{Y})$, and $\mathbf{R}_{\mathrm{xy}} = E(\mathbf{X}^{\mathrm{T}}\mathbf{Y})$.

The objective specified by Eq. (3.2) is equivalent to solving the following constrained optimization problem:

$$\emptyset = \mathbf{J}^{\mathrm{T}}\mathbf{R}_{\mathrm{xy}}\mathbf{L} + \lambda_{\mathrm{x}}(\mathbf{I}_{\mathrm{x}} - \mathbf{J}^{\mathrm{T}}\mathbf{R}_{\mathrm{xx}}\mathbf{J}) + \lambda_{\mathrm{y}}\left(\mathbf{I}_{\mathrm{y}} - \mathbf{L}^{\mathrm{T}}\mathbf{R}_{\mathrm{yy}}\mathbf{L}\right) \tag{3.3}$$

where $\mathbf{I}_x$ and $\mathbf{I}_y$ are identity matrices of appropriate dimensions and λ_x and λ_y are the Lagrange constants. The solution to Eq (3.3) commences with differentiating the function with respect to **J** and **L** and solving the resulting pair of simultaneous equation below:

$$d\emptyset/d\mathbf{J} = \mathbf{L}^{\mathrm{T}}\mathbf{R}_{\mathrm{yx}} - \mathbf{2}\lambda_{\mathrm{x}}\mathbf{J}^{\mathrm{T}}\mathbf{R}_{\mathrm{xx}} = 0 \tag{3.4}$$

$$d\emptyset/d\mathbf{L} = \mathbf{J}^{\mathrm{T}}\mathbf{R}_{\mathrm{xy}}\mathbf{L} - \lambda_{\mathrm{y}}\mathbf{L}^{\mathrm{T}}\mathbf{R}_{\mathrm{yy}} = 0 \tag{3.5}$$

The solution is given by:

$$SVD\left(\mathbf{R}_{\mathrm{xx}}^{-1/2}\mathbf{R}_{\mathrm{xy}}\mathbf{R}_{\mathrm{yy}}^{-1/2}\right) = \hat{\mathbf{J}}\mathbf{S}\hat{\mathbf{L}}^{\mathrm{T}} \tag{3.6}$$

$$\mathbf{J} = \mathbf{R}_{\mathrm{xx}}^{-1/2}\hat{\mathbf{J}};\ \mathbf{L} = \mathbf{R}_{\mathrm{yy}}^{-1/2}\hat{\mathbf{L}} \tag{3.7}$$

The main diagonal of the **S** matrix contains the correlation coefficients. The combined operation of Eq. (3.6) and Eq. (3.7) is referred to as the generalized singular value decomposition (GSVD) of $\mathbf{R}_{\mathrm{xy}}$.

CVA is conceptually similar to DPLS, in that both method seek to extract a subspace representation of the correlation between two blocks of data set. A comparison of Balanced, PLS, CV state space realization by Negiz and Cinar (1997b) revealed that the three approaches were all capable of identifying a minimal state order model but concluded that the CV state space realization offered a much more robust tool for system identification in state space than PLS and the balanced realization methods. The main advantage offered by CVA realization is that it generates states that are orthogonal at zero lag and requires a one-step SVD algorithm to arrive at the states. The classical PLS algorithm, however, requires an additional SVD step in order for the

PLS states to be orthogonal (Negiz and Cinar, 1997b). The diagonal state covariance matrix offered by CVA is preferred over PLS and balanced realization methods as it provideds a better conditioned covarance matrix to facilitate the extraction of the state matrices via least squares estimation, as will be demonstrated in subsequent subsections.

3.2.2 State Space Modelling

The first application of the canonical correlation analysis method to stochastic realization theory was done by Akaike (Akaike, 1975; Akaike, 1976). The state space model proposed back then had a number of limitations due to its simplicity, it had no system inputs, no additive measurement noise, and was computationally intensive involving numerous single value decomposition (SVDs). Other researchers have made improvements to Akaike's state space approach and his canonical correlation method such as (Larimore, 1983; Larimore, 1990). The improvements included generalisation to system with additive noise and the inclusion of inputs in the state space model for feedback control. A summary of the different state space models that have been proposed in the various literatures are as follows:

i) State Space (Innovation) model, no exogenous inputs, has correlated noise term, state space representation employed when representing the process as an autoregressive moving average ARMA model (Negiz and Cinar, 1997b):

$$\mathbf{x}_{t+1} = \boldsymbol{A}\mathbf{x}_t + \boldsymbol{B}\mathbf{w}_t$$
$$\mathbf{y}_t = \boldsymbol{C}\mathbf{x}_t + \mathbf{w_t} \tag{3.8}$$

ii) State Space Models with exogenous inputs, noise term maybe correlated or not (Borjas and Garcia, 2010; Van Overschee and De Moor, 1994):

$$\mathbf{x}_{t+1} = \boldsymbol{A}\mathbf{x}_t + \boldsymbol{B}\mathbf{u}_t + \mathbf{w}_t$$
$$\mathbf{y}_t = \boldsymbol{C}\mathbf{x}_t + \boldsymbol{D}\mathbf{u}_t + \mathbf{v}_t \tag{3.9}$$

$$\mathbf{x}_{t+1} = \boldsymbol{A}\mathbf{x}_t + \boldsymbol{B}\mathbf{u}_t + \mathbf{K}\mathbf{v}_t$$
$$\mathbf{y}_t = \boldsymbol{C}\mathbf{x}_t + \boldsymbol{D}\mathbf{u}_t + \mathbf{v}_t \tag{3.10}$$

iii) State Space Models with exogenous inputs and correlate and uncorrelated noise terms

$$\mathbf{x}_{t+1} = \boldsymbol{A}\mathbf{x}_t + \boldsymbol{B}\mathbf{u}_t + \mathbf{w}_t$$
$$\mathbf{y}_t = \boldsymbol{C}\mathbf{x}_t + \boldsymbol{D}\mathbf{u}_t + \boldsymbol{K}\mathbf{w}_t + \mathbf{v}_t$$

(3.11)

iv) An Iterative Bilinear CVA State Space Model was proposed by (Lakshminarayanan, et al. 2001):

$$\mathbf{x}_{t+1} = \boldsymbol{A}\mathbf{x}_t + \boldsymbol{B}\mathbf{u}_t + \mathbf{N}(\mathbf{x}_t \otimes \mathbf{u}_t) + \mathbf{w}_t$$
$$\mathbf{y}_{\boldsymbol{t}} = \boldsymbol{C}\mathbf{x}_{\boldsymbol{t}} + \boldsymbol{D}\mathbf{u}_{\boldsymbol{t}} + \boldsymbol{K}\mathbf{w}_{\boldsymbol{t}} + \mathbf{v}_{\boldsymbol{t}}$$

(3.12)

Eq. (3.11) accounts for the correlation between the residuals of the state and output equations by inclusion of the **K** matrix. This facilitates the development of a more parsimonious state space model for a given process. The resulting state space model can be completely defined using less state variables than that of Eq. (3.9) which only retains the uncorrelated noise terms (Larimore, 1990).

For the purpose of monitoring defining state space models with an exogenous input term is not particularly necessary. It will be demonstrated later in the work on an independent state space CVA approach how exploiting such may provide an alternative development approach that is more computationally efficient and gives good results in terms of its fault detection capabilities.

3.2.3 State Vector Derivation

The approximation of the states of the process using canonical variate analysis was proposed by Larimore (1983) in which he introduced the concept of defining the past and future vector of the process. At some reference time instance *t* we define a vector of past inputs containing both time delayed past input and output samples as:

$$\boldsymbol{P}_t^T = \left[\boldsymbol{y}_{t-1}^T, \boldsymbol{y}_{t-2}^T, \ldots.\boldsymbol{y}_{t-l_y}^T, \boldsymbol{u}_{t-1}^T, \boldsymbol{u}_{t-2}^T, \ldots.\boldsymbol{u}_{t-l_u}^T\right]^T$$

(3.13)

If we seek to develop the state space model reflecting of the ARMA model representation of Eq. (3.10) then the past vector representation would be given by:

$$\boldsymbol{P}_t^T = \left[\boldsymbol{y}_{t-1}^T, \boldsymbol{y}_{t-2}^T, \dots . \boldsymbol{y}_{t-l_y}^T\right]^T \tag{3.14}$$

and the vector containing the output information in the future as

$$\boldsymbol{F}_t^T = \left[\boldsymbol{y}_t^T, \boldsymbol{y}_{t+1}^T, \dots . \boldsymbol{y}_{t+f}^T\right]^T \tag{3.15}$$

where $l_{y,}$ and l_u are the window length of the dynamic lag elements of the input and output samples. The length of future observation window is given by f. To the author's best knowledge, in the majority of the publications the window length for all the process variables comprising the input or output matrix were all set to the same number of time shifts, see (Negiz and Cinar, 1997a; Schaper, et al., 1994; Russell, et al., 2000). Simoglou, et al. (2002) speculated that the use of this common lag order for all the inputs and outputs in the past vector construction may impose some limitations with the use of the method as different variables may exhibit different dynamics and should therefore be included with a different number of lagged values in the past vector. This has the potential of reducing the model complexity and optimising on the information content that is retained by the past vector. In Simoglou, et al. (1999b), CVA and PLS were analysed and compared in terms of their system identification capabilities, the lag order of the past vectors were made to be different for the different variables. Some simulations were carried out in this study to see if there were any benefits to be gained from using process variable specific lag orders instead of a common window length, the results thus far are inconclusive.

Irrespective of the realization being pursued (PLS, Balanced, or Canonical), defining the truncated form of the infinite Hankel matrix from the future and past stacked measurements, will be relevant to the derivation of the state space model.

The Hankel matrix is defined as follows:

$$\mathbf{H} = E\{\mathbf{P}^T\mathbf{F}\} = \mathbf{E}\left\{\begin{bmatrix}\mathbf{y}_{t-1}^T\\ \mathbf{y}_{t-2}^T\\ \vdots\\ \mathbf{y}_{t-l_y}^T\end{bmatrix}\begin{bmatrix}\mathbf{y}_t^T & \mathbf{y}_{t+1}^T & \cdots & \mathbf{y}_{t+f}^T\end{bmatrix}^{\mathrm{T}}\right\}$$

$$= \begin{bmatrix}\Lambda_1 & \Lambda_2 & \cdots & \Lambda_f\\ \Lambda_2 & & & \Lambda_{f+1}\\ \vdots & & & \vdots\\ \Lambda_{l_y} & \Lambda_{l_y+1} & \cdots & \Lambda_{f+l_y}\end{bmatrix} \tag{3.16}$$

where for a stationary process $\Lambda_k = \mathbf{y}_t^T\mathbf{y}_{t+k}^T = \mathbf{y}_{t-k}^T\mathbf{y}_t^T$.

The canonical variate realization is given by

$$\mathbf{x}_t = \mathbf{J}\mathbf{P}_t^T \tag{3.17}$$

In Eq. (3.17) the states computed for any given time instance *t* are arranged as a column vector. **J** is the transformation matrix obtained from the SVD of the scaled Hankel matrix:

$$(\mathbf{P}^T\mathbf{P})^{-1/2}\mathbf{H}(\mathbf{F}^T\mathbf{F})^{-1/2} = \mathbf{U\Sigma V}^T \tag{3.18}$$

$$\mathbf{J} = (\mathbf{P}^T\mathbf{P})^{-1/2}\mathbf{U} \tag{3.19}$$

The choice of **J** will result in the states having identity covariance matrix. For the balance realization approach the covariance matrix of the state would be based on the correlation matrix of the past and future vector **Σ**, the definition of **J** would be given by:

$$\mathbf{J} = (\mathbf{P}^T\mathbf{P})^{-1/2}\mathbf{U}\mathbf{\Sigma}^{\mathbf{1/2}} \tag{3.20}$$

The conditional state covariance matrix for the balance realization is not diagonal. Also, it is possible that the state covariance matrix may be singular depending upon condition of the covariance matrix of the past observation matrix **P** (Negiz and Cinar, 1997b).

3.2.4 Stochastic estimation of the state space matrices

Once the state variables for the model have been determined the next step is to estimate the state-matrices of the model. A stochastic estimation of the state-space matrices was first proposed by Larimore (1983) for the model given by Eq. (3.8):

$$\mathbf{x}_{t+1} = \boldsymbol{A}\mathbf{x}_t + \boldsymbol{B}\mathbf{w}_t$$
$$\mathbf{y}_t = \boldsymbol{C}\mathbf{x}_t + \mathbf{w}_\mathrm{t}$$

By computing the state vector sequence and applying multiple least square, the **A**, **B** and **C** matrix of the innovation model was determined. By multiplying the state equations by $\mathbf{x}_\mathrm{t}^\mathrm{T}$ and noting the fact that the residue $\mathbf{e}_\mathrm{t}$ and state vector $\mathbf{x}_\mathrm{t}^\mathrm{T}$ are orthogonal and therefore uncorrelated to each other, we obtain:

$$E\{\mathbf{x}_{\mathrm{t}+1}\mathbf{x}_\mathrm{t}^\mathrm{T}\} = \boldsymbol{A}E\{\mathbf{x}_\mathrm{t}\mathbf{x}_\mathrm{t}^\mathrm{T}\}$$
$$E\{\mathbf{y}_\mathrm{t}\mathbf{x}_\mathrm{t}^\mathrm{T}\} = \boldsymbol{C}E\{\mathbf{x}_\mathrm{t}\mathbf{x}_\mathrm{t}^\mathrm{T}\}$$

(3.21)

Therefore:

$$\begin{bmatrix}\widehat{\mathbf{A}}\\ \widehat{\mathbf{C}}\end{bmatrix} = E\left\{\begin{bmatrix}\mathbf{x}_{\mathrm{t}+1}\\ \mathbf{y}_\mathrm{t}\end{bmatrix}\mathbf{x}_\mathrm{t}^\mathrm{T}\right\}E\{\mathbf{x}_\mathrm{t}\mathbf{x}_\mathrm{t}^\mathrm{T}\}^{-1}$$

(3.22)

The prediction errors for the state and output variables can now be computed using the estimates of **A** and **C**:

$$\widehat{\boldsymbol{x}}_{t+1} = \mathbf{x}_{\mathrm{t}+1} - \widehat{\mathbf{A}}\mathbf{x}_\mathrm{t}$$

$$\widehat{\boldsymbol{y}}_t = \mathbf{w}_t = \mathbf{y}_t - \widehat{\mathbf{C}}\mathbf{x}_\mathrm{t}$$

(3.23)

Multiplying through by the transpose of the state and output residuals we obtain:

$$E\left\{\begin{bmatrix}\widehat{\mathbf{x}}_{t+1}\\ \widehat{\mathbf{y}}_t\end{bmatrix}\begin{bmatrix}\widehat{\mathbf{x}}_{t+1}^T & \widehat{\mathbf{y}}_t^T\end{bmatrix}\right\} = \begin{bmatrix}\widehat{\mathbf{x}}_{t+1}\widehat{\mathbf{x}}_{t+1}^T & \widehat{\mathbf{x}}_{t+1}\widehat{\mathbf{y}}_t^T\\ \widehat{\mathbf{y}}_t\widehat{\mathbf{x}}_{t+1}^T & \widehat{\mathbf{y}}_t\widehat{\mathbf{y}}_t^T\end{bmatrix} = \begin{bmatrix}\widehat{\mathbf{B}}\boldsymbol{\Phi}\widehat{\mathbf{B}}^T & \widehat{\mathbf{B}}\boldsymbol{\Phi}\\ \boldsymbol{\Phi}\widehat{\mathbf{B}}^T & \boldsymbol{\Phi}\end{bmatrix} = \begin{bmatrix}S_{11} & S_{12}\\ S_{21} & S_{22}\end{bmatrix}$$

(3.24)

where **Φ** is the covariance matrix of the output noise component e_t.

By comparing sub-matrix terms:

$$\boldsymbol{\Phi} = \mathbf{S}_{11} = \hat{\mathbf{y}}_t\hat{\mathbf{y}}_t^T \tag{3.25}$$

$$\widehat{\mathbf{B}} = \mathbf{S}_{12}\mathbf{S}_{22}^{-1} \tag{3.26}$$

For the state space model representation employed by Larimore (1997), the procedure is fundamentally the same but more involved computationally due to the added complexity of the model:

$$\boldsymbol{x}_{t+1} = \boldsymbol{A}\boldsymbol{x}_t + \boldsymbol{B}\boldsymbol{u}_t + \boldsymbol{w}_t$$
$$\mathbf{y}_t = \boldsymbol{C}\mathbf{x}_t + \boldsymbol{D}\mathbf{u}_t + \boldsymbol{K}\mathbf{w}_t + \mathbf{v}_t$$

This time the state equations are both multiplied through by the transpose of the state and input vectors:

$$E\left\{\begin{bmatrix}\mathbf{x}_{t+1}\\ \mathbf{y}_t\end{bmatrix}\begin{bmatrix}\mathbf{x}_t^{\mathrm{T}} & \mathbf{u}_t^{\mathrm{T}}\end{bmatrix}\right\} = \begin{bmatrix}\widehat{\mathbf{A}} & \widehat{\mathbf{B}}\\ \widehat{\mathbf{C}} & \widehat{\mathbf{D}}\end{bmatrix} E\left\{\begin{bmatrix}\mathbf{x}_t\\ \mathbf{u}_t\end{bmatrix}\begin{bmatrix}\mathbf{x}_t^{\mathrm{T}} & \mathbf{u}_t^{\mathrm{T}}\end{bmatrix}\right\} \tag{3.27}$$

Again we note that the noise components are assumed to be uncorrelated with the inputs and so the matrices can be derived as follows:

$$\begin{bmatrix}\widehat{\mathbf{A}} & \widehat{\mathbf{B}}\\ \widehat{\mathbf{C}} & \widehat{\mathbf{D}}\end{bmatrix} = E\left\{\begin{bmatrix}\mathbf{x}_t\\ \mathbf{u}_t\end{bmatrix}\begin{bmatrix}\mathbf{x}_t^{\mathrm{T}} & \mathbf{u}_t^{\mathrm{T}}\end{bmatrix}\right\} E\left\{\begin{bmatrix}\mathbf{x}_{t+1}\\ \mathbf{y}_t\end{bmatrix}\begin{bmatrix}\mathbf{x}_t^{\mathrm{T}} & \mathbf{u}_t^{\mathrm{T}}\end{bmatrix}\right\}^{-1} \tag{3.28}$$

The second step as before uses the residuals to determine the **G** matrix and extract the noise covariance matrices as follows:

$$\hat{\mathbf{x}}_{t+1} = \mathbf{x}_{t+1} - \left(\widehat{\mathbf{A}}\mathbf{x}_t + \widehat{\mathbf{B}}\mathbf{u}_t\right) = \mathbf{v}_t$$
$$\hat{\mathbf{y}}_t = \mathbf{y}_t - \left(\widehat{\mathbf{C}}\mathbf{x}_t + \widehat{\mathbf{D}}\mathbf{u}_t\right) = \mathbf{K}\mathbf{v}_t + \mathbf{w}_t \tag{3.29}$$

$$E\left\{\begin{bmatrix}\hat{\mathbf{x}}_{t+1}\\ \hat{\mathbf{y}}_t\end{bmatrix}\begin{bmatrix}\hat{\mathbf{x}}_{t+1}^T & \hat{\mathbf{y}}_t^T\end{bmatrix}\right\} = \begin{bmatrix}\hat{\mathbf{x}}_{t+1}\hat{\mathbf{x}}_{t+1}^T & \hat{\mathbf{x}}_{t+1}\hat{\mathbf{y}}_t^T\\ \hat{\mathbf{y}}_t\hat{\mathbf{x}}_{t+1}^T & \hat{\mathbf{y}}_t\hat{\mathbf{y}}_t^T\end{bmatrix} = \begin{bmatrix}\mathbf{\Pi} & \hat{\mathbf{K}}\mathbf{\Pi}\\ \mathbf{\Pi}\hat{\mathbf{K}}^T & (\hat{\mathbf{K}}\mathbf{\Pi}\hat{\mathbf{K}}^T + \mathbf{\Phi})\end{bmatrix} = \begin{bmatrix}S_{11} & S_{12}\\ S_{21} & S_{22}\end{bmatrix} \quad (3.30)$$

whereas before **Φ** is the covariance matrix of the uncorrelated output noise component $\boldsymbol{w}_t$ *and* **Π** is the covariance matrix of the state noise $\mathbf{v}_t$:

$$\mathbf{\Pi} = \mathbf{S}_{11} = \hat{\mathbf{x}}_{t+1}\hat{\mathbf{x}}_{t+1}^T = \mathbf{v}_t^{\mathrm{T}}\mathbf{v}_t \quad (3.31)$$

$$\hat{\mathbf{K}}\mathbf{S}_{11} = \mathbf{S}_{\mathbf{12}}; \quad \hat{\mathbf{K}} = \mathbf{S}_{12}\mathbf{S}_{11}^{-1} \quad (3.32)$$

$$\hat{\mathbf{K}}\mathbf{S}_{11}\hat{\mathbf{K}}^T + \mathbf{\Phi} = \mathbf{S}_{22}; \quad \mathbf{\Phi} = \mathbf{S}_{22} - \hat{\mathbf{K}}\mathbf{S}_{11}\hat{\mathbf{K}}^T;$$

$$\mathbf{\Phi} = \mathbf{S}_{22} - \mathbf{S}_{12}(\mathbf{S}_{12}\mathbf{S}_{11}^{-1})^{\mathbf{T}} \quad (3.33)$$

The covariance of the total noise process $\mathbf{Kv}_{\mathrm{t}} + \mathbf{w}_{\mathrm{t}}$ is therefore given by:

$$\Delta = \hat{\mathbf{K}}\mathbf{\Pi}\hat{\mathbf{K}}^T + \mathbf{\Phi} \quad (3.34)$$

3.3 N4SID and MOESP

Besides the subspace method of CVA, the method of Numerical Algorithms for Subspace State Space system identification (N4SID) and Multivariable Output-Error State Space (MOESP) modelling are the among the most common used subspace algorithms (Borjas and Garcia 2010). Similar to CVA, both algorithms derive the state sequences directly from input/output observations without knowledge of the model. N4SID and MOESP apply either orthogonal or oblique projection of input and output data using linear algebra tools (QR and SVD) to arrive at the Kalman filter states. Both N4SID and MOESP derive the actual system matrices **A,B,C,D**, and **K** from the observability matrix while the CVA matrix employs the canonical variate estimates of the states and least square regression to obtain the system matrices. Figure 3.1 outline the differences in subspace algorithm derivation and parameterization procedure. The derivation paths employed by the three algorithms are indicated below the figure.

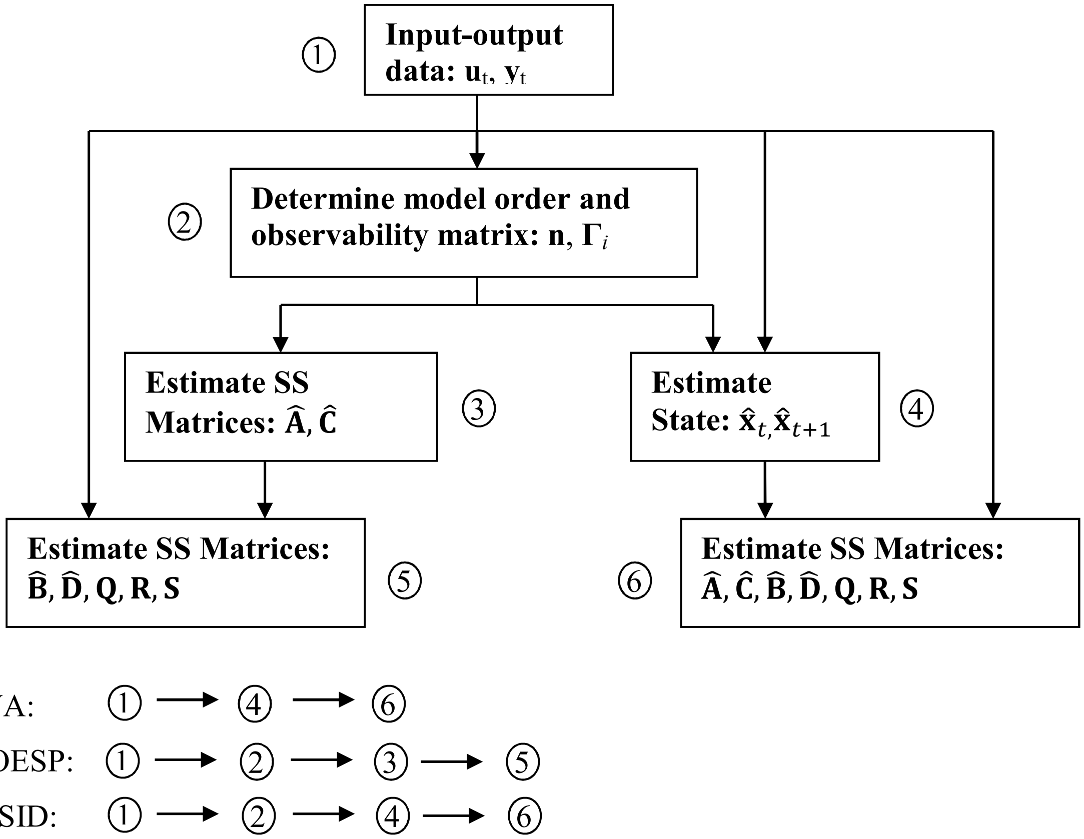
①
Input-output data: $\mathbf{u}_t$, $\mathbf{y}_t$
②
Determine model order and observability matrix: n, $\boldsymbol{\Gamma}_i$
Estimate SS Matrices: $\hat{\mathbf{A}}, \hat{\mathbf{C}}$
③
Estimate State: $\hat{\mathbf{x}}_{t,}\hat{\mathbf{x}}_{t+1}$
④
Estimate SS Matrices: $\hat{\mathbf{B}}, \hat{\mathbf{D}}, \mathbf{Q}, \mathbf{R}, \mathbf{S}$
⑤
⑥
Estimate SS Matrices: $\hat{\mathbf{A}}, \hat{\mathbf{C}}, \hat{\mathbf{B}}, \hat{\mathbf{D}}, \mathbf{Q}, \mathbf{R}, \mathbf{S}$
CVA: ① ⟶ ④ ⟶ ⑥
MOESP: ① ⟶ ② ⟶ ③ ⟶ ⑤
N4SID: ① ⟶ ② ⟶ ④ ⟶ ⑥

Figure 3.1 Comparing the subspace development algorithm stage of N4SID, MOESP, and CVA

Repeated iterations of the output equation of Eq. (3.10) generates:

$$\boldsymbol{Y}_f = \boldsymbol{\Gamma}_i \mathbf{X}_f + \mathbf{H}_i^d \mathbf{U}_f + \mathbf{H}_i^s \mathbf{V}_f \tag{3.35}$$

where the subscript *f* represents the future, the superscript *d* makes reference to the deterministic component of the system while *s* refers to the stochastic components of the system.

The extended observability matrix $\boldsymbol{\Gamma}_i$ is given by:

$$\boldsymbol{\Gamma}_i = \begin{bmatrix} \mathbf{C} \\ \mathbf{CA} \\ \cdots \\ \mathbf{CA}^{i-1} \end{bmatrix} \tag{3.36}$$

$\mathbf{H}_i^d$ is a lower block triangular Toeplitz matrix given by:

$$\mathbf{H}_i^d = \begin{bmatrix} \mathbf{D} & 0 & 0 & \dots & 0 \\ \mathbf{CB} & \mathbf{D} & 0 & \dots & 0 \\ \mathbf{CAB} & \mathbf{CB} & \mathbf{D} & \cdots & 0 \\ \dots & \dots & \dots & \dots & \dots \\ \mathbf{CA}^{\mathrm{i-2}}\mathbf{B} & \mathbf{CA}^{\mathrm{i-3}}\mathbf{B} & \dots & \mathbf{CB} & \mathrm{D} \end{bmatrix} \tag{3.37}$$

While the covariance matrix $\mathbf{H}_i^s$ is given by:

$$\mathbf{H}_i^d = \begin{bmatrix} \mathbf{\Lambda}_i & \mathbf{\Lambda}_{i-1} & \mathbf{\Lambda}_{i-2} & \dots & \mathbf{\Lambda}_1 \\ \mathbf{\Lambda}_{i+1} & \mathbf{\Lambda}_i & \mathbf{\Lambda}_{i-1} & \dots & \mathbf{\Lambda}_2 \\ \mathbf{\Lambda}_{i+2} & \mathbf{\Lambda}_{i+1} & \mathbf{\Lambda}_i & \cdots & \mathbf{\Lambda}_3 \\ \dots & \dots & \dots & \cdots & \dots \\ \mathbf{\Lambda}_{2i-1} & \mathbf{\Lambda}_{2i-2} & \dots & \mathbf{\Lambda}_{i+1} & \mathbf{\Lambda}_i \end{bmatrix} = \mathbf{\Gamma}_i \mathbf{\Delta}_i^s \text{ and } \mathbf{\Lambda}_i = \begin{cases} \mathbf{CA}^{\mathrm{i-1}}\mathbf{G} & i > 0 \\ \mathbf{\Lambda}_i & i = 0 \\ \left[\mathbf{CA}^{\mathrm{i-1}}\mathbf{G}\right]^{\mathrm{T}} & i < 0 \end{cases} \tag{3.38}$$

The **G** matrix is a cross-covariance matrix defined as:

$$G = E\{\mathbf{x}_k \mathbf{y}_k^{\mathbf{T}}\}. \tag{3.39}$$

The past and future input and output block-Hankel matrices are defined as:

$$\mathbf{U}_p = \begin{bmatrix} \mathrm{u}_0 & \mathrm{u}_1 & \mathrm{u}_2 & \cdots & \mathrm{u}_{j-1} \\ \mathrm{u}_1 & \mathrm{u}_2 & \mathrm{u}_3 & \cdots & \mathrm{u}_j \\ \vdots & \vdots & \vdots & \cdots & \vdots \\ \mathrm{u}_{i-2} & \cdots & \cdots & \cdots & \mathrm{u}_{i+j-3} \\ \mathrm{u}_{i-1} & \mathrm{u}_i & \mathrm{u}_{i+1} & \cdots & \mathrm{u}_{i+j-2} \end{bmatrix} \quad \mathbf{U}_f = \begin{bmatrix} \mathrm{u}_i & \mathrm{u}_{i+1} & \mathrm{u}_2 & \cdots & \mathrm{u}_{i+j-1} \\ \mathrm{u}_{i+1} & \mathrm{u}_{i+2} & \mathrm{u}_{i+3} & \cdots & \mathrm{u}_{i+j} \\ \vdots & \vdots & \vdots & \cdots & \vdots \\ \mathrm{u}_{2i-2} & \cdots & \cdots & \cdots & \mathrm{u}_{2i+j-3} \\ \mathrm{u}_{2i-1} & \mathrm{u}_{2i} & \mathrm{u}_{2i+1} & \cdots & \mathrm{u}_{2i+j-2} \end{bmatrix} \tag{3.40}$$

where $u_k \in \mathbb{R}^m$ is the input vector observation at the *k*th time instance. The output $\mathbf{Y}_p$, $\mathbf{Y}_f$, and noise $\mathbf{V}_p$, $\mathbf{V}_f$ Block-Hankel are all similarly constructed.

The MOESP solves the subspace problem by first deriving an approximation of the extended observability matrix $\mathbf{\Gamma}_i$. This is achieved by eliminating the last two terms in the right side of Eq. (3.35) and is carried out in two steps:

i) An orthogonal projection of Eq. (3.35) is performed into the row space of $\boldsymbol{U}_f^{\perp}$ and yields:

$$\boldsymbol{Y}_f/\boldsymbol{U}_f^{\perp} = \mathbf{\Gamma}_i\mathbf{X}_f/\boldsymbol{U}_f^{\perp} + \mathbf{H}_i^d\mathbf{U}_f/\boldsymbol{U}_f^{\perp} + \mathbf{H}_i^s\mathbf{V}_f/\boldsymbol{U}_f^{\perp} \tag{3.41}$$

Applying one of the properties of orthogonal projection ($\mathbf{U}_f/\boldsymbol{U}_f^{\perp} = 0$), Eq. (3.41) can be simplified to:

$$\boldsymbol{Y}_f/\boldsymbol{U}_f^{\perp} = \mathbf{\Gamma}_i\mathbf{X}_f/\boldsymbol{U}_f^{\perp} + \mathbf{H}_i^s\mathbf{V}_f/\boldsymbol{U}_f^{\perp} \tag{3.42}$$

ii) To eliminate the noises term in Eq. (3.42), the equation is multiplied by an instrumental variable $Z = \left(\mathbf{U}_p^T\mathbf{Y}_p\right)^T$ and this yields:

$$\boldsymbol{Y}_f/\boldsymbol{U}_f^{\perp}\boldsymbol{Z} = \mathbf{\Gamma}_i\mathbf{X}_f/\boldsymbol{U}_f^{\perp}\boldsymbol{Z} + \mathbf{H}_i^s\mathbf{V}_f/\boldsymbol{U}_f^{\perp}\boldsymbol{Z} \tag{3.43}$$

Since it is assumed that the noise is uncorrelated with the input and output past data then that would mean $\mathbf{V}_f/\boldsymbol{U}_f^{\perp}\boldsymbol{Z} \;\; = \mathbf{0}$ and therefore Eq. (3.43) is further simplified to:

$$\boldsymbol{Y}_f/\boldsymbol{U}_f^{\perp}\boldsymbol{Z} = \mathbf{\Gamma}_i\mathbf{X}_f/\boldsymbol{U}_f^{\perp}\boldsymbol{Z} \tag{3.44}$$

From Eq. (3.44) the estimates of the Kalman filter state is given by $\widehat{\mathbf{X}}_f = \mathbf{X}_f/\boldsymbol{U}_f^{\perp}\boldsymbol{Z}$ and the column space of $\mathbf{\Gamma}_i$ can be calculated from the SVD of $\boldsymbol{Y}_f/\boldsymbol{U}_f^{\perp}\boldsymbol{Z}$**.**

N4SID arrives at an alternative subspace model solution to the problem by means of an approximation of the past and future Kalman filter state sequence. First an oblique projection of Eq (3.35) is carried out along the row space of $\mathbf{U}_{\mathrm{f}}$ onto the row space of **Z:**

$$\boldsymbol{Y}_f/_{U_f}\boldsymbol{Z} = \boldsymbol{\Gamma}_i\mathbf{X}_f/_{U_f}\boldsymbol{Z} + \mathbf{H}_i^d\mathbf{U}_f/_{U_f}\boldsymbol{Z} + \mathbf{H}_i^s\mathbf{V}_f/_{U_f}\boldsymbol{Z} \tag{3.45}$$

The last two terms of the Eq. (3.45) are zero by the property of oblique projection and based upon the assumption that the noise is uncorrelated with input and output past data. Based upon theorem in Overschee and Moor (1996), Eq. (3.45) can be written as:

$$\boldsymbol{\Xi}_i = \boldsymbol{\Gamma}_i\widehat{\mathbf{X}}_i \tag{3.46}$$

where $\widehat{\mathbf{X}}_i = \mathbf{X}_f/_{U_f}\boldsymbol{Z}$ and $\boldsymbol{\Xi}_i = \boldsymbol{Y}_f/_{U_f}\boldsymbol{Z}$**.**

It was shown in Overschee and Moor (1996) that **t**he column space and of $\boldsymbol{\Gamma}_i$ can be calculated from the SVD of $\boldsymbol{\Xi}_i$**:**

$$\boldsymbol{\Gamma}_i = U_1S_1^{1/2} \tag{3.47}$$

With $\boldsymbol{\Gamma}_i$ and $\boldsymbol{\Xi}_i$ known the state sequence $\widehat{\mathbf{X}}_i$ can be computed easily by applying Eq. (3.46) and the next state can also be calculated as:

$$\widehat{\mathbf{X}}_{i+1} = \boldsymbol{\Gamma}_{i-1}^{-1}\boldsymbol{\Xi}_{i+1} \tag{3.48}$$

where $\boldsymbol{\Xi}_{i+1} = \boldsymbol{Y}_f^-/_{U_f^-}\boldsymbol{Z}_p^+$ and $\boldsymbol{\Gamma}_{i-1}$ denotes the matrix $\boldsymbol{\Gamma}_i$ without the last l rows.

Several other subspace algorithms have been proposed in the literature for identification of combine deterministic-stochastic systems. The subspace algorithm proposed by Viberg, et al. (1993) in an instrumental variable framework was shown to be an equivalent to N4SID algorithms in terms of how the model order and observability matrix $\boldsymbol{\Gamma}_i$ are determined (Overschee and Moor, 1995). More recently Borjas and Garcia (2010) proposed an hybrid algorithm merging the N4SID method with the MOESP approach. The algorithm employs the MOESP method to extract the obervability matrix and then use the N4SID method to calculate the matrices A,B,C,D through least squares regression.

An interpretation of Larimore's CVA subspace method in an effort to summarize the similarities and difference that exist between the method versus MOESP and N4SID subspace identification methods is presented in Overschee and Moor (1995). Reference was made to the analysis and description of the CVA method Larimore provided (Larimore, 1990). In order to compare the method with the N4SID and MOESP approach it was necessary to establish the parallels between the notations employed by Larimore and those used previously in describing the N4SID and MOESP method, the definition are as follows:

i) the past inputs and outputs matrix

$$\boldsymbol{p} \overset{\text{def}}{=} \begin{pmatrix} \boldsymbol{U}_p \\ \boldsymbol{Y}_p \end{pmatrix} \tag{3.49}$$

ii) the future outputs

$$\boldsymbol{f} \overset{\text{def}}{=} \boldsymbol{Y}_f \tag{3.50}$$

iii) and the future inputs (not included in the analysis in Section 3.2)

$$\boldsymbol{u} \overset{\text{def}}{=} \boldsymbol{U}_f \tag{3.51}$$

In relation to the analysis presented in Section 3.2 the notations $\boldsymbol{p}$ and $\boldsymbol{f}$ are equivalent to **P** and **F** respectively.

The primary goal of a system identification model can be categorized as given in Overschee and Moor (1995):

i) *Optimal prediction*. To arrive at a model that will sufficiently accurately predict the behaviour of the process variables. For the linear subspace system identification case this may be formulated mathematically as finding the optimal linear combination of the past input-outputs $\boldsymbol{p}$ and future inputs $\boldsymbol{u}$ to predict the future state of the outputs $\boldsymbol{f}$:

$$\boldsymbol{min}_{\boldsymbol{L_p},\boldsymbol{L_u}} \left\| \boldsymbol{f} - (\boldsymbol{L}_p \quad \boldsymbol{L}_u) \begin{pmatrix} \boldsymbol{p} \\ \boldsymbol{u} \end{pmatrix} \right\|_F^{\mathbf{2}} \tag{3.52}$$

where $\boldsymbol{L}_p \in \mathbb{R}^{\boldsymbol{li} \times (\boldsymbol{m}+\boldsymbol{l})\boldsymbol{i}}$e and $\boldsymbol{L}_u \in \mathbb{R}^{\boldsymbol{li} \times \boldsymbol{mi}}$

The optimal combination of the past input/outputs $\boldsymbol{p}$ to predict the future $\boldsymbol{f}$ can be geometrically interpreted as the oblique projection of the row space of $\boldsymbol{f}$ along the row space of $\boldsymbol{p}$:

$$\boldsymbol{\Theta} \overset{\text{def}}{=} \boldsymbol{L}_p \boldsymbol{p} \tag{3.53}$$

ii) *Complexity reduction*. A second goal is that for a given model accuracy, the complexity of the model should be limited to its minimal dimension. This second requirement can be mathematically formulated as:

$$\boldsymbol{min}_{\boldsymbol{\mathcal{R}}} \|\boldsymbol{W}_1(\boldsymbol{\Theta} - \boldsymbol{\mathcal{R}})\boldsymbol{W}_2\|_F^{\mathbf{2}} \tag{3.54}$$

where $\boldsymbol{\mathcal{R}} \in \mathbb{R}^{li\,\mathbf{x}\,j}$, $\mathbf{W}_1 \in \mathbb{R}^{li\,\mathbf{x}\,li}$ and $\mathbf{W}_2 \in \mathbb{R}^{j\,\mathbf{x}\,j}$. The choice of the weighting matrices $\boldsymbol{W}_1$ and $\boldsymbol{W}_2$ determines the information retained by the reduced subspace representation $\boldsymbol{\mathcal{R}}$ of the model $\boldsymbol{\Theta}$. The choice of weightings, as shown in Table 3.1, is also the basis of distinction between the different subspace methods covered in this literature review. The solution to Eq. (3.54) for the optimal reduction is given by:

$$\boldsymbol{\mathcal{R}} = \boldsymbol{W}_1^{-\mathbf{1}} \boldsymbol{U}_1 \boldsymbol{S}_1 \boldsymbol{V}_1^{\mathrm{T}} \boldsymbol{W}_2^{-\mathbf{1}} \tag{3.55}$$

where the following SVD gives:

$$\boldsymbol{W}_1 \boldsymbol{\Theta} \boldsymbol{W}_2 = (\boldsymbol{U}_1 \quad \boldsymbol{U}_2) \begin{pmatrix} \boldsymbol{S}_1 & 0 \\ 0 & 0 \end{pmatrix} \begin{pmatrix} \boldsymbol{V}_1^{\mathrm{T}} \\ \boldsymbol{V}_2^{\mathrm{T}} \end{pmatrix} \tag{3.56}$$

The order of the system is equal to the number of non-zero singular values in Eq.(3.56) For further details and derivation proof of the summary description provided in the Table 3.1 refer to Overschee and Moor (1995).

Table 3.1 Interpretation of three different subspace algorithms in a unifying framework

Weightings	**Acronym**		
	N4SID	**MOESP**	**CVA**
$\mathbf{W_1}$	$\mathbf{I}_{li}$	$\mathbf{I}_{li}$	$[\boldsymbol{f}/\boldsymbol{u}^{\perp}(\boldsymbol{f}/\boldsymbol{u}^{\perp})^{\boldsymbol{T}}]^{-\mathbf{1/2}}$
$\mathbf{W_2}$	$\mathbf{I}_j$	$\Pi_{\mathbf{U}_f^{\perp}}$	$\Pi_{\mathbf{u}^{\perp}}$

3.4 Model order selection and past and future vector lag sizing

Typically, the number of lags are decided upon first and then the number of state variables to be used is determined. In most of the publications the past and future vector window length are set equal to each other. Various approaches have been adopted for the selection of the length of the past vector for CVA state space modelling. Negiz and Cinar (1997b) proposed a method of deciding upon the number of lags to use by applying the minimum number of significant lags after which the autocorrelation of the autoregressive (AR) residuals would be considered statistically insignificant.

Another means of selecting the number of states to be used is to include the states having non-zero canonical correlation coefficients or singular values of the Hankel matrix (Negiz and Cinar, 1997). This method is only applicable if the state vectors are select using a balance realization approach. Juricek et al. (1998) applied a cross-validation approach. A number of other model order selection procedure and criterions have been proposed and applied in the literature, the list below gives the criterions for which an overview is provided in the proceeding subsections:

i) Akaike Information Criterion, AIC

ii) Normalized Residual Sum of Squares

iii) Multiple Correlation Coefficient

iv) Adjusted Multiple Correlation Coefficient

v) Overall F-test of the loss function, OVF

vi) Final prediction error ,FPE criterion

vii) Bayessian estimation criterion, BIC

viii) Law of iterative logarithms criterion, LILC

3.4.1 Akaike Information Criterion

Akaike information criterion is a measure of the fitness of a statistical model in the context of quantifying the trade off between bias and variance of the statistical model, that is, model accuracy versus model complexity. The criterion was first published by Akaike (1974a). Larimore (1983) applied the Akaike information criterion AIC by generating ARX time series models of varying orders. The model order that minimized the AIC would define the optimal length of the past vector. This approach would involve regression of the output vector **Y** unto to past vector **P**:

$$\mathbf{Y} = \mathbf{BP} + \mathbf{E} \quad \text{with} \quad \mathbf{B} = \mathbf{YP}^{\mathrm{T}}(\mathbf{PP}^{\mathrm{T}})^{-1} \tag{3.57}$$

The general form of the AIC is defined in terms of the sum of the log likelihood function and the number of free parameters may be expressed as:

$$\mathrm{AIC(k)} = \sum \ln p\left(y_i \middle| x_i, u_i, \theta_k\right) + 2 f_M M_k \tag{3.58}$$

As it pertains to Akaike original work, the correction factor f_M has a value of unity, the correction term was introduced by Hurvich, et al. (1990) to apply correction to the AIC order selection for cases of limited number of samples, the correction factor is given by:

$$f_N = N / \left\lfloor N - \left(m_k / n_y\right) - \left(n_y + 1\right) / 2 \right\rfloor \tag{3.59}$$

The commonly used equation for computing the number of free parameters as applied in the literature (Schaper, et al. 1994; Simoglou, et al. 1999a) is given by:

$$m_k = k(2n_y + n_u) + n_y n_u + n_y(n_y + 1)/2 \qquad (3.60)$$

where k is the number of states, n_u is the number of inputs, and n_y is the number of outputs. The origin of the Eq. (3.60) is tied to the number of parameters required to parameterize the general state-space canonical form (Candy, et al., 1979). The number was reported to be far less than the number of elements in the various state-space matrices.

Eq. (3.58) has been translated and applied in terms of exact model parameters via different equations in different publications (Simoglou, et al., 1999a; Liu, et al., 2004):

$$AIC(k) = N\left[n_y(1 + \ln 2\pi) + \ln\left|\Sigma_{ee}(k)\right|\right] + 2f_M M_k \qquad (3.61)$$

$$AIC(k) = Nn_y\left[\ln 2\pi + \ln\left|\Sigma_{ee}(k)\right|\right] + 2f_M M_k \qquad (3.62)$$

where Σ_{ee} is the error covariance matrix (the sample covariance is equal to the normalized residual sum squares NRSS).

The AIC criterion has also been applied to selecting the number of states to include in the states space model. One method of doing this is to create a one-step ahead ARX prediction model by regressing the output **Y** unto the states **X** and choosing the state vector size based upon minimizing the AIC criterion (Juricek, et al., 1999):

$$\mathbf{Y} = \mathbf{BX} + \mathbf{E} \quad \text{with} \quad \mathbf{B} = \mathbf{YX}^{\mathrm{T}}(\mathbf{XX}^{\mathrm{T}})^{-1} \qquad (3.63)$$

It is cautioned that the AIC is a model-specific criterion. For example, the AIC when applied in the above case or used to determine the number of lags to be included in the past vector using the ARX least square regression model approach, the value of M_k would be set equal to the number of parameters in the **B** matrix, however when applied directly to the state-space model of the process, Eq. (3.60) would apply (Simoglou, et al. 1999a). So as to not make premature conclusions about which of the forms of the equation was best suited for computing the number of free parameters M_k, given the state space representation employed in my research, both Eq. (3.60) and Eq. (3.61) along with independently derived equations for M_k were used in the test simulations documented in the case study of Chapter 4.

3.4.2 Normalized Residual Sum of Squares

The Normalized Residual Sum of Squares (NRSS) is a lack of fit metric, also commonly known as the Mean Squared Error MSE and is essentially the mean of the squared residuals across all reconstructed/predicted response for all observations:

$$NRSS = \frac{1}{N}\sum_{j=1}^{m}\sum_{i=1}^{N} e_{ij}^{2} \tag{3.64}$$

where *m* is the number of process variables and *N* is the number of observations. Typically the model that gives the lowest value is used to define the model order or number of lags to use in the case of an ARX model. This fitness measure can be applied to any model as it is based purely on the model error. To avoid over-fitting the model when applying this criterion it is advisable to using one set of data to build the model and a second set of unseen data to determine the model order.

3.4.3 Multiple correlation coefficient

The multiple correlation coefficient R^2 is given by:

$$R^2 = 1 - \frac{RSS}{TSS} \tag{3.65}$$

where the residual sum of squares *RSS* is defined as:

$$RSS = \sum_{j=1}^{m}\sum_{i=1}^{N} e_{ij}^{2} = \sum_{j=1}^{m}\sum_{i=1}^{N}\left(y_{ij} - \hat{y}_{ij}\right)^{2} \tag{3.66}$$

and the total sum of squares *TSS* is given by:

$$TSS=\sum_{j=1}^{m}\sum_{i=1}^{N}\left(y_{ij}-\bar{y}_j\right)^2 \tag{3.67}$$

Where y_{ij} is the ith observation of the jth variable, $\hat{y}_{ij}$ is the model predicted response and $\bar{y}_j$ is the mean of the jth variable. If the data is autoscaled prior to modeling then the ratio of *RSS* to *TSS* is essentially a measure of the ratio of the residual on the *jth* variable to its observed size. The more accurate the model the more this ratio will tend to zero and the R^2 value tends to one. Again, this criterion as before is prone to over-fitting.

The Adjusted Multiple Correlation Coefficient, R_a^2 , was proposed by Draper and Smith (1998) to reduce over-fitting by taking into account the degrees of freedom in a model, it is given by:

$$R_a^2=1-\left(1-R^2\right)\left(\frac{N-1}{N-m_k}\right) \tag{3.68}$$

where m_k is the number of model parameters. Like in the case of the multiple correlation coefficient, the aim is to attain a model that gives a value R_a^2 close to unity.

3.4.4 The Overall F-Test of the loss function

The overall F-test of the loss function OVF proposed by Haber and Unbenhauen (1990 is given by:

$$OVF=\left(\frac{TSS-RSS}{RSS}\right)\left(\frac{N-1}{N-m_k}\right) \tag{3.69}$$

the terms appearing are as defined previously. The OVF can be alternatively expressed as:

$$OVF=\left(\frac{1}{1-R^2}-1\right)\left(\frac{N-1}{N-m_k}\right) \tag{3.70}$$

Therefore, as R^2 tends to 1 the OVF value gets larger. This criterion compares the models under investigation against a fix *TSS* value and the model that gives the highest *OVF* is then selected.

3.4.5 The Final prediction error criterion

The Final Prediction Error Criterion (FPE) (Akaike, 1969) is given by:

$$FPE = N\left[\ln(NRSS) + \ln\left(\frac{N + m_k}{N - m_k}\right)\right] \tag{3.71}$$

where the NRSS is the Normalized Residual Sum of Squares (NRSS) defined in Eq. (3.64). The FPE like the AIC criterion has a model fitness term and a model complexity term that influences its value. The model order selected corresponds to the order that minimizes the FPE.

3.4.6 The Bayesian Information Criterion

The Bayesian information criterion (BIC) (Schwarz, 1978) is given by:

$$BIC = -2\ln p(Y, U, \Theta) + m_k \ln(N) \tag{3.72}$$

The BIC differs from the AIC only in its complexity term which includes the natural log of N. This results in the BIC complexity term tending to produce larger values than its AIC counterpart and as such this leads to lower order models being identified by BIC and additional parameters being more heavily penalized. Another important property of BIC, as was noted by Li, et al. (2001), is that as the sample size $N \to \infty$, the probability of selecting the true model order approaches unity. In Li, et al. (2001) the BIC was employed to avoid model over-fitting and to evaluating and compare their proposed Box-Tidwell transformation based partial least squares BTPLS model with several other nonlinear and a linear PLS model, the translation of Eq. (3.72) used by the authors was given by:

$$BIC = \log(RSS) + \frac{plog(N)}{N} \tag{ 3.73}$$

where p represented the number of unknown parameters of the model and all other terms are as previously defined.

3.4.7 The Law of Iterated Logarithms Criterion

The Law of Iterated Logarithms Criterion LILC was also developed to address the problem of model over-fitting, Hannan and Quinn (1979) proposed the following criterion:

$$LILC = -2\ln p(Y, U, \Theta) + cm_k \ln(N) \tag{3.74}$$

where c is a multiplicative constant (>1). The constant is typically assigned a value between 2 and 4 when the information criterion is used for identifying the order of an ARMAX model. This c term increases the complexity of identifying the true order of the model as the optimal value of c has to be identified prior to the identification of the true order.

The previously summarized list of criterions can be categorized into a few general groups: the first two methods are only based on evaluating model fitness while the others incorporate some form of model complexity term. The model complexity maybe incorporated as a multiplicative term or additive term. In the case of the last four methods on the list and the AIC criterion the complexity term was addictive, however in the case of the Overall F-test criterion and the adjusted multiple correlation coefficient criterion, the term was multiplicative.

3.5 Nonlinear Extension to PCA and PLS

If the underlying linear functional relationship characterizing the projection methods covered in Chapter 2 is replaced with a non-linear function then we have a non-linear adaptation of the traditional PLS, CCA or PCA method. Performance monitoring and prediction of process variables for processes characterized by significant nonlinearities necessitates the use of such nonlinear modelling methods.

Even multi-way PCA and data unfolding methods in some way seeks to mitigate for the presence of process non-linearity by accounting for the time trajectory on the average value of the process variable during scaling. Likewise moving window PCA and adaptive or recursive PCA (Li, et al., 2000) takes into account the shift in the process characteristic that may occur over time. However, with such extension to PCA described in the previous chapter, the scores or latent variables or derived states are nonetheless linear functions of the process variables and or past values of the process variables (for the dynamic case). For processes which have inherent non-linear characteristics and dynamics or the range of variability of the process variables about the operating point results in nonlinearity in the process variables correlation then several nonlinear extensions to the standard PCA, PLS techniques have been proposed in the literature.

3.5.1 Nonlinear PCA (NLPCA)

A number of approaches have been proposed in the literature to adapt the linear model based approach of PCA to be more effectively model non-linear correlation structure between process variable. An early approach proposed by Gnanadesikan (1977), refer to as "Generalized PCA", is to expand the *m* dimensional data matrix **X** with non-linear functions of its elements and then apply the standard PCA method. Another method proposed by Etezadi-Amoli and McDonald (1983) is to apply non-linear factor analysis in which *l* dimensional polynomials are used to approximate the *m*-dimensional data space, where $l < m$. The coefficients of the polynomial are then derived using a linear least squares method.

An algorithm called principal curves was first proposed by Hastie and Stuetzle (1989) to solve the non-linear problem and yielded much success where implementation of NLPCA was concerned and spawned spin off algorithms for extracting the principal curves. Hastie and Stuetzle (1989) defined a principal curve as a smooth, one-dimensional curve that passes through the centre of an *m* dimensional data set. The principal curves are defined by the property of self-consistency, that is, each point of the curve is the average of all data points that project to it, and as such that point is the closest point on the curve for the data points. Whereas for PCA the objective is to project the data set onto a linear manifold, the goal in constructing a principal curve is to project the set onto a nonlinear manifold. The iterative algorithm proposed by Hastie and Stuetzle (1989) starts with first or largest linear principal component and after which the principal component is successively reshape if it is deemed not to be a principal curve based on local projection and expectation computation.

A one-dimensional curve in an m-dimensional space is defined by a vector ***f(λ)*** comprising l functions of a single variable λ:

$$\boldsymbol{f}(\lambda) = [\, f_1(\lambda) \quad f_2(\lambda) \quad \cdots \quad f_l(\lambda)]$$

(3.75)

The variable λ parameterizes the curve such that for every point on the non-linear principal component curve, the length of the curve is used as its index. This length will completely determine the point as the curve is one-dimensional.

The principal curve gives the minimal of all orthogonal deviations among all smooth curves. Thus, for a given data set the first principal curve is its first non-linear principal component. After the first nonlinear principal component is computed, successive components are derived using the residuals:

$$\begin{aligned} X &= f_1(t_1) + E_1 \\ E_{i-1} &= f_i(t_i) + E_i \qquad (i > 1) \end{aligned}$$

(3.76)

The algorithm developed by Hastie and Stuetzle (1989) iterates between a projection step and expectation step and maybe summarized as follows:

i) Let $\boldsymbol{f}^0(\lambda)$ be the first principal component line for **X**. Set j = 1.

ii) Define $\boldsymbol{f}^{\mathrm{j}}(\lambda) = \boldsymbol{E}\left(\mathbf{X} | \lambda_{\boldsymbol{f}^{j-1}}(\mathbf{X}) = \lambda\right)$

iii) Set $\lambda_{\boldsymbol{f}^j}(\mathbf{X}) = max\{\lambda : \|\mathbf{X} - \boldsymbol{f}^j(\lambda)\| = min_\tau \|\mathbf{X} - \boldsymbol{f}^j(\tau)\|\}$ for all $X \in \mathbb{R}^d$

iv) Compute $\Delta(\mathbf{f}^j) = E\left\|\mathbf{X} - \boldsymbol{f}^j\left(\lambda_{\boldsymbol{f}^j}(\mathbf{X})\right)\right\|^2$ and check $\left|\Delta(\mathbf{f}^j) - \Delta(\mathbf{f}^{j-1})\right| <$ threshold. If less than threshold then stop, otherwise, let $j = j + 1$ and return to step (ii).

Whereas the principal curve algorithm was a breakthrough for solving the NLPCA problem, it does not yield a NLPCA model that could be used for prediction. Dong and McAvoy (1994) presented an NLPCA method which integrated the principal curve algorithm with a five-layer auto-associative neural network while Harket et al. (2003) used a similar structured radial basis function (RBF) network. The RBF network comprises of two three layer NN with the output of one being the input to the other. The three layer networks are independently trained using standard training algorithms such as backpropagation (Werbos, 1977; Rumelhard et al, 1986). Dong and McAvoy (1994) used the conjugate gradient learning method (Leonard & Kramer, 1990; Fletcher and Powell, 1963).

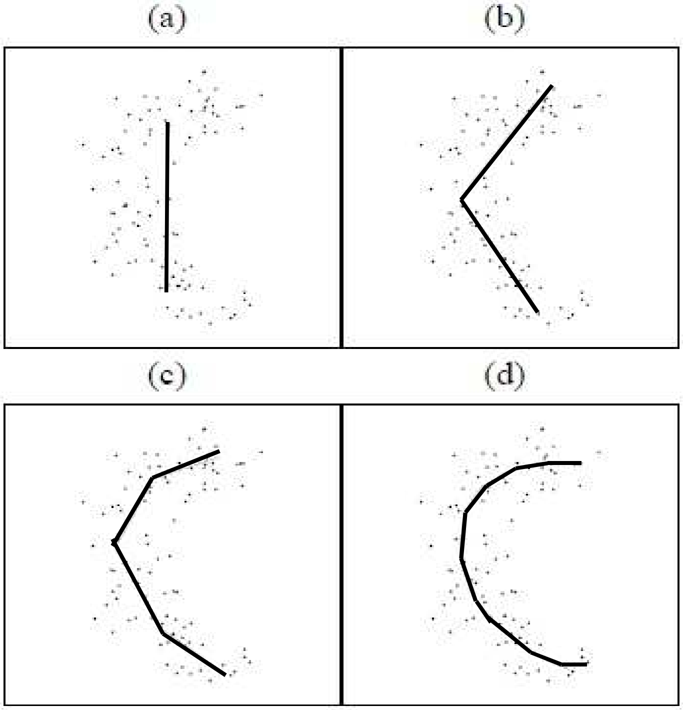

Figure 3.2 The polygonal line algorithm

Another algorithm proposed for extracting the principal curves was proposed by Kegl, et al. (1999) in their work they redefined and represented principal curves as polygonal lines. The principal curve algorithm was initialized by using the first linear principal component of the data set. The algorithm then iteratively identifies new segment vertices by adding one vertex to polygonal curve in each iteration step. The new position of each vertex was determined by minimizing an average squared distance criterion penalized by a measure of the local curvature.

The stopping criterion is based on a heuristic complexity measure, determined by the number of segments k, the dimension of data matrix, and the average squared distance of the polygonal line from the data points. A pictorial illustration of the algorithmic process unfolding is provided in Figure 3.2.

The algorithm was proven to be more robust than the Hastie and Stuetzle algorithm due to the heuristics it uses to adapt the smoothing term and the number of line segments to the data**.** The estimation bias is eliminated by minimizing the average distance from the curve rather than from the vertices of the curve (this also separates it from other algorithms based on vector quantization, such as the self-organizing map SOM or the generative topographic mapping). The algorithm is also faster especially for large data sets.

3.5.2 Non-linear Projection to latent spaces (NLPLS)

Based on the literature reviewed, NLPLS implementations all share one thing in common, the linear inner relationship mapping the Y scores to the X scores of the PLS algorithm is replaced by a non-linear function:

$$\mathbf{T} = \mathbf{X}\mathbf{P}^{T} + \mathbf{E} \tag{3.77}$$

$$\mathbf{U} = \mathbf{Y}\mathbf{Q}^{T} + \mathbf{F} \tag{3.78}$$

$$\mathbf{U} = f(\mathbf{T}) \tag{3.79}$$

A number of different methods of defining/deriving the nonlinear inner relationship for the PLS algorithm have been proposed in the literature:

i) Early publications of Wold, et al. (1989) and Hoskuldsson (1992) established the framework for the quadratic nonlinear extension to the linear PLS approach. The work of Wold, et al. (1989) was revisited by Baffi, et al. (1999b) and they recommended three improvements to Wold's algorithm to improve its applicability to modelling highly nonlinear data sets.

ii) Wold (1992) later applied a spline function approach in which a smooth bivariate spline function (piecewise polynomial functions - quadratic or cubic) was applied as the inner relation to fit a nonlinear mapping between the pair of latent variables. The spline function approach provided more generality and flexibility in defining the non-linear relationship of the inner relationship than the QPLS approach (Wold, et al., 1989). However, both these approaches are essentially a pseudo-linear fit and in the case of a defining a complicated nonlinear relationship, nonlinear parameter estimation would be required. Li, et al. (1999) therefore proposed combining an efficient nonlinear parameter estimation algorithm in the form of a numeric genetic algorithm within the nonlinear PLS algorithm. Identifying that the adaptation of the linear PLS weight selection process was a critical issue for the different non-linear PLS methods, Hassel et al. (2001) proposed an estimation of the weight vector based upon the principle of weighted averages and reciprocal variance criterion.

iii) Qin and McAvoy (1992) generalized the PLS model to a nonlinear framework by imbedding feedforward neural networks into PLS modelling. The feedforward network implementation developed a single feedforward network to map the inner relations between each pair of scores generated sequentially. As such this approach decomposed the multivariate regression problem into a number of univariate nonlinear regressors. Malthouse, et al. (1997) conducted simulation exercises to compare the NLPLS feedforward model with pursuit regression based and neural network modelling approaches and concluded that NLPLS did give much advantage over other projection-based algorithms such as pursuit regression based algorithms and neural networks. Apart from feedforward networks other neural networks can be applied to map the non-linear relationship, such as radial basis networks, see Baffi, et al. (1999a). However, RBF networks are considered superior to the sigmoidal feedforward networks because the training is simpler and faster. The NN approach has been demonstrated to provide a stable and generic (no prior assumption is made about the nonlinear nature of the process) modelling tool.

3.5.3 Non-Linear Canonical Correlation Analysis (NLCCA)

The non-linear approach via neural network implementation has also been applied to implementation of NLCCA using essential the same approach as described earlier. Figure 3.3 illustrates the three-layer NN structured used by Hsieh (2001) which implement a NLCCA method to study the relationship between the tropical Pacific sea level pressure (SLP) and sea surface temperature (SST) fields. The input NN is used to map the **x** and **x** blocks to the **u** and **v** canonical variates respectively. The two output-side NNs are used to generate the non-linear de-mapping function to reconstruct the inputs **x** and **y**. Hyperbolic activation functions ($\mathbf{h}^{(x)}$, $\mathbf{h}^{(y)}$, $\mathbf{h}^{(u)}$, and $\mathbf{h}^{(v)}$) were used for both the input mapping and output inverse-mapping hidden layer implementation.

The input network is trained to maximise the covariance between **u** and **v** since there exist no alternate derivation of **u** and **v** to facilitate a Euclidean error-base training of the network. However, after the forward mapping is completed, the output network is trained to minimize the mean-square error (mse) between the NN output ($\mathbf{x}^{/}$ and $\mathbf{y}^{/}$) and the original data (**x** and **y**).

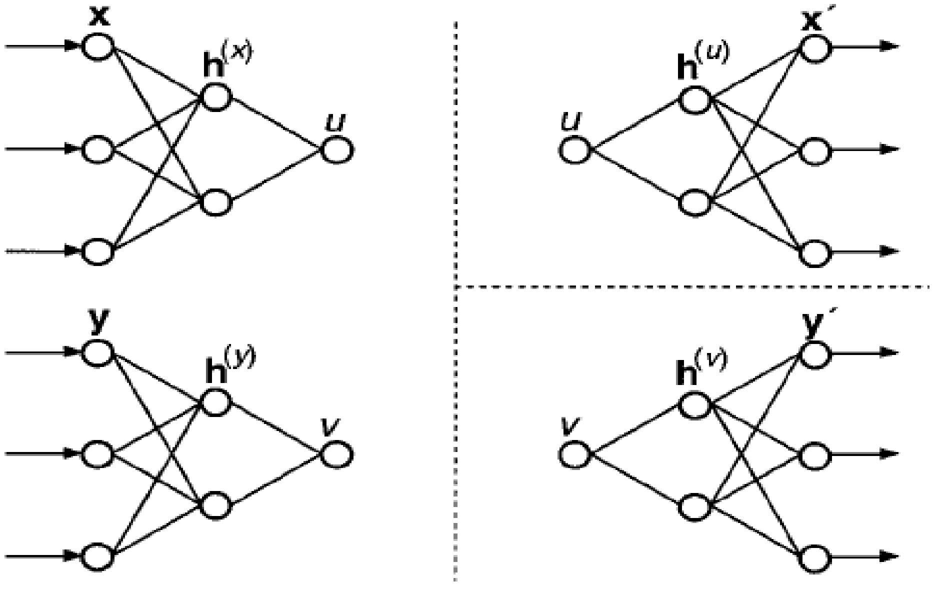

Figure 3.3 Architecture of neural network used to implement NLCCA. Hsieh (2001)

3.6 Hybrid Data Driven/ Mechanistic Model based Approaches

Prior to the proliferation of the data based black-box models for process modelling, first principle mechanistic models were used to determine whether a process was operating desirably. Mechanistic models are particularly appealing because of the following reasons:

i) The challenges of making process monitoring more robust and reliable especially for dynamic and or highly non-linear processes could be improved if known chemical and physical relationships about the process could be incorporated in the process monitoring scheme.

ii) Mechanistic models based upon actual chemistry and design of the process affords tracing and understanding of the nature and source of process upsets to be linked to specific process variables or unit operations.

iii) Data based black-box models do not give much insight into the underlying process behaviours and diagnosis and interpretation of process upset can be subjective. Improving the reliability and confidence in the diagnosis maybe accomplished by the inclusion of known and designed relationship existing between the process variables.

One of the methods that have been explored briefly in the literature to combat and address the issue of providing robust reliable monitoring of non-linear batch and continuous processes characterized by grade changes is model-based PCA proposed by Wachs and Lewin (1999). This was one of the earliest published papers in which the concept of combining a first principle mechanistic model of the process with a database statistical model was explored. The concept which is illustrated in Figure 3.4 is premised on existence of a first principle model of the process which is sufficiently accurate such that the process non-linearity characteristic and whatever serial correlation that exist between the process variables are captured. Then the process of subtracting the model outputs from the real plant data would result in residuals free of non-linearity and autocorrelation. The residuals could therefore be treated using any standard linear statistical multivariate technique such as PCA.

In theory a perfect model would result in the residuals being essentially white noise and as such any process disturbance, faulty sensor, or equipment failure would manifest itself in the residual space without the need for the application of any additional multivariate stochastic methods. However, in an industrial environment there is almost no such thing as a perfect model and as such the residuals space will retain some amount of cross and auto correlation to the extent to which there exist model mismatch:

$$y_e(k) = G_p u(k) + n(k) - G_m u(k) = (G_p - G_m)u(k) + n(k) = G_e u(k) + n(k) \qquad (3.80)$$

Where $y_e(k)$ is the residual vector, u(k) is the input vector, n(k) is the process white noise and G_m and G_p are the process model and actual plant transfer function respectively.

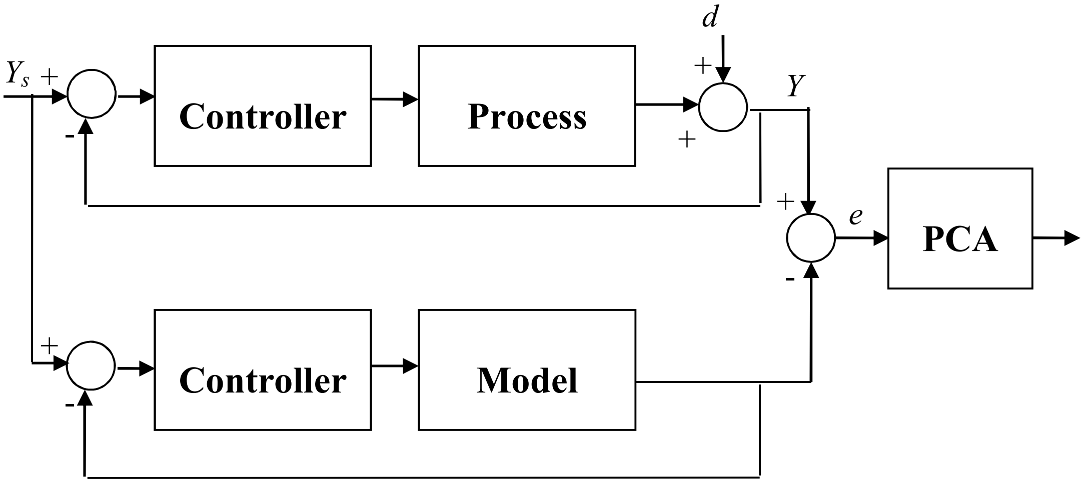

Figure 3.4 Model based PCA

This model mismatch was noted as a primary concern by Wachs and Lewin (1999) and they proposed a fault detection factor that would offer some form of quantitative measure of the extent to which a model mismatch impacted its fault detection applicability. The fault detection factor, F_{MB}, is calculated as the Euclidean norm of the scaled perturbations of the scores:

$$F_{MB} = \sqrt{\sum_{i=1}^{k} \left(\Delta t_i^d / \Delta t_i\right)} \qquad (3.81)$$

where Δt_i^d is the mean in the scores during normal operating condition (NOC) to its value when an alarm is generated for a given fault, and Δt_i is the range of variability of the score during normal operating condition. The more detectable a disturbances is or unaffected by model uncertainty then the greater F_{MB} is. Values of $F_{MB} < 1$ indicate faults that are difficult to detect. Another measure of model mismatch measurement suggested in a publication by Rotem et al. (2000) is to apply the Durbin-Watson test to elucidate the autocorrelation retained in the residuals:

$$\rho = \frac{\sum_{k=2}^{n+1}\left[e(k) - e(k-1)\right]^2}{\sum_{k=1}^{n} e(k)^2} \tag{3.82}$$

where e(k) and e(k-1) are the sample residuals one time sample apart.

If the numerator term is expanded, then the following is obtained:

$$\sum_{k=2}^{n}\left[e(k)^2 - 2e(k)e(k-1) + e(k-1)^2\right] \tag{3.83}$$

and if the samples are uncorrelated then $\sum_{i=2}^{n+1} e(k)^2 = \sum_{i=2}^{n+1} e(k-1)^2$ and the summation of the product term should tend to zero and hence ρ tends to a value of 2. Positive autocorrelation would be indicated in the range of $0 \leq \rho < 2$ and negative autocorrelation would give values in the range $2 < \rho \leq 4$.

Recognising the limitations of model-based PCA in that unless the model was a perfect one, the residuals could still retain serial and autocorrelation structure, McPherson, et al. (2002) proposed a super-model based approach to monitoring of batch processes. The concept is illustrated in Figure 3.5 and the idea behind it is that an additional stage (error model) would be incorporated to augment the mechanistic plant model to end of removing whatever remaining structure that may exist in the first stage residuals.

The final residuals would therefore have independent identically distributed and follow normal distribution. This would then enable the application of PCA, or multi-way PCA, or any standard linear multivariate projection technique for monitoring. The error model was implemented using a number of different approaches, PLS, NLPLS, DPLS, and dynamic CCA.

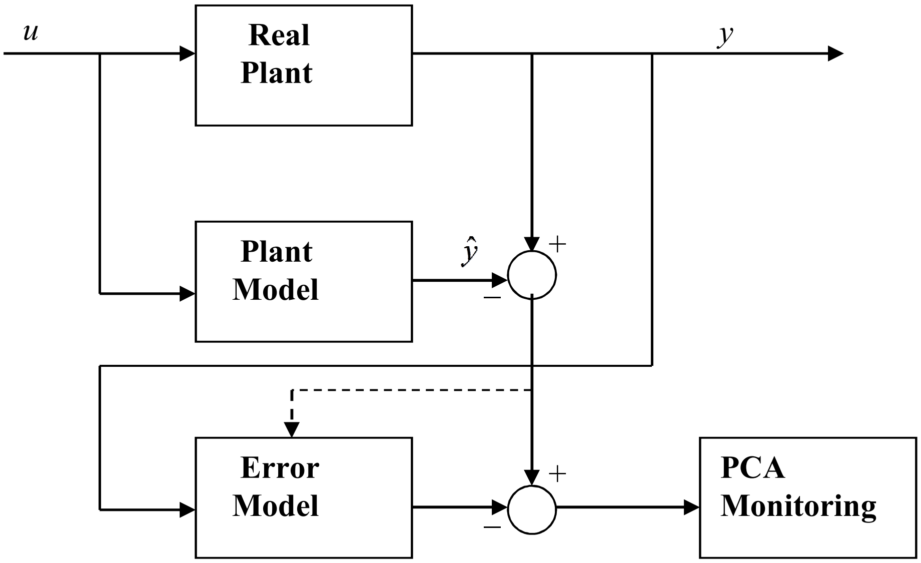

Figure 3.5 Super-model based PCA

A similar concept was adopted by Boudreau, et al. (2006) in which a dynamic error model was used as a second stage to model and eliminate whatever structure retained in the residuals obtained from the difference in the profile output from the 'real plant' and 'virtual plant'.

The general hybrid framework combining statistical linear or nonlinear data driven methods with known kinetics, material balance equations, and other first principle or heuristic knowledge of a given system, has been extensively applied in the literature (Lee, et al., 2005; Oliveira, 2004; Peres, et al., 2001; Psichogios and Ungar, 1992). One particular recent bioprocess modelling application employing this approach by Stosch, et al. (2011), incorporated a nonlinear partial least squares model NPLS with known material balance equations. The material balance equations were used to capture the dynamics of the bioprocess – both the cellular and bioreactor system. The model was evaluated on a fed-batch production of a recombinant protein – *Bordetella Pertussis* batch cultivation and demonstrated better prediction accuracy over alternative non-hybrid approaches at implementing a dynamic model.

Hybrid approaches involving the integration of different statistical data driven modeling techniques are also quite common in the literature. Yan (2010) developed a soft sensor for detection of naptha dry point using an Hybrid Artificial Neural Network HANN. The HANN network employed a partial least square regression PLSR model to remove the multicolinearity among the hidden layer neuron outputs and to enhance the relational model between the hidden and output layer neuron outputs.

3.7 Summary

Three subspace method were reviewed – CVA, N4SID and MOESP. The literature review sought to identify the commons traits of each of the three subspace method in terms of the central objective of representing a data set in a lower order dimensional space. The differences were also highlighted and suitability of the CVA method for process monitoring applications based upon comparative studies conducted by several researchers was the motivating factor to pursue and a proposed a CVA state space model based dynamic modelling approach in this thesis.

The review also explored a number of successfully proposed methods of adapting linear statistical methods of PCA and PLS to tackle nonlinear process modelling and monitoring applications. More specifically, several algorithmic approaches to implementing principle curves in the case of NLPCA were reviewed. The review also covered several methods of modifying the linear PLS algorithm to incorporate a neural network based or polynomial inner relationship.

Several hybrid model based approaches for prediction and performance monitoring across both batch and continuous processes were reviewed. The class of hybrid models included those combining mechanistic (first principle model) with data driven model based approaches and those non-mechanistic approach combining statistical data driven methods of different paradigms such as linear versus nonlinear data based modelling techniques.

Chapter 4 : A Simplified CVA State Space Modelling Approach for Process-Monitoring Specific Applications

4.1 Introduction

The use of state space models for the modelling, control and monitoring of dynamic processes have been reported to be superior to other multivariate statistical methods. In the area of system identification and predictive modelling, Juricek, et al. (2005) demonstrated that subspace models based on canonical variate analysis (CVA) and numerical algorithm for subspace identification (N4SID) outperformed regression models based on partial least squares (PLS) and constraint categorical regression (CCR). They also demonstrated that of the two subspace modelling methods, the CVA model was more accurate than its N4SID counterpart. Other comparative analysis works carried out by Simoglou, et al. (1999a) and Negiz and Cinar (1997b) have also provided support for the superior performance of CVA based state space models .

A few variants of the state space model representations have also been explored and presented on in the literature. Typically, the form of CVA based state-space representation is one that can be used in applications ranging from process modelling, control and monitoring. Such a model generally requires the estimation of five matrices to fully parameterize the model. In control system applications the representation is necessary, as control of the plant is achieved via methods involving the application of calculated input signal(s) based upon the past output measurements. Thus far very little emphasis has been placed on selecting a state-space model based upon its intended application and most if not all recent papers employing state space models for process monitoring applications have resorted to this full model representation (Lee, et al., 2006; Yao and Gao, 2008; Odiowei and Cao, 2010).

An adaptation of the state-space model representation and CVA based derivation for the specific purpose of process monitoring is proposed in this chapter. The proposed state space model employs a significantly reduced number of parameters. The reduced dimensionality of the model in conjunction with a slightly amended method of constructing the past vector, provides for a much simpler and more efficient stochastic estimation method for deriving the state matrices.

Using the benchmark Tennessee Eastman processor simulator under close-loop control, a comprehensive fault detection analysis is carried out using the Hotelling's T^2 statistics and squared prediction error (Q) statistics of the state and output residuals. The results were compared with reported fault detection performance from previous publications (Russell, et al., 2000; Detroja, et al., 2007), both of papers published fault detection results on the same set of 21 faults reviewed in this paper. Russell, et al. (2000) evaluated three different fault detection models: the traditional CVA state space modelling technique, standard and dynamic principal component analysis (D)PCA. While Detroja, et al. (2007) evaluated the detection performance of the Hotelling's T^2 statistics and Q statistics based upon a statistical method called correspondence analysis (CA). The results from these previous publications points to the traditional CVA state space model being overall the best performing model. The results of this research demonstrates that the proposed CVA state space model can offer at least the same and in some cases better fault detection capabilities in terms of detection delay time when compared with the fault detection performance of the traditional CVA state space model.

The chapter is organised as follows: Section 4.2 highlights the differences between the proposed state space model and state variable derivation with that of the models and methods pioneered by Larimore (Larimore, 1990) and reviewed in Chapter 3. Section 4.3 delves into the application of several model selection criterions and how they were employed for the selection of the appropriate state vector dimension used to construct the state space model. Section 4.4 seeks to justify the model suitability via simulation results confirming the model's prediction accuracy while Section 4.5 provides a summary of the results obtain from the TE simulator on the proposed CVA state space model fault detection capabilities compared against that of previous publications for the Tennessee Eastman Application. Section 4.6 summarises the conclusions arrived at and closes the chapter.

4.2 The CVA State Space Modified Approach

4.2.1 The Proposed Representation and Redefining of the Past Vector

The well-known state space model representation is given in Eq. (4.1). The state space model is premised on the stochastic process exhibiting Markov properties (Akaike, 1975). In the strict sense definition of a Markov process, the future state of the process, that is, the conditional probability of future transitions should only be dependent upon the current state of the process. Hence the proposed representation given by Eq. (4.2) is not in contradiction to a Markovian representation and quite accurately aligns with the definition.

$$\mathbf{x}_{t+1} = \boldsymbol{A}\mathbf{x}_t + \boldsymbol{B}\mathbf{u}_t + \mathbf{e}_\mathrm{x};\ \mathbf{y}_t = \boldsymbol{C}\mathbf{x}_t + \boldsymbol{D}\mathbf{u}_t + \boldsymbol{G}\mathbf{e}_\mathbf{x} + \mathbf{e}_\mathbf{y} \tag{4.1}$$

$$\mathbf{x}_{t+1} = \boldsymbol{A}\mathbf{x}_t + \boldsymbol{G}\mathbf{e}_\mathrm{y} + \mathbf{e}_\mathrm{x}\ ;\ \mathbf{y}_t = \boldsymbol{B}\mathbf{x}_t + \mathbf{e}_\mathbf{y} \tag{4.2}$$

For both state space representation $\mathbf{e}_\mathrm{x} \in \mathbb{R}^{N\,\mathrm{x}\,k}$ is the state residuals and $\mathbf{e}_\mathrm{y} \in \mathbb{R}^{N\,\mathrm{x}\,m}$ is the uncorrelated output residuals. The representation given by Eq. (4.2) retains the **G** matrix but incorporates it in the state transition equation as opposed to the output equation. The correlation **G** matrix is somewhat similar to the innovation term employed in Kalman filter designs (Brown and Hwang, 1992; Welch and Bishop, 2006), like Kalman filters, the state estimation is iteratively improved by using the innovations or residuals of the output equation. The proposed state space representation, therefore, more closely aligns its representation with that of the Kalman filter design but makes the assumption that the covariance of the measurement data is constant.

According to Larimore (1990), accounting for the correlation between the state and output residual ensured a minimum order hidden Markov state space representation. The proposed state space representation similarly guarantees a minimum order hidden Markov model, however, the size of the state vector is determined via a cross-validation procedure using the state transition equation as opposed to the output equation as is the case for Larimore's model given by Eq. (4.1).

From a control system point of view the essential difference between the two representations is that the five matrix representation, Eq. (4.1) explicitly accounts for the input vector $\mathbf{u}_t$ and therefore finds its use in control systems applications. For the purpose of fault and disturbance detection, the proposed model, Eq. (4.2) would then suffice adequately and be even more desirably, given the advantages it provides in terms of simplification of representation and stochastic estimation equations. As can be observed, the state space representation of Eq. (4.2) is more concise than Eq. (4.1) with the removal of the current input vector $\mathbf{u}_t$. In order to retain the information component provided by the input vector $\boldsymbol{u}_t$ the author has proposed a redefining Larimore's past vector representation, which was defined in the previous chapter according to the following:

$$\boldsymbol{P}_t^T = \left[\boldsymbol{y}_{t-1}^T, \boldsymbol{y}_{t-2}^T, \dots . \boldsymbol{y}_{t-l_y}^T, \boldsymbol{u}_{t-1}^T, \boldsymbol{u}_{t-2}^T, \dots . \boldsymbol{u}_{t-l_u}^T\right]^T \tag{4.3}$$

To account for the removal of the $\boldsymbol{u}_t$ input in the proposed state space representation, the following redefining of the past vector **P** is proposed in this paper:

$$\boldsymbol{P}_t^T = \left[\boldsymbol{y}_{t-1}^T, \boldsymbol{y}_{t-2}^T, \dots . \boldsymbol{y}_{t-l_y}^T, \boldsymbol{u}_t^T, \boldsymbol{u}_{t-1}^T, \dots . \boldsymbol{u}_{t-l_u}^T\right]^T \tag{ 4.4}$$

The subtle amendment is the inclusion of the $\boldsymbol{u}_t$ vector in the past matrix definition such that the process of deriving the states would retain what information that is contain by the current time input vector $\boldsymbol{u}_t$.

The state vector of the proposed model would be similarly derived according to the canonical variate analysis theory presented in the previous chapter, that is, the state vector $\mathbf{x}_t$ is computed from the canonical variate transform **J** of the past vector:

$$\mathbf{x}_t = \mathbf{J}\mathbf{P}_t^T \;;\; \mathrm{GSVD}\left(\mathbf{R}_{pf}\right) = \mathbf{JSL}^{\mathrm{T}} \tag{4.5}$$

subject to $\mathbf{J}^{\mathrm{T}}\mathbf{R}_{\mathrm{pp}}\mathbf{J} = \mathbf{I}_{\mathrm{m}}$ and $\mathbf{L}^{\mathrm{T}}\mathbf{R}_{\mathrm{ff}}\mathbf{L} = \mathbf{I}_{\mathrm{q}}$, where $\mathbf{R}_{\mathrm{pp}} = \mathbf{P}^{\mathrm{T}}\mathbf{P}$, $\mathbf{R}_{\mathrm{pf}} = \mathbf{P}^{\mathrm{T}}\mathbf{F}$, and $\mathbf{R}_{\mathrm{ff}} = \mathbf{F}^{\mathrm{T}}\mathbf{F}$.

The definition of the future vector remains unchanged:

$$\boldsymbol{F}_t^T = \left[\boldsymbol{y}_t^T, \boldsymbol{y}_{t+1}^T, \ldots . \boldsymbol{y}_{t+f}^T\right]^T \tag{4.6}$$

where l_y, and l_u are the window length of the dynamic lag elements of the input and output samples. The length of future observation window is given by f.

4.2.2 Simplification of the State Matrices Derivation

Larimore's stochastic estimation procedure covered in detail in chapter 3 is summarised by Eq. (4.7) to Eq. (4.10). The stochastic algorithm first derives estimates for the matrices **A**, **B**, **C**, and **D** and then proceeds to simultaneously derive the covariance matrices of the state and output residuals (Φ_{x}, Φ_{y}) along with the parameters of the **G** matrix:

$$\begin{bmatrix} \widehat{\boldsymbol{A}} & \widehat{\boldsymbol{B}} \\ \widehat{\boldsymbol{C}} & \widehat{\boldsymbol{D}} \end{bmatrix} = \begin{bmatrix} \mathbf{x}_{t+1}^T\mathbf{x}_t & \mathbf{x}_{t+1}^T\mathbf{u}_t \\ \mathbf{y}_t^T\mathbf{x}_t & \mathbf{y}_t^T\mathbf{u}_t \end{bmatrix} \begin{bmatrix} \mathbf{x}_t^T\mathbf{x}_t & \mathbf{x}_t^T\mathbf{u}_t \\ \mathbf{u}_t^T\mathbf{x}_t & \mathbf{u}_t^T\mathbf{u}_t \end{bmatrix}^{-1} \tag{4.7}$$

$$\mathbf{e}_{\mathrm{x}} = \mathbf{x}_{t+1} - (\widehat{\mathbf{A}}\mathbf{x}_t + \widehat{\mathbf{B}}\mathbf{u}_t) \tag{4.8}$$

$$\tilde{\mathbf{y}}_t = \mathbf{y}_t - (\widehat{\mathbf{C}}\mathbf{x}_t + \widehat{\mathbf{D}}\mathbf{u}_t) \tag{4.9}$$

$$\begin{bmatrix} \Phi_{\mathrm{x}} & \Phi_{\mathrm{x}}\boldsymbol{G} \\ \boldsymbol{G}^T\Phi_{\mathrm{x}} & \boldsymbol{G}^T\Phi_{\mathrm{x}}\boldsymbol{G} + \Phi_{\mathrm{y}} \end{bmatrix} = \begin{bmatrix} \mathbf{e}_{\mathrm{x}} \\ \tilde{\mathbf{y}}_t \end{bmatrix} [\mathbf{e}_{\mathrm{x}} \quad \tilde{\mathbf{y}}_t]^T \tag{4.10}$$

where $\boldsymbol{\Phi}_{\mathrm{x}} = \mathbf{e}_{\mathrm{x}}^{\mathrm{T}}\mathbf{e}_{\mathrm{x}}$, $\Phi_{\mathrm{x}} = \mathrm{e}_{\mathrm{y}}^{\mathrm{T}}\mathrm{e}_{\mathrm{y}}$ and the total output equation residuals $\tilde{\mathbf{y}}_t = \mathbf{G}\mathbf{e}_{\mathrm{x}} + \mathbf{e}_{\mathrm{y}}$.

We shall now expand Eq. (4.7) to reveal the true complexity behind Larimore's stochastic algorithm when applied to the CVA modelling approach using a five matrices state space model representation. We begin by first deriving the inverse matrix term appearing in Eq. (4.7):

$$\begin{bmatrix} \mathbf{x}_t^T\mathbf{x}_t & \mathbf{x}_t^T\mathbf{u}_t \\ \mathbf{u}_t^T\mathbf{x}_t & \mathbf{u}_t^T\mathbf{u}_t \end{bmatrix} \begin{bmatrix} \boldsymbol{S}_{11} & \boldsymbol{S}_{12} \\ \boldsymbol{S}_{21} & \boldsymbol{S}_{22} \end{bmatrix} = \begin{bmatrix} \boldsymbol{I} & 0 \\ 0 & \boldsymbol{I} \end{bmatrix} \tag{4.11}$$

The sub-matrices $\mathbf{S}_{11}$, $\mathbf{S}_{12}$, and $\mathbf{S}_{22}$ are therefore derivable from the following relations:

$$\mathbf{x}_t^T\mathbf{x}_t\boldsymbol{S}_{11} + \mathbf{x}_t^T\mathbf{u}_t\boldsymbol{S}_{21} = \boldsymbol{I} \tag{4.12}$$

$$\mathbf{u}_t^T\mathbf{x}_t\boldsymbol{S}_{11} + \mathbf{u}_t^T\mathbf{u}_t\boldsymbol{S}_{21} = \mathbf{0} \tag{4.13}$$

$$\mathbf{x}_t^T\mathbf{x}_t\boldsymbol{S}_{12} + \mathbf{x}_t^T\mathbf{u}_t\boldsymbol{S}_{22} = \mathbf{0} \tag{4.14}$$

$$\mathbf{u}_t^T\mathbf{x}_t\boldsymbol{S}_{12} + \mathbf{u}_t^T\mathbf{u}_t\boldsymbol{S}_{22} = \boldsymbol{I} \tag{4.15}$$

By rearranging Eq. (4.13) and Eq. (4.14) the following are obtained:

$$\boldsymbol{S}_{21} = -[\mathbf{u}_t^T\mathbf{u}_t]^{-1}\mathbf{u}_t^T\mathbf{x}_t\boldsymbol{S}_{11} \tag{4.16}$$

$$\boldsymbol{S}_{12} = -[\mathbf{x}_t^T\mathbf{x}_t]^{-1}\mathbf{x}_t^T\mathbf{u}_t\boldsymbol{S}_{22} \tag{4.17}$$

By substituting Eq. (4.16) into Eq. (4.12) and Eq. (4.17) into Eq. (4.15) we obtain:

$$\boldsymbol{S}_{11} = [\mathbf{x}_t^T\mathbf{x}_t - \mathbf{x}_t^T\mathbf{u}_t[\mathbf{u}_t^T\mathbf{u}_t]^{-1}\mathbf{u}_t^T\mathbf{x}_t]^{-1} \tag{4.18}$$

$$\boldsymbol{S}_{22} = [\mathbf{u}_t^T\mathbf{u}_t - \mathbf{u}_t^T\mathbf{x}_t[\mathbf{x}_t^T\mathbf{x}_t]^{-1}\mathbf{x}_t^T\mathbf{u}_t]^{-1} \tag{4.19}$$

Finally, returning to Eq. (4.7) the estimates of the state matrices can now be obtained:

$$\begin{bmatrix} \widehat{\boldsymbol{A}} & \widehat{\boldsymbol{B}} \\ \widehat{\boldsymbol{C}} & \widehat{\boldsymbol{D}} \end{bmatrix} = \begin{bmatrix} \mathbf{x}_{t+1}^T\mathbf{x}_t & \mathbf{x}_{t+1}^T\mathbf{u}_t \\ \mathbf{y}_t^T\mathbf{x}_t & \mathbf{y}_t^T\mathbf{u}_t \end{bmatrix} \begin{bmatrix} \boldsymbol{S}_{11} & \boldsymbol{S}_{12} \\ \boldsymbol{S}_{21} & \boldsymbol{S}_{22} \end{bmatrix} \tag{4.20}$$

$$\widehat{\boldsymbol{A}} = [\mathbf{x}_{t+1}^T\mathbf{x}_t - \mathbf{x}_{t+1}^T\mathbf{u}_t[\mathbf{u}_t^T\mathbf{u}_t]^{-1}\mathbf{u}_t^T\mathbf{x}_t]\boldsymbol{S}_{11} \tag{4.21}$$

$$\widehat{\boldsymbol{B}} = [\mathbf{x}_{t+1}^T\mathbf{u}_t - \mathbf{x}_{t+1}^T\mathbf{x}_t[\mathbf{x}_t^T\mathbf{x}_t]^{-1}\mathbf{x}_t^T\mathbf{u}_t]\boldsymbol{S}_{22} \tag{4.22}$$

$$\widehat{\boldsymbol{C}} = [\mathbf{y}_t^T\mathbf{x}_t - \mathbf{y}_t^T\mathbf{u}_t[\mathbf{u}_t^T\mathbf{u}_t]^{-1}\mathbf{u}_t^T\mathbf{x}_t]\boldsymbol{S}_{11} \tag{4.23}$$

$$\widehat{\boldsymbol{D}} = [\mathbf{y}_t^T\mathbf{u}_t - \mathbf{y}_t^T\mathbf{x}_t[\mathbf{x}_t^T\mathbf{x}_t]^{-1}\mathbf{x}_t^T\mathbf{u}_t]\boldsymbol{S}_{22} \tag{4.24}$$

The computation load in terms of the number of floating point operations required to derive the **A**, **B**, **C**, and **D** matrix based upon Eq. (4.21) to Eq. (4.24) is actually less than that required to extract the matrices based upon Eq. (4.7) because its computationally cheaper to find the inverse of a $n_u \times n_u$ and a $k \times k$ dimensional matrix separately than to find the inverse of $(n_u + k) \times (n_u + k)$ dimensional matrix. Also, one could employ computation and storage of reusable sub-blocks common to the different equations in the set spanning Eq. (4.16) to Eq. (4.24), to further reduce the computation requirements. Nevertheless, either approach would prove computationally more intensive than the reduce set of equations to be derived for the modified state space modelling approach. The derivation is outlined by Eq. (4.25) to Eq. (4.33) and shows how redefining of the past vector **P** and the change in the model representation can lead to a significantly reduced and simplified set of equations.

With reference to Eq. (4.2), the **B** matrix is derived so as to minimize the squared output residuals:

$$\mathbf{e}_y\mathbf{e}_y^T = \mathbf{y}_t\mathbf{y}_t^T - 2\mathbf{y}_t\mathbf{x}_t^T\mathbf{C}^T + \mathbf{C}\mathbf{x}_t\mathbf{x}_t^T\mathbf{C}^T \tag{4.25}$$

Note that the state variables of Eq. (4.1) and Eq. (4.2) share common properties, in particular, the covariance of the state vector is still given by an identity matrix as a result of the common CVA procedure employed in extracting the state variables. Applying this special condition to Eq. (4.25) and setting the derivative function to zero, yields the following results:

$$\frac{d(\mathbf{e}_y\mathbf{e}_y^T)}{d\mathbf{B}} = -2\mathbf{y}_t\mathbf{x}_t^T + 2\mathbf{C} = \mathbf{0} \tag{4.26}$$

$$\mathbf{C} = \mathbf{y}_t\mathbf{x}_t^T \tag{4.27}$$

Likewise, the parameters of the **A** and **G** matrices are found from minimizing the squared residuals of the next state equation with respect to **A** and **G**:

$$\mathbf{e}_x\mathbf{e}_x^T = \mathbf{x}_{t+1}\mathbf{x}_{t+1}^T - 2\mathbf{x}_{t+1}\mathbf{x}_t^T\mathbf{A}^\mathbf{T} - 2\mathbf{x}_{t+1}\mathbf{e}_y^T\mathbf{G}^\mathbf{T} + \mathbf{A}\mathbf{x}_t\mathbf{x}_t^T\mathbf{A}^\mathbf{T} + \mathbf{G}\mathbf{e}_y\mathbf{e}_y^T\mathbf{G}^\mathbf{T} + 2\mathbf{A}\mathbf{x}_t\mathbf{e}_y^T\mathbf{G}^\mathbf{T} \tag{4.28}$$

Eq. (4.28) can be simplified by setting $\mathrm{x_t x_t^T} = \mathrm{I_k}$, $\mathbf{x}_{t+1}\mathbf{x}_{t+1}^T = \mathbf{I}_k$ and noting that $\mathrm{x_t e_y^T}$= 0, these assumptions result in:

$$\boldsymbol{e}_x\boldsymbol{e}_x^T = \mathrm{I_k} - 2\mathbf{x}_{t+1}\mathbf{x}_t^T\mathbf{A}^\mathbf{T} - 2\mathbf{x}_{t+1}\mathbf{e}_y^T\mathbf{G}^\mathbf{T} + \mathbf{A}\mathbf{A}^\mathbf{T} + \mathbf{G}\mathbf{e}_y\mathbf{e}_y^T\mathbf{G}^\mathbf{T} \tag{4.29}$$

The solutions are obtained by setting the partial derivatives with respect to **A** and **G** to zero:

$$\frac{\partial(\mathbf{e}_x\mathbf{e}_x^T)}{\partial\mathbf{A}} = -2\mathbf{x}_{t+1}\mathbf{x}_t^T + 2\mathbf{A} = 0 \tag{4.30}$$

$$\frac{\partial(\mathbf{e}_x\mathbf{e}_x^T)}{\partial\mathbf{G}} = -2\mathbf{x}_{t+1}\mathbf{e}_y^T + 2\mathbf{e}_y\mathbf{e}_y^T\mathbf{G} = 0 \tag{4.31}$$

$$\mathbf{A} = \mathbf{x}_{t+1}\mathbf{x}_t^T \tag{4.32}$$

$$\mathbf{G} = \mathbf{x}_{t+1}\mathbf{e}_y^T\left[\mathbf{e}_y^T\mathbf{e}_y\right]^{-1} \tag{4.33}$$

Derivation of the state matrices of the simpler proposed model shows that no matrix inversion operation is required to generate the solution for the **A** and **C** matrices of the model.

Table 4.1 compares the proposed and traditional stochastic estimation algorithms in terms of the numbers of floating point operations (FLOPs) needed to compute the two models. The matrix inversion operation involved in the computation of the A-B and A-B-C-D matrices of the state space models is separately shown so as to highlight its computational load. Online available educational material on matrix inverse computation provided by researchers from the University of South Florida (http://numericalmethods.eng.usf.edu/simulations) demonstrates that matrix inversion operation using LU Decomposition method requires significantly less FLOPs over a Gaussian Elimination based technique. The matrix inversion FLOPS given in Table 4.1 is based on LU decomposition, however, this serves as a reference for comparison and does not necessarily represent the most efficient inversion considering that the LU decomposition could be substituted for by a Cholesky decomposition. The Cholesky decomposition is a special case of the general LU decomposition that is numerically more stable and efficient than LU decomposition but is applicable only to positive definite symmetric matrices.

Table 4.1 Computational complexity (FLOPs) of proposed and traditional CVA methods

Computer Operations	Model Type	
	ABG	ABCDG
A to D Matrix: Multiplications and Additions	$2n(n_u n_y + k^2)$	$4n\left[\left(k + n_u + n_y\right)k + \left(n_y + n_u\right)n_u\right]$ $+2(k + n_u)^3$
A to D Matrix: Matrix Inversion Operation	0	$\frac{4(k + n_u)^3}{3} + \frac{3(k + n_u)^2}{2} - \frac{5(k + n_u)}{6}$
G-Matrix: Computation	$2nq\left(k + n_y\right) + \frac{4n_y^3}{3} + \frac{3n_y^2}{2} - \frac{5n_y}{6}$	

n_u – number of inputs; n_y – number of outputs; n – length of training data; k – number of state vectors

4.3 State matrix sizing and other modelling considerations

Development of a CVA state space model requires the selection of several sizing parameters: the window lengths of the past and future vectors and the number of state vectors comprising the state matrix. Additionally, consideration must also be given as to whether to apply separate lag/lead order per process variable when constructing the past or future vector.

Simoglou, et al. (1999a) presented an overview of several criteria that have been reported in the literature for state vector dimension selection, namely Akaike information criterion (AIC), cross-validation procedures, and selection based on the eigenvalues of the Hankel matrix. In addition to these, there exist several other model order selection criteria such as Final Prediction Error (FPE), Bayesian Information Criterion (BIC), and Law of Iterated Logarithm Criterion (LILC).

AIC is the first of these and the most extensively used in such endeavours. Larimore (1983) proposed using AIC for determination of the lag-order and several other researchers have done likewise (Simoglou, et al., 1999a; Juricek, et al., 1999). Simoglou, et al. (2002) speculated that the use of this common lag order for all the inputs and outputs in the past vector construction may impose some limitations with the use of the method as different variables may exhibit different dynamics and should therefore be included with different numbers of lagged values in the past vector. Negiz and Cinar (1997b) proposed using the autocorrelation trend of the process variables to select the past window lag on a per-variable basis.

The model development carried out in this research employed a common lag-window size for the past and future vectors. The choice was driven by the need to simplify the model development procedure. To the authors' best knowledge, in the majority of the publications the window lengths for all the process variables were set to the same number of time shifts (Simoglou, et al., 1999b; Simoglou, et al., 2002; Negiz and Cinar, 1997a). Also, simulation results shown in Figure 4.1 indicate that the choice of lag-window size is not very critical to the accuracy of the developed model and that the state vector size selection is a more influential factor. This result was based upon simulation data using a multi-input multi-output (MIMO) autoregressive model with exogenous input (ARX), defined by Eq. (4.34) to Eq. (4.36). The ARX time series model employed for the simulation is an expanded and more involved version of the single-input two-output ARMAX time series model used by Negiz and Cinar (1997a). Additive measurement noise with a signal to noise ratio of 10% is added to input and output measurements.

The model simulates three output signals from three independent inputs:

$$y_1(t) = 0.95y_1(t-1) - 0.35y_1(t-2) + 0.8u_1(t) \tag{4.34}$$

$$y_2(t) = 0.35y_2(t-1) + u_1(t) + 0.4u_2(t) \tag{4.35}$$

$$y_3(t) = 0.6y_1(t-1) - 0.3y_2(t-1) + 0.88u_3(t) \tag{4.36}$$

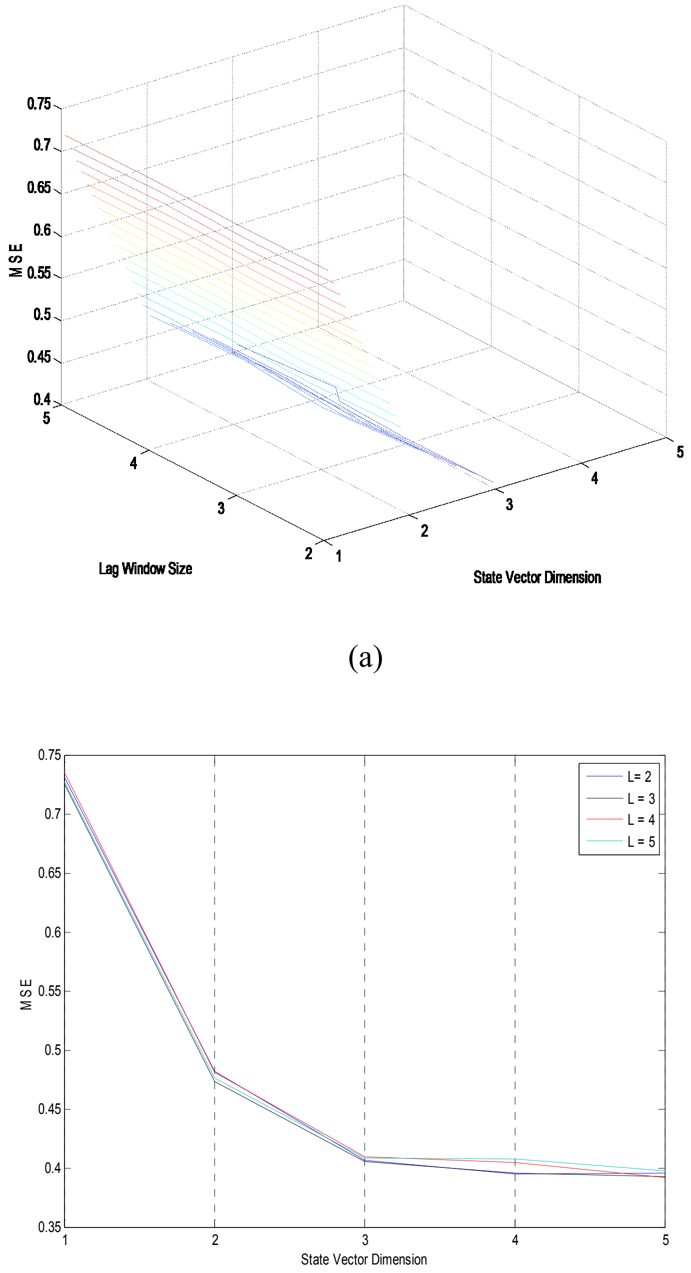

(a)

(b)

Figure 4.1 a) 3-D plot of model error vs. state vector and lag window sizes; b) Equivalent 2-D family of plots for different lag size L - MSE versus state vector dimension.

Both the 3-D contour plot shown in Figure 4.1(a) and the family of mean squared error (MSE) plots in Figure 4.1(b) demonstrate that the choice of lag window size is of less impact on the performance of the model. Figure 4.1(b) also shows that the cross validation MSE plateaus beyond the use of more than three/four states which is consistent with the fact that there are three independent variables in the data set along with one time delayed output term included in the second order time series equation defining output y_1. The MSE plots will later be shown to characterize the shape of the model fitness (maximum likelihood) terms employed by a number of model order selection criteria.

Simoglou, et al. (1999b) also investigated the noise-sensitivity of several model order selection criteria by observing the impact of measurement noise in the data on the selected model order. They concluded that the most suitable model order was dependent upon the purpose of the model, whether it was employed for prediction or monitoring, and was also dependent upon other specifics about the particular data based model. A list of the criteria investigated in this paper for finding the minimum state vector size is given in Table 4.2. The list shows that AIC, BIC, and LILC all use the maximum likelihood term to estimate the model fitness and only differ in the term used to quantify model complexity. The maximum likelihood term is itself a function of the covariance of the model residual:

$$\ln p(\mathbf{Y}, \mathbf{U}, \mathbf{\Theta}) = nn_y(\ln 2\pi + \ln||\mathbf{E}||) \tag{4.37}$$

where n is the number of observations, n_y is the number of output variables and $\mathbf{E}$ is the vector of model residuals for the regression model $\mathrm{Y} = \mathrm{U\Theta} + \mathrm{E}$ **.**

Therefore, for a given training data set, the maximum likelihood function is only a logarithmic function of the error covariance of the form:

$$\ln p(\mathbf{Y}, \mathbf{U}, \mathbf{\Theta}) = a + b \ln ||\mathbf{E}|| \tag{4.38}$$

where a and b are constants related to the model training data dimension.

Table 4.2 A list of model size selection criteria

Criterion	Equation
Akaike Information Criterion - AIC, (Akaike, 1973)	$\mathrm{AIC} = -2\ln p(\mathbf{Y}, \mathbf{U}, \mathbf{\Theta}) + 2m_k$ where m_k is the number of model parameters
Bayesian Information Criterion - BIC, (Hannan and Quinn, 1979)	$\mathrm{BIC} = -2\ln p(\mathbf{Y}, \mathbf{U}, \mathbf{\Theta}) + 2m_k \ln(N)$ where N is the number of observations in the training data set
Law of Iterated Logarithm Criterion - LILC, (Hannan and Quinn, 1979)	$\mathrm{LILC} = -2\ln p(\mathbf{Y}, \mathbf{U}, \mathbf{\Theta}) + 2m_k \ln(\ln N)$
Final Prediction Error - FPE, (Akaike, 1970). The criterion converges towards the AIC for large values of N.	$FPE = N\left[\ln \|\|E\|\| + \ln\left(\frac{N + m_k}{N - m_k}\right)\right]$

The desirable parabolic shape obtained when these criteria are employed is therefore a function of the rate or magnitude of decline of the likelihood function curve as the model residual diminishes versus the rate or magnitude of growth of the model complexity term employed as is illustrated in Figure 4.2. As such, the point at which the particular criterion employed achieves a minimum (if one is achieved) is subject to the trend of the model residual decline with increasing model parameters and the complexity term employed. In the case of the proposed CVA state space model, the commonly used equation for computing the number of free parameters, as applied in several papers (Simoglou, et al. 1999a; Schaper, et al. 1994), is given by:

$$m_k = k(2n_y + n_u) + n_y n_u + n_y(n_y + 1)/2 \tag{4.39}$$

where k is the number of states, n_u is the number of inputs, and n_y is the number of outputs.

The origin of Eq. (4.39) is tied to the number of parameters required to parameterize the general state space canonical form which is far less than the number of elements in the various state space matrices (Candy, et al., 1979). However, the number of parameters making up the matrices of the proposed state space model versus Larimore's model are given by Eq. (4.40) and Eq. (4.41) respectively:

$$m_k = 2kn_y + k^2 \tag{4.40}$$

$$m_k = k(2n_y + n_u) + n_y n_u + k^2 \tag{4.41}$$

The model complexity term of Eq. (4.41) yields larger values than Eq. (4.39) for state order size selection satisfying:

$$k \geq \sqrt{n_y(n_y + 1)/2} \tag{4.42}$$

However, the model complexity term applicable to the simplified state space model, Eq. (4.40) would always yield smaller values than Eq. (4.41) for any state vector size *k*. Comparing with Larimore's model complexity term Eq.(4.39), Eq. (4.40) would yield larger values only when:

$$k^2 + kn_u \geq n_y(n_y + 1)/2 + n_y n_u \tag{4.43}$$

This is essentially satisfied once the state order *k* exceeds the number of model outputs n_y.

Due to the large values returned by the likelihood function computation as shown in Figure 4.2(a), it is desirable to choose a model complexity term (Eq. (4.39) to Eq.(4.41)) that yields the largest m_k value and the choice as demonstrated previously is therefore driven by the state space model being employed. The subjective nature of the process therefore requires that the model complexity term be specific to the model so as to guarantee arriving at the true model order. With that said, the BIC plot of Figure 4.2 best approximates a parabolic shape with its minimum located at the state order of four consistent with the observation from the MSE plots in Figure 4.1.

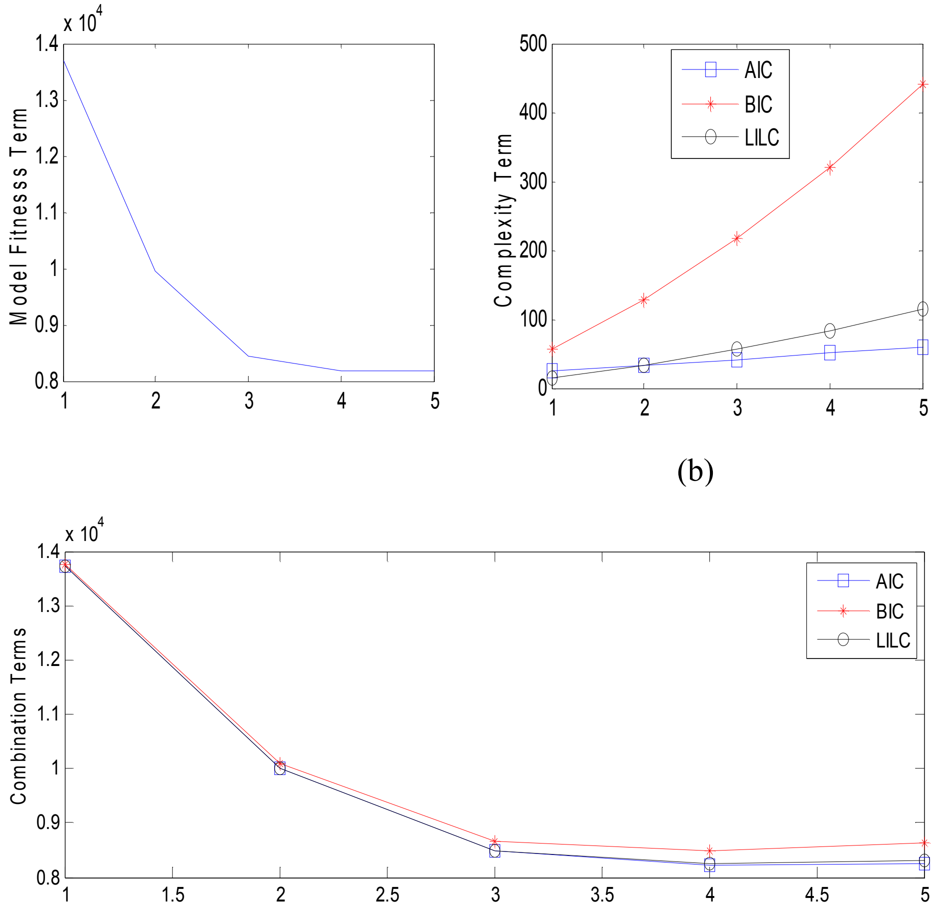

(b)

(c)

Figure 4.2 Plots of the AIC, BIC, LILC criteria dissected in terms of model complexity term and model fitness term

An alternative method for identifying the state order of the model is to rely on the MSE cross-validation plots. The stopping criterion employed is based upon a minimum gradient specification:

$$\Delta(k) = \frac{mse(k) - mse(k-1)}{mse(k) - mse(k_{int})} \tag{4.44}$$

where k is the current state vector size and k_{int} is the initial chosen dimension. The initial state order dimension is typically chosen to be $\min\{n_u,n_y\}$ for the model under evaluation. The final state vector size is then selected when $\Delta(\mathrm{k})$ falls below a pre-determined value, which is typically a small positive value for example 0.01.

The simplification of the state space model parameterization equations facilitates a sequential procedure such that for each past vector window size selected, the state vector size is increased by one in each step until a plateau (minimum gradient change) or minimum point of the MSE plot is detected. The state output error can be updated sequentially for each additional state vector employed by expanding the **B** matrix by a single row when a new state vector is included in the model and then updating the residual vector computation:

i) Compute the *k*th row-vector of the **B** matrix:

$\mathbf{b}_k^T = \mathbf{Y}_{tr}^T\mathbf{x}_{tr}^k$ where $\mathbf{Y}_{tr}^T$ is an $N \times m$ matrix of training output measurements and $\mathbf{x}_{tr}^k$ is the *k*th state vector derived as the canonical variate using the training data.

ii) Update the output prediction: $\widehat{\mathrm{Y}}_{\mathrm{k}} = \widehat{\mathrm{Y}}_{\mathrm{k\text{-}1}} + \mathrm{b}_{\mathrm{k}}\mathrm{x}_{\mathrm{v}}^{\mathrm{k}}$

iii) Update residual matrix: $\mathbf{E}_k = \mathbf{Y}_v - \widehat{\mathbf{Y}}_k$.

Steps (i) to (iii) are repeated until the MSE converges to a minimum value. The state vector dimension and lag-order is then selected based upon the convergence value obtained over the range of past vector window sizes employed.

4.4 Simulation 1: Evaluating the Proposed CVA SS model Accuracy and Predictive Capabilities

The derived state-matrices and covariance matrices for the two state-space models are given below. The covariance matrix of the state variables in both cases was checked to confirm consistency with the theory and both models return an identity matrix.

ABCDG Model :

$\mathbf{x}(t+1) = \mathbf{Ax}(t) + \mathbf{Bu}(t) + \mathbf{e}_{\mathbf{x}}(t)$

$\mathbf{y}(t) = \mathbf{Cx}(t) + \mathbf{Du}(t) + \mathbf{Ee}_{\mathbf{x}}(t) + \mathbf{e}_{\mathbf{y}}\mathbf{(t)}$

$$A = \begin{bmatrix} 0.575 & 0.081 & -0.061 \\ -0.772 & 0.076 & 0.203 \\ 0.226 & -0.459 & 0.730 \end{bmatrix} \qquad B = \begin{bmatrix} 0.850 \\ -0.610 \\ 0.020 \end{bmatrix}$$

$$C = \begin{bmatrix} -1.101 & 0.251 & 0.001 \\ -0.965 & -0.0284 & -0.001 \end{bmatrix} \qquad D = \begin{bmatrix} -0.002 \\ 0.008 \end{bmatrix}$$

$$G = \begin{bmatrix} 0.287 & 1.324 & -0.359 \\ -0.244 & 0.585 & -0.373 \end{bmatrix}$$

ABG Model

x(t+1) = **Ax**(t) + **e**$_{\mathbf{x}}$(t)

y(t) = **Bx**(t) + **Ge**$_{\mathbf{x}}$(t) + **e**$_{\mathbf{y}}$**(t)**

$$A = \begin{bmatrix} 0.575 & 0.081 & -0.061 \\ -0.772 & 0.076 & 0.203 \\ 0.226 & -0.459 & 0.730 \end{bmatrix}; B = \begin{bmatrix} 0.850 \\ -0.610 \\ 0.020 \end{bmatrix}; C = \begin{bmatrix} -1.101 & 0.251 & 0.001 \\ -0.965 & -0.0284 & -0.001 \end{bmatrix}$$

The autocorrelation plots of the residuals shown in Figure 4.3 and Figure 4.4 reveals that both state space models produced residuals whose autocorrelation falls off steeply and is statistically zero after a lag shift of two samples. The results validate the use of the proposed state space model and estimation algorithm as a suitable alternative to the 5 matrices state space representation and Larimore’s stochastic algorithm.

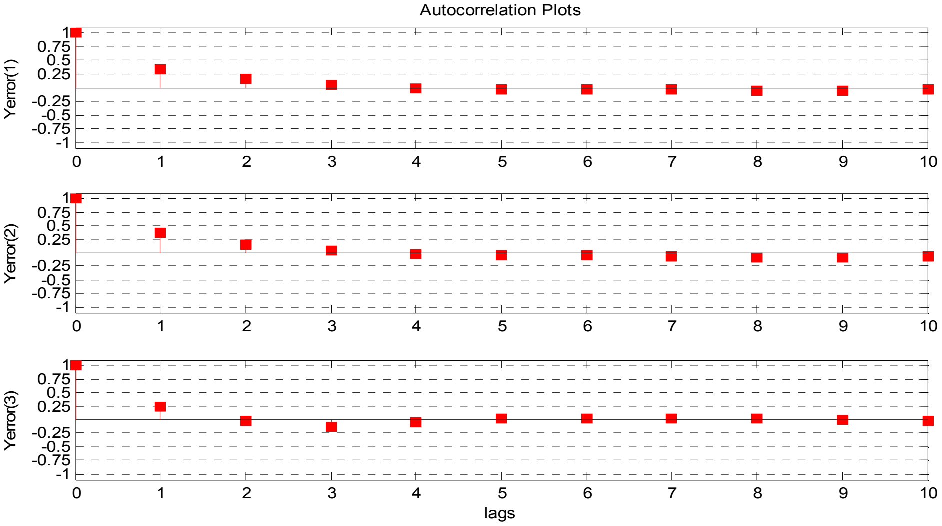

Figure 4.3 Autocorrelation plots of the output residuals ABG state space model

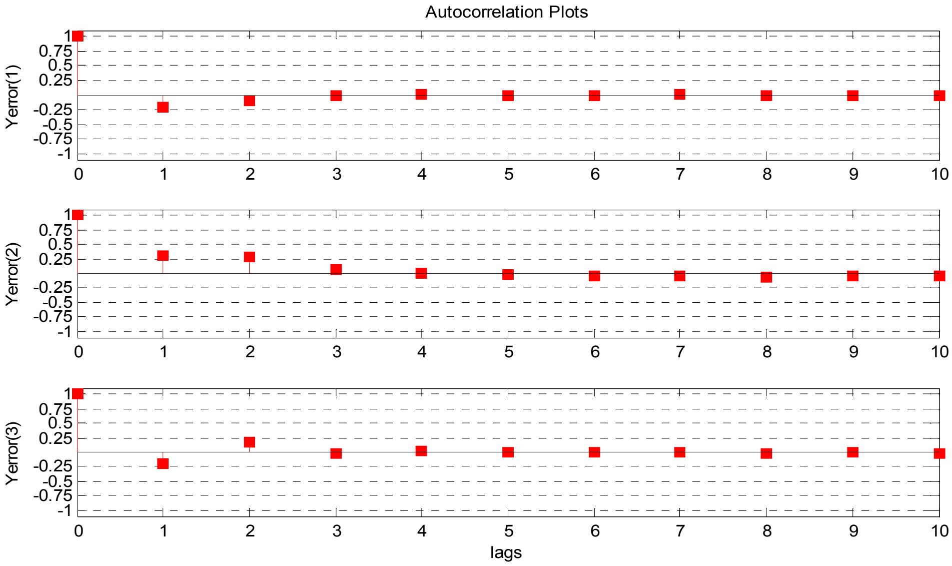

Figure 4.4 Autocorrelation plots of the output residuals ABCDG state space model.

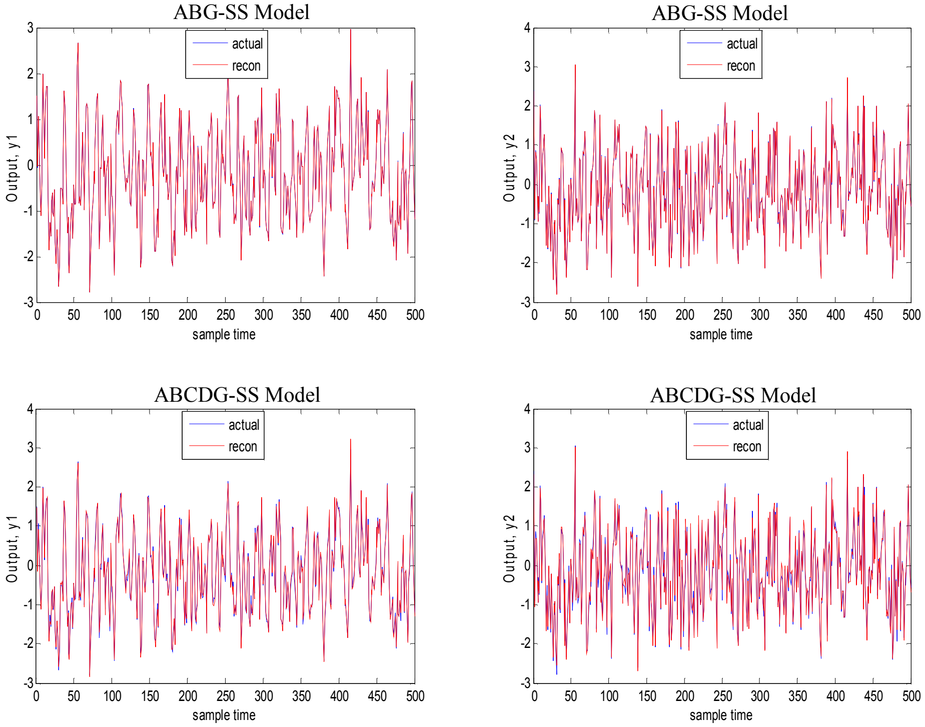

Figure 4.5 Reconstruction of outputs for both CVA State Space models

Figure 4.5 shows the reconstruction of the output and state variables in contrast to the actual output and computed CVA states for both state space models. The accuracy of the reconstruction appears to be very much on spot. Note that the reduce-dimension SS model gives a more exact fit to the actual output with the red-line plot virtually overlapping the blue-line plot. The distribution of the residuals shown in Figure 4.6 also appear to exhibit an expected white-noise Gaussian distribution consistent with residuals void of correlation structure.

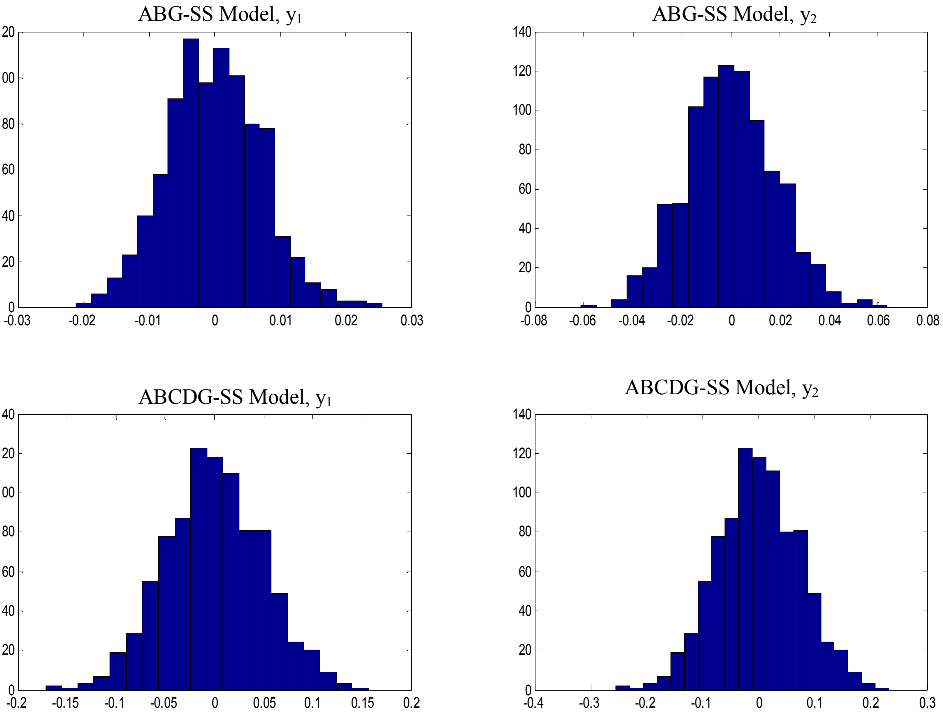

Figure 4.6 Histogram plot of the output residual distribution for both CVA SS models

4.5 Simulation 2: Fault Detection Capabilities Based on TE Simulator

4.5.1 The Tennessee Eastman Process

The Tennessee Eastman (TE) process is a benchmark process simulator that has been used extensively for studying process control technology and strategies and more recently process monitoring schemes. The process, as shown in Figure 4.7, consists of five major unit operations: a reactor, product condenser, a vapour-liquid separator, a recycle compressor, and a product stripper. The simulated faults and a description of the open loop TE simulation is provided in Downs and Vogel (1993). The close-loop TE simulator adopted for the simulation runs to be described is a control strategy proposed by Lyman and Georgakis (1995). The control strategy is a plant-wide control scheme with the control structure arranged in a multi-tiered framework in which SISO control loops are classified according to their level of importance to performance of the plant as a whole. The four tiers in order of relative importance are production and inventory control, product specification control, equipment and operating constraints, and economic performance enhancement.

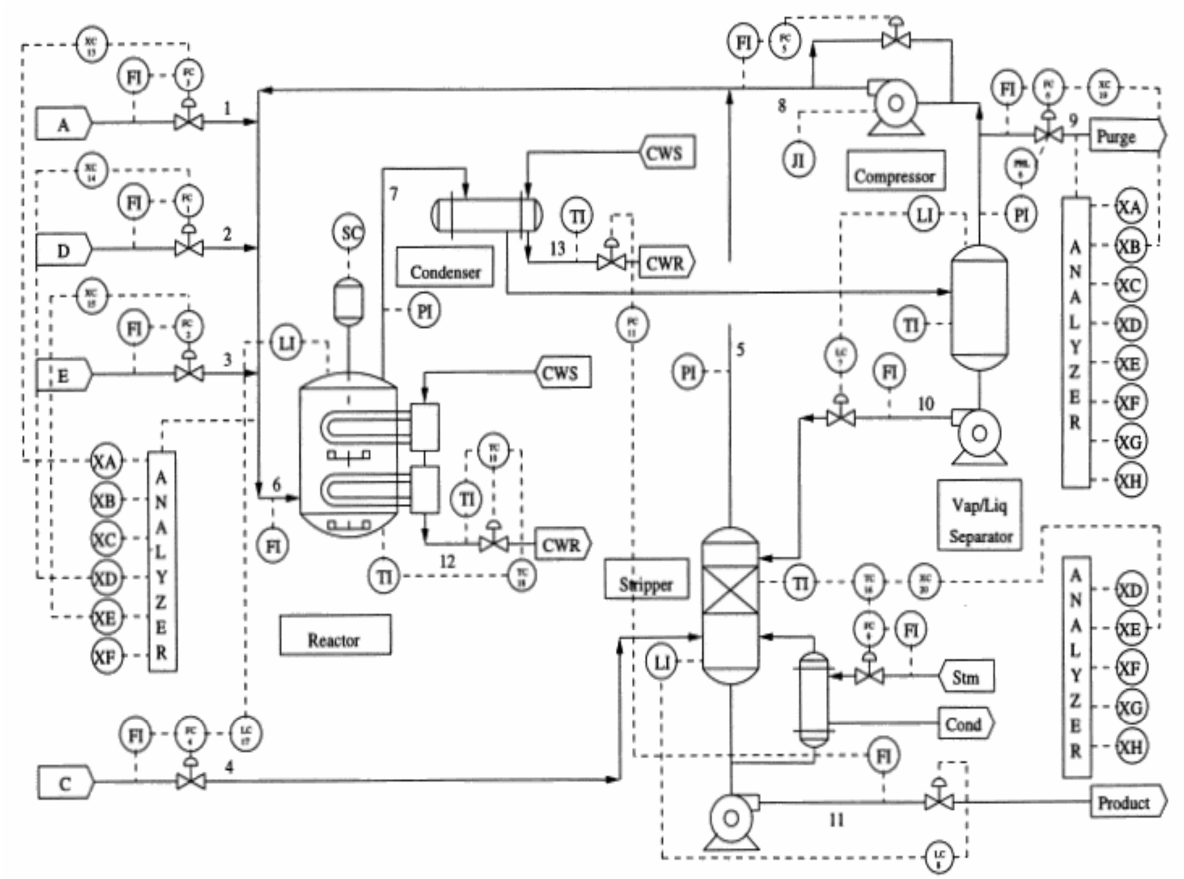

Figure 4.7 Diagram of the Tennessee Eastman process simulator under Lyman and Georgakis control scheme. (Lyman and Georgakis, 1995)

Twenty one pre-programmed faults, summarized in Table 4.3, were tested and the detection delays were computed. The data sets used were downloaded from http://brahms.scs.uiuc.edu. The statistical model was built from the normal operation data consisting of 500 samples and the cross-validation was carried out using a second unseen data set of 900 samples. All manipulated and measurement variables were used except the agitation speed of the reactor stirrer, making it a total of 52 variables The model is defined by 34 states and uses a lag order of 2 for the past and future vector. Even with the same state vector dimension, the proposed state space model provided a reduction in the number of parameters by $k(n_y + n_u)$, where k is the number of states, n_u is the number of inputs and n_y are the number of outputs.

Table 4.3 List of simulated disturbances and faults

Fault	Fault Description	Fault Type
F(1)	A/C feed ratio, B composition constant (Stream 4)	Step
F(2)	B composition, A/C ratio constant (Stream 4)	Step
F(3)	D feed temperature (Stream 2)	Step
F(4)	Reactor cooling water inlet temperature	Step
F(5)	Condenser cooling water inlet temperature	Step
F(6)	A feed loss (Stream 1)	Step
F(7)	C header pressure loss- reduced availability	Step
F(8)	A, B, C feed composition (Stream 4)	Random variation
F(9)	D feed temperature (Stream 2)	Random variation
F(10)	C feed temperature (Stream 4)	Random variation
F(11)	Reactor cooling water inlet temperature	Random variation
F(12)	Condenser cooling water inlet temperature	Random variation
F(13)	Reaction Kinetics	Slow drift
F(14)	Reactor cooling water valve	Sticking
F(15)	Condenser cooling water valve	Sticking
F(16)	Unknown	
F(17)	Unknown	
F(18)	Unknown	
F(19)	Unknown	
F(20)	Unknown	
F(21)	Stream 4 valve fixed at the steady state position	Constant position

The manipulated process variables, process feeds and measured disturbance variables were all assigned as inputs variables, the remaining process variables were assigned as output variables. With respect to the manipulated variables, one could have alternatively assigned such process measurements as output variables seeing they represent intermediate outputs driven by the plant controllers. Most importantly is that all variables that may indicate the development of a fault or disturbance is included in the model. For further details of the simulator the publication of Downs and Vogel (1993) can be consulted.

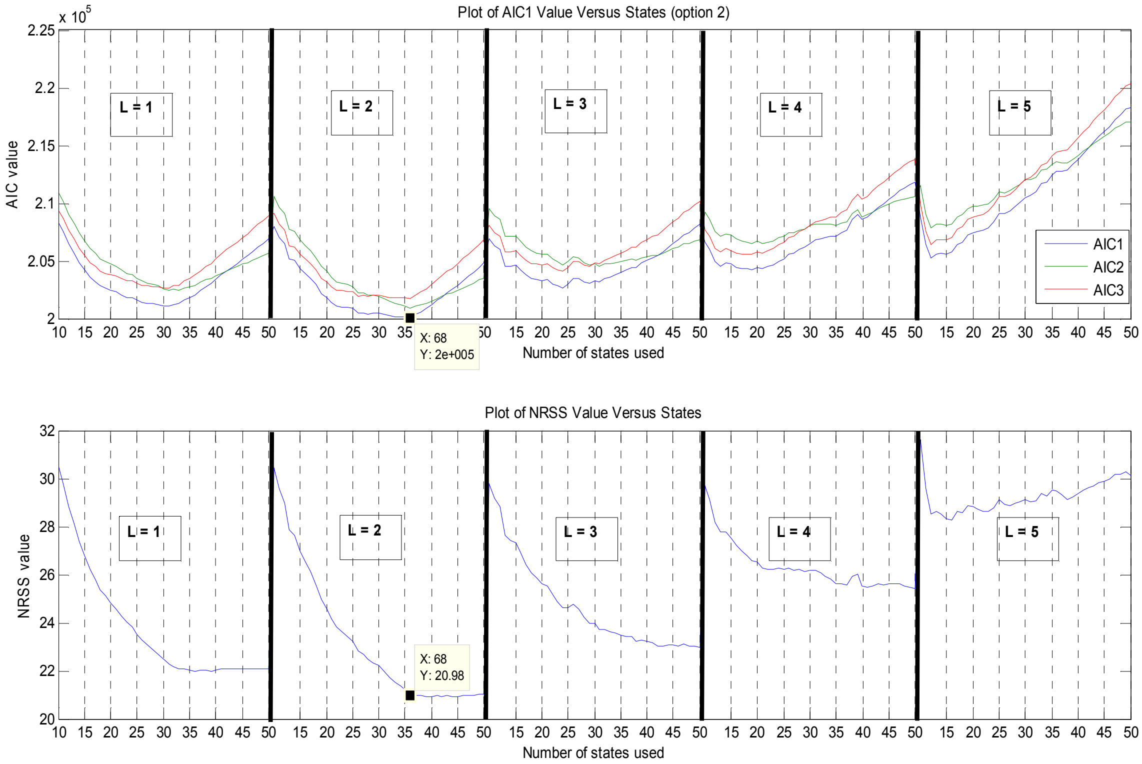

AIC1 – Eq. 4.39 AIC2 – Eq. 4.40 AIC2 – Eq. 4.41

Figure 4.8 AIC and NRSS computation for the monitoring-specific SS models (ABG) spanning lag size from 1 to 5 and state order from 10 to 50.

The AIC criterion proved to be most suitable for prediction of the model state order and lag-order for both the proposed and traditional state space models. The plots in the top row of Figure 4.8 all show a family of AIC plots each one corresponding to one of the three different complexity terms discussed earlier (Eq. 4.39 – 4.41). The AIC plot proved to be less sensitive to the choice of complexity term and all the plots fairly followed each other in terms of parabolic fitness. However, the fix size lag/lead order employed for the dynamic expansion to construct the past and future matrices proved to be of more influence on the model selection criterion. In the end, a lag order ***L*** of 2 gave AIC curves with minimum points most consistent with the state order return by the MSE plots shown in the bottom row of Figure 4.8 and the state order as determine by the algorithm proposed in section 4.3. The lag order of two also corresponds to the minimum MSE attainable as can be observed from the various plots.

Both the BIC and LLIC failed to converge and indicate the true state order for the model as can be observed in Figure 4.9. The LLIC plots generate parabolic shape curves but the minimum points of the curve can be observed to be achieved at a much lower-sate order in comparison to the state order observed by both the AIC and MSE plots of Figure 4.1.

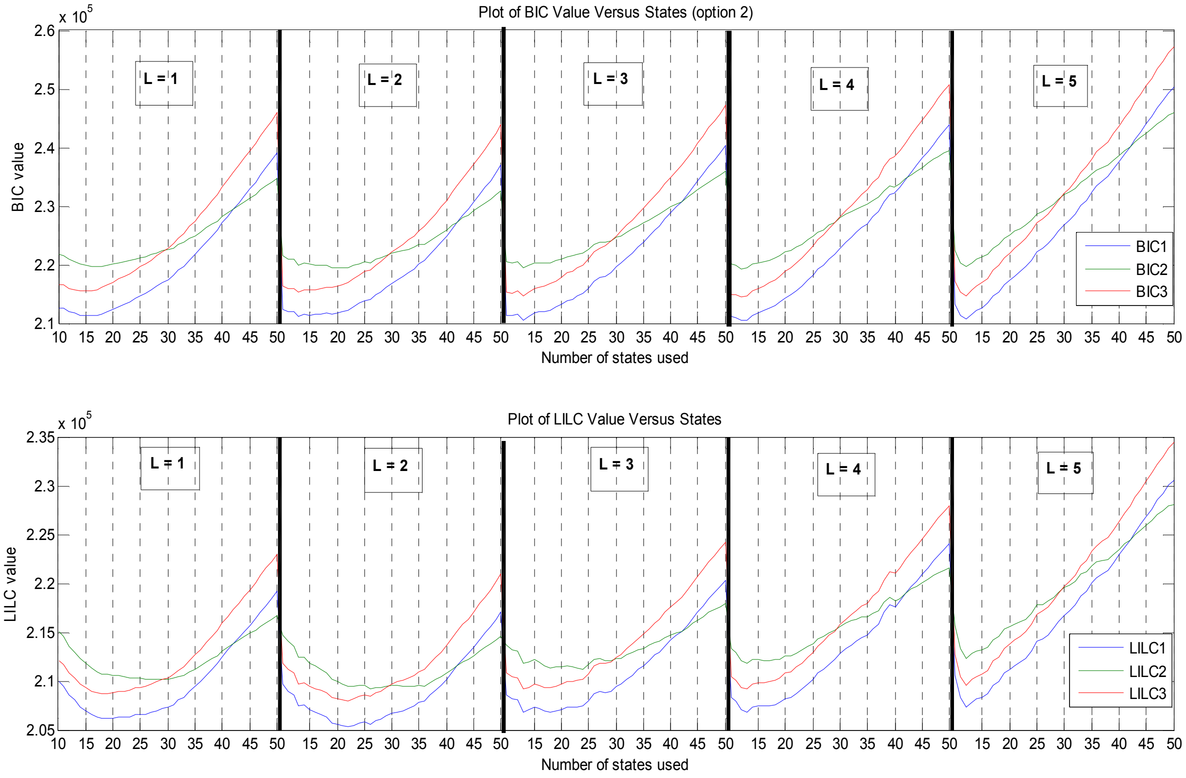

BIC1/LLIC1 – Eq. 4.39 BIC2/LLIC2 – Eq. 4.40 BIC2/LLIC2 – Eq. 4.41

Figure 4.9 BIC and LLIC computation for the monitoring-specific SS models (ABG) spanning lag size from 1 to 5 and state order from 10 to 50.

4.5.2 Fault Monitoring Statistics and Results

Similar statistics common to those used for PCA can be adopted and applied for CVA state space analysis. The computation of the covariance matrices in Section 4.2.2 is necessary to facilitate computation of the Hotelling's T^2 statistics on the state and output residuals. Hotelling's T^2 statistics based on the first k CVA states, Eq. 4.45, was used by Negiz and Cinar (1997a) and Simoglou, et al. (1999b). The covariance matrix of the k-dimensional state vector Σ_k, appearing in Eq. 4.45, is of unity covariance for the models developed due to method of CVA employed in deriving the states. Hotelling's T^2 and Q (SPE) statistics based on the residuals of the state and output matrix, as proposed by Simoglou, et al. (2002), were also employed, they are all listed as Eq. (4.45) to (4.49).

$$T_x^2 = \mathbf{x}\mathbf{\Sigma}_{\mathrm{x}}\mathbf{x}^{\mathbf{T}} \tag{4.45}$$

$$Q_{ey}^2 = \boldsymbol{e}_y\boldsymbol{e}_y^T \tag{4.46}$$

$$Q_{ex}^2 = e_x\boldsymbol{e}_x^T \tag{4.47}$$

$$\mathrm{T}_{\mathrm{ey}}^2 = \mathrm{e}_{\mathrm{y}}\Theta_{\mathrm{y}}^{-1}\mathrm{e}_{\mathrm{y}}^{\mathrm{T}} \tag{4.48}$$

$$\mathrm{T}_{\mathrm{ex}}^2 = \mathrm{e}_{\mathrm{x}}\Theta_{\mathrm{x}}^{-1}\mathrm{e}_{\mathrm{x}}^{\mathrm{T}} \tag{4.49}$$

The control limits were established on the same statistical assumption referenced by both Negiz and Cinar (1997a) and Simoglou (1999), that is, the statistics follow an F-distribution:

$$T_k^2 = \frac{k(n^2-1)}{n(n-k)}F_\alpha(k, n-k) \tag{4.50}$$

where n is the number of observations and $F_\alpha(k, n\text{-}k)$ is the value of the F-distribution with k and $(n - k)$ degrees of freedom for a significance level of α.

The two CVA state space models were developed using MATLAB (the model codes can be found in Appendix B). Attempts were made to measure the time lapsed from the start and completion of the code used to execute each model. The result was consistent with the expected improved model computational efficiency of the proposed ABG state space CVA model, this was elaborated on with reference to Table 4.1.

Table 4.4. Detection delay times of proposed CVA model with previously reported results.

	Delay	Statistics	PCA T^2	PCA Q	DPCA T^2	DPCA Q	CA Q	CA T^2
F1	**3**	T^2_{ey}/T^2_{ex}	21	9	18	15	6	33
F2	**12**	T^2_{ey}	51	36	48	39	33	36
F4	**3**	$T^2_{ey}/T^2_{ex}/Q_{ey}$	F	9	453	3	3	F
F5	**3**	All	48	**3**	6	6	3	27
F6	**3**	All	30	**3**	33	**3**	**3**	24
F7	**3**	All	**3**	**3**	**3**	**3**	**3**	**3**
F8	**24**	T^2_{ey}	60	60	69	63	60	87
F10	**72**	Q_{ey}	288	147	303	150	81	186
F11	**18**	T^2_{ey}/Q_{ex}	912	33	585	**21**	33	567
F12	**3**	T^2_{ey}/T^2_{ex}	66	24	9	24	9	63
F13	**90**	T^2_{ey}	147	111	135	120	123	147
F14	**3**	$T^2_{ey}/T^2_{ex}/T^2_{X}/Q_{ey}$	12	**3**	18	**3**	**3**	F
F15	**30**	T^2_{ey}	F	F	F	F	F	F
F16	**18**	T^2_{ey}	936	591	597	588	30	108
F17	**48**	T^2_{ey}	87	75	84	72	66	468
F18	228	T^2_{ey}	279	252	279	252	**225**	288
F19	**6**	Q_{ex}	F	F	F	246	441	F
F20	**189**	T^2_{ey}	261	261	267	252	222	252
F21	**765**	T^2_{x}	1689	855	1566	858	780	1527

Hotelling's T^2 and Q statistics on output residuals: T^2_{ey}/Q_{ey}; Hotelling's T^2 and Q statistics on state residuals: T^2_{ex}/Q_{ex}; Hotelling's T^2 statistics on the state variables: T^2_{X}.

Table 4.4 summarizes and compares the result obtained from the simulation runs and compares the detection delay time of the best performing monitoring statistics of the proposed model with previously published results of other statistical methods: correspondence analysis CA and (dynamic) principal component analysis (D)PCA carried out on the same simulator, see (Russell, et al., 2000; Detroja, et al., 2007). The method of declaring a fault was also adopted from these cited publications. A fault condition was declared to exist after the established control limit for any one of the statistics was exceeded for six (6) consecutive sample instance. The detection delay is then expressed as the time delay in number of samples between fault introduction and its detection.

The label "F" in Table 4.4 indicates that the fault was not detected. The five monitoring statistics given in Eq. (4.45) – Eq. (4.49) were applied independently and the best performing detection statistics for each fault case was noted. The statistics and model giving the quickest detection for a given fault is highlighted in bold in the table. Fault detection using the proposed CVA model not only detected faults quicker in most cases but was also able to detect faults (e.g. F15) for which the other statistics were not able to flag.

The bar charts in Figure 4.10 compare the fault detection performance of the proposed CVA based state space model (ABG) with Larimore's CVA based state space model (ABCDG). Some faults were readily detectable while others proved more difficult to detect or undetectable, this general categorization is differentiated in Figure 4.10. The undetectable or more difficult to detect faults are grouped and shown to the right-hand-side of the figure (Faults 3, 9, 15, and 21).

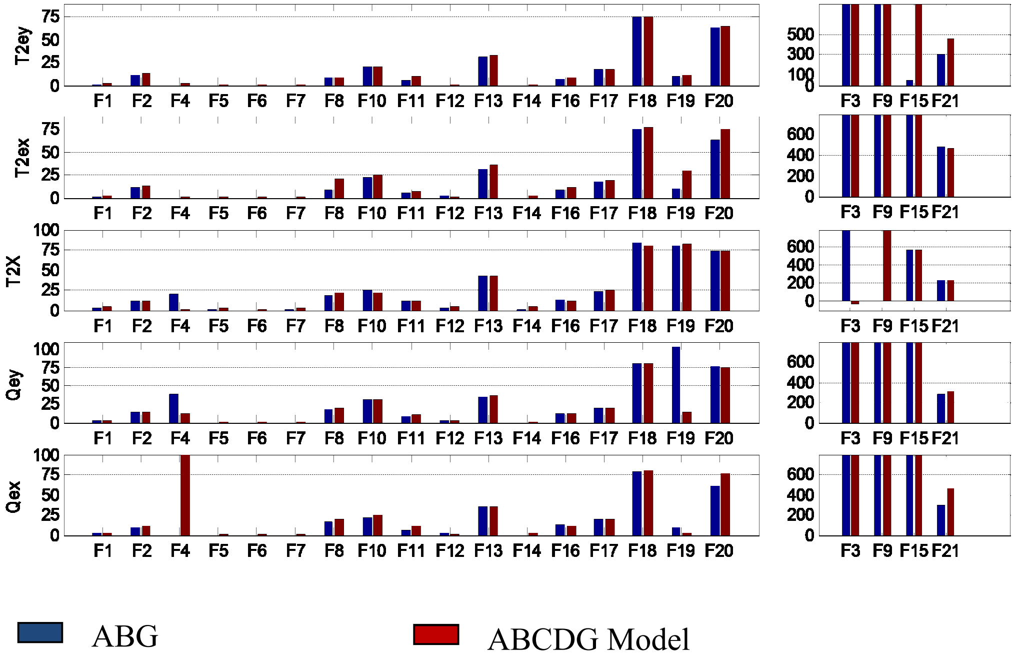

Figure 4.10. Fault detection delay time comparison of the 5 monitoring statistics across the 2 CVA state space models. Missing bars indicate zero detection delay time, negative bars indicate false alarm condition and full length bars indicate failed/missed detections.

Overall the performance of the proposed model is for the most part on par or in some cases slightly better than Larimore's state space model. Figure 4.11 shows the detection of Fault # 15 (cool water valve sticking fault) base on the five independent monitoring statistics using both the ABG and ABCDG CVA state space models. The results indicate that only the Hotelling's statistics on the output error $\boldsymbol{T_{ey}^2}$ of the ABG model was able to give early detection of the fault. All publications uncovered prior to 2010 reported failed detection of this particular fault. The Q statistics based on the proposed CVA model also provided modest improvement in the detection of Faults 20 and 21.

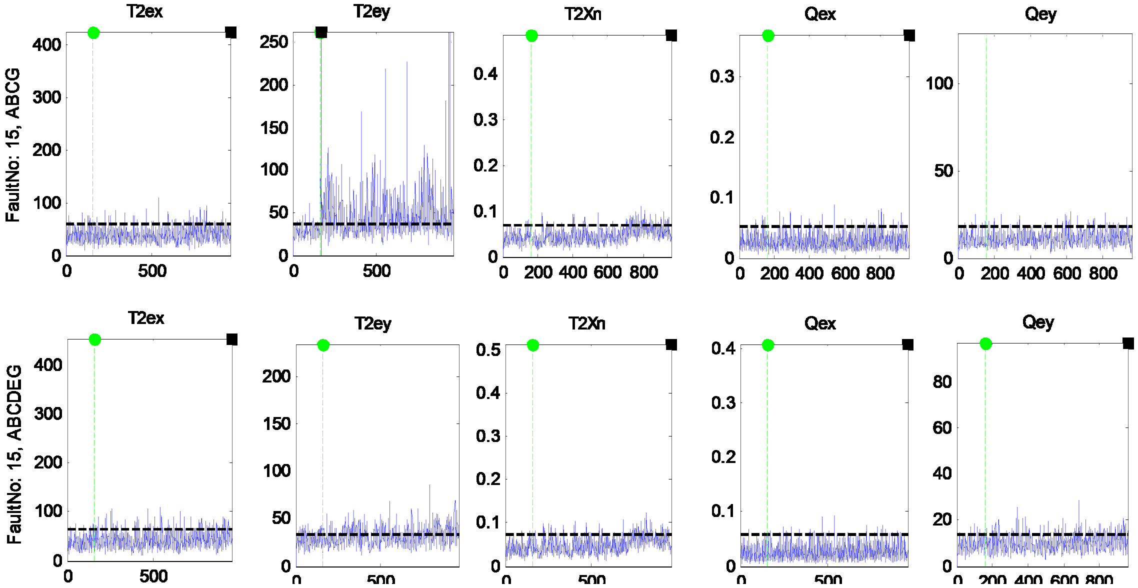

Figure 4.11. Detection of fault No. 15 using ABG and ABCDG state space models

Detection of a select set of faults using one the Hotelling's statistics computed on the output residuals ($\boldsymbol{T_{ey}^2}$) and applying the proposed ABG model is shown Figure 4.12. For some of the plots – the control limit line is not readily visible because of the scale of the y-axis for the particular fault monitoring statistics profile. A red circle appearing on the x-axis of each plot indicates the point of detection of the fault.

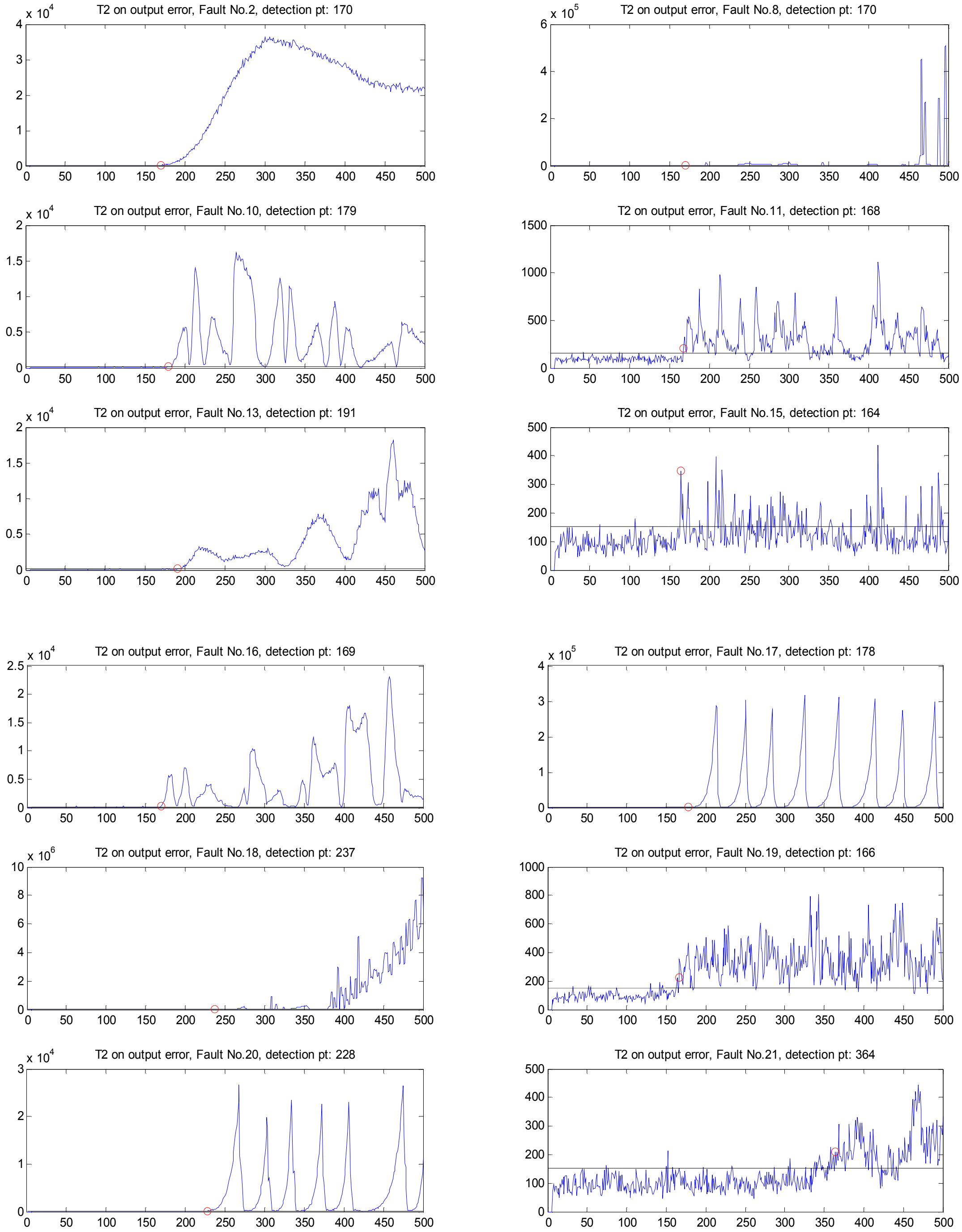

Figure 4.12 Fault detection performance of the Hotelling's T^2 statistics on the output residuals (ABG model).

A more recent publication by Odiowei and Cao (2010) also conducted a comparative analysis of their proposed state space independent component analysis SSICA approach against the performance of the CVA and dynamic independent component analysis DICA approach. The SSICA is essentially a combination of a first stage CVA state space model and a second stage independent component analysis ICA approach. The authors attributed the improved performance of SSICA over the usual DICA approach due to the fact that CVA SS model is better suited for capturing the dynamics of a process than a dynamic principal component analysis DPCA method upon which DICA is based. ICA method is said to be better suited for process characterised by non-Gaussian distribution.

Both detection delay times and percentage reliability metrics were analysed, Table 4.5 compares extracts of their results with the fault monitoring performance of the proposed CVA state space performance. The percentage reliability is defined as the percentage of the samples outside the control limits. The proposed model outperformed or detected on par with the SSICA/DICA method in terms of detection delay time for faults 1,2,4,5,6,7,11,12,13,14,16,17 and 19 but performed inferior for the remaining faults not including fault 21 which was not included in Odiowei and Cao (2010) fault simulation and analysis study.

In particular, Odiowei and Cao (2010) have reported successful detection of faults # 3 and # 9 with relatively high reliability. Based on the authors' literature review, no other publications have reported achieving such. Beside these two faults, the fault detection reliability was above 97% for all detectable faults for the proposed CVA state space model and therefore gave an overall better fault performance than both the DICA and SSICA schemes in that regards.

Table 4.5 Fault detection performance comparison of CVA versus DICA and SSICA

	Detection Delay time (mins)			Detection Reliability (%)		
Fault	**CVA***	**DICA**	**SSICA**	**CVA***	**DICA**	**SSICA**
1	3	9	9	98.58	99.75	99.75
2	12	15	12	99.44	99.50	99.63
3	-	21	15	-	19.48	73.03
4	3	6	6	99.80	99.88	99.88
5	3	6	6	99.88	99.88	99.88
6	3	6	6	99.90	99.88	99.88
7	3	6	6	98.61	99.88	99.88
8	24	33	18	98.52	98.75	99.88
9	-	48	18	-	46.82	91.64
10	72	96	18	97.54	96.13	96.75
11	18	18	18	99.44	99.38	99.38
12	3	15	15	99.58	99.50	99.50
13	90	96	18	97.60	96.13	96.25
14	3	6	6	98.57	99.88	99.88
15	30	15	12	99.68	99.50	99.63
16	18	21	18	98.75	99.25	99.38
17	48	48	18	98.75	98.13	98.38
18	228	21	21	99.80	99.25	99.25
19	6	6	6	98.57	99.88	99.88
20	189	72	18	98.61	97.13	97.63

4.6. Conclusions

The detection performance of a given fault detection scheme (model and statistics) is dependent upon both components of the system. A particular parameterization of a model may favour detection of certain types of fault over others. Hence, for some faults analysed, the detection delay time was sensitive to specification of the model in terms of state vector dimension and lead/lag window size.

A simplified CVA based state-space model design for the specific purpose of process monitoring was achieved using a simpler and more efficiently estimation of a reduced set of state space parameter matrices. The performance integrity of the state space model was maintained in conjunction with a dramatic reduction in the number of model parameters and simplification of the set of stochastic estimation equations used to derive the model parameters. Application results on the Tennessee Eastman benchmark process indicate that the proposed state space representation and model development technique provides comparable, and in many cases better, fault detection performance than the traditional CVA state space modelling technique. Most notable is the detection of fault No. 15 in the Tennessee Eastman benchmark process and the significant reduction in detection delay time achieved for the more difficult to detect faults. The overall best performing monitoring statistics in terms of fault detection and detection delay time is the Hotelling's T^2 statistics of the output residuals T^2_{ey}.

The fault detection performance also faired comparably to that reported for the DICA and SSICA schemes (Odiowei and Cao 2010) save for the unprecedented detection of faults # 3 and 9. However, for those faults detectable by the proposed CVA method, the percentage performance reliability was better on average than that of DICA and SSICA. Future research could explore what further fault performance improvements could be yield from combining the ICA approach with a CVA state space model as proposed in this paper.

Chapter 5 : Hybrid Model Based Approach to Process-Monitoring

5.1 Introduction

Previous researchers have proposed several different hybrid framework for process monitoring and modeling. Some methods have included hybrid approaches involving integration of different data driven modeling techniques, Yan (2010). Other approaches have considered combining linear or nonlinear data driven model based approaches with mechanistic model based approaches when there exist information about known kinetics, material balance equations, and other first principle or heuristic knowledge of the system being modeled or monitored (Lee, et al., 2005; Oliveira, 2004; Peres, et al., 2001; Psichogios and Ungar, 1992).

As it relates to the specific application of process performance monitoring and fault detection, Wachs and Lewin (1998) proposed model-based PCA and more recently McPherson et al (2002) proposed a super-model base approach to monitoring of batch processes. The main difference or improvement of super model-based PCA over model-base PCA proposed by Wachs and Lewin (1998) is that the hybrid model incorporated the use of an additional stage referred to as an error model. The error model was used to augment the mechanistic plant model to remove whatever remaining structure that may exist in its residuals, that is, the plant-mechanistic model residuals.

This chapter contributes to research and exploration into the suitability and advantages that a hybrid model architecture may offer to fault detection and process monitoring applications. Specific improvements and implementation considerations are given to the hybrid mechanistic-data driven model based monitoring scheme applicable to close-loop process operations. The impact of model-plant mismatches on the fault detection and monitoring performance is also considered. The work presented in this chapter demonstrates the feasibility of combining a statistical data based model with a mechanistic model implementation that does not require implementation of the plant control loops to perform fault detection.

The effectiveness of the hybrid mechanistic-data driven fault monitoring scheme and the problems arising from plant model mismatch when employing mechanistic first principle models are both analyzed using a simulated CSTR process with a recycle via a heat exchanger. The results provide evidence that both the prediction and fault detection performance of the mechanistic model can be enhanced by compensating the mechanistic or first principle model with a data-driven based statistical model. Linear PLS data-based modeling and a non-linear PLS implementation based on a quadratic PLS (QPLS) implementation originally proposed by Wold et. al (1989) were employed. Both data-based models proved to offer effective compensation for the mechanistic models implemented and the associated plant-model mismatch. The most suitable model for fault detection was identified from fault detection simulation analysis results.

An alternative hybrid scheme combining two different types of statistical data driven models was also explored. The hybrid architecture combines a neural network model with an ordinary least squares (OLS) regression model to map the nonlinear plant dynamics of a simulated distillation column developed using ChemCad version 6.

The remainder of the chapter is organized as follows. Section 5.2 provides an overview of the first principle equations applied in the development of the simulated CSTR. The subsection also explains the method used to introduce and evaluate the plant-model mismatch issue. In section 5.3 several hybrid modelling schemes are proposed and evaluated to assess what improvement the hybrid approaches bring to bear on the residual whitening and model predictive capabilities. In section 5.4 a subset of the hybrid models presented in section 5.3 is further analyzed and combined with Hotelling's T^2 and Q statistics to evaluate their fault detection performance. Section 5.5 documents an alternative hybrid data driven model scheme which combines two different classes of statistical data modelling approaches. The hybrid scheme was evaluated and applied to performance monitoring of a simulated distillation column.

5.2 The Plant, Model, and Fault Simulator

5.2.1 CSTR Plant Simulator

The CSTR system shown in Figure 5.1 is an adaptation of a similar model used by Zhang et al (1996) to evaluate the detection and diagnostic capable of principal component analysis PCA based monitoring scheme. The reaction model is one of an irreversible heterogeneous catalytic exothermic conversion of a reactant A to a product B. The control objective is to maintain the product concentration at a desired level by indirect control of the temperature, residence time and mixing conditions in the CSTR. A recycle product stream circulated via a heat exchanger (HTX) is used to facilitate the temperature control and ensure well-mixed condition. The reactor temperature is controlled by manipulating the flow rate of the cold water feed to the heat exchanger via a cascade control loop. The residence time is controlled by maintaining the level in the reactor.

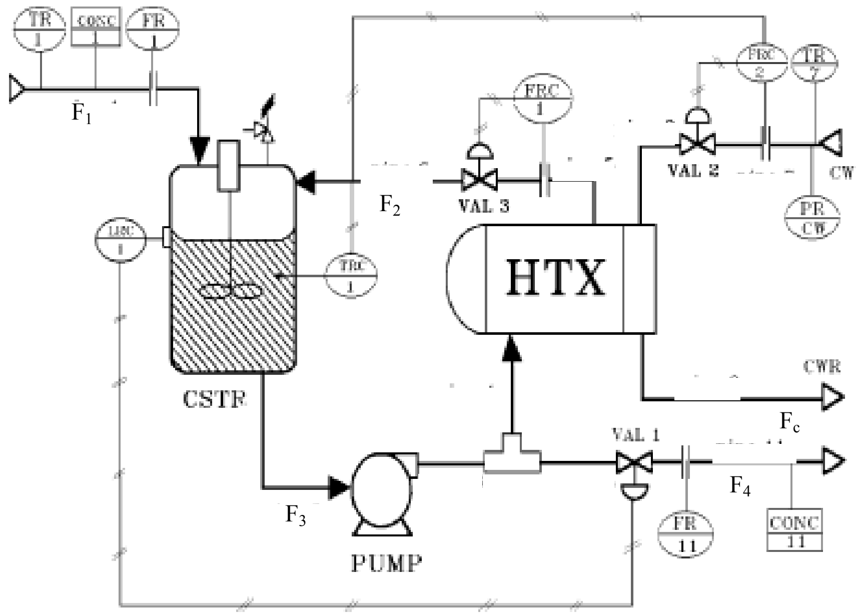

Figure 5.1. Continuous Stirred Tank Reactor CSTR with recycle loop via Heat Exchanger HTX.

The reaction and dynamics of the reactor was modelled using Eq.(5.1) through to Eq(5.6).

The rate of change of the liquid level *H* in the reactor is given by:

$$\frac{dH}{dt} = \frac{1}{A}(F_1 + F_2 - F_3) \tag{5.1}$$

where F_1 is the flow rate of the inlet stream, F_2 is the flow rate of the recycle stream and F_3 is the flow rate of the stream exiting in the reactor.

The rate of change of the reactant concentration C_r in the reactor is given by:

$$\frac{dC_r}{dt} = \frac{F_1 C_{r0}}{AH} + \frac{C_r}{AH}(F_2 - F_3) - a_r e^{-b_r/T} C_r^n \tag{5.2}$$

From the mass-balance applied around the reactor $F_2 – F_3 = -F_1$ therefore Eq. (5.2) maybe written as:

$$\frac{dC_r}{dt} = \frac{F_1}{AH}(C_{r0} - C_r) - a_r e^{-b_r/T} C_r^n$$

The rate of change of the product concentration C_p in the outlet stream F_4 is net of that being converted (generated) in the reactor, that which already exist in the tank outlet stream F_3 and the amount being taken away by the recycle stream F_2:

$$\frac{dC_p}{dt} = a_r e^{-b_r/T} C_r^n + \frac{C_p}{AH}(F_3 - F_2) \tag{5.3}$$

Again applying the mass balance equation Eq.(5.3) may alternatively be expressed as:

$$\frac{dC_p}{dt} = a_r e^{-b_r/T} C_r^n + \frac{F_1}{AH} C_p$$

The rate of change of the temperature in the reactor is given by:

$$AHB_2 \frac{dT_r}{dt} = B_1 F_1 (T_1 - T_r) - B_2 F_2 (T_r - T_2) + H_r a_r e^{-b_r/T} C_r^n \tag{5.4}$$

where T_1 is the temperature of stream F_1, T_2 is the temperature of stream F_2, and T_r is the temperature of the reactor.

The dynamics of the heat exchanger was modeled by the non-linear first order equation given by:

$$B_2 V \frac{dT_2}{dt} = B_2 F_2 (T_r - T_2) - \left(\frac{aF_c^b}{F_c + 0.5aF_c^b}\right) \rho_c c_c F_c (T_2 - T_c) \tag{5.5}$$

where $B_1 = \rho_r c_r C_{r0} + (1 - C_{r0})\rho_s c_s$ and $B_2 = \rho_r c_r (C_r + C_p) + (1 - C_r - C_p)\rho_s c_s$.

The pressure at the base of the tank is given by:

$$P_0 = H(\rho_r (C_r + C_p) + (1 - C_r - C_p)\rho_s) \tag{5.6}$$

The description of all the constants and variables for the model along with their assign values and steady state condition is provided in Table 5.1.

Table 5.1 CSTR Plant and Model Simulator Constants

CSTR Constants & Variables	Value	CSTR Constants & Variables	Model
Cross-sectional area of reactor, A	300 cm^2	Reactor liquid level, *H*	30.0 cm
Volume of heat exchanger, V	$1x10^3$ cm^2	Inlet Stream flow-rate, F_1	300.0 cm^3/s
Heat of reaction constant, H_r	$4.3x10^7$J/g	Recycle Stream flow-rate, F_2	200.0 cm^3/s
Constant specific to reactor, a_r	0.8 g/sec	Tank outlet Stream flow rate, F_3	500.0 cm^3/s
Constant specific to reactor, b_r	66.9 °C	Product Stream, F_4	300.0 cm^3/s
Constant of heat exchanger, a	$1.6x10^3$	Temperature of Reactor, T_r	50 °C
Constant of heat exchanger, b	0.5	Temperature of inlet, T_1	25 °C
Density of reactant/solvent, ρ_r / ρ_s	1.2 g/cm^3	Temperature of Recycle, T_2	- °C
Density of coolant, ρ_c	1.1 g/cm^3	Temperature of Cool-Water, T_c	25 °C
Specific heat cap. of reactant, c_r	0.9 J/g °C	Recycle Pump Pressure, ΔP	200 g/cm^2
Specific heat cap. of solvent, c_s	0.8 J/g °C	Cool-Water Inlet Pressure, P_c	200 g/cm^2
Valve Constant, valve 1	2.607	Conc. of reactant in inlet stream	0.8
Valve Constant, valve 2	7.8213	Conc. of product in reactor	0.7
Valve Constant, valve 3	1.134	Conc. of reactant in reactor	0.1
Reaction order, *n*	1		

5.2.2 The CSTR Simulator with Model Plant Mismatch

To understand the impact of model plant mismatches when applying mechanistic models for fault monitoring applications, model parameter errors of a specified magnitude were deliberately introduced in specifying the constants of the model. As such a subset of the plant constants were made to be different from the values used to implement the CSTR plant simulation model. The subset of constants and whether they were adjusted by a negatively or positively offset from the true constant value was randomly selected. The magnitudes of the offsets/error associated with each of the selected model parameters were defined to be a percentage of the true value of the constant. Table 5.2 provides an example of a randomly generated plant versus model constant assignment.

Other model-plant mismatches were experimented with by developing a mechanistic model based upon a simplified model of the actual CSTR equations along with the model constant errors. The simplification involved replacing the dynamic equations governing the heat exchanger with steady state equivalents Eq. (5.7) and Eq. (5.8) outline the changes made to derive the mechanistic model from the actual plant model. In the end, the simplified mechanistic model was aborted and deemed not useable because it resulted in controller output saturation problems and would therefore introduce undesirable non-linearity and discontinuity problems.

The steady state equation for the heat exchanger is derived from Eq. (5.5) by setting the rate of change of the recycle loop temperature term to zero:

$$T_2 = \frac{B_2 F_2 T_r + \left(\frac{aF_c^b}{F_c + 0.5aF_c^b}\right)\rho_c c_c F_c T_c}{\left(\frac{aF_c^b}{F_c + 0.5aF_c^b}\right)\rho_c c_c F_c + B_2 F_2} \tag{5.7}$$

For the case where the constant are given the assignments a = 2 and b = 1 the above reduces to:

$$T_2 = \frac{B_2 F_2 T_r + \rho_c c_c F_c T_c}{\rho_c c_c F_c + B_2 F_2} \tag{5.8}$$

Table 5.2 Model Mismatch Case: Plant vs Model Constants Employed

CSTR Model Constants	**Plant**	**Model**
Cross-sectional area of reactor, **A**	300 cm^2	300 cm^2
Volume of heat exchanger, **V**	$1x10^3$ cm^2	$1x10^3$ cm^2
Heat of reaction constant, $\mathbf{H_r}$	$4.3x10^7$J/g	$4.68x10^7$J/g
Constant specific to reactor, $\mathbf{a_r}$	0.8 g/sec	0.75 g/sec
Constant specific to reactor, $\mathbf{b_r}$	66.9 °C	68.2 °C
Constant of heat exchanger, a	$1.6x10^3$	$1.68x10^3$
Constant of heat exchanger, b	0.5	0.55
Density of reactant/product	1.2 g/cm^3	1.31 g/cm^3
Density of coolant	1.1 g/cm^3	1.08 g/cm^3
Specific heat cap. of reactant, c_r	0.9 J/g°C	0.913 J/g°C
Specific heat cap. of product	0.8 J/g°C	0.787 J/g°C
Valve Constant, valve 1	2.607	2.744
Valve Constant, valve 2	7.8213	8.568
Valve Constant, valve 3	1.134	1.11
Reaction order	1	1.044

Figure 5.2 illustrates the impact of the model plant mismatch for a subset of the process variables generated by the model. The deviation/offset of the model outputs from those of the actual plant is shown to increase with increasing percentages of model-mismatches. Note, however, that the difference in the plant-model outputs is bounded for the entire simulation run time for all cases of model-plant mismatch presented. This is a necessary condition for any model to be used for fault detection applications.

An independent index proposed by this study to quantify the plant-model mismatch is given by Eq. (5.9). The index computes the ratio of the squared residuals to that of the squared value of the steady state plant measurements, summed across all the process variables:

$$\gamma(i) = \frac{\sum_{j=1}^{m} \left(Y_{ij} - \hat{Y}_{ij}\right)^2}{\sum_{j=1}^{m} Y_{ij}^2} \tag{5.9}$$

where m is the number of process variables and i is the sample instance.

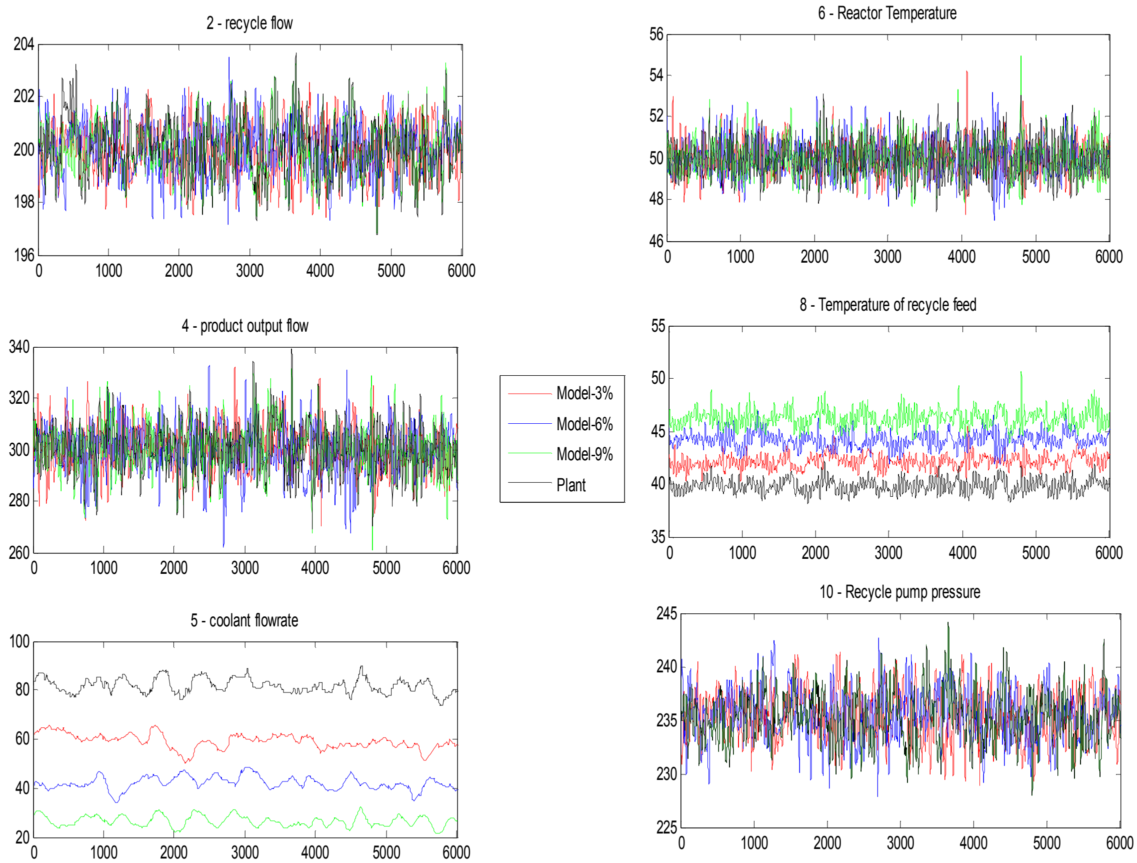

Figure 5.2 Plant vs Mechanistic Model Outputs for different size plant-model mismatch error.

Figure 5.3 provides a plot of the proposed index γ computed at several sample instances throughout the duration of the simulation. One can observe the dramatic increase in the impact of the model plant mismatches for relatively small percentage increase in the offset error associated with the model parameters. It can also be observed that the fluctuations in γ over duration of the simulation is more pronounced for larger plant-model mismatch error, indicating that the residuals in such cases will exhibit variability with more nonlinearity present.

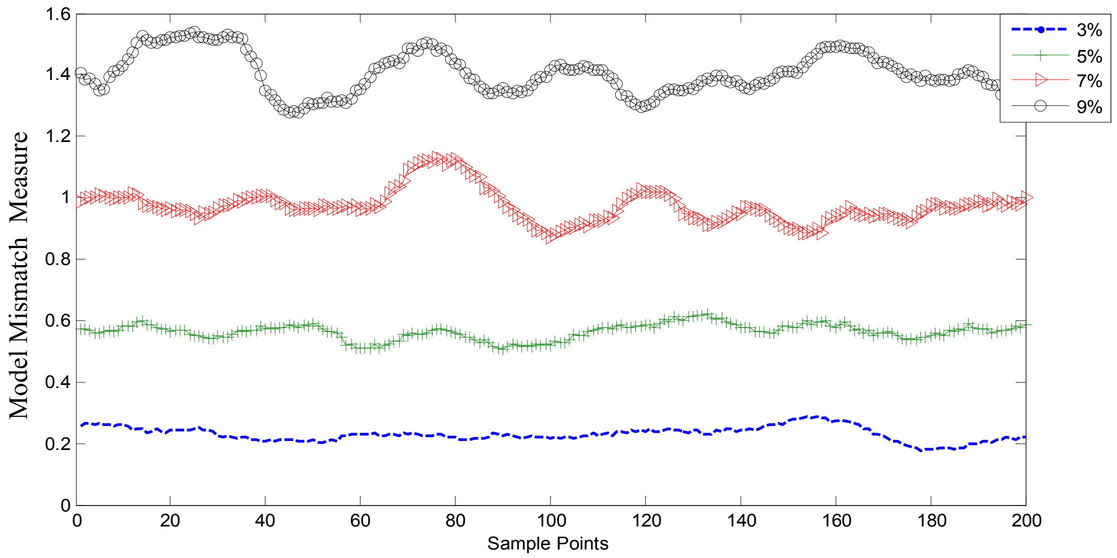

Figure 5.3 Mismatch index plot monitoring for four different level of plant-model mismatch.

5.3. Exploring Data Driven and Hybrid Model based Approaches

Figure 5.4Figure 5.4 shows two alternative plant-model interfacing of a process model to the process for online monitoring applications. The approach in Figure 5.4(a) is an approach proposed in previous publications (McPherson, 2007; Wachs and Lewin, 1999). In this approach, the model and process would share identical disturbance/load inputs and the plant controller implementation is included in the model. However, due to the model plant mismatch, in order for the feedback signal (control variables) of the plant and model to be maintained about the same set-point condition, the controller outputs (manipulated variables) would deviate from that of the actual plant controller outputs.

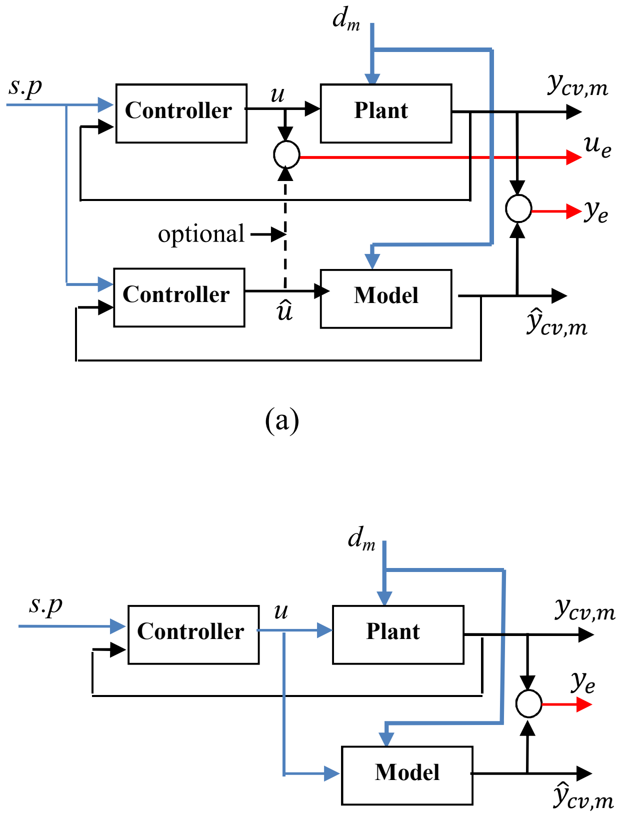

(a)

(b)

Figure 5.4. Mechanistic Model-Plant interfacing options along with compensation data driven model (a) Traditional Mechanistic Model-Plant interface (b) Proposed mechanistic-plant interface.

The second suggested interfacing shown in Figure 5.4(b) provides greater validation of the extent to which the process model actually approximates the real process. In this approach, the plant and the model shares identical actuating signals as it is possible to acquire the controller output signal directly from the data acquisition and control system. This approach would also alleviate the need for incorporating and ensuring correct replication of the plant controllers within the plant model.

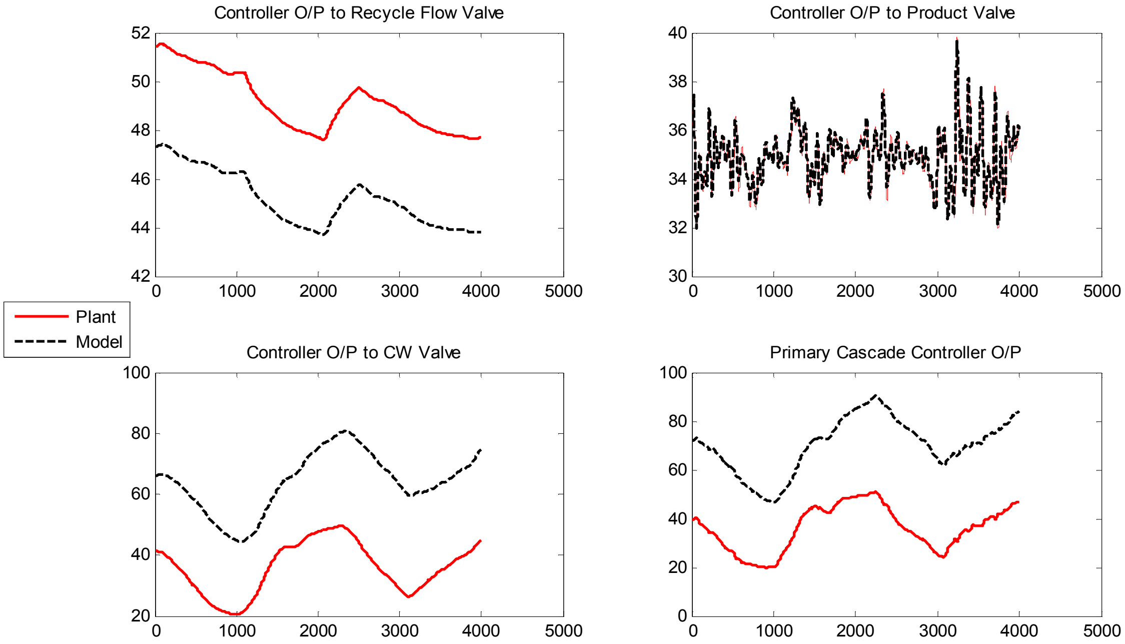

Figure 5.5 Plant-model offset in controller output (manipulated variables) due to mechanistic model implementation approach of Figure 5.7(a).

The difference in the two hybrid approach is further illuminated using the CSTR simulation model case study. Table 5.3 shows the list of all measured variables generated by the simulation and assignment as input or output variables depending on the mechanistic interface approached employed. Note the proposed interface possess far fewer residual outputs as the controller outputs would serve as inputs to the mechanistic model instead of output variables. The controller output being common to both the plant and mechanistic model will also facilitate fault diagnostic endeavours as the number of residuals to monitor to isolate the fault would be significantly less. Figure 5.5 illustrates the difference in the controller output observed when the traditional mechanistic model development is pursued. Three of the controller outputs deviated from that of the actual plant due to 9% model plant mismatch applied to some of the model parameters for the plant. Given these reasons, the option proposed in Figure 5.4(b) is a more attractive alternative.

Table 5.3 Simulated Process Variables – Input/Output Classification

PV No.	CSTR Process Variable	Proposed Mechanistic Interface	Traditional Mechanistic Interface
1	Reactant-Input Flow rate	Input	Input
2	Recycle Flow-rate	Output	Output
3	Outlet Flow-rate exiting Reactor	Output	Output
4	Product Output Flow-rate	Output	Output
5	Coolant Flow-rate	Output	Output
6	Reactor Temperature	Output	Output
7	Temperature of Input Stream	Input	Input
8	Temperature of Recycle Stream	Output	Output
9	Temperature of Cold-Water Stream	Input	Input
10	Recycle Pump Pressure	Input	Input
11	Cold-Water Pump Pressure	Input	Input
12	Reactant Conc. in Input Stream	Input	Input
13	Reactant Conc. In Product Stream	Output	Output
14	Reactor Liquid Level	Output	Output
15	Controller O/p to Recycle Flow Valve	Input	Output
16	Controller o/p to Downstream Flow Valve	Input	Output
17	Controller o/p to CW Valve	Input	Output
18	Primary Controller o/p Cascade loop	Input	Output
19	Reactor Temperature Setpoint	Input	Input
20	Reactor Level Setpoint	Input	Input
21	Recycle Flow-rate Setpoint	Input	Input

The residuals of the plant-model interface could be compensated using a data-driven linear or nonlinear statistical model as shown in Figure 5.6. The data based models are one-step ahead predictive model and generates an estimate of the residuals of the plant-model interface and subtract this estimate from the actual residuals to obtain a residual free from offsets, serial and cross correlation structures. The two implementations shown in Figure 5.6 is essentially a hybrid approach employing both a data-based model and a mechanistic model which is incorporated within the Plant-Model Interface block.

The specifics of the Plant-Model Interface block implementation and subsequently that of the hybrid compensation design may vary and is dependent on whether mechanistic plant-model interface approach of Figure 5.4(a) or Figure 5.4(b) is being applied. In the case of the favoured approach proposed in Figure 5.4(b), the controller outputs u instead of the setpoint inputs $s.p$ would serve as inputs to the compensation model and there would exist no controller output residual term u_e, refer to Figure 5.6(b). The data-based compensation model implementation may also differ along the choice of delay feedback inputs, Figure 5.6(a) uses the residuals as feedback inputs while Figure 5.6(b) shows the alternative of using the past plant and mechanistic model outputs instead to serve as feedback input.

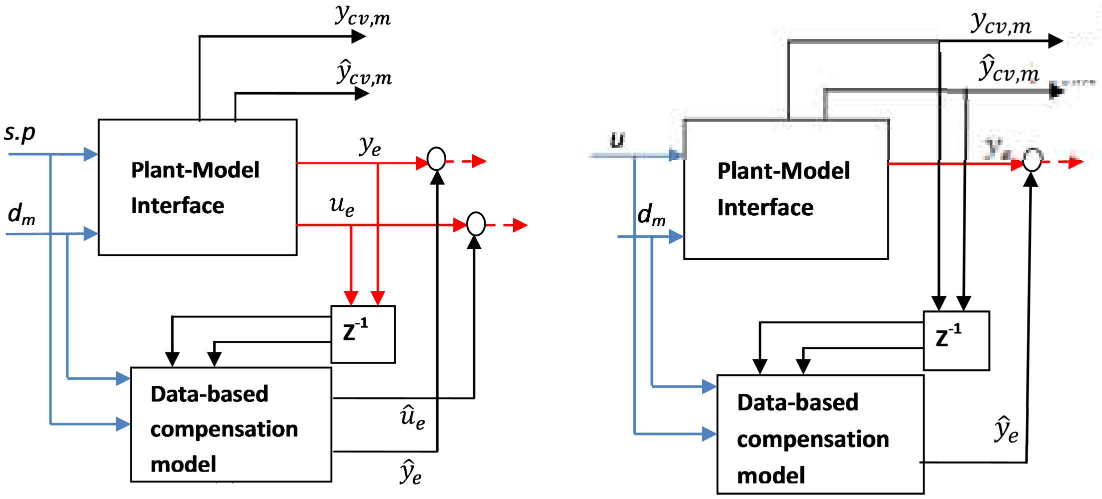

Figure 5.6 Data-based compensation model employing delayed feedback output of the plant and mechanistic model

All approaches described would ultimately derive a dynamic data-based model capable of capturing what remaining structure is still retained in the residuals of the plant-mechanistic model interface. For a dynamic system the current values of the variables are also dependent upon the past values. Thus, the model would be required not only to capture the linear relationship between $\mathbf{X}(t)$ but also $\mathbf{X}(t\text{-}1)$, $\mathbf{X}(t-2)$, and so forth. PLS can be extended to dynamic systems by carrying out a matrix expansion of the original data matrix with time-shifted duplicate vectors. By appropriate selection of the number of lags l to be included $\mathbf{X}(t-l)$, both the static and dynamic relationship between the variables can be captured.

$$\mathbf{X_d = [X}(t\text{-}1)\ \mathbf{X(}t\text{-}2)\ \mathbf{......X}(k\text{-}l)\mathbf{]} \qquad (5.10)$$

For the application reported in this paper, the **X** matrix composed of both input/disturbance measurements and past time-delayed output variables(control, manipulated, and monitored measurements). Implementation of a one-step ahead predictive model also meant that the response vector or matrix **Y** would comprise of the set of output variables at the current time instance:

$$\mathbf{Y} = [\mathbf{Y}_{\mathrm{m}}(t),\mathbf{Y}_{\mathrm{cv}}(t),\mathbf{U}_{\mathrm{cv}}(t)] \qquad (5.11)$$

where $\boldsymbol{Y}_{\mathrm{cv}}$(t) is the set of contol variables and $\boldsymbol{U}_{\mathrm{cv}}$(t) is the set of manipulated input variables and $\boldsymbol{Y}_{\mathrm{m}}$(t) is the set of monitored output variables not belonging to the two previously stated groups.

The non-linear QPLS model employed the same set of data for its input **(X)** and outputs **(Y)** matrix. In the case of the QPLS, several methods of parameterization of the quadratic inner relation were explored based upon the original work of Wold et al.(1989) and three variants of that approach investigated by Baffi et al.(1999b). All QPLS updating alternatives are linked by the Newton-Raphson linearization of the quadratic inner relation and for this specific case study there was no distinctive performance difference between the alternatives and so ultimately the original algorithm by Wolds et al. (1989) was used. For both the linear and nonlinear QPLS model the number of latent vectors employed by the model was automatically selected based upon cross-validation and convergence specification tolerance.

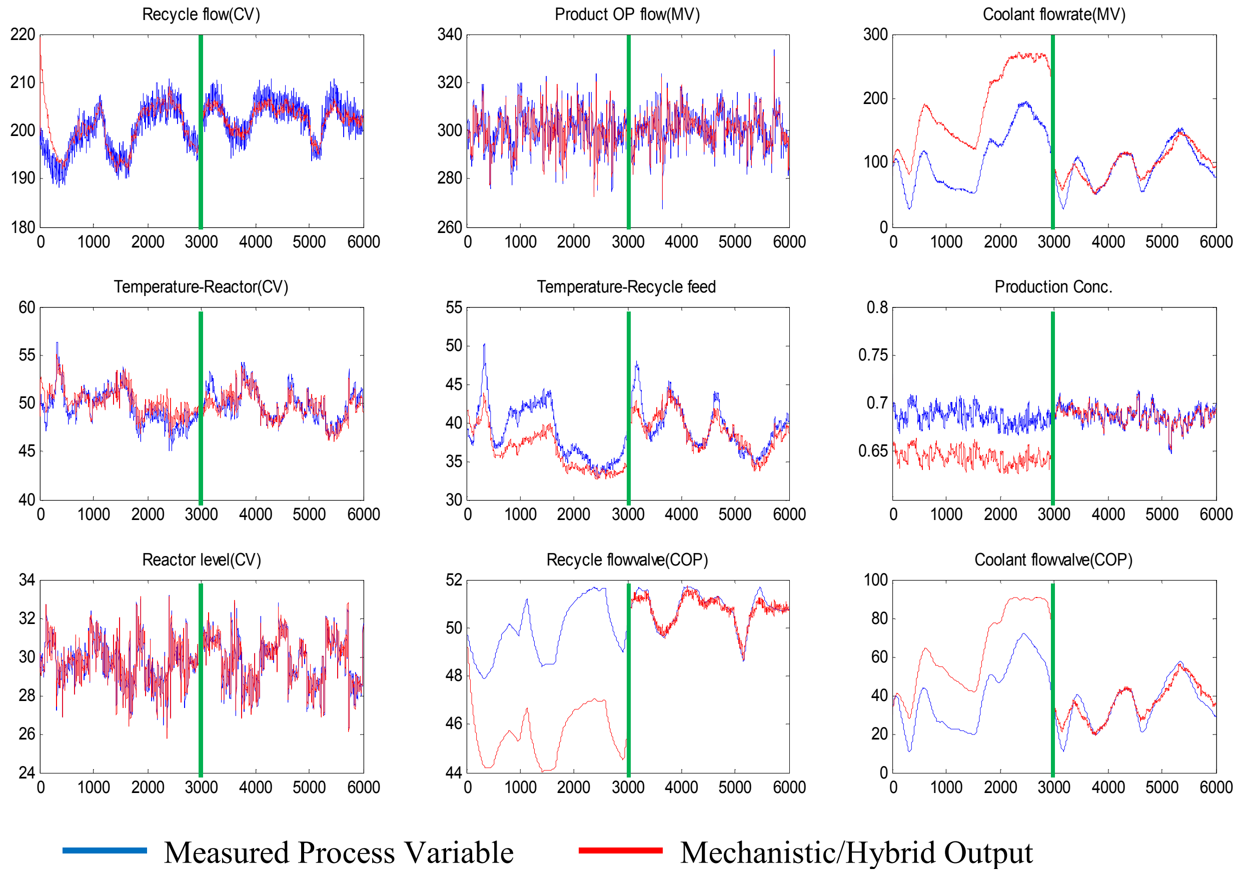

Figure 5.7 Mechanistic (left pane) versus PLS1 hybrid (right pane) one-step ahead prediction of plant measured variables. Mechanistic implementation of Figure 5.4(a) employed.

The impact of the data base compensation model is visually evident regardless of the mechanistic interface approach applied. Figure 5.7 demonstrates the improvement achieved after the PLS1 data based model is applied to the traditional mechanistic interface approach outline in Figure 5.4(a). Note that the model plant mismatches are not significantly manifested in any of the control variables (CVs) of the plant. This is expected as the control loops implementation in the mechanistic model will maintain the CVs about set-point regardless of the model plant mismatches. However, the manifestation is suppressed in the CVs at the expense of the manipulated variables (MVs) and controller outputs (COP) showing significant deviations relative to the actual plant measurement outputs. The improvement achieved by addition of the PLS1 model to form a linear hybrid implementation is shown in the right pane of each split figure window.

Even better results were obtained using the proposed mechanistic model interface strategy, Figure 5.8 shows the before and after impact of incorporating the PLS1 model as a data-based compensation model to implement an hybrid model, refer to Figure 5.6(b). In this approach the plant-model mismatch is not masked by the control loop since its driven by the same control output signals as the plant, hence there exist a more measurable difference between the plant and model control variables (CVs). However, the compensation data base model is more effective with this mechanistic interface approach because it is able to exploit the information content in the controller output signal to provide better correction, estimation (one-step ahead predictive tracking) of the other plant variables.

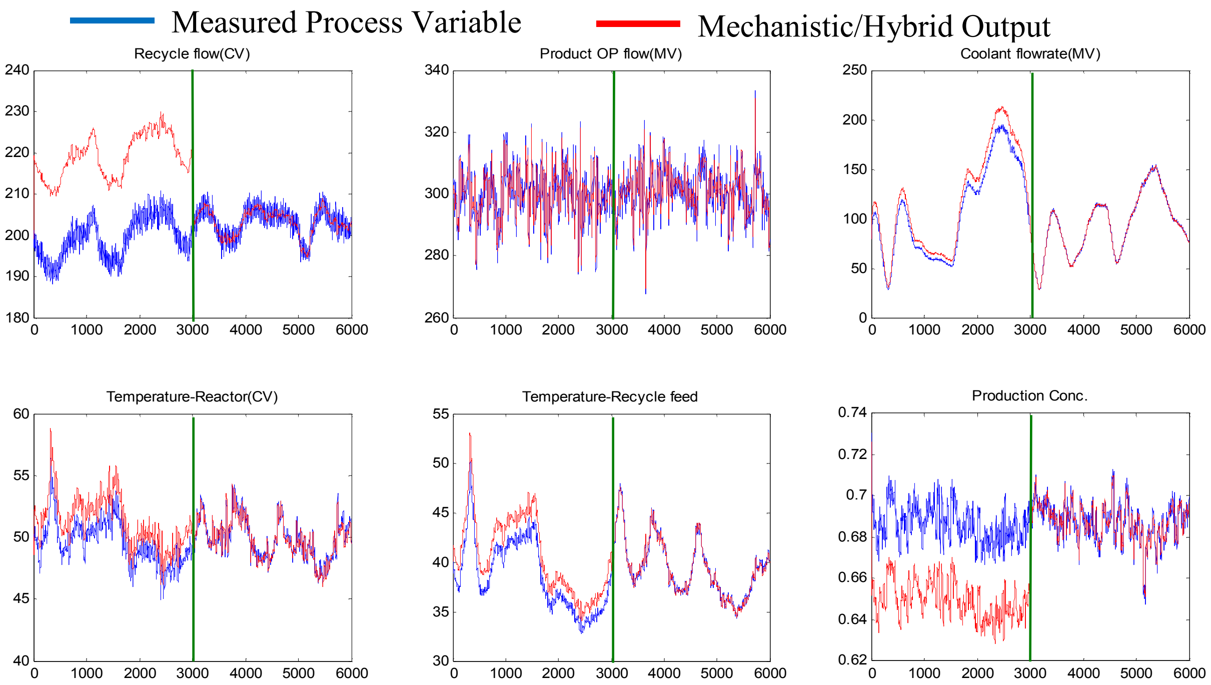

Figure 5.8 Mechanistic (left pane) vs PLS1 hybrid (right pane) prediction of plant measured variables. Mechanistic implementation of Figure 5.4(b) employed.

Table 5.4 compares the mean square error of the measured residuals of the compensated (hybrid) and uncompensated mechanistic model for both the traditional and proposed implementation. From the analysis thus far it is clear that the mechanistic online monitoring interface approach proposed and presented diagrammatically in Figure 5.4(b) is the most suitable implementation to pursue. Consequently all other hybrid alternatives to be investigated will apply the proposed mechanistic model interface approach.

Table 5.4 Process variables prediction MSE given as a percentage of the steady state process variable mean values

Output Variables	Traditional Implementation		Proposed Implementation	
	Mechanistic	Hybrid	Mechanistic	Hybrid
Recycle Flow (CV-MV)	0.004%	0.0058%	0.856%	0.004%
Product O/P Flow (MV)	0.0063%	0.0060%	0.004%	0.004%
Coolant Flow (MV)	116.2%	3.405%	1.577%	0.0087%
Temperature Reactor (CV)	0.021%	0.013%	0.937%	0.0030%
Temperature-RecycleFeed	0.6369%	0.092%	0.2172%	0.0020%
Product Concentration	0.324%	0.0015%	0.2357%	0.0011%
Reactor Level	0.0069%	0.0048%	0.0455%	0.0026%
Recycle FlowValve	0.682%	0.0020%	common	common
Coolant FlowValve	76.86%	3.365%	common	common
Product FlowValve	0.0024%	0.0019%	common	common

Table 5.4 summarizes the hybrid model variants that were employed for the fault monitoring experiments. A linear subspace modelling technique based on a PLS1 implementation and a nonlinear QPLS implementation were both employed. The hybrid alternatives are also differentiated by the type of feedback approach employed – feedback of the past residuals as shown in Figure 5.6(a) or the feedback of the past outputs as demonstrated in Figure 5.6(b).

Table 5.5 Summary of the Hybrid Mechanistic–Data Driven Modelling Schemes Investigated

Hybrid Model	Mechanistic Model Interface	Feedback	Statistical Method
HM1	Figure 5.4(b)	Residuals (y_e)	PLS
HM2	Figure 5.4(b)	Residuals (y_e)	QPLS
HM3	Figure 5.4(b)	Outputs($y_{cv,m}$)	PLS
HM4	Figure 5.4(b)	Outputs ($y_{cv,m}$)	QPLS

Figure 5.9 shows the plot of the normalized residual square error (NRSE) per output for the hybrid models HM1 to HM4. The results indicate that the nonlinear data based hybrid model accuracy of estimation is impervious to the choice of feedback as the red plots (HM2 and HM4) are essentially the same, giving roughly the same value for the total normalized residual sum squared error (NRSE) index. However, in the case of the linear PLS1 model, a significant improvement in the hybrid model output prediction is observable with a reduction in the total NRSE of more than 50% obtained when the hybrid model employs feedback of the actual plant and model outputs as oppose to feedback of the residuals.

The normal probability plot of the residuals before and after the data based compensation model is introduced also reveals the residual whitening effect achieved by the hybrid model. Figure 5.10 shows the normal probability plot of the residuals of HM2 against the residuals before the data based compensation model is added. The residuals of the Hybrid model all demonstrate a better approximation of a normal distribution free of any correlation structure.

If the fault detection capabilities of a model was entirely based on and directly correlated to its predictive capabilities then the two hybrid model of choice would have been HM2 and HM4 – the two hybrid approaches using a non-linear data based compensation model, one employing residual feedback and the other output feedback. However, as will be discovered in the next subsection, the best performing fault detection model turn out to be those based on the linear PLS1 data based compensation model.

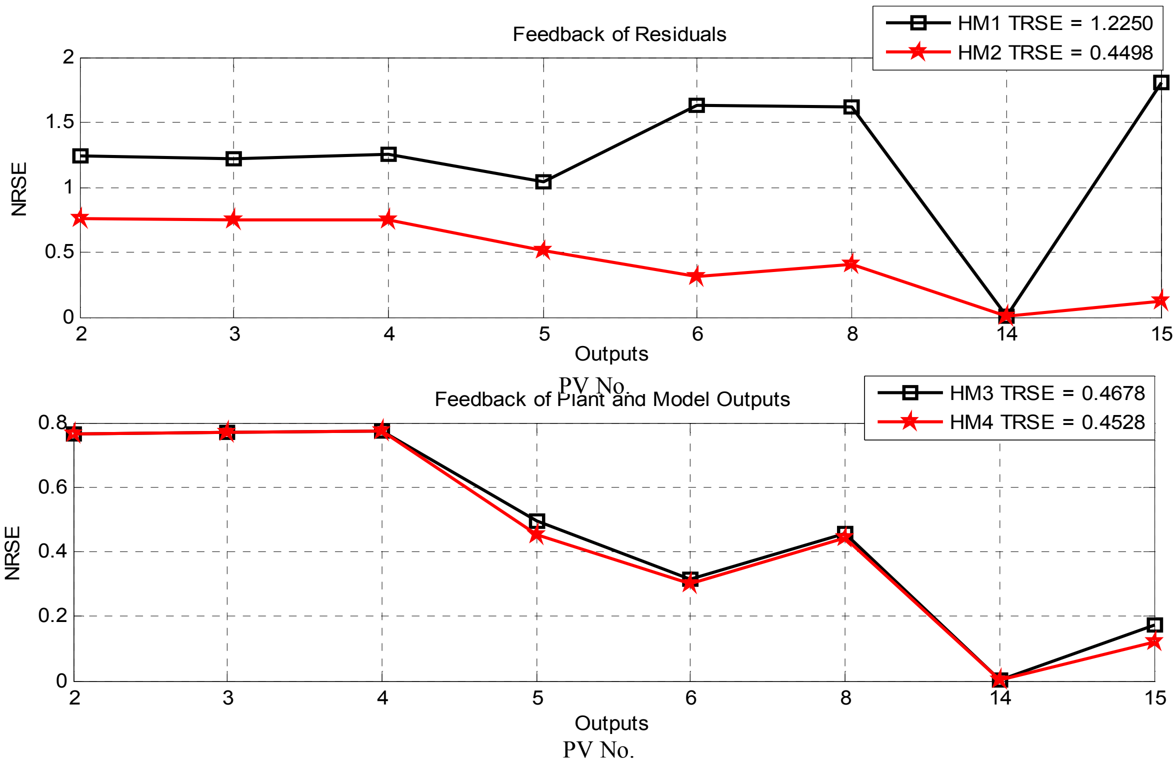

Figure 5.9 NRSE plots per output for hybrid model alternatives

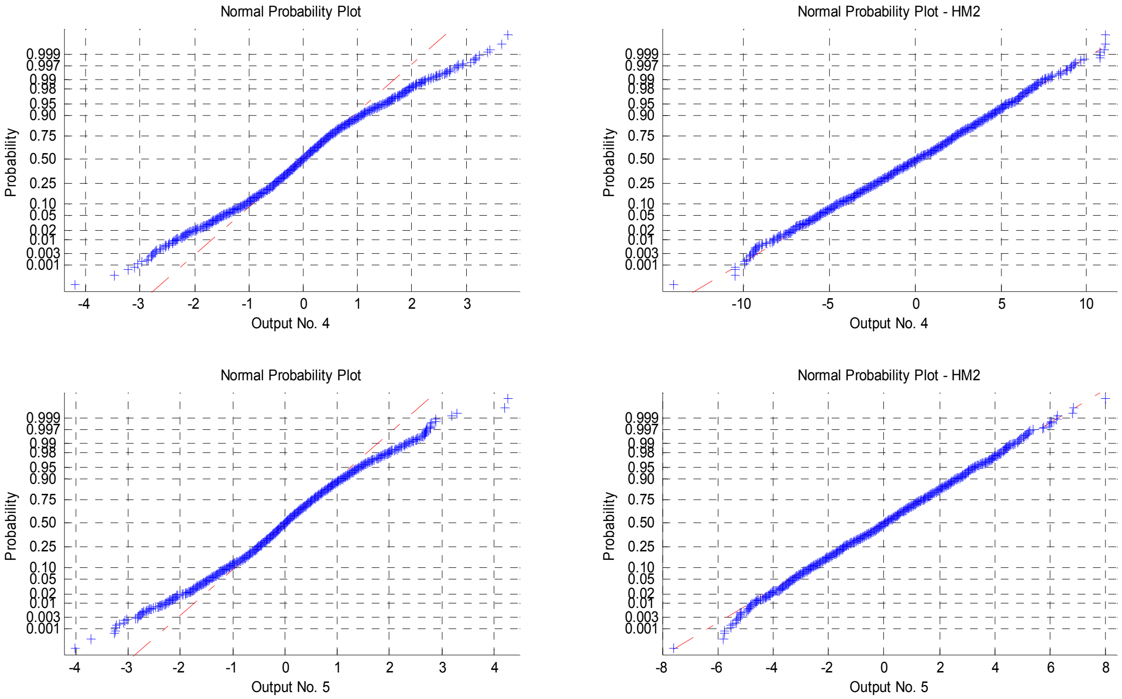

Figure 5.10 NN Hybrid model HM2 and uncompensated mechanistic model normal probability plot on residuals

For all of the model evaluation conducted and discussed in this section, the training data was acquired by applying pseudo random perturbations injected via the designated disturbance inputs of the CSTR process. The maximum level of the perturbations was set to be less than or equal to 5%. Additive measurement noise with a signal to noise ratio SNR of 5% was also simulated and added to the outputs of the CSTR including those used as feedback measurements for the various control loops. Figure 5.11 provides an illustration example of the perturbation applied to what are considered as input/disturbance variables of the CSTR model.

For the fault analysis section to be described in the subsequent section, the same process variable perturbations were applied. However, several single (independent) incipient faults were additionally simulated to investigate the fault detection capabilities of the proposed strategies in the presence of normal process background noise and perturbations.

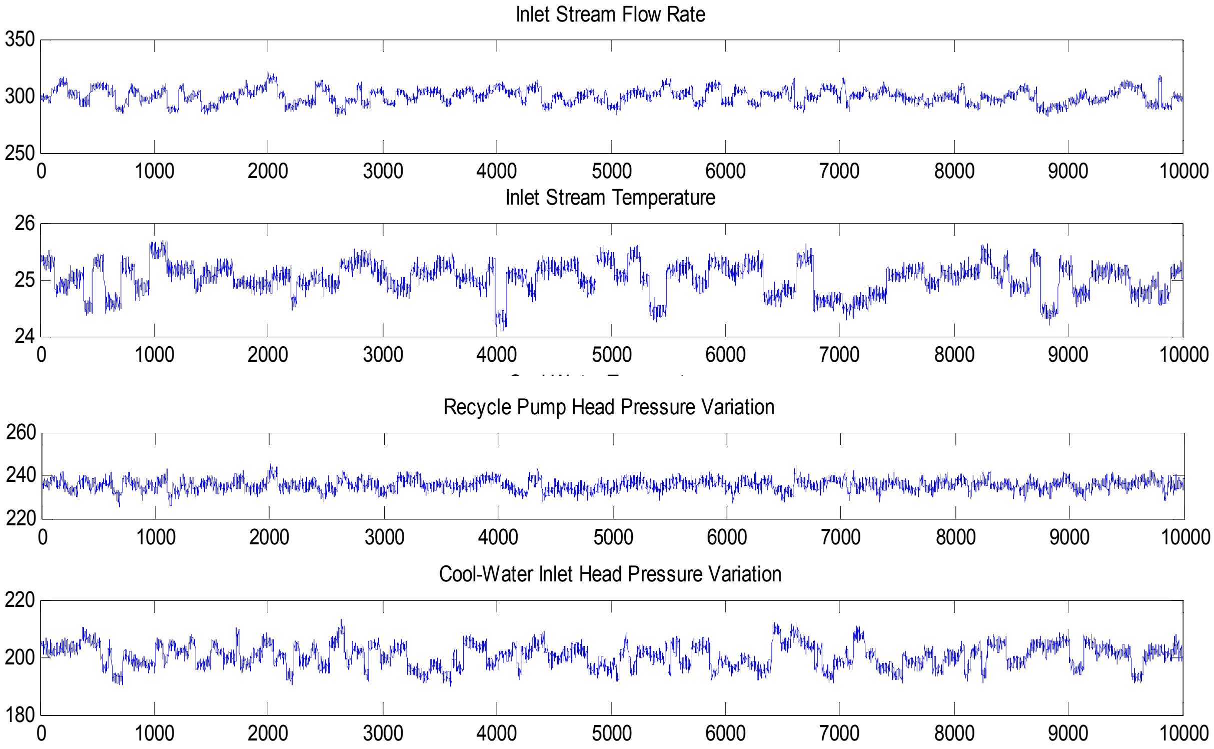

Figure 5.11 Simulated perturbations of CSTR input variables with additive noise.

5.4 Performance Comparison of Mechanistic and Hybrid Fault Detection Monitoring Schemes

5.4.1 The Fault Simulations

Figure 5.12 provides block diagram overview of a controlled process. Typical measurements available are categorized according to control variables y_{cv}, manipulated variables u_{mv}, and monitored variables y_m, and measured disturbance/input variables d_m. The diagram also classifies and indicates the general type of faults that maybe associated with a given process. The faults range from sensor errors such as calibration drift error, to unit operation faults such as heat exchanger fouling, pump pressure loss, to valve sticking faults. The three general fault categories are:

Fault Type 1 (F_p): This is an actuator or unit operation based fault such as a control valve sticking, heat exchanger fouling, a pump failure, etc.

Fault Type 2 (F_s): This is a sensor based fault such as sensor drift, offsets, and failure. The sensor in this case is located within a control loop and therefore may propagate its failure and affect other variables or parameters under control.

Fault Type 3 (F_s): This is also a sensor fault but the sensor in this case is not located within a control loop and may represent the measurement of a disturbance variable or some other monitored variable.

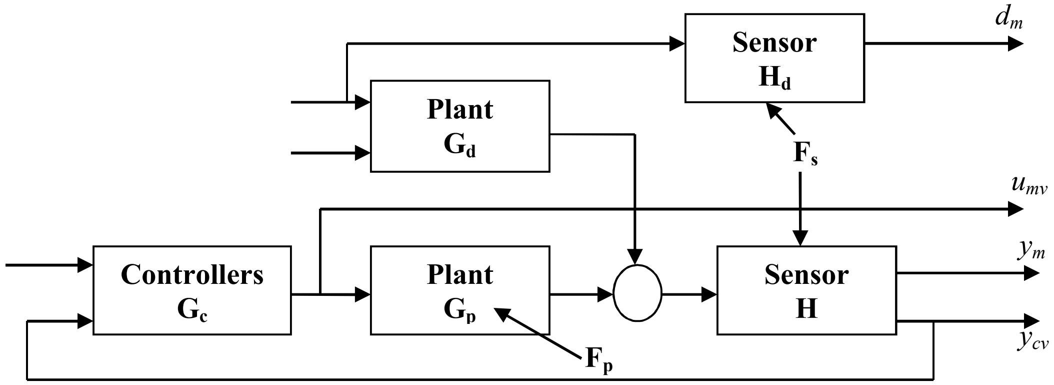

Figure 5.12. Plant overview showing unit operation faults F_p and sensor faults F_s within and outside the process control loop.

The manifestation of the faults in terms of process variables affected was dependent upon the type of fault and its location. Faults generated within control loops, be it of the sensor or unit operation type, tend to be more readily detected because of the propagating effect of the control loop. Other faults resulted in more subtle shift in the mean level of the auto-scaled process variables which would not be easily detected by an operator, relying on visual observation of trend charts, until perhaps the fault magnitude was much more severe. An example of such a fault scenario is shown in Figure 5.13(a), this is a developing pipe blockage fault and can only be observed to impact the mean deviation on the downstream flow controller output signal to the valve.

The valve sticking faults are of a dynamic nature and were only detectable under significant valve stem movement. The example provided in

Figure 5.13 Figure 5.13(b) is shown to generate unstable oscillatory effects, impacting the frequency content and standard deviation spread of the process variables affected.

The effect of a given fault on the process variable deviation, as shown in the two examples provided, can be very subtle and difficult to detect by mere visual monitoring of one or more of the process variables. An effective model-based fault monitoring system should, however, be able to detect such faults and do so within an acceptable time window relative to the onset of the fault. Subsequently, the time delay to the detection of a fault will be one of the key metrics used to evaluate the performance of the proposed hybrid schemes that will follow in the proceeding sections. It can also be observed that the impact of the fault on the monitored process variables is dependent on the specific fault in terms of its location and type. Case in point, the cool-water valve sticking fault impact is most visible via the onset of oscillation in the cool-water flow-rate measurements whereas the pipe blocking fault effect is more subtle and does not result in the onset of any oscillation.

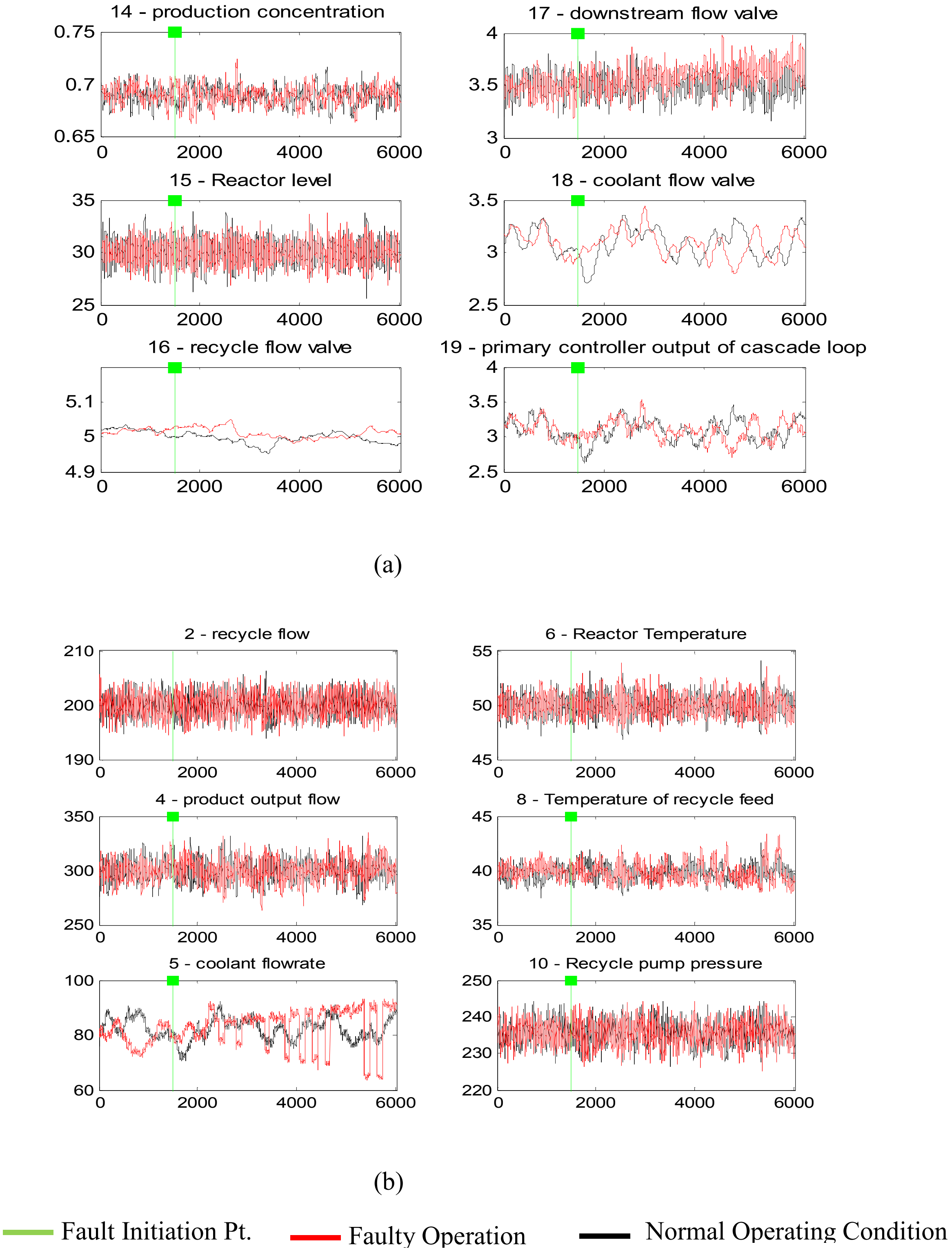

(a)

(b)

Figure 5.13 (a) Incipient fault - Product Stream Pipe Blockage (b) Incipient faults – Cool-water (CW) valve sticking

All faults were initiated at sample instance 1500. The incipient type faults were implemented using a constant drift percentage to produce a linear deviation from the true nominal reading over time. The incipient grow rate of the simulated faults differed, however, all sensor faults were implemented such that the maximum deviation at the end of each simulation run (5500 samples) was set to 10% of the measured process variable nominal value. Table 5.16 gives a list of the faults simulated and the fault type category classification of each.

Table 5.6 Simulated Fault Summary

Fault No.	Fault Description	Fault Type
1	Reactor temp. sensor drift	2
2	Reactant input stream temp. sensor drift	3
3	Recycle temp. sensor drift	3
4	CW feed temperature sensor drift	3
5	Recycle pump pressure sensor drift	3
6	CW feed pump pressure sensor drift	3
7	Reactor level sensor	2
8	Input stream - flow sensor drift	3
9	Recycle loop - flow sensor drift	2
10	Product-output flow sensor drift	3
11	Cool-water flow sensor drift	2
12	Heat exchanger fowling	1
13	Pipe Blockage-Recycle loop	1
14	Pipe Blockage-Product Stream	1
15	Pipe Blockage-CoolingWater Feed	1
16	Recycle Pump Failure	1
17	Valve Sticking – CoolWater Valve	1
18	Valve Sticking – Product Valve	1

5.4.2 Fault Detection

In this subsection the fault detection capabilities of the hybrid model variants proposed in Table 5.5 are analysed. The fault detection capabilities of the models were investigated by application of the both *SPE (Q)* and T^2 statistics on the hybrid scheme residuals and model input variables. The Hotelling's T^2 statistics was applied to the input variables such as the controller/manipulated variables input to the plant/mechanistic model. To do so the covariance matrix of the data set was first estimated from training data generated under normal operating conditions. The Q statistics was employed for monitoring of the residuals. The data base compensation incorporated in the hybrid schemes ensured that the residuals where void of structure thereby making them ideal candidates for Q statistics monitoring.

$$T^2 = \boldsymbol{u}^T \boldsymbol{\Sigma}^{-1} \boldsymbol{u} \tag{5.12}$$

$$\boldsymbol{Q} = \boldsymbol{y}_e^T \boldsymbol{y}_e \tag{5.13}$$

where $\boldsymbol{u}$ are set of input variables inclusive of process variable measurements on input streams and controller output to manipulating elements, Σ is the covariance matrix of the input vector of variables $\boldsymbol{u}$ and $\boldsymbol{y_e}$ is the set of residuals inclusive of monitored plant variables on the output streams and unit operations, manipulated variables, and control variables.

A combined index statistics as used in Yue and Qin (2010) was also employed for fault monitoring, the statistics was defined as:

$$\varphi = \frac{Q}{\delta^2} + \frac{T^2}{\tau^2} \tag{5.14}$$

where δ is the control limit on the Q statistics and τ is the control limit on the T^2 statistics. The method of deriving the control limits for the two statistics were elaborated on in Chapter 2.

A *Q* statistics was applied directly to the residuals of the mechanistic model-plant interface without any compensation data based model included. However, the fault monitoring approach proved to not be very effective having a detection success of about 50% across the 18 fault simulated. Some examples of the fault detection performance of this non-hybrid approach employing only the mechanistic model is shown in Figure 5.14.

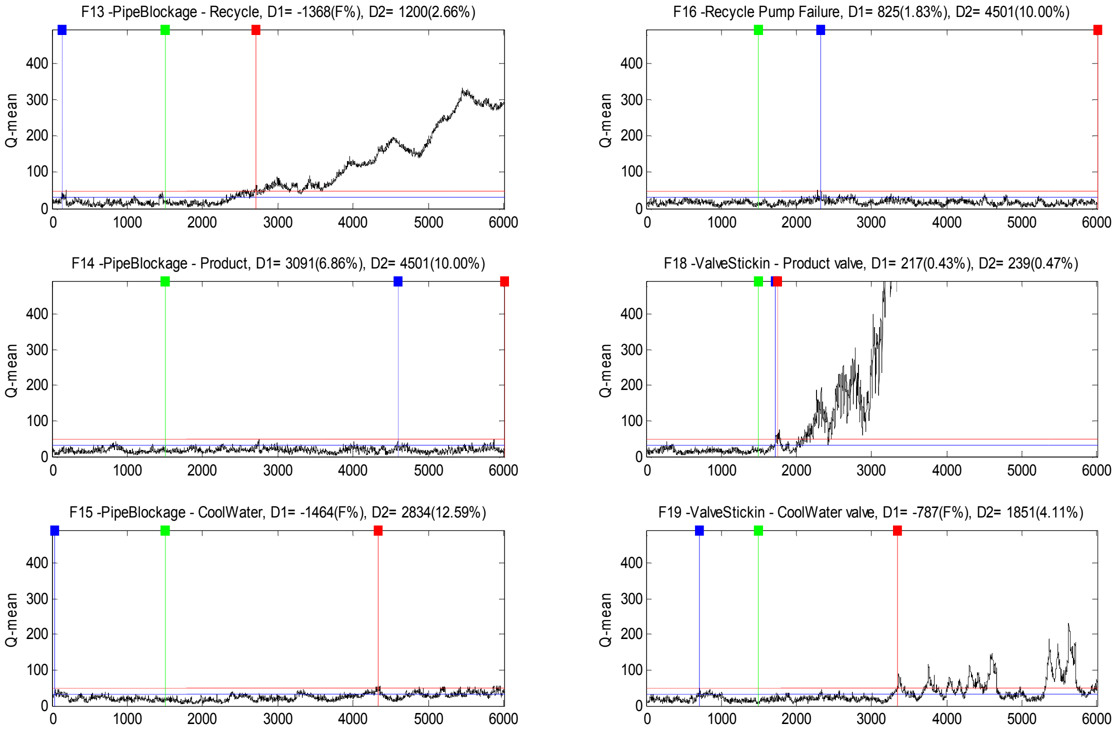

Figure 5.14 Fault Detection Performance of Mechanistic Model (non-hybrid approach) using a Q statistics monitoring index.

A possible reason behind the failure of the mechanistic monitoring approach to detect certain faults is revealed in Figure 5.15 by way of highlighting the impact of the heat exchanger fouling fault on the measured process variables and outputs of the mechanistic model. Examination of Figure 5.15(a) shows that only two of the nine variables shown are impacted by the fault. These two particular variables – a manipulated variable and a controller output variable have a persistent offset between the actual process measurement and the simulated mechanistic output equivalent due to the model plant mismatch. The deviation of the actual plant variables due to the fouling of the heat exchanger is in such a direction that actually diminishes the offset between the mechanistic outputs and the plant variables relative to what pre-existed before the fault condition was simulated. Therefore, as the *Q* statistics is based on the summation of the square residuals across all the variables, Figure 5.15(b) illustrates why the summation statistics would retreat and remain below the normal operating condition control limit instead of growing and exceeding the control limit.

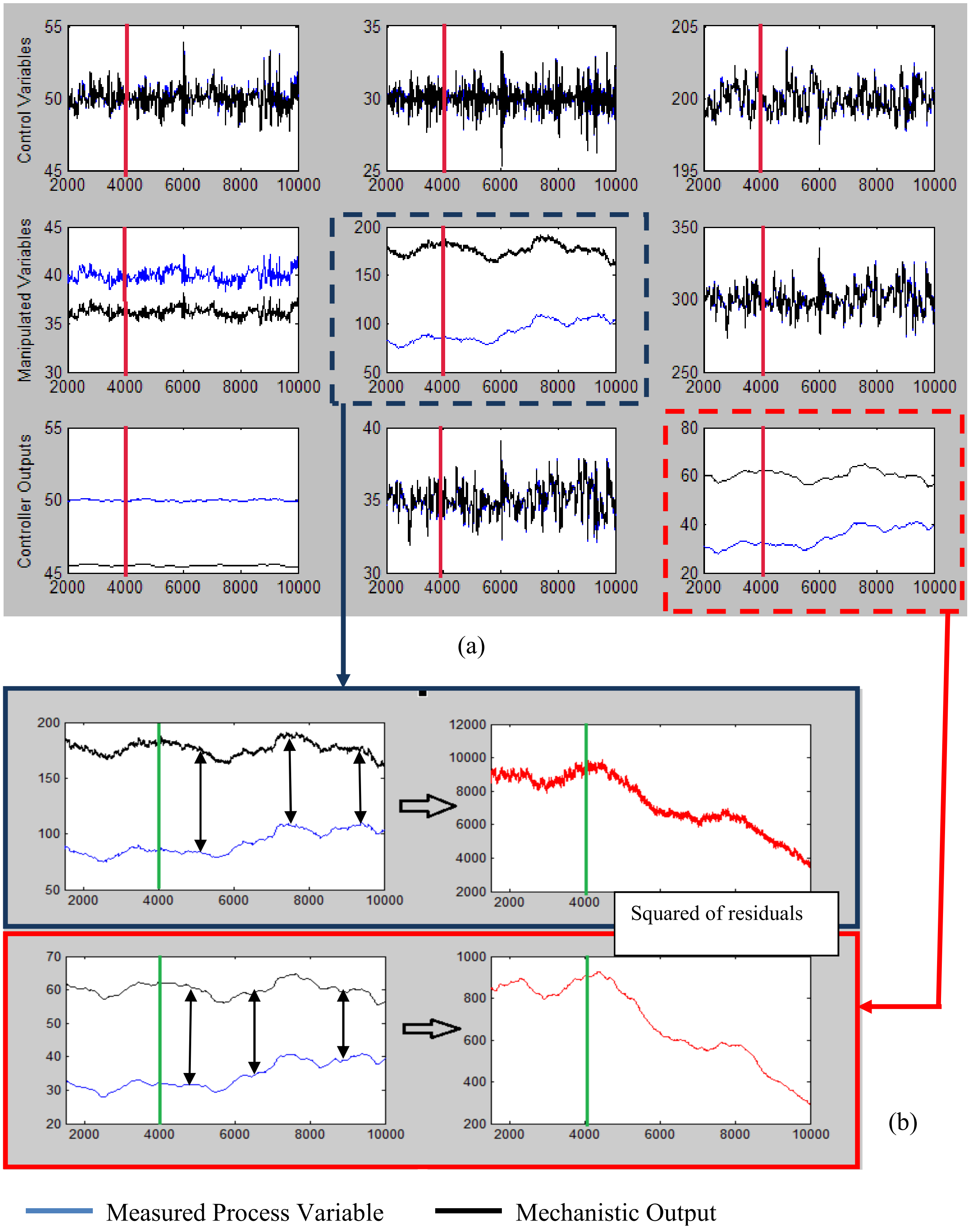

Figure 5.15 **(a) The impact of the heat exchanger fouling fault on the measured process variables and mechanistic model output (b) The gradual decline in the magnitude of the squared residual after the fault is initiated.**

The detection success is dramatically improved when the data based model is included to create the hybrid model based approach and Figure 5.16 demonstrates why this is the case. The impact of the same heat exchanger fouling fault analysed earlier for the case of the mechanistic model based only approach is again considered. Monitoring statistics derived from separately monitoring the output residuals and input variables is shown to provide reliable detection of the developing fault. The Q statistics based on the residuals was, however, able to give a faster detection of the fault.

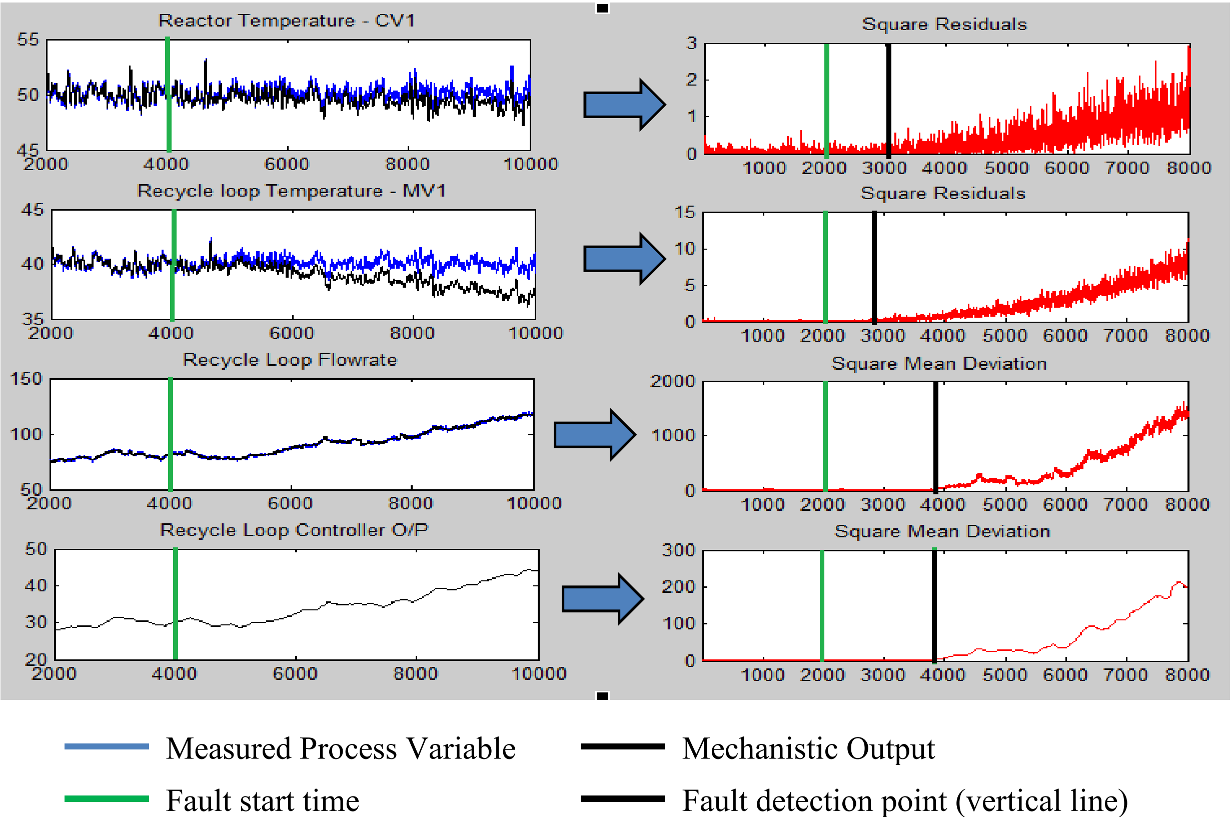

Figure 5.16 Heat exchanger fouling fault impact and detection via hybrid mechanistic – data driven model

The success of the *Q* statistics is further demonstrated in Figure 5.17. The *Q* statistics monitoring of the four hybrid models (HM1 to HM4) were analysed across the 18 simulated faults, Figure 5.17 provides a sample of the results obtained. For all the faults that were detectable (faults 1 to 16) using the *Q* statistics, hybrid model implementation HM3 proved to be the most sensitive *Q* statistics based monitoring metric providing the sharpest gradient of ascent as the fault magnitude increased.

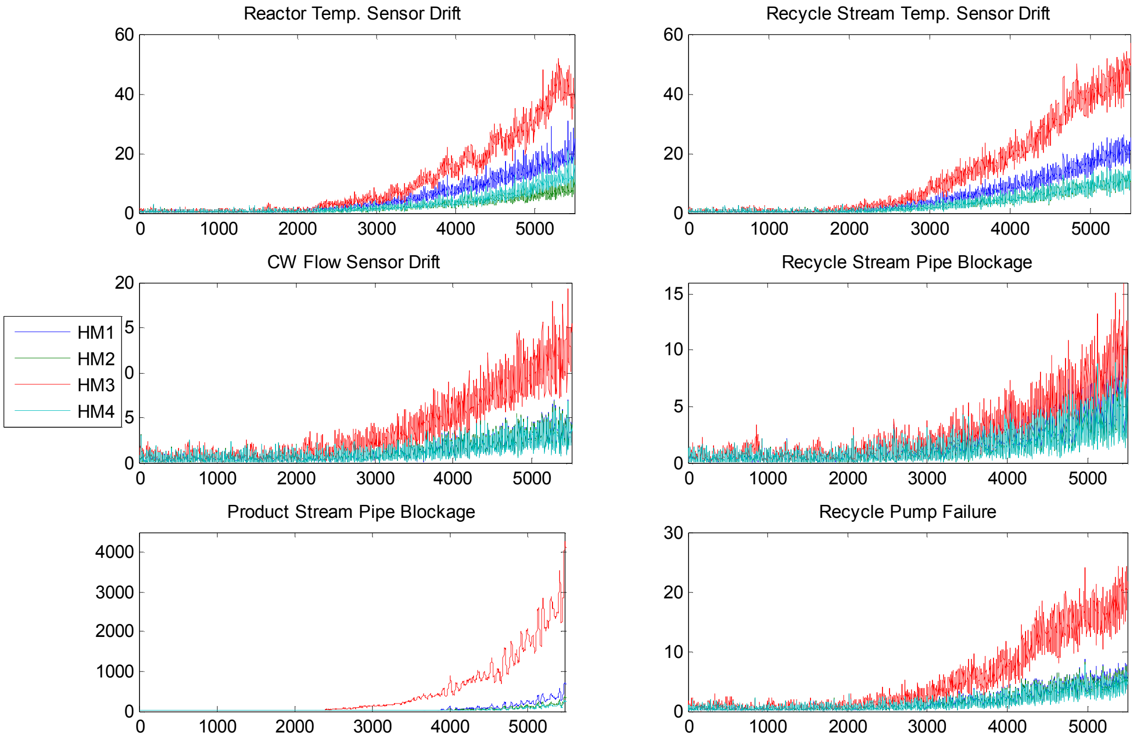

Figure 5.17 Fault detection monitoring using Q statistic applied to the residuals of the 4 different hybrid model variants.

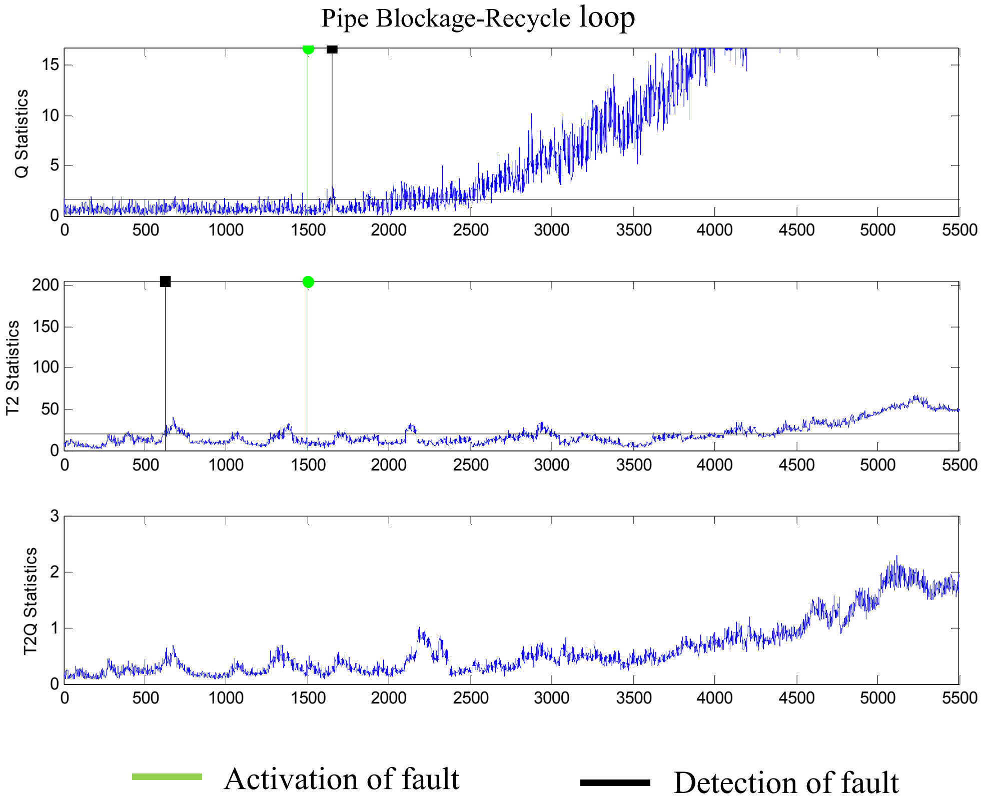

Figure 5.18 Detection of recycle pipe blockage fault using Q, T^2 and combine index monitoring statistics on the hybrid HM3 model.

The combined index statistics proved to provide no additional detection capabilities than the two independent Q and T^2 statistics. That is, if detection of the fault was not achieved by either the Q or T^2 statistics then the combine index statistic also failed to detect. Further, the detection using a combine index monitoring was sometimes degraded if one of the Q or T^2 statistics failed to give good detection. In the case of the recycle loop pipe blockage detection shown in Figure 5.18, the T^2 statistics was ineffective, however, the statistic was more responsive than the Q statistics for the level sensor drift fault shown in Figure 5.19. Table 5.7 provides a fault detection delay summary of the 18 faults analysed, a negative detection delay time indicates an early premature detection (false alarm) and the letter “F’ is to indicate no detection achieved.

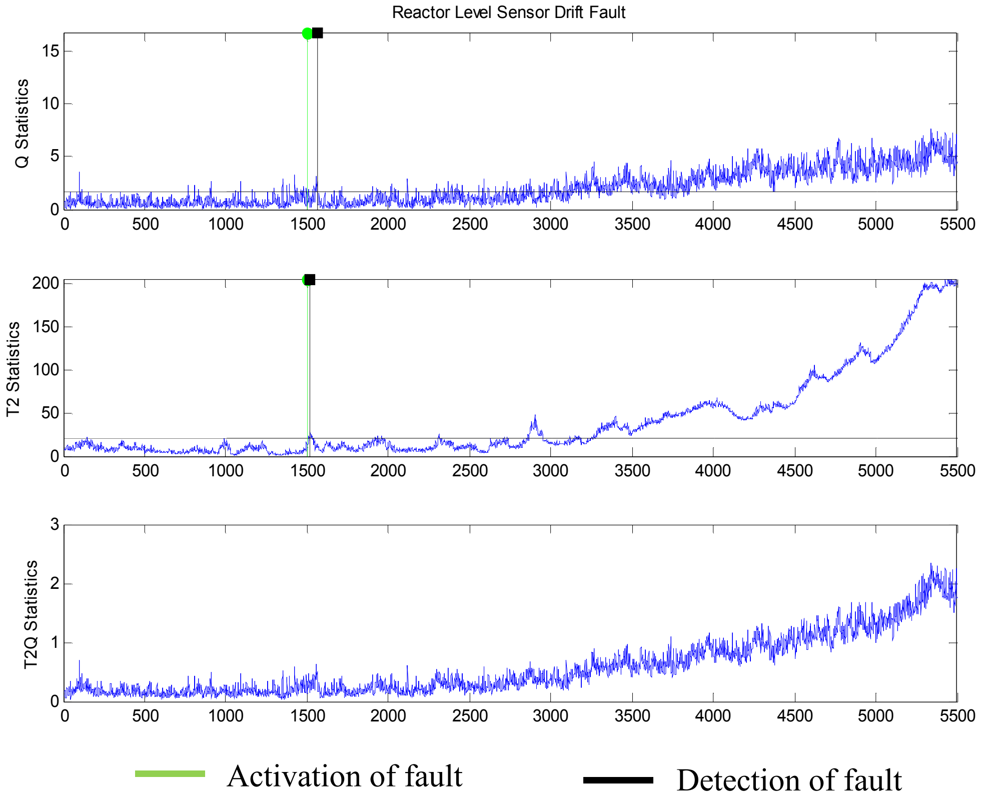

Figure 5.19 Detection of reactor level sensor drift using Q, T^2, and combine index statistics on the hybrid HM3 model.

The Q statistics, even for the HM3 model, did not give 100% detection success, for a few of the faults, detection relied on the Hotelling's T^2 statistics, case in point – recycle pump pressure sensor drift (fault no.5). Only two of the eighteen faults simulated - the valve sticking faults, proved undetectable by either statistics. However this was not surprising as such a fault has explained earlier would not be detectable during a typical steady state plant operation. The fault manifestation at best would be transient and only for the case of setpoint changes or if the plant disturbances required sizeable and significant movement of the particular valve opening to maintain desirable operating conditions

The Hotellings T^2 statistics was found to be more subject to false alarm conditions because the statistics was computed using the autoscaled process variables that served as input to the mechanistic model. This meant that unlike the residuals which would essentially be free of correlation structure, the input variables distribution would not be consistent with that of a normal distribution. Figure 5.18 gives an example of a misdetection occurrence using the T^2 statistics.

Table 5.7 Fault detection delay times for all hybrid models

Fault No.	HM1 - Q	HM2 - Q	HM3 - Q	HM4 - Q	T^2
1	889	1354	736	1354	-769
2	2054	3045	830	3190	1529
3	716	1283	605	1253	F
4	3009	F	901	F	-1107
5	F	F	F	F	298
6	3072	3167	1801	3170	615
7	1681	3061	62	2753	15
8	850	1128	179	1163	2173
9	1063	1319	808	1319	705
10	1123	1506	22	1506	360
11	2300	2300	651	2300	F
12	1008	1279	1005	1279	400
13	1871	2173	154	2241	-873
14	1006	1077	311	1144	3000
15	1874	2057	1119	2057	F
16	F	F	F	F	580

The chart shown in Figure 5.20 provides related results to those presented in Table 5.7, it provides a measure of how early each fault was detected in terms of the extent to which the fault had progressed or developed. The measure is given as a percentage deviation from the correct output measurement in the case of a faulty sensor or a percentage deviation from the nominal level or ideal parameter value as in the case of the heat transfer coefficient *U* value which was adjusted to simulate the heat exchanger fouling effect. The simulated faults were not implemented with all the same incipient growth rate so an identical detection delay time does not necessarily translate into the same fault magnitude condition at the point of detection. The chart provides an insight into the minimum level of a sudden fault that would be detectable by each hybrid model using the Q statistics on the hybrid model residuals.

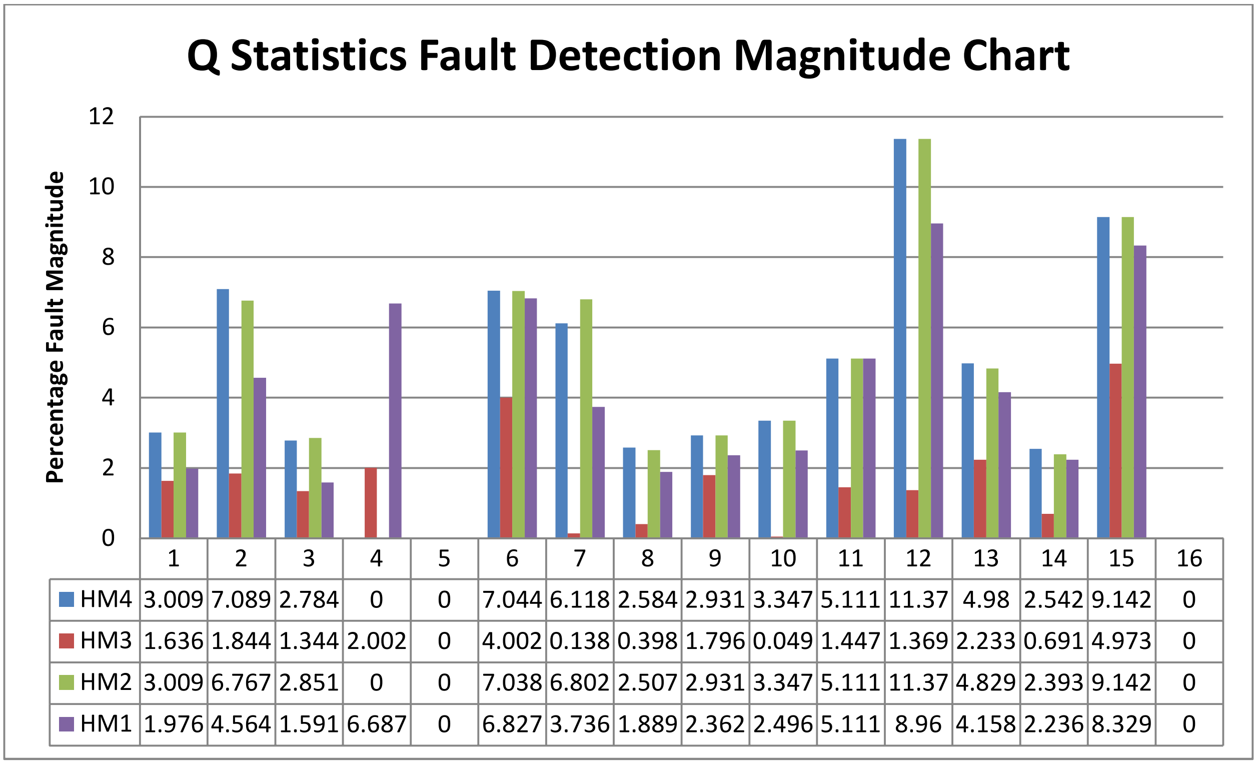

	1	2	3	4	5	6	7	8	9	10	11	12	13	14	15	16
🟦 HM4	3.009	7.089	2.784	0	0	7.044	6.118	2.584	2.931	3.347	5.111	11.37	4.98	2.542	9.142	0
🟥 HM3	1.636	1.844	1.344	2.002	0	4.002	0.138	0.398	1.796	0.049	1.447	1.369	2.233	0.691	4.973	0
🟩 HM2	3.009	6.767	2.851	0	0	7.038	6.802	2.507	2.931	3.347	5.111	11.37	4.829	2.393	9.142	0
🟪 HM1	1.976	4.564	1.591	6.687	0	6.827	3.736	1.889	2.362	2.496	5.111	8.96	4.158	2.236	8.329	0

Figure 5.20 Fault Magnitudes at the point of detection for the Q-statistics of the four hybrid models.

5.5 Distillation column, hybrid model, and disturbance overview

A simple dynamic distillation process model was developed using CHEMCAD to investigate the fault/disturbance detection performance using a hybrid data driven model architecture and its applicability to distillation column monitoring. Three independent feed condition changes were simulated:

i) change in feed flow rate

ii) change in feed composition

iii) change in feed temperature

Sufficiently severe enough changes in any of the above three conditions can lead to column flooding – vapour or liquid flooding condition. Also investigated was the effect of the combine fault scenarios:

i) simultaneous change in feed flowrate and temperature

ii) simultaneous change in feed temperature and composition

The purpose of this particular case study was to investigate the applicability of hybrid approaches which do not incorporate a mechanistic or first principle model of the plant. Quite often developing a sufficiently accurate mechanistic model is not feasible for many real life applications. This may be the case either because of insufficient information about the plant dynamics or due to the sheer complexity of the plant, such undertaking might be too costly and time consuming. As such the hybrid model implementation employed for fault monitoring for the case study employed the use of a NN model and multiple ordinary least squares (OLS) regression models. The objective being to approximate a quasi time-variant model by developing several localised OLS models optimized about different operating points for the plant. The artificial neural network model was use to provide a mapping between the coefficients of the OLS models for the various operating points of the plant. The NN model therefore essential serves the function of switching in the appropriate OLS model based upon the observed short-term mean value of select process variables used to identified the current operating point of the plant. Further details and results into the implementation of the column and faults, hybrid model, and fault detection performance will be provided in the subsequent subsections to follow.

The distillation column implementation for this case study consists of 30 stages and uses a partial condenser, the column and control structures are shown in Figure 5.21. The overhead condenser and reboiler unit of the distillation column unit operation shown in the diagram were disabled during configuration of the column unitop in CHEMCAD. The reboiler and condenser utilities were then externally implemented above and below the column icon as indicated in the diagram. This facilitated access to specific streams, sensors and unit operations for which various fault conditions could be implemented and simulated.

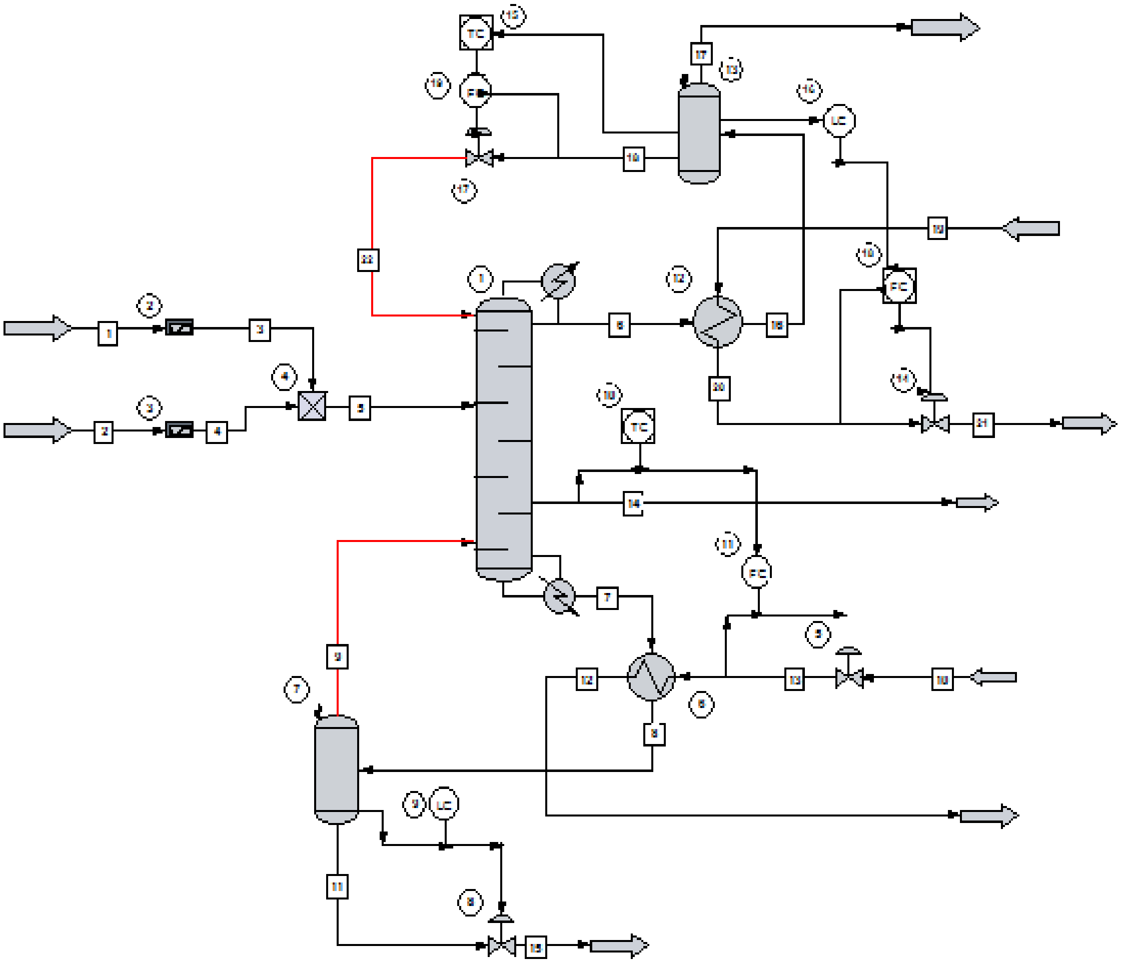

Figure 5.21 Dynamic Distillation Column with feed composition and condition switch implementation

Two input streams are fed to a mixer and a dynamic RAMP module available in CHEMCAD. The RAMP unit is used to switch between the feeds and/or to change a property of a given stream. An example of this is provided in Table 5.8, the RAMP modules shown in Figure 5.21 are used to adjust the feed flow-rate of the two feed streams shown in the diagram. One module is used to adjust Feed1 from 19800Kg/hr to 0Kg/hr while another module simultaneously adjusts the feed flow-rate of Feed2 from 0Kg/hr to 20000Kg/hr and effects a change in composition also.

The column is in steady state before the change of feed and works properly with the condenser specified with a reflux ratio of 3 and the reboiler specified to have a bottoms temperature of 157^{o}C. The top pressure for the column is maintained at 15 bar. The reflux ration is controlled by a cascade loop base upon the top plate temperature. A similar loop is used to control the steam utility of the reboiler via a bottom plate temperature measurement. A cascade loop is also used to control the level in the condenser via control of the cool-water flow-rate. Finally the reboiler level is maintained via a level-control loop that regulates the bottoms flow rate.

Table 5.8 Feed composition change condition used in simulation

	Stream Name	Feed1	Feed2
	Temperature C	50	50
	Press bar	15	15
	Flowrate	19,800	20,000
Components, Kg/hr	Ethane	1200	1473
	Propane	3400	3156.4
	I-Butane	4000	3787.7
	N-Butane	4100	4839.8
	I-Pentane	2500	1893.8
	N-Hexane	1300	1262.6
	N-Heptane	800	841.7
	N-Octane	500	430.3

5.6 Hybrid Model Development and Fault Detection Scheme

The monitoring of the column performance using the data driven hybrid model was conducted via the monitoring of the residuals of the process variables and controller outputs indicated in Table 5.9. The hybrid model architecture is shown in Figure 5.22, the neural network model used as input the short-term moving average of selected past output and inputs of the OLS model. The short-term moving average inputs provides a means of identify the current nominal levels or operating point of the plant/ChemCad model. The NN model provides a method of mapping and identify the most suitable coefficients of the linear OLS model for the current operating point.

Table 5.9 Process variable measurements used as inputs and outputs of Hybrid Data Driven Model.

Stream/Unit OP ID	Assignment	Variable
Stream 5	Input	Feed Temperature
Stream 5	Input	Feed Mass Flow Rate
Unit OP 9	Input	Reboiler Level Controller OP
Unit OP 11	Input	Steam Flow Rate Controller OP
Unit OP 19	Input	Reflex Flow Rate Controller OP
Unit OP 18	Input	CW Flow Rate Controller OP
Stream 18/22	Output	Reflux Temperature
Stream 18/22	Output	Reflux Flow Rate
Stream 17	Output	Distitillate (Tops) Flow Rate
Stream 17	Output	Distitillate (Tops) Temperature
Unit Op 1	Output	Tray Temperature plate – 24
Stream 15	Output	Bottom Product Flow Rate
Stream 15	Output	Bottom Product Temperature

The neural network fraction of the hybrid model was trained separately and after the OLS component of the system was identified. Several OLS models were derived one for each operating point which was established. By coding the vector of OLS model parameters derived (b_0, b_1, .. b_n) along with the a priori information of the established mean operating conditions of the feed stream, a three-layer sigmoid activation function NN model was then trained to develop a mapping function between the steady state condition and the collection of OLS model for each output variable. The complete monitoring system involving several hybrid network structure is shown in Figure 5.23. In that diagram the blocks labelled 'Hybrid ANN + OLS Models' encapsulates the more details presented in Figure 5.22.

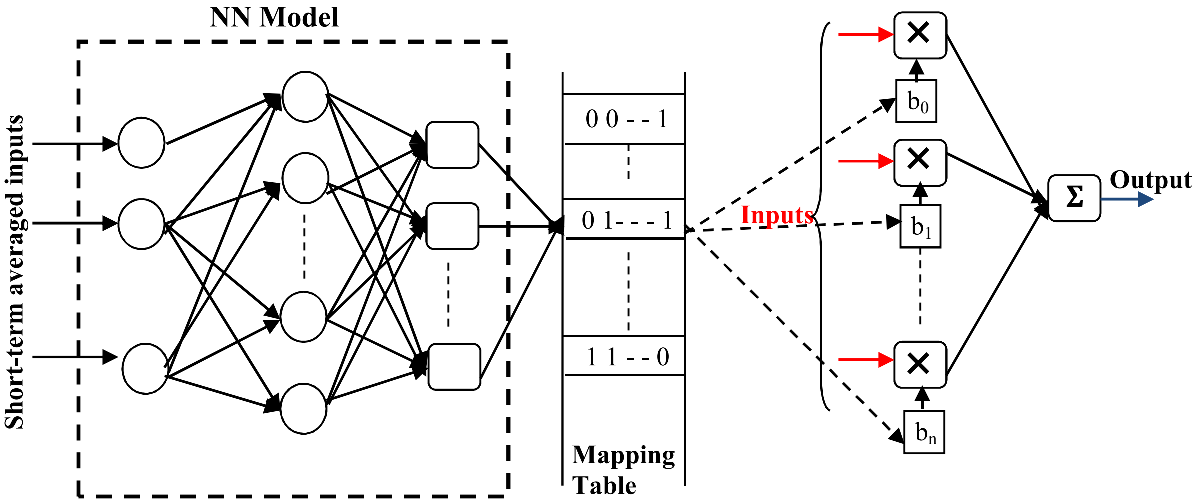

Figure 5.22 Hybrid data driven model architecture comprising an ANN and an OLS model. One network is developed for each output variable.

The monitoring scheme applied PCA to the data matrix consisting of the input variables and the output residuals of the plant and hybrid model. The residuals were extracted as indicated in Figure 5.23. The PCA T^2 and Q statistics were then applied for monitoring of the plant.

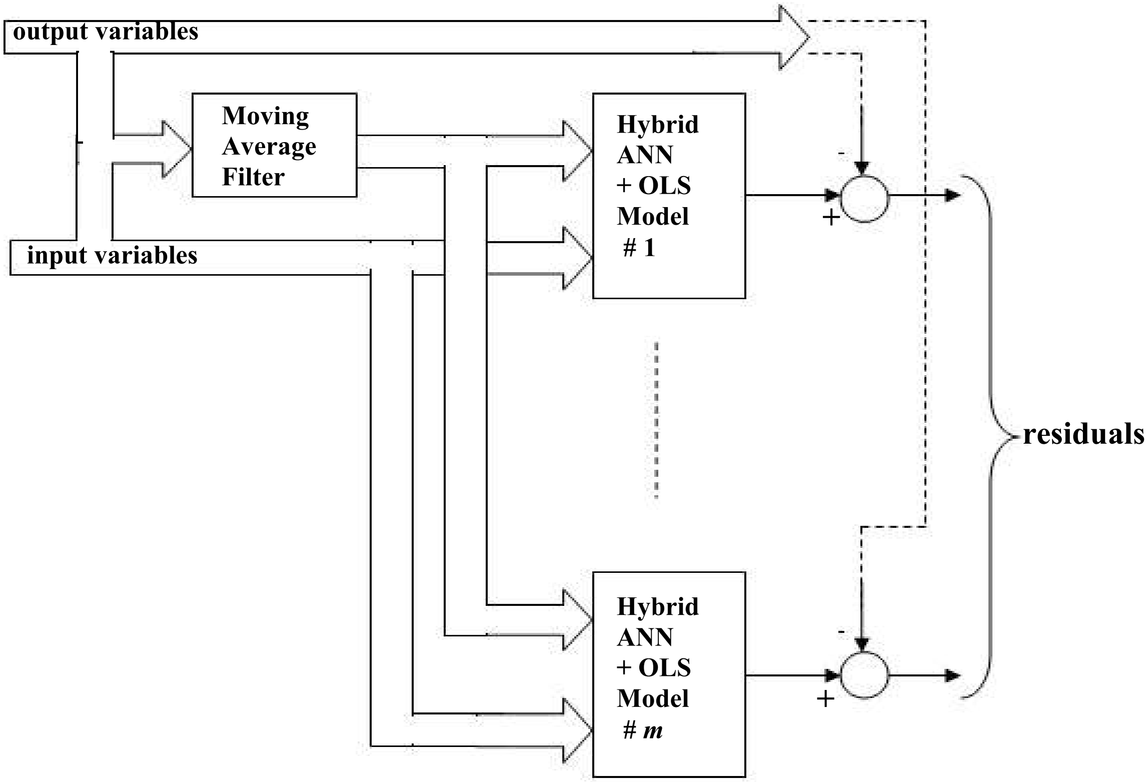

Figure 5.23 Complete multi-network hybrid data driven model base monitoring scheme.

The hybrid data based model was developed using training data generated by applying pseudo random and sine wave perturbations to the flow and temperature variables of the feed stream. To develop a non-linear hybrid data based model capable of dealing with operating shifts, the perturbations were applied about several nominal feed conditions (operating point). The set of varying feed conditions included adjustments to the nominal state of the temperature, flow-rate, and composition of the feed. The plots of Figure 5.24 provide an example of the training data used for model development. A separate set of data was generated and used for validation of the model after training.

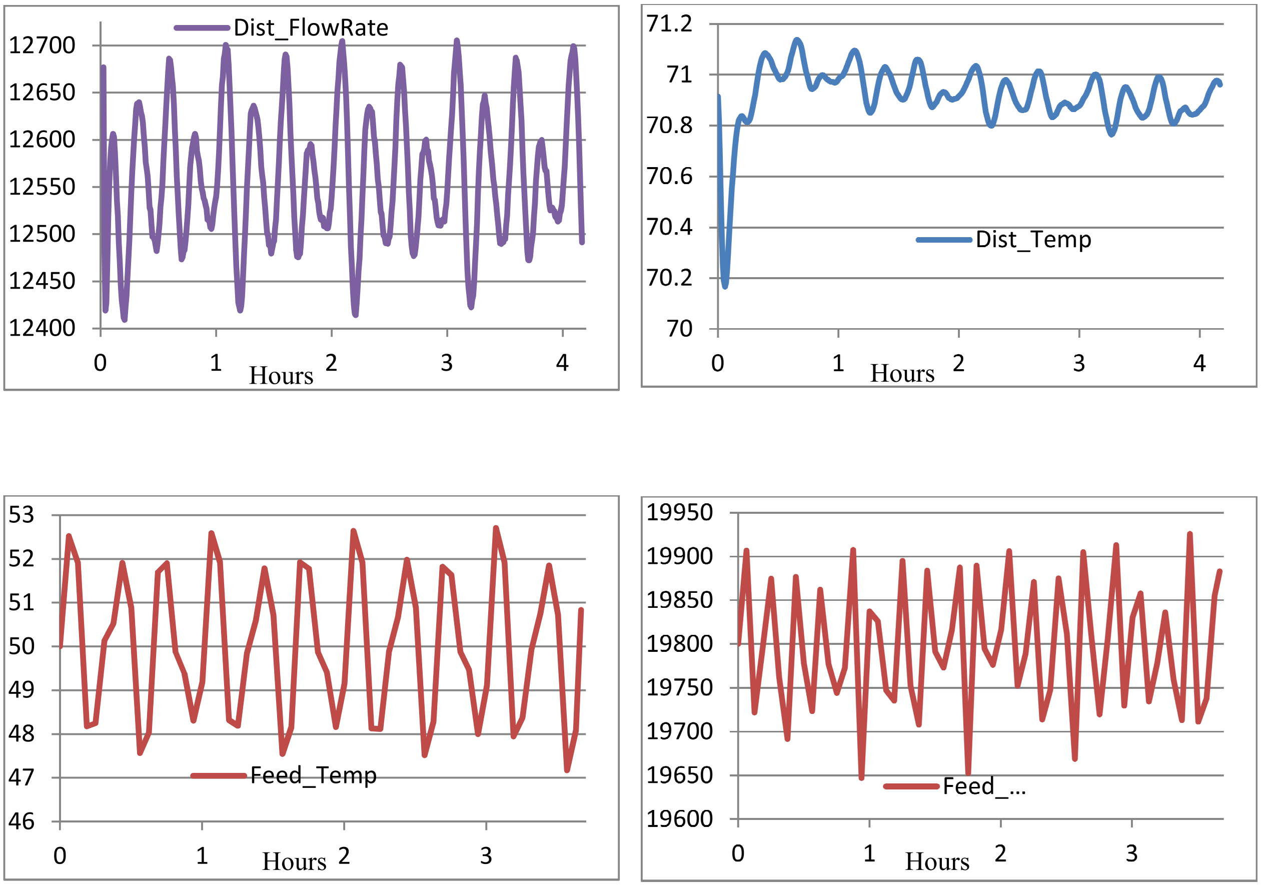

Figure 5.24 Training data profile of some of the process variable measurements used as input and output of the hybrid data driven base process performance monitoring scheme

5.7 Impact Analysis and Detection of Simulated Disturbances

5.7.1 Feed Temperature Change

Figure 5.25 shows the impact on the temperature and flow rate condition of the distillate stream due to the feed temperature change from 50^{o}C to 60^{o}C. The temperature can be observed to only be transiently affected, the maximum deviation from its steady state temperature was a 0.2^{o}C change which by any real-world practical scenario can be considered insignificant. Consequently the composition of the stream remained fairly unaffected by the feed stream temperature disturbance. The effect on flow rate was also transient but exhibited a fairly significant spike at the initial onset of the fault, refer to Figure 5.25(a).

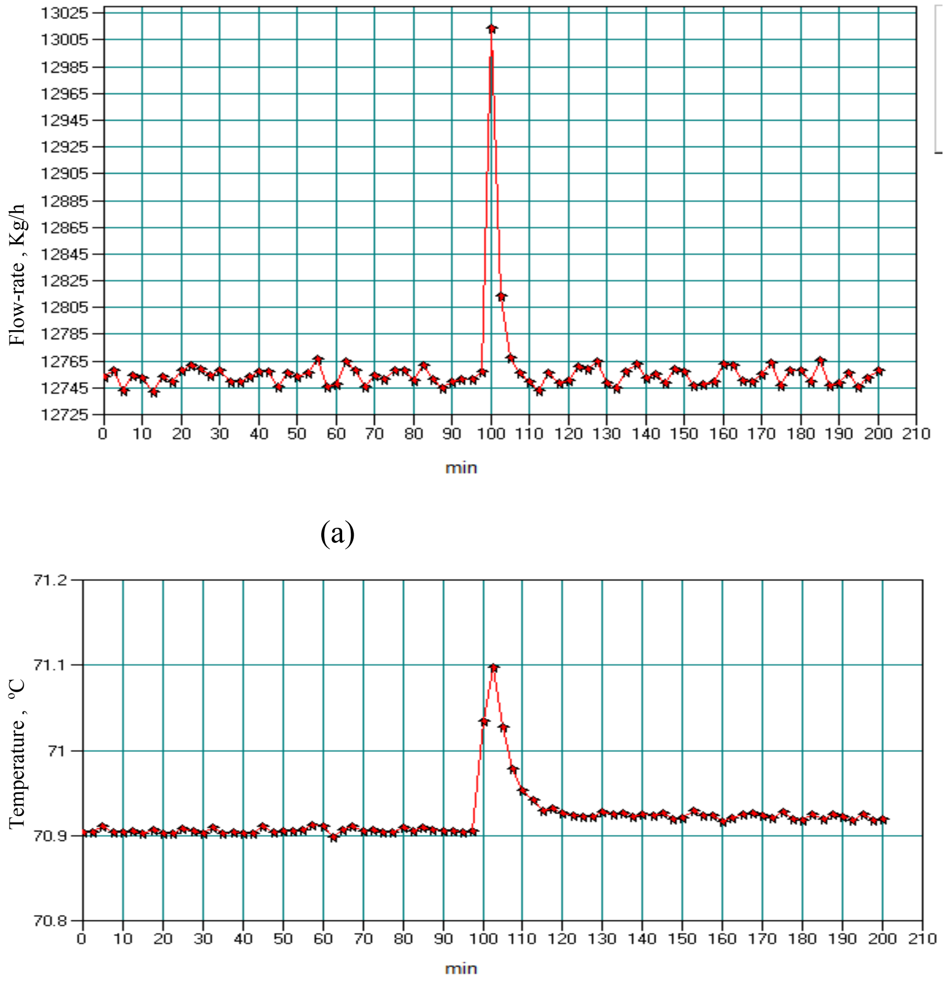

(a)

(b)

Figure 5.25 Impact of feed temperature change on distillate stream (a) flow rate plot (b) temperature plot.

The minimal impact on the distillate stream temperature and composition condition is due to reflux flow-rate and top product temperature control loops effectiveness in correcting for the disturbance. Both the PCA T^2 and Q statistics was able to reveal the presence of the disturbance, however, the Q statistics failed to show the persistence of the fault condition, refer to Figure 5.26.

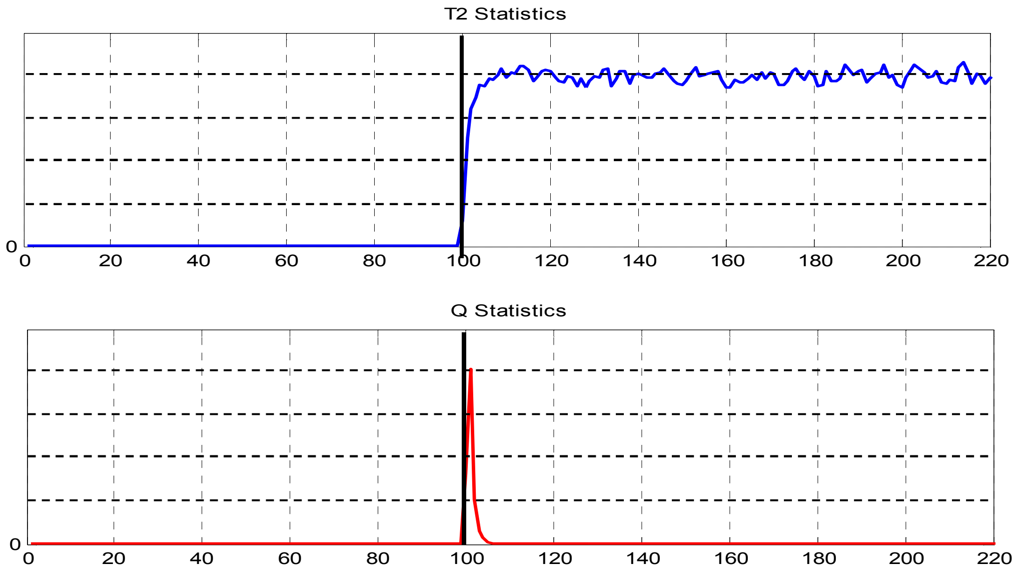

Figure 5.26 Detection of feed temperature disturbance using T2 and Q statistics

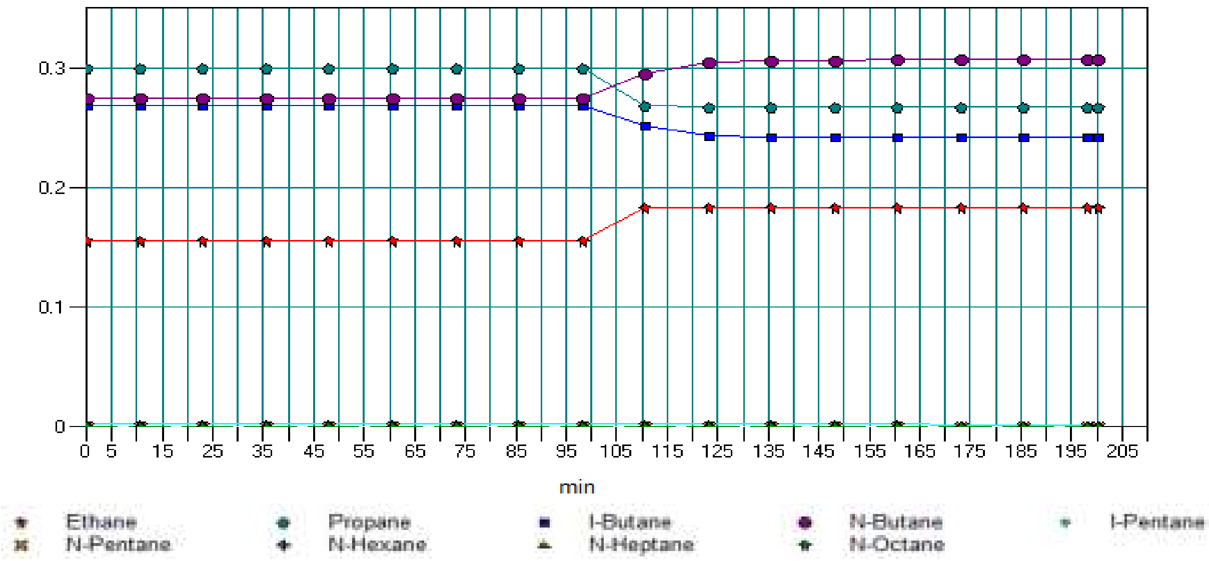

Figure 5.27 Impact of feed composition change on composition of top product.

5.7.2 Feed Composition Change

The feed composition was adjusted as specified in Table 5.8 and the resulting composition change of the top product is shown in Figure 5.27, the plots shows the more volatile components of higher concentration present in the distillate, exhibiting notable shift in mole concentration. The impact on the temperature of the distillate stream was transient and minimal as can be observed in Figure 5.28(a). However, the disturbance resulted in a significant and permanent increase in the distillate flow-rate as shown by Figure 5.28(b). The change in the distillate flow-rate is indicative of the potential column flooding impact that feed composition changes can lead to.

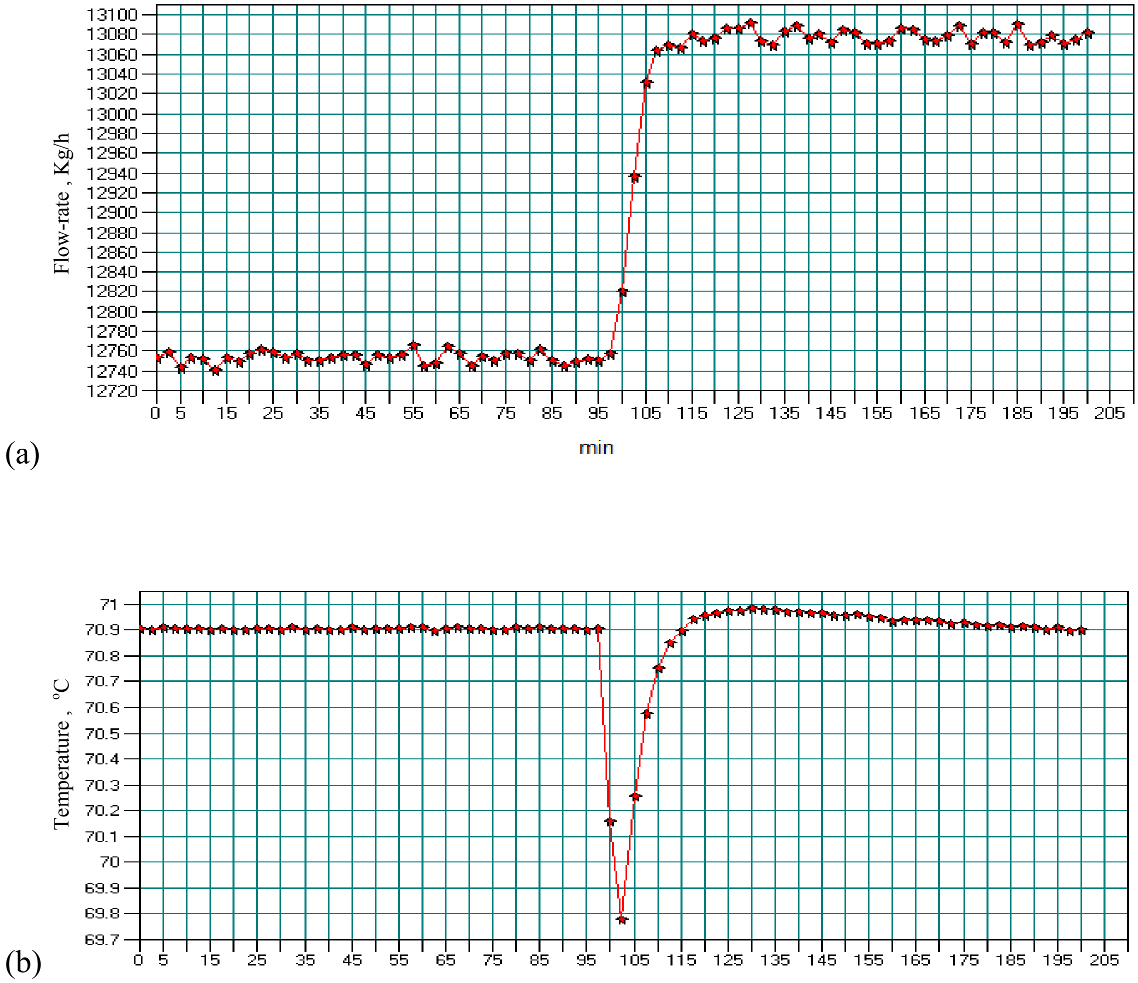

Figure 5.28 Impact of feed composition change on distillate stream (a) flow rate plot (b) temperature plot.

Both the T^2 and Q statistics proved effective in detection of the composition disturbance with the T^2 statistics being slightly quicker and aggressive in its detection, see Figure 5.29. Both statistics also indicate that the fault/disturbance persists.

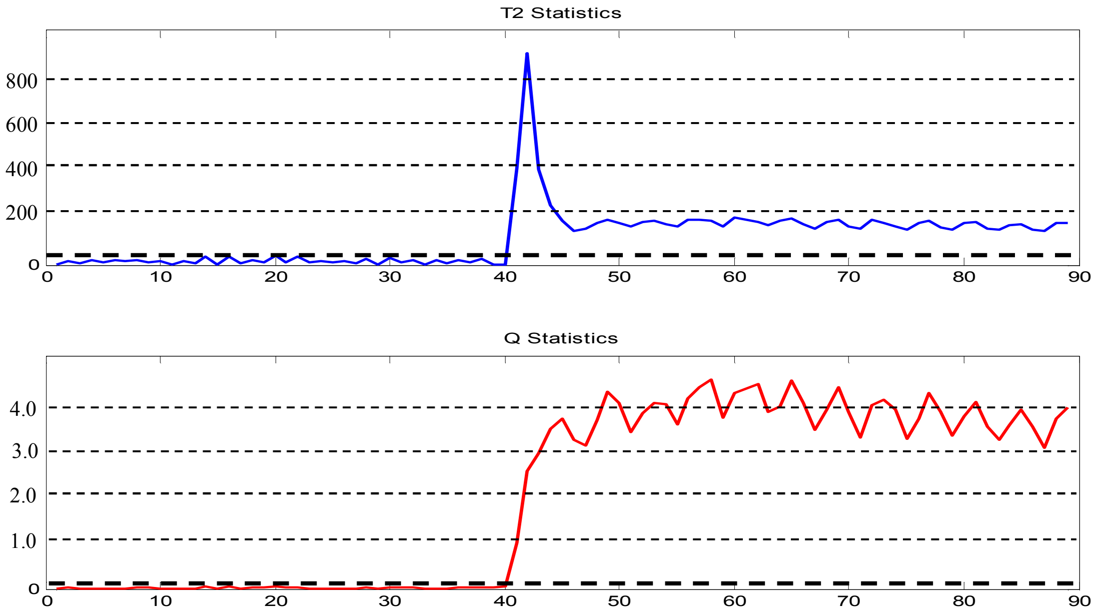

Figure 5.29 PCA based T2 and Q Statistics detection of composition disturbance.

5.7.3 Change in Feed Flow Rate

The feed flow rate change appears only to have an impact on the distillation stream mass flow rate variable as shown in Figure 5.30(a), both temperature and composition was unaffected by the fault. Figure 5.30(b) shows the detection of this disturbance using T^2 and Q statistics computed from applying PCA on the residuals only.

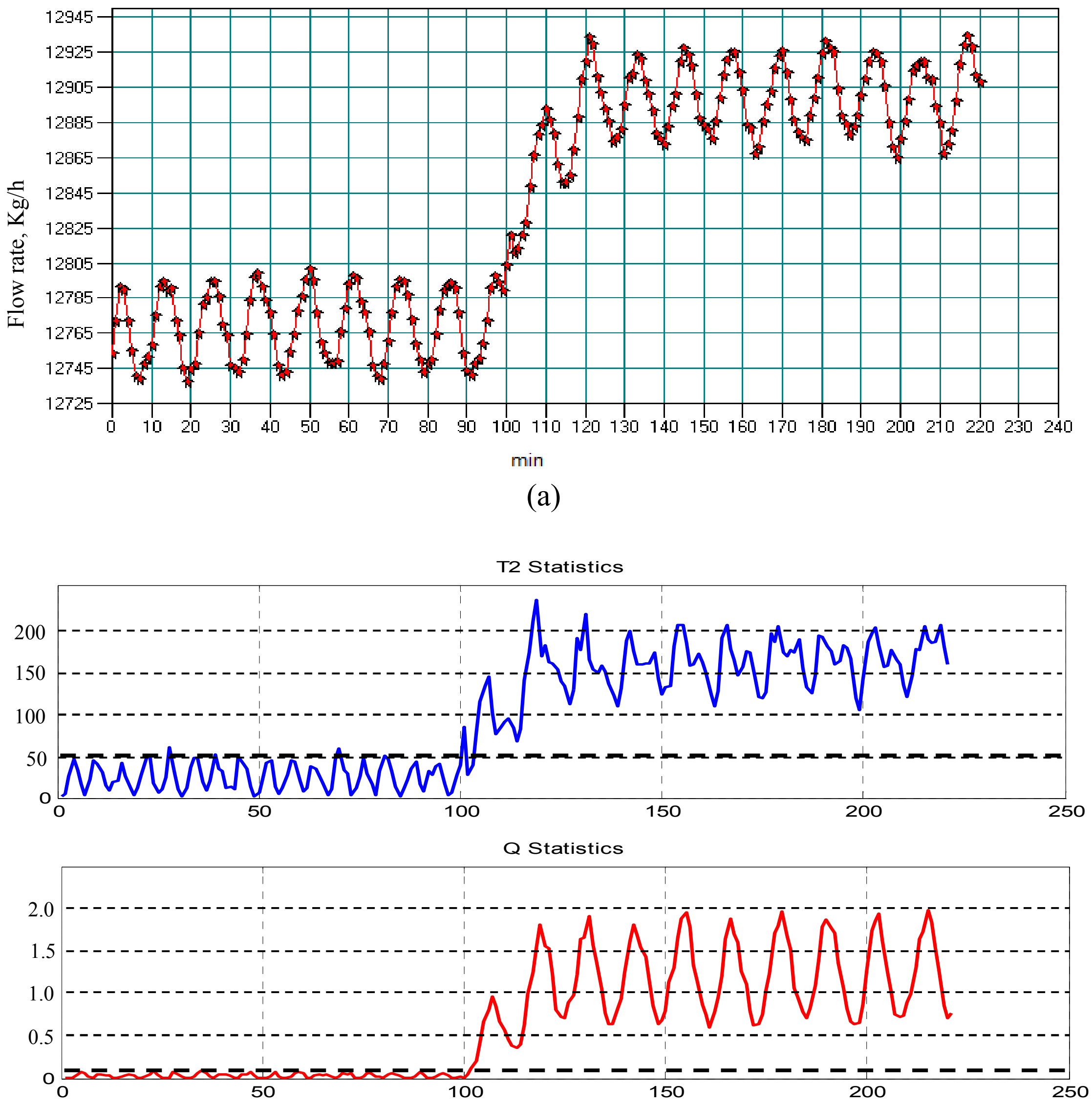

(a)

(b)

Figure 5.30 (a) Impact of feed flow disturbance based on the distillate steam flow rate (b) Detection of the feed flow rate disturbance using T^2 and Q statistics.

5.7.4 Combine fault Detection

A common curiosity is often how well or whether or not a monitoring scheme that demonstrates successful detection of single fault scenarios would be able to successfully detect combined simultaneous faults. This was proven to be the case for the two combinations of two-fault scenarios analysed.

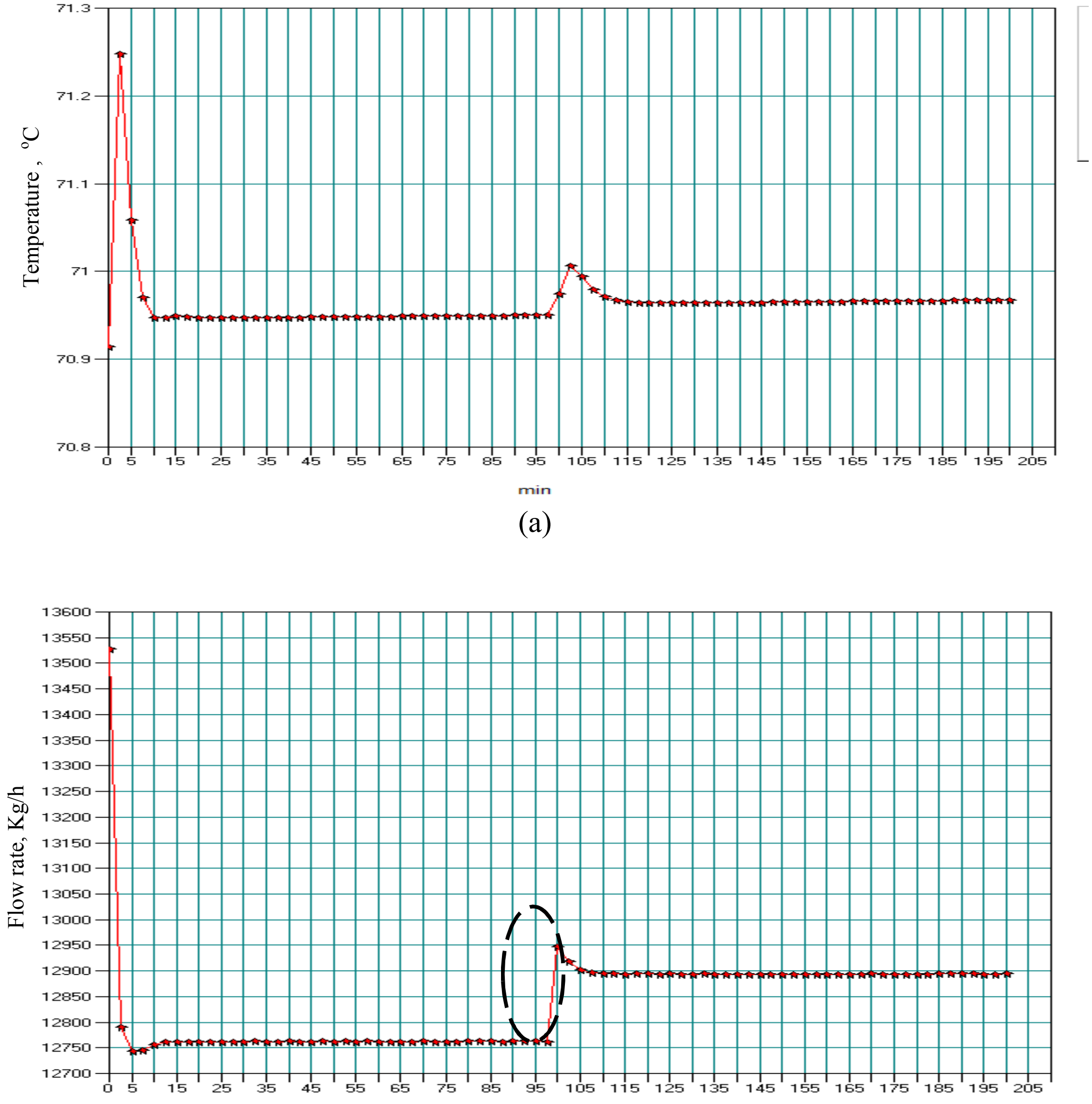

(a)

(b)

Figure 5.31 Distillate stream process variable profiles before and after feed flow-rate and temperature change (a) Temperature (b) Mass flow-rate.

The impact on the distillate temperature and flow-rate profile shown in Figure 5.31 is due to the feed temperature and flow rate combined disturbance. Note that effect the combine effect on the stream equates the superposition of the two independent effects. The temperature spike is totally due to the change in temperature of the stream and unrelated to the impact of the feed flow rate change. Likewise, the flow rate impact on the distillate stream is for the most part due to the adjustment in the feed flow rate and not its temperature.

Figure 5.32 shows the detection of two simultaneous fault scenario using the PCA T^2 statistics. The detection speed of response for the simultaneous change in temperature (50°C to 60°C) and flow rate (19800 kg/h to 2000 kg/h) was as quickly detected as the simultaneous fault scenario of temperature and composition shift.

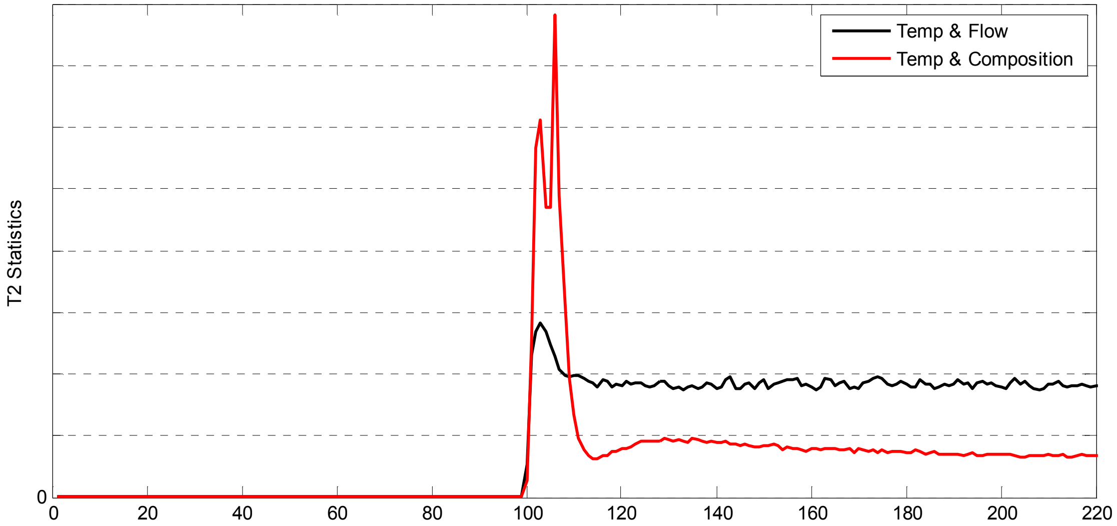

Figure 5.32 T^2 detection of simultaneous fault conditions – (i) temperature and flow rate change (ii) Temperature and composition change.

5.8 Conclusions

The degree of success of a mechanistic model to effectively monitor plant and detect faults arising is largely dependent on the extent of plant model mismatch that exist (model error). It was shown that such model parametric errors can lead to offset between the process variables and plant model output variability and this in some cases inhibits fault detection.

Compensation via linear or non-linear data based model can dramatically improve the fault detection by providing compensation to correct the inaccuracy of the mechanistic model process variable estimation. The residual whitening effect of the data based compensation model not only facilitates fault detection but also improves the reliability of the statistics against false alarm condition.

A non-mechanistic hybrid approach comprising a NN and OLS model, prove to have the same degree of success with regards to mitigating false alarm conditions due to shift in processing operating point and nonlinear process variability. The scheme was also very effective in detecting the simulated disturbances associated with the column feed stream for both single and dual simultaneous fault scenarios. In most cases the ability to detect two independent faults normally translates to being able to detect both faults if occurring simultaneously.

Based upon the analysis study conducted on the impact of several different fault scenarios on the process variables, one can conclude that a perfect fault diagnosis system capable of automatically linking a given fault condition to a specific fault scenario case, may not be feasible in all cases. This being the conclusion as it was observed that for some cases faults of different origins can affect the same subset of process variables with very similar characteristics. For cases like this a fault diagnostic system may only be able to narrow the search by identifying a set of possible fault conditions.

Chapter 6 : Batch Process Monitoring Using Multi-way and Interval PLS methods

6.1 Introduction

The importance and applications of batch and fed-batch processes in the chemical and biotech industry have increased dramatically in recent years. Batch fermenters in early years were run to completion under a fixed recipe with nothing added except air and some agent to control foam. Today, most bioprocessing incorporates adjustments to the medium to control conditions and to supply nutrients and compounds that promote biosynthesis of the target product. The enlightenment to the fact that making changes to the batch process could influence formation of the product and that these changes could be controlled by additions was spawned from early investigations in the making of penicillin. Fed-batch approach does come with some disadvantages. A general feature of batch bio-processes is that small changes in the operating conditions during some critical periods may degrade the quality and yield of the final product, see Nomikos and MacGregor (1995). Some changes are not immediately obvious and may gradually grow and adversely affect the final product quality. Furthermore, product quality variables, the key indicators of process performance, are often examined off-line in a laboratory. Hence the need for monitoring and on-line estimators is essential to the efficient running of such processes in that fault conditions can be detected early and corrective actions can be taken before the loss of an entire batch (Chen and Liu, 2002).

Over the years several techniques have been proposed for batch process monitoring, the method of particular interest is multi-way partial least squares (MPLS) for batch process monitoring. The multi-way technique of transforming a three dimensional data set into a two dimensional representation was first introduced and applied to principal component analysis (PCA) and PLS by Wold, et al. (1987), and was followed up by several other key publications (Nomikos and MacGregor, 1995; Nomikos and McGregor, 1994; Kosanovich, et al., 1994). Since then there have been many publications on the applications of MPCA, MPLS, and their variants such as batch dynamic PCA and PLS (Chen and Liu, 2002; Hu and Yuan, 2008). Some of these publications proposed batch monitoring using nonlinear models such as nonlinear PCA (Dong and McAvoy, 1996a).

In recent years the method of interval partial least squares (iPLS) has been applied successfully to the monitoring and prediction of quality variables using the mid-infrared (FTIR) and near-infrared (NIR) spectrum. The technique has been reported in applications ranging from pharmaceutical medicinal explorations - measuring the content of flavone an active ingredient in a rare medicinal plant called snow lotus (Chen, et al., 2010), determination of total polyphenols content in green tea (Chen, et al., 2008), and for simultaneous active substance detection in pharmaceutical formulations (Silva, et al., 2009), to the detection of quality parameters in biodiesel/diesel blends (Ferrao, et al., 2011) and the detection of contaminants in lubricating oil (Borin and Poppi, 2005). The principle of this method involves splitting a spectrum or batch duration into several equidistance sub-intervals or regions and then developing a PLS model for each sub-interval using a selected number of latent variables.

In this thesis the method of interval partial least squares (iPLS) is synergistically combined with multi-way partial least square (MPLS) to generate a superior statistical model for fed-batch process monitoring and product quality variable prediction. The iPLS implementation differs from previously published papers in two key ways:

i) The first is that the allocation of the subintervals is not equally spaced but the interval slicing is optimally selected based upon an algorithm to minimize the over-all root mean squared error (RMSE) of prediction.

ii) Secondly, all subintervals are employed as the objective of the model is to support the detection of fault condition developing at any stage in the batch which may have adverse impact on the target product quality.

The iPLS model is developed and applied to the batch-wise unfolded data set to produce a Multi-way iPLS (MiPLS) monitoring and predictive model. The model's improved fault detection performance and quality variable prediction capabilities are demonstrated using data generated from the well-known benchmark fed-batch penicillin fermentation simulator – Pensim (Birol, et al., 2002). It will also be shown that optimal splitting of the interval can dramatically diminish the number of subintervals required and subsequently the number of PLS models required to represent the full spectrum or duration of the batch process.

The chapter is structured as follows. Section 6.2.1 introduces the concept of batch duration interval splicing and proposes a method of synergistically combining two data unfolding methods with the interval splicing approach. The novel algorithm proposed by the authors to achieve optimal interval splicing is described in detail in subsection 6.2.2. Section 6.3 gives a descriptive overview of the fed-batch penicillin process simulator and provides specifics on the development of the process monitoring and predictive models employed in this work. Section 6.4 presents simulation results and analysis obtained using the proposed process monitoring and prediction models. Section 6.5 concludes the paper with a summary of the major conclusions and findings obtained.

6.2. Combining Data Unfolding and Interval Splicing Techniques

6.2.1 Three-dimensional data unfolding

Multi-way partial least squares MPLS is an extension of PLS to deal with data in three dimension arrays. MPLS is essentially the equivalent of PLS applied to the unfolded three dimension data set **X** (***I*** x ***J*** x ***K***) where ***I*** is the number of batches ***J*** is the number of variables and ***K*** represents the number of measurement samples for the duration of the batch run. As was shown in Figures 2.4 to 2.6 of chapter 2, the data can be unfolded in one of three different modes: i) Time ii) Batch and iii) Variable. The approach adopted for this application employed a merger of both time and batch unfolding methods shown in Figure 6.1.

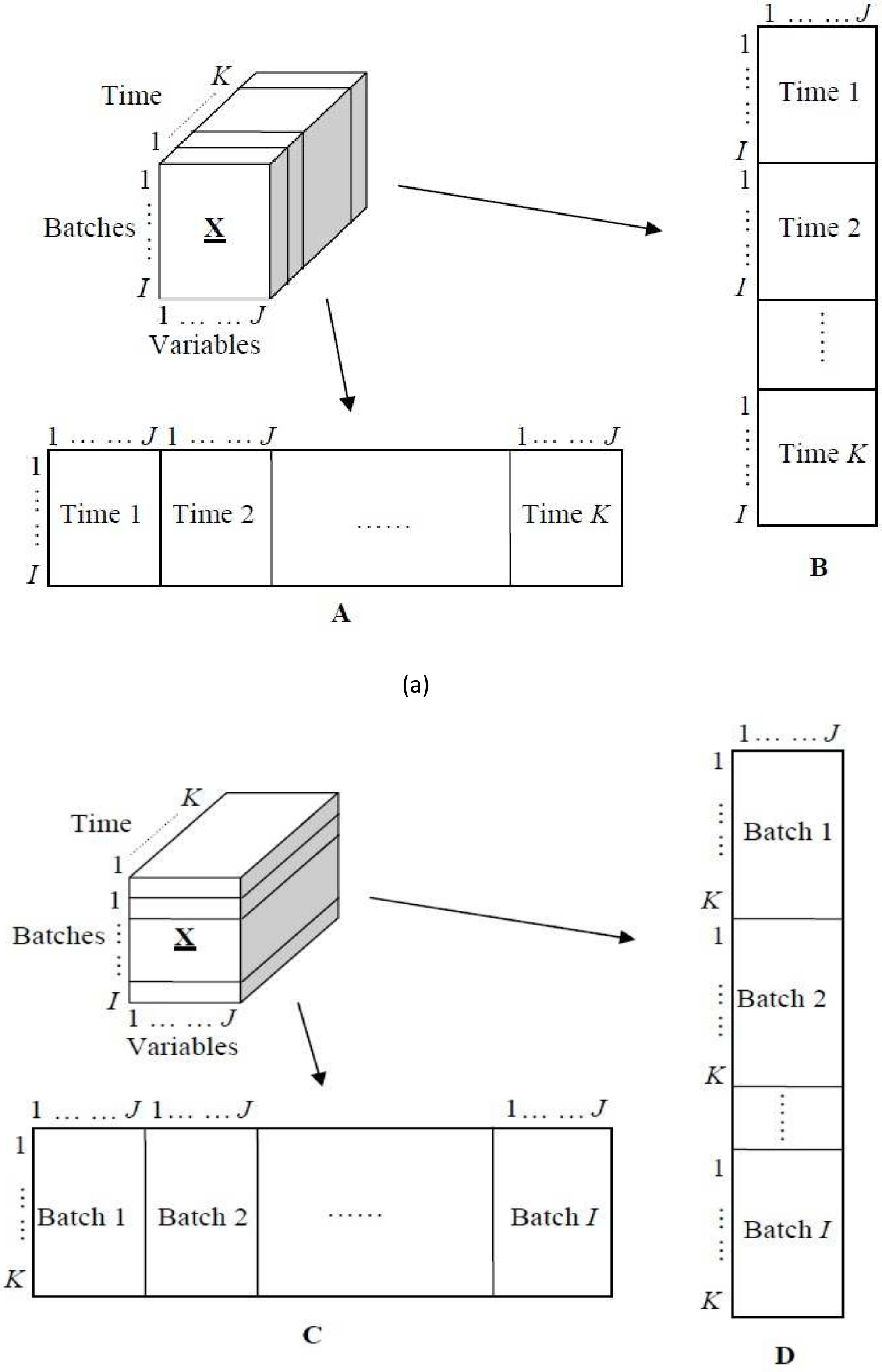

(a)

Figure 6.1 a) Time Unfolding b) Batch-mode Unfolding

The process involves first splitting the batches along identical time slice intervals. Each subinterval is then unfolded according to option D in Figure 5.1(b). Data blocks extracted from identical intervals across each batch are combined into *r* subinterval grouping and a PLS model is constructed for each subinterval as shown in Figure 6.2.

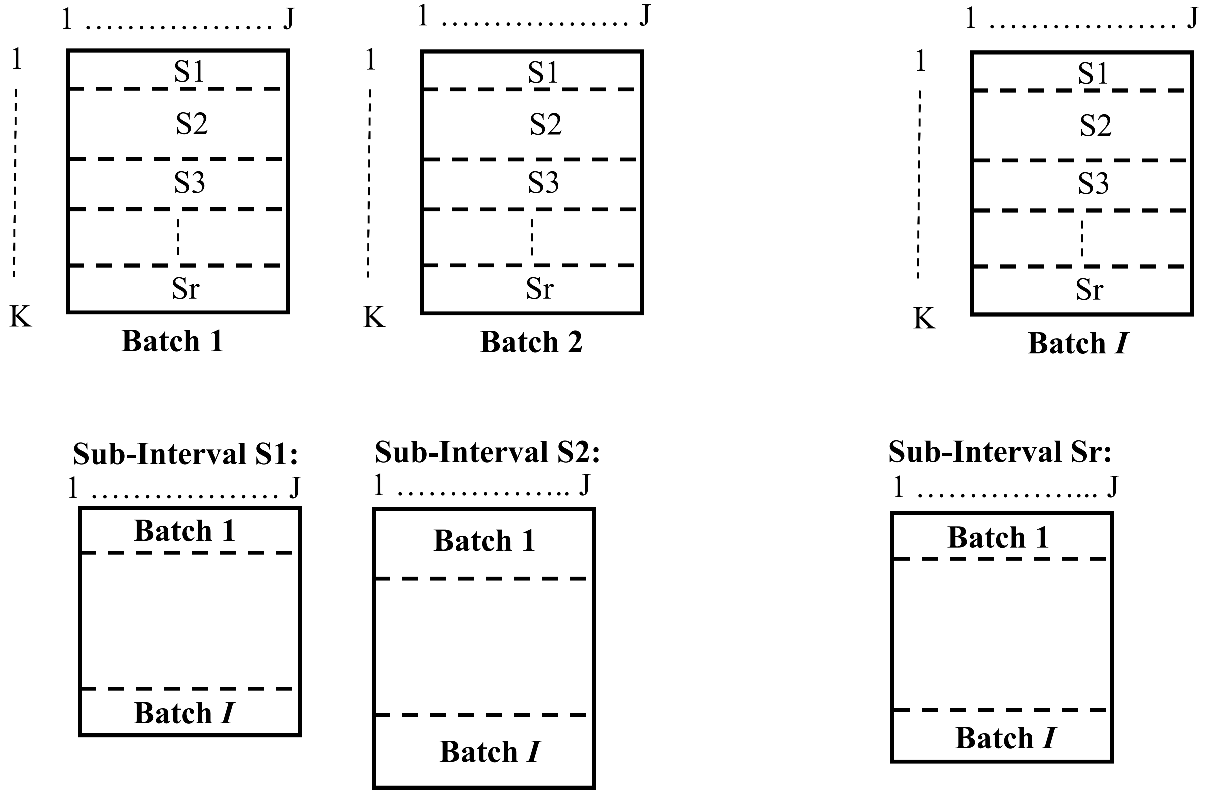

Figure 6.2 Batch-wise interval segmented unfolding of data set.

6.2.2 A binary dividing search algorithm approach for subdivision length selection

Critical to the success of this method is the process of arriving at the ideal interval subdivision across all batches or the selection of a subset of the intervals which will minimize the overall RMSE. Chen et al. (2010) applied genetic algorithm (GA) programming to select a subset of the intervals that most efficiently contributes to the prediction of the quality parameter sought to be quantified. In this subsection we describe a novel procedure which has been effectively applied to derive the best interval subdivision across all batches. The approach renders the selection of subintervals unnecessary as it will be demonstrated that if the spectrum or batch duration is optimally spliced then the number of subintervals required is significantly less than choosing an arbitrary fixed-length subinterval.

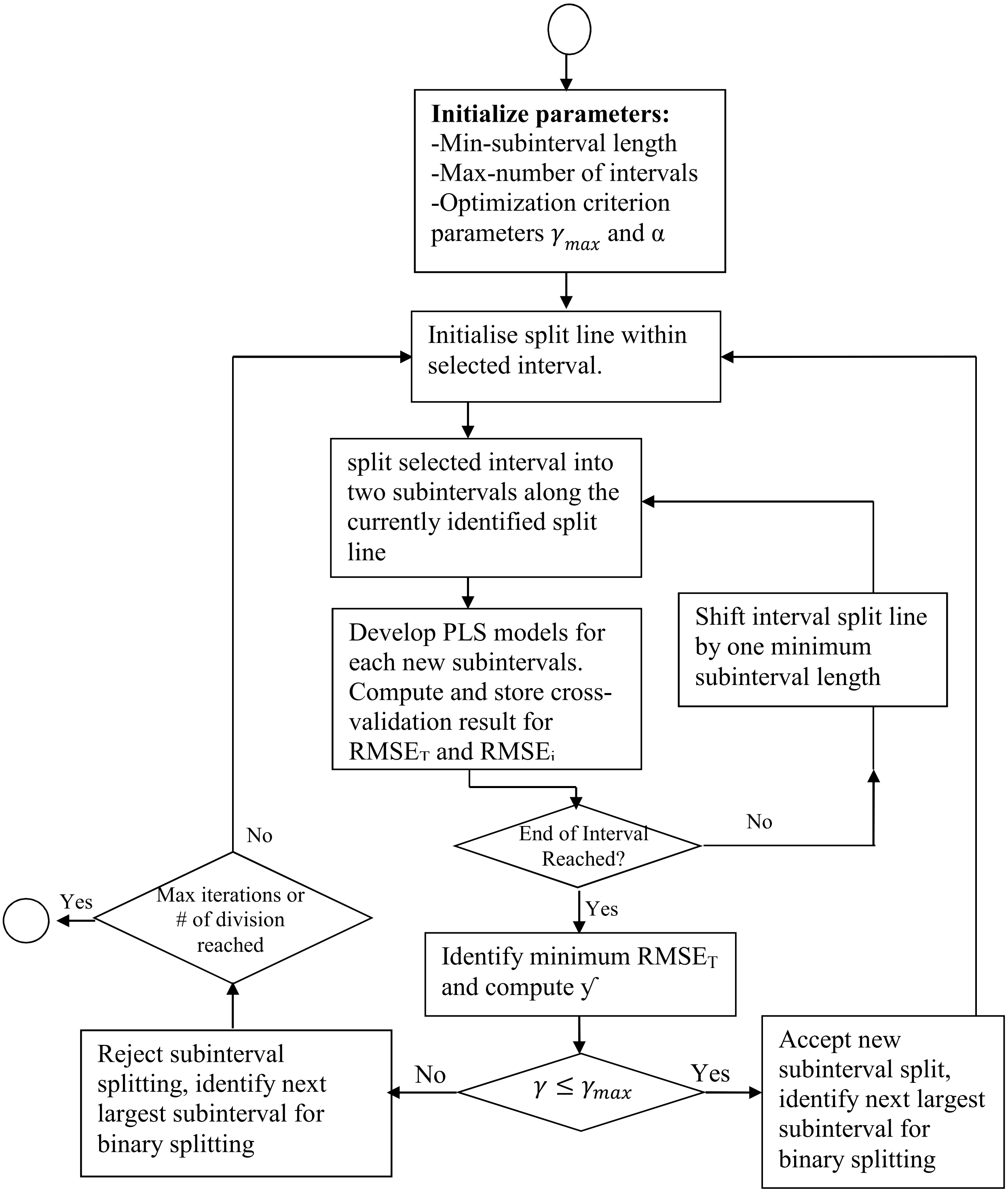
Initialize parameters:
-Min-subinterval length
-Max-number of intervals
-Optimization criterion parameters γ_{max} and α
Initialise split line within selected interval.
split selected interval into two subintervals along the currently identified split line
Develop PLS models for each new subintervals. Compute and store cross-validation result for RMSE$_T$ and RMSE$_i$
Shift interval split line by one minimum subinterval length
End of Interval Reached?
No
Yes
Identify minimum RMSE$_T$ and compute γ
$\gamma \leq \gamma_{max}$
No
Yes
Accept new subinterval split, identify next largest subinterval for binary splitting
Reject subinterval splitting, identify next largest subinterval for binary splitting
Max iterations or # of division reached
No
Yes

Figure 6.3 **Flowchart of binary interval splitting algorithm**

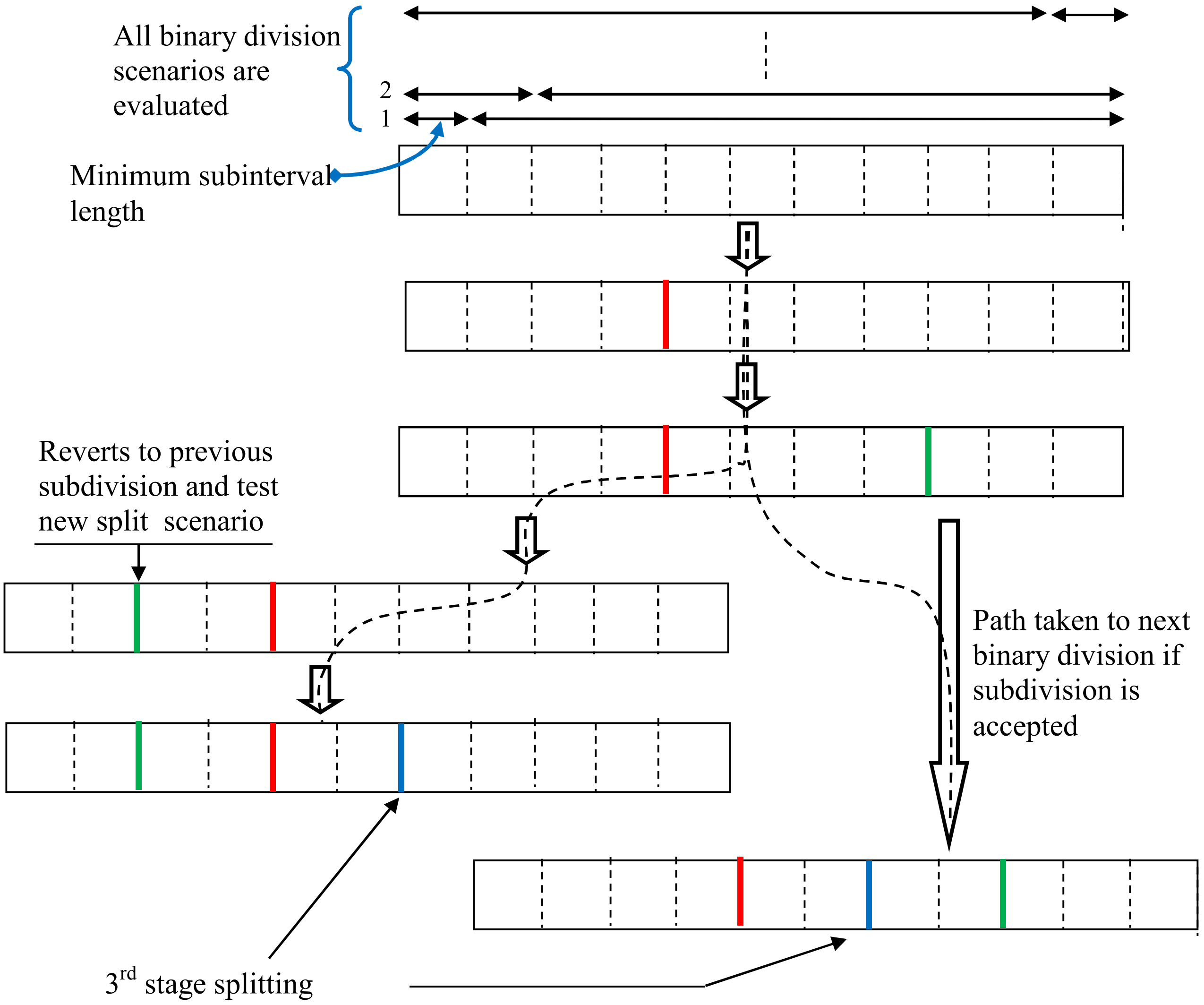
All binary division scenarios are evaluated
2
1
Minimum subinterval length
Reverts to previous subdivision and test new split scenario
Path taken to next binary division if subdivision is accepted
3rd stage splitting

Figure 6.4 Illustrative example of binary division algorithm for interval splitting

The algorithm was inspired by an algorithm proposed by Kegl, et al. (1999) for constructing principal curves using polygonal line segments. The principal curve algorithm was initialized by using the first linear principal component of the data set. The algorithm then iteratively identifies new segment vertices by adding one vertex to polygonal curve in each iteration step. The new position of each vertex was determined by minimizing an average squared distance criterion penalized by a measure of the local curvature. The stopping criterion is based on a heuristic complexity measure, determined by the number of segments k, the dimension of data matrix, and the average squared distance of the polygonal line from the data points.

The proposed algorithm is initialized by defining first a minimum subinterval length or step size, all subsequently selected interval lengths are integer multiples of this minimum interval spacing. The process could be best described as an iterative binary subdivision process that terminates when either a predefined maximum number of subdivisions is reached or the algorithm deems that further subdivision of the intervals would not achieve any significant improvement in the RMSE of prediction. To evaluate the degree of success or failure of a given subdivision stage, we define two measurement - the total and segment RMSE, given by Eq. (6.1) and Eq. (6.2) respectively, note that the total batch RMSE is computed as a weighted sum of the interval RMSE such that the largest subinterval will have the most influence on the overall value.

$$RMSE_T = \sum_{i=1}^{r} \frac{n_i}{N} RMSE_i \tag{6.1}$$

$$RMSE_i = \sqrt{\frac{\sum(\hat{y} - y)^2}{n_i}} \tag{6.2}$$

where n_i is the length of the *i*th subinterval, *N* is the full length of the batch duration and *r* is the total number of segments the batch is currently divided into, $\hat{y}$ is the estimated/predicted value of the quality variable measurement *y* based upon the PLS model of the *i*th subinterval.

Identifying the best binary split of any given segment is a sequential process of evaluating all split scenarios as illustrated in the flowchart of Figure 6.3 and the example of Figure 6.4. The partitioning is adjusted in discrete step size defined by the minimum subinterval. The binary division algorithm compares the segment RMSE value ($RMSE_i$) before a split ($RMSE_i^-$) with the weighted sum of the RMSE of the split version of the given interval ($RMSE_i^+$) to determine whether splitting the segment into two parts achieves any improvement over keeping the segment as a single block. Additionally, the impact of a given subinterval binary splitting on the total RMSE ($\mathrm{RMSE_T}$) is factored in by considering the ratio of the combined weighted RMSE across all subintervals before and after the most recent binary split:

$$\gamma_i = \alpha \frac{RMSE_T^+}{RMSE_T^-} + (1-\alpha)\frac{RMSE_i^+}{RMSE_i^-} \tag{6.3}$$

where $RMSE_T^+$ is the evaluated total RMSE after a given subinterval is trialed split and $RMSE_T^-$ is the total RMSE before. The weight parameter α takes on values over the range from 0 to 1, setting the parameter closer to 1 allows more emphasis to be placed on improving the total RMSE of the fit. By design, therefore, γ will take on values less than 1 if a given trial split of a subinterval reduces the overall RMSE and will be equal to or greater than 1 if the experimental splitting of the batch fails to improve the prediction fit.

Based upon the criterion of Eq. (6.3), the algorithm is biased to splitting of the largest subinterval in any given stage since a registered improvement in the segment RMSE resulting from binary splitting exercise will impact the $\mathrm{RMSE_T}$ value more if that particular subinterval represents a larger proportion of the total batch duration. Therefore, as indicated in Figure 6.4, the flow of the program will first target the largest subinterval and may either revert to the previous state if the split is rejected or proceed, in either case targeting the next largest subinterval for splitting.

After the optimal subdivision of the batch duration is arrived at, the final stage of the process involves developing a partial least squares model to fit each interval:

$$E_{k+1} = X - \sum_{i=1}^{k} T_i p_i \quad \text{and} \quad F_{k+1} = Y - \sum_{i=1}^{k} U_i q_i \tag{6.4}$$

where k is the number of latent variables used to defined a given interval, X is the process measurements, Y is the process quality variables. The process measurement and quality variable are therefore simultaneously decomposed into a set of scores **T** and **U** using a matrix of loading vectors ***p*** and ***q***, respectively. A linear inner relation between the scores ensures that the scores of **X** are generated to be most correlated while being highly predictive of **Y**.

The binary division interval splicing algorithm was first evaluated using simulated data defined by Eq. (6.5), the coefficients a_1 and a_2 of the equation were designed to take on different parameter values over different time interval range. Subsequently, the linear relationship between the response variable y and predictor variables x_1 and x_2 is dependent upon the current time or sample instance. The data is corrupted with random noise of n(t) with zero mean and variance equal to 10% that of the true measurement variances. Three different scenarios experimented with are provided in the leftmost column of Table 1.

$$y(t) = a_1 x_1(t) + a_2 x_2(t) + n(t) \tag{6.5}$$

Ten batches of data each spanning a batch duration of 300 samples (a matrix of data with the size 3 x 300 for each batch) were generated and the multiway unfolding and interval splitting algorithm was applied. The final results obtained and the number of iterations used to arrive at the interval subdivision outcomes are summarized in Table 6.1. The number of stages required in case was equal to twice the number of subdivision as the algorithm before terminating would iterates through each discovered subinterval to determine whether further binary splitting was necessary.

It was found that the algorithm gave best results when the weight parameter α and the value of $\gamma_{\max}$ were assigned values in the range: 0.6 < α < 1.0 and 0.8 < $\gamma_{\max}$ < 0.9 respectively. If $\gamma_{\max}$ was chosen too close to the value of 1.0 and or α chosen to be 0.5 or less, the binary division algorithm was found to be too sensitive to provide improvement in the segment RMSE – RMSE$_i$ and had the tendency of overshooting the actual number of segment intervals required in some cases. The number of iterations per stage is a function of the minimum subinterval length (S$_{\min}$) and the subdivision discovery path taken by the algorithm. Figure 6.5 shows the prediction fitting evolution for the response variable y as the algorithm discovered the optimal splicing of batch data set range.

Table 6.1 Simulation Results Evaluating the Capability and Accuracy of Proposed Interval Division Algorithm

Case 1	Boundaries Discovered		Iterations per stage		Total RMSE $RMSE_T$	
	S_{min} = 20	S_{min} = 15	S_{min} = 20	S_{min} = 15	S_{min} = 20	S_{min} = 15
$a_1 = 0.75;\ a_2 = 0.15;\ \ 0 < t \leq 100$	No Split	No Split	1		0.2840	
$a_1 = 0.10;\ a_2 = 0.75;\ \ 100 < t \leq 160$	100	225	14	9	0.1335	0.1302
$a_1 = 0.35;\ a_2 = 0.35;\ \ 160 < t \leq 225$	220	105	9	14	0.0492	0.0503
$a_1 = 0.50;\ a_2 = 1.25;\ \ 225 < t \leq 300$	160	165	5	7	0.0266	0.0290
Case 2	**Boundaries Discovered**		**Iterations per stage**		**Total RMSE $RMSE_T$**	
	S_{min} = 20	S_{min} = 15	S_{min} = 20	S_{min} = 15	S_{min} = 20	S_{min} = 15
$a_1 = 0.75;\ a_2 = 0.15;\ \ 0 < t \leq 65$	No Split	No Split	1		0.2548	
$a_1 = 0.10;\ a_2 = 0.75;\ \ 65 < t \leq 160$	220	225	14	9	0.1364	0.1282
$a_1 = 0.35;\ a_2 = 0.35;\ \ 160 < t \leq 225$	60	60	10	14	0.0587	0.0519
$a_1 = 0.50;\ a_2 = 1.25;\ \ 225 < t \leq 300$	160	165	7	10	0.0359	0.0301
Case 3	**Boundaries Discovered**		**Iterations per stage**		**Total RMSE $RMSE_T$**	
	S_{min} = 20	S_{min} = 15	S_{min} = 20	S_{min} = 15	S_{min} = 20	S_{min} = 15
$a_1 = 0.75;\ a_2 = 0.15;\ \ 0 < t \leq 80$	No Split	No Split	1		0.2950	
$a_1 = 0.10;\ a_2 = 0.75;\ \ 80 < t \leq 120$	180	180	14	19	0.1945	0.1945
$a_1 = 0.35;\ a_2 = 0.35;\ \ 120 < t \leq 180$	80	75	8	11	0.1472	0.1479
$a_1 = 0.50;\ a_2 = 1.25;\ \ 180 < t \leq 250$	240	255	5	7	0.0740	0.0419
$a_1 = 1.15;\ a_2 = 0.25;\ 250 < t \leq 300$	120	120	4	6	0.0621	0.0319

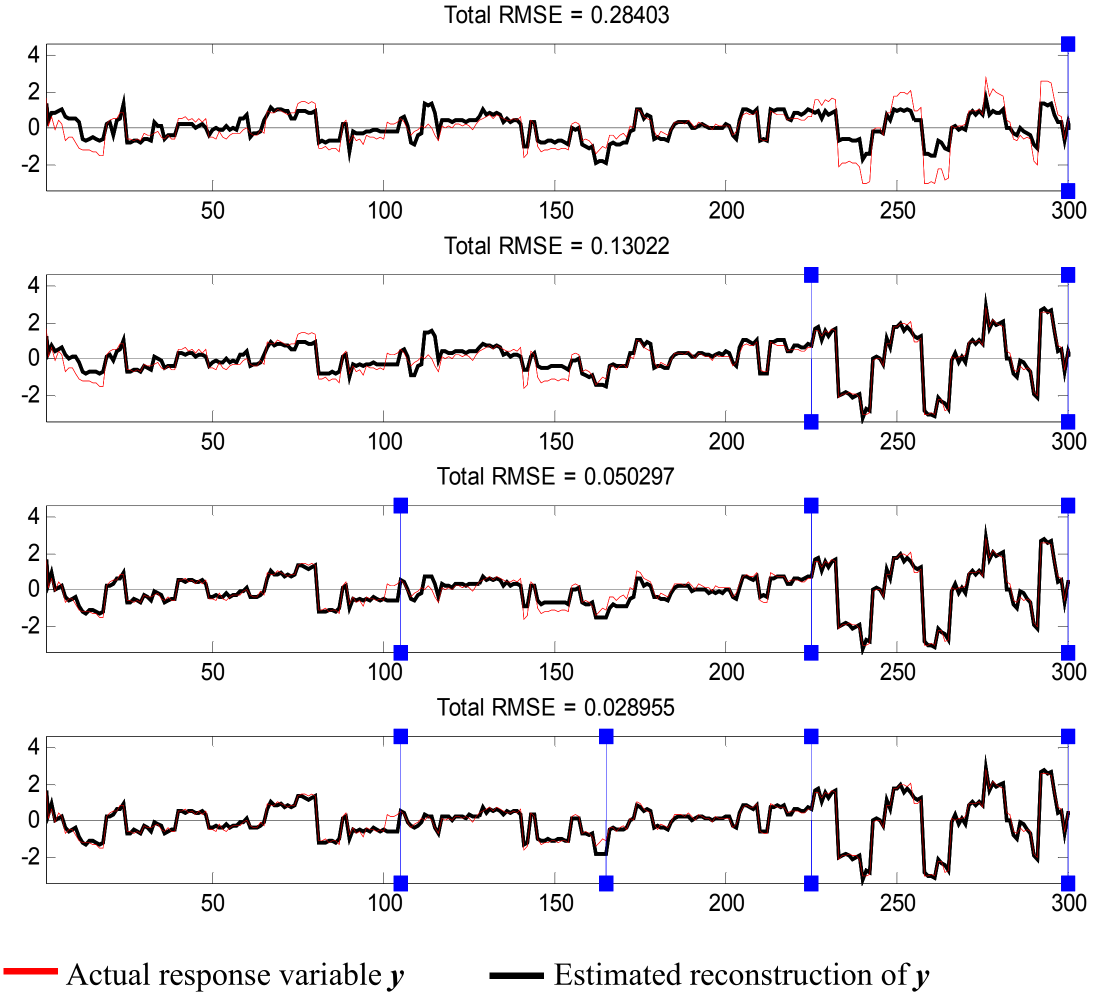

Figure 6.5 Plot of predicted response versus actual response through different stages of the interval splitting algorithm for case 1 with S_{min} = 15.

6.3 Fed-batch penicillin simulator prediction and fault monitoring

6.3.1 Fed-batch Penicillin Production Process Simulator Overview

The proposed MiPLS model was used to detect faults in a simulated fed-batch penicillin cultivation process. The penicillin model upon which the simulator was developed by Birol, et al. (2002) represents an extended more involved version of an earlier model develop by Bajpaj and Reuss (1980). The more recent model by Birol, et al. (2002) accounted for additional input variables to the process such as agitation power and aeration rate. The other input variables are: substrate feed rate and substrate feed temperature; the manipulated variables are: acid/base and heating/cooling water flow rates; the internal state variables are: culture volume, generated heat, carbon dioxide, dissolved oxygen, biomass, penicillin and substrate feed concentrations; and the controlled variables are: pH and bioreactor temperature. The typical offline measurements of biomass and penicillin concentration were assigned as the process quality variable for which the predictive model was developed. The control loop setup is shown in Figure 6.6.

The relationship between these variables is characterized by non-linear dynamic equations and the process is multistage in nature. In the initial pre-culture stage most of the necessary cell mass is usually generated after which penicillin production commences at the exponential growth phase. Penicillin production then continues until cell growth reaches the stationary phase. To ensure high penicillin productivity a minimum cell growth rate is maintain by feeding glucose continuously into the system during cultivation instead of applying it all at once. The duration of each batch is 400 h, comprising a pre-culture stage (about 45 h) and a fed-batch stage (about 355 h). All batches are of the same duration and measurement samples are of collected on a sampling interval of 0.5 h making each batch essentially comprising of approximately 800 samples. The set-point for the control variables and initial conditions of the input variables are given in Table 6.2.

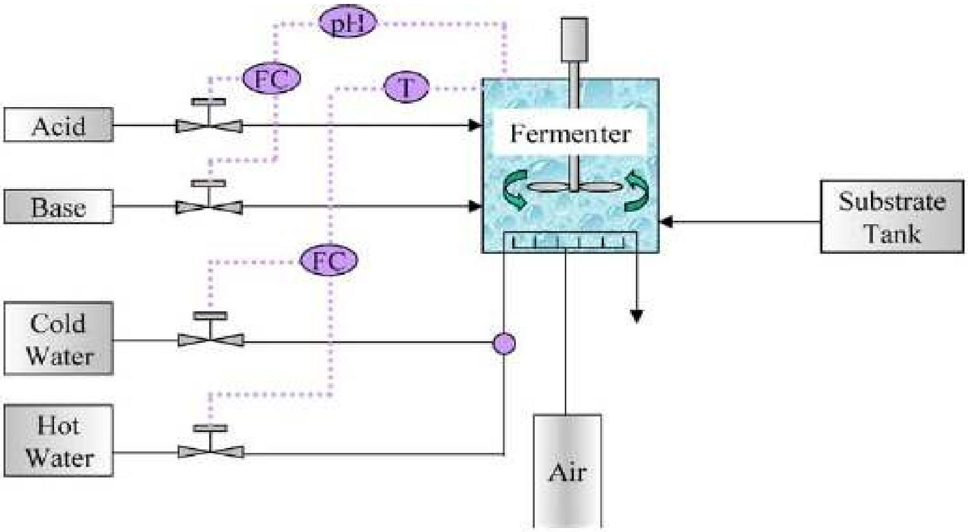

Figure 6.6 Flow sheet of Penicillin Cultivation Process

Table 6.2 Initial Conditions and Set-points used by Penicillin Simulator

Input and Manipulated Variables	**Initial Condition Range**
Substrate Concentration (g/L)	15
Dissolved Oxygen Concentration (mmol/L)	1.16
Biomass Concentration (g/L)	0.1
Penicillin Concentration (g/L)	0.0
Culture Volume (L)	100
Carbon dioxide concentration	0.50
pH	4.5 – 5.5
Bioreactor Temperature (K)	295 - 300
Control Variables	**Setpoint**
Aeration Rate (g/h)	8.6
Agitation Power (W)	30
Substrate feed flow rate (L/h)	0.039 – 0.045
Substrate feed temperature (K)	295 - 296
Bioreactor Temperature	297-298
pH	5.0

The simulation and detection of three different fault conditions were explored. For two of the three faults both incipient and abrupt fault scenarios were investigated as shown in Table 6.3. For each type of fault and occurrence (abrupt or incipient), four batches were generated, with different fault commencement times as indicated in Table 6.3.

Table 6.3 Summary of Fault Scenarios in Simulated Penicillin Cultivation Process

Fault Description	Fault Start time (hrs)	Fault Magnitude/Rate
pH controller Failure	50,100, 150, 200	N/A
Decrease in substrate flow rate	50, 100, 150, 200	-15% / -0.002
Decrease in agitator Power	50, 100, 150, 200	-15% / -0.002

6.3.2 Prediction and Process Monitoring

The input/output structures of the predictive and process monitoring models are both shown in Figure 6.7. The PLS2 predictive model estimates the quality variables – biomass and penicillin concentration using eleven process measurement variables. The same set of input variables were employed to develop the process monitoring model. The process monitoring model is actually an aggregation of PLS1 models with each PLS1 model providing an output that is representative of the estimation of one of the six selected online measured variables (highlighted in red bold in Figure 6.7) from the eleven predictor variables.

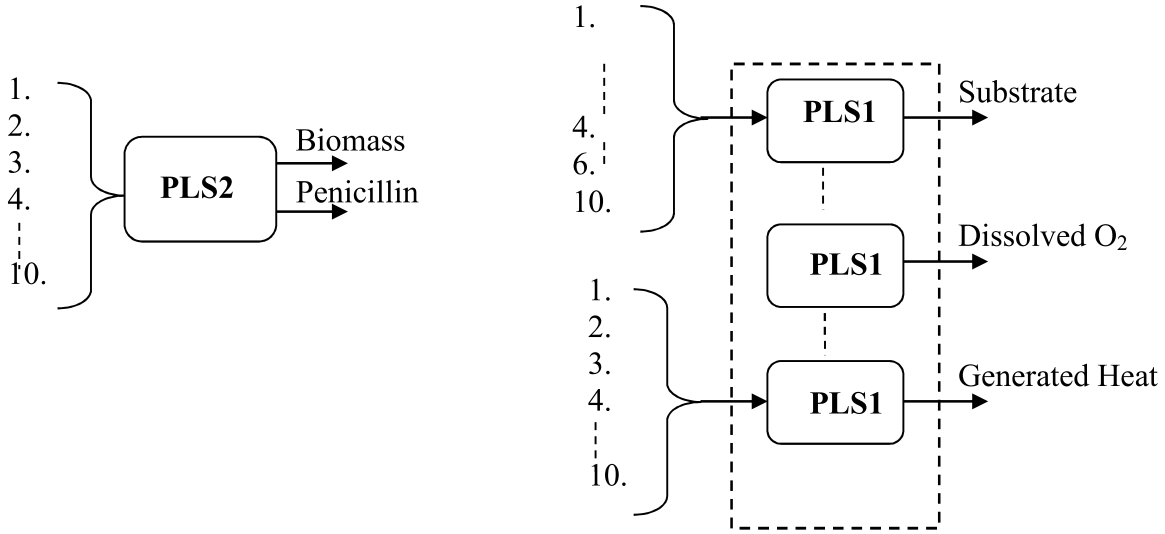

1. Aeration Rate **2.** Agitation Power **3.** Substrate feed rate **4.** Substrate feed temp. **5.** **Substrate conc.**
6. **Dissolved 0_2 conc**. **7.** Culture Volume **8.** **$C0_2$ conc.** **9.** **pH** **10.** **Reactor temp.** **11.** **Generate Heat**

Figure 6.7 PLS2 and PLS1 implementation of a) Predictive model b) Fault monitoring model

Estimation or reconstruction of a given output variable is based on the remaining ten variables or subset thereof consisting of input (load) variables, control and manipulated variables. Along with employing an interval PLS approach, the model development also incorporates variable selection to identify the minimum subset of the ten remaining process variables that is most reflective of the particular output variable being estimated. Table 6.4 provides details of each iPLS1 model indicating the interval segmentation and selected process variables employed by each model for a given output variable estimation. The process variables for which ‘Not used’ appears in the ‘Predictor Variables’ column, indicates that they are input/independent variables and as such no PLS model was constructed to predict or estimate/reconstruct these variables. For those variables that were estimated by a PLS1 model, the selected variables used by the PLS model as inputs are indicated by their index number. It was discovered that no more than four segments were needed to create the optimal MiPLS1 model.

Table 6.4 Specifications of the iPLS models used to Implement Process Monitoring Strategy

Process Variables	Model Outputs		
	Predictor Variables	Intervals	Interval Variance
1. Aeration Rate	Not Used	Not Used	Not Used
2. Agitator Power	Not Used	Not Used	Not Used
3. Substrate feed rate	Not Used	Not Used	Not Used
4. Substrate feed Temp.	Not Used	Not Used	Not Used
5. Substrate Conc.	1, 2, 4, 6, 7, 11	0-90, 91-801	2.72x10^{-4}, 1.59x10^{-5}
6. Dissolved O_2 Conc.	1, 3, 5, 9, 10, 11	0-90, 91-600, 601-801	8.39x10^{-6},2.63x10^{-6},1.79x10^{-6}
7. Volume	Not Used	Not Used	Not Used
8. CO_2 Conc.	1,10,11	0 - 801	1.9x10^{-3}
9. H^+ Conc. (pH)	1, 3, 5, 6, 7, 10, 11	0-90, 91-270, 271-801	3.54x10^{-5},7.39x10^{-5},1.06x10^{-5}
10. Reactor Temp.	1- 9, 11	1-330,331-420,421-801	1.7x10^{-3}, 1.2x10^{-3}, 5.2x10^{-3}
11. Generated Heat	1 – 10	1-90, 91-210, 211-300, 301-801	2.1x10^{-3},11x10^{-2}, 1.2x10^{-3}, 14.2x10^{-3}

The PLS1 fault model residuals, computed as the difference between the estimation and actual output measurement, are then combined to form monitoring metric. Both the squared prediction error statistics SPE and Hotelling's T^2 were experimented with as possible monitoring metrics:

$$SPE_k = \sum_{i=1}^{m} e_{ik}^2 \tag{5}$$

$$T_k^2 = \sum_{i=1}^{m} \frac{e_{ik}^2}{\sigma_k} \tag{6}$$

where k is the sample instance, m is the number of variables for which the residuals are computed and σ_k is a time varying covariance computed and applied as done in Lee, et al. (2004). The same monitoring statistics have been used by other process monitoring studies using the penicillin simulator (Lee, et al., 2004; Birol, et al., 2002). Note, however, that in this study it was necessary to apply a time dependent variance to compute the T^2 statistics due to difference in variance characterizing the different intervals of the iPLS model.

For the PLS models developed with and without variable selection, the generally adopted bootstrapped PLS regression algorithm (Zhao, et al., 2006) was employed. The algorithm incorporation within an iterative variable selection procedure is shown in Table 6.5, essentially the subsection spanning from lines 3 to 16. The selection of the number of latent variables ***A*** to employ was in all cases done via cross-validation, step 16, which decides the number of iterations of the innermost loop. The outermost loop in each stage eliminates one predictor variable by identifying the best performing PLS model based on the subset of predictor variables $\mathbf{X}_{\mathbf{jc}}$. In a given stage *j* one PLS model is constructed for each unique set of predictor variables $\mathbf{X}_{\text{jc}}$ which differ from each other based on the selected variable that is removed. When removal of predictor variables fail to yield further improvements in the RMSE error the algorithm terminates. The overall algorithm is a nested three loop structure.

Table 6.6 documents the design of the MiPLS2 predictive model alternatives considered for predicting biomass and penicillin concentration. One model was developed using all available online measurements while the other employed variable selection in addition to the interval PLS modelling scheme. For both scenario analyzed, the order in which the interval segmentation unfolds is listed as stages. The progressive reduction in RMSE with each stage is listed alongside the interval boundaries.

Table 6.5 Bootstrap PLS algorithm Integrated Within Variable Selection Algorithm

Step 1	Initiate outermost loop iteration to start at first column c = 1; set j = 1;
Step 2	Mean center and scale **X** and **Y**;
3	Remove a predictor variable (column c from **X**) and save the remaining variables as $\mathbf{X}_{\mathbf{jc}}$, set $\mathbf{E}_0 = \mathbf{X}_{\mathbf{jc}}$ and $\mathbf{F}_0 = \mathbf{Y}$ and $k = 1$.
4	Set $\boldsymbol{u}_{\mathrm{k}}$ to the first column of $\boldsymbol{F}_{\mathrm{k-1}}$
5	$\boldsymbol{w}_k = \boldsymbol{E}_{k-1}^T\boldsymbol{u}_k \big/ (\boldsymbol{u}_k^T\boldsymbol{u}_k)$
6	scale $\boldsymbol{w}_{\mathrm{k}}$ to unit length: $\boldsymbol{w}_k = \boldsymbol{w}_k / \lVert\boldsymbol{w}_k\rVert$
7	$\boldsymbol{t}_k = \boldsymbol{E}_{k-1}\boldsymbol{w}_k$
8	$\boldsymbol{q}_k = \boldsymbol{F}_{k-1}^T\boldsymbol{t}_k \big/ (\boldsymbol{t}_k^T\boldsymbol{t}_k)$
9	scale $\boldsymbol{q}_{\mathrm{k}}$ to unit length: $\boldsymbol{q}_k = \boldsymbol{q}_k / \lVert\boldsymbol{q}_k\rVert$
10	$\tilde{\boldsymbol{u}}_k = \boldsymbol{F}_{k-1}^T\boldsymbol{q}_k \big/ (\boldsymbol{q}_k^T\boldsymbol{q}_k)$
11	Check for convergence. set $\boldsymbol{u}_k = \tilde{\boldsymbol{u}}_k$
12	If converges go to step 13 else return to step 5
13	$\boldsymbol{E}_{\mathrm{k-1}}$ loadings: $\boldsymbol{p}_k = \boldsymbol{E}_{k-1}^T\boldsymbol{t}_k / (\boldsymbol{t}_k^T\boldsymbol{t}_k)$
14	Regress $\boldsymbol{u}_{\mathrm{k}}$ unto $\boldsymbol{t}_{\mathrm{k}}$: $b_k = \boldsymbol{u}_k^T\boldsymbol{t}_k / (\boldsymbol{t}_k^T\boldsymbol{t}_k)$
15	Compute Residuals: $\boldsymbol{E}_k = \boldsymbol{E}_k - \boldsymbol{t}_k\boldsymbol{p}_k^T$ and $\boldsymbol{F}_k = \boldsymbol{F}_k - b_k\boldsymbol{t}_k\boldsymbol{p}_k^T$
16	Apply cross-validation to determine whether to generate additional latent structure if required then return to step 5 else move to step 17.
17	Execute interval splicing algorithm, repeating steps 3 to 16 to identify optimal interval splitting; save best iPLS model.
18	If c is less than columns of **X** then set c = c + 1 and return to step (2) else step 19;
19	Identify best PLS model based on RMSE comparison and set new **X** = $\mathbf{X}_{\mathbf{jc}}$ (best case);
20	If j > 1 compare current best case PLS model with previous if RMSE if lower then set j = j + 1 and return step 1 else terminate outermost loop;

Table 6.6 Predictive Model Description for Penicillin and Biomas Concentration

	With Variable Selection		Without Variable Selection	
Predictor Variables	1, 3-7, 9-11		1 - 11	
	Interval Boundaries	Total RMSE	Interval Boundaries	Total RMSE
Stage 1	Whole	11 x 10^{-4}	Whole	0.4046
Stage 2	120	4.5 x 10^{-4}	90	0.164
Stage 3	480	3.948 x 10^{-4}	270	0.113
Stage 4	150	3.862 x 10^{-4}	180	0.028
Stage 5	690	3.798 x 10^{-4}	30	0.009

6.4 Prediction and Monitoring Results

6.4.1 Predictive Model Performance of MiPLS Approach

The plot in Figure 6.8 illustrates the improvement in the reconstruction/prediction of biomass concentration and penicillin concentration when a MiPLS approach is employed in contrast to a non-interval PLS method is used. In all cases studied the interval splicing achieved reduction of the initial RMSE to less than 30% of its initial value. The results was obtained using five batch of unseen data after building the model using a separate five batch of data generated by the simulator. The performance of the MiPLS predictive model depicted in Figure 6.8 for one of the test batch runs is reflective of the improve prediction/reconstruction achieved across the all the five unseen batch data set. The evolution and reduction in the overall RMSE through the several stages of the binary division algorithm used to identify the boundaries of the intervals employed by the MiPLS scheme for the same testing batch data is also shown in Figure 6.9. It can be observed that the initial RMSE corresponding to the scenario of a non-iPLS model, that is, a standard MPLS approach, is dramatically improved when the final MiPLS is evolved.

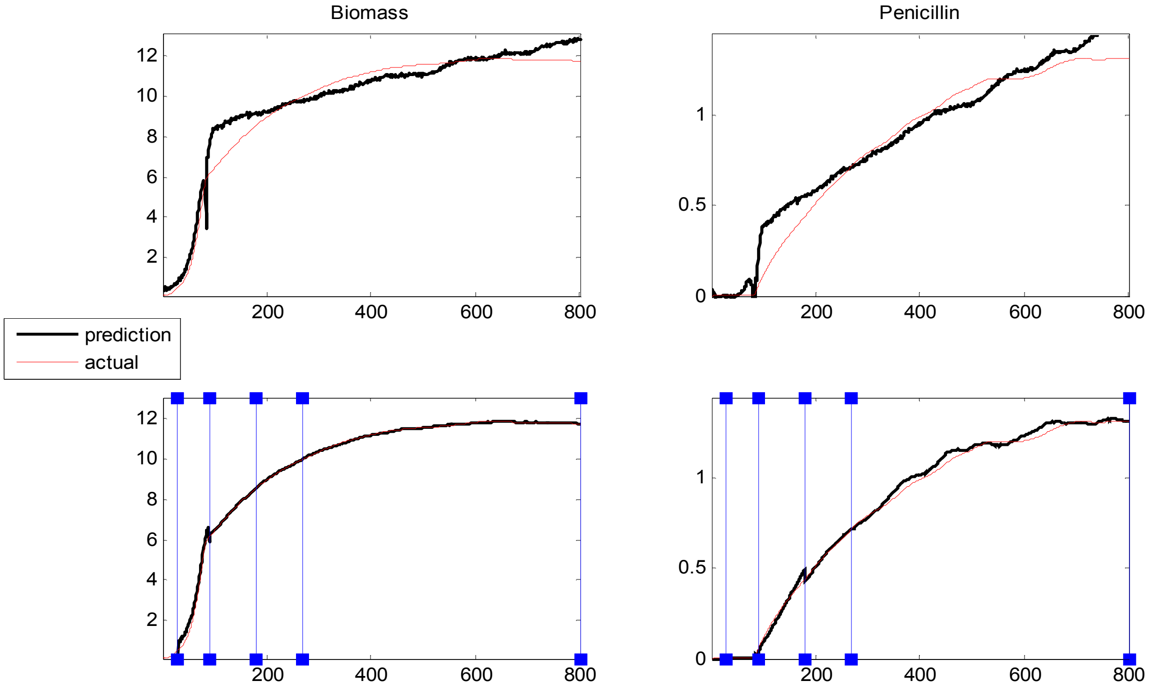

Figure 6.8. Plot comparing prediction of Penicillin and Biomass concentration using online measurements a) Standard PLS model b) proposed MiPLS model

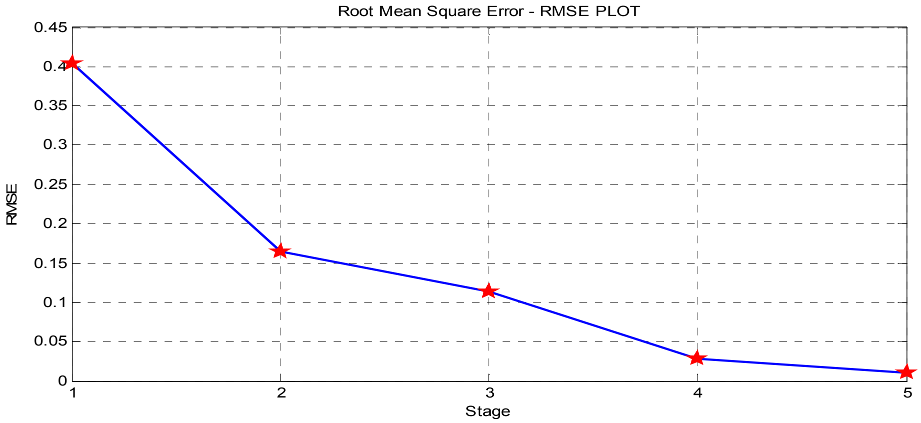

Figure 6.9. Plot of root-mean square error RMSE reduction with discovery of the intervals

The authors believe that the multiple PLS model approach of interval PLS scheme provides a strategy advantage over the use of a single PLS model created from the two dimensional unfolded data set through the increase flexibility and degrees of freedom inherent to the method. Employing subinterval dividing and the development of independent PLS models for each interval segment provides for more effective capturing and representation of the process dynamics and nonlinearities. Instead of just one general PLS model, we have several models with the freedom to select the best number of latent variables for each specific model to most accurately capture the dominant process features characterizing the specific interval within the batch duration.

6.4.2 Process Monitoring Performance

Both abrupt and incipient faults were simulated and detection capabilities of the square prediction error and Hotelling's T^2 statistics monitoring statistics, previously described and defined by Eq.(6.5) and (6.6), were evaluated. The early detection of these faults are crucial as the impact of the fault on the process quality variable would not be detectable in actual operation given that these are typically offline measurements. An example of the impact of a 50% step decrease in substrate feed rate on the penicillin and biomass conc. is depicted in Figure 6.10

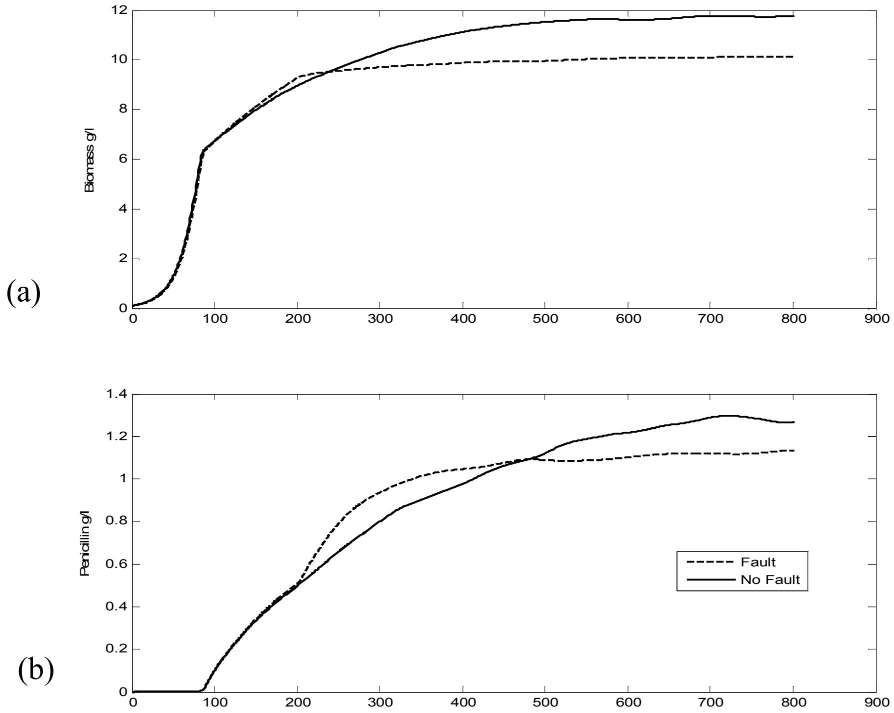

Figure 6.10 Impact of a 50% step decrease in substrate feed rate (Fault #2) on a) Biomass concentration b) Penicillin Concentration

As shown in Figure 6.11 all three faults analyzed were detectable by both the Hotelling's T^2 statistics and the SPE statistics. In comparison to fault detections reported by both Lee, et al. (2004) and Birol, et al. (2002) using multiway principal component analysis MPCA, the proposed model gives remarkably more aggressive detection of the faults 1 and 3 with the monitoring statistics significantly exceeding the control limits after the activation of the fault conditions. Detection of Fault #2 was not as quick and for the most part went undetected by the SPE statistics, however, similar tentative detection was also reported by Lee, et al. (2004).

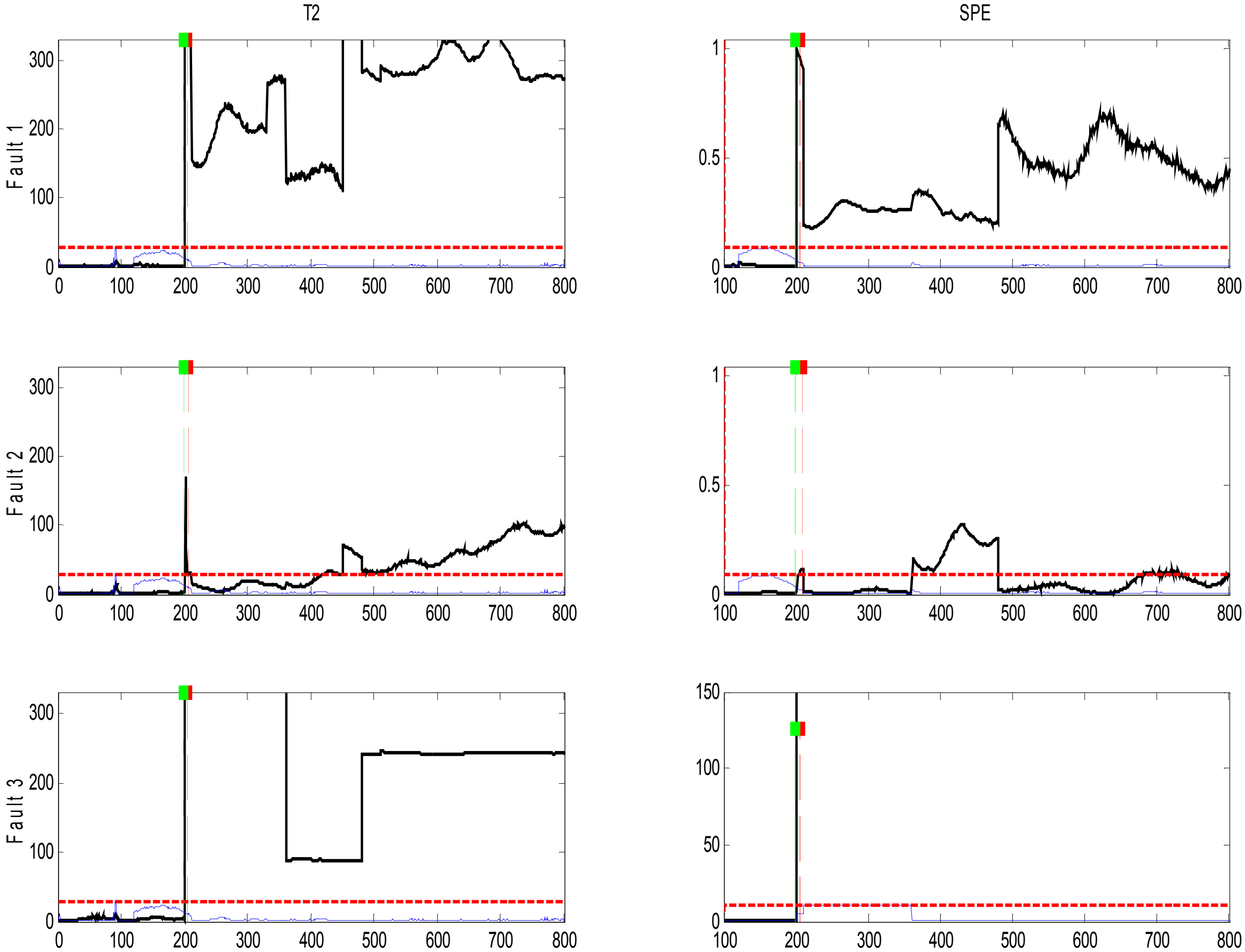

Figure 6.11 Detection of sudden faults 1 through to 3 using T^2 and *SPE* statistics

Overall, therefore, the Hotelling's T^2 statistics performed more reliably than the SPE statistics because it accounted of the difference in the residual variance across the different intervals of the

PLS model fit. To prevent false alarm condition for the SPE statistics it may be advisable to employ a variable control limit over different interval time span of the batch duration, similar to the control limits employed by Lee, et al. (2004).

Figure 6.12 compares the incipient fault detection of both fault 1 and 3 for the fault initiation time of t = 150 hr. The detection of incipient fault # 1 is achieved more readily than incipient fault # 3.

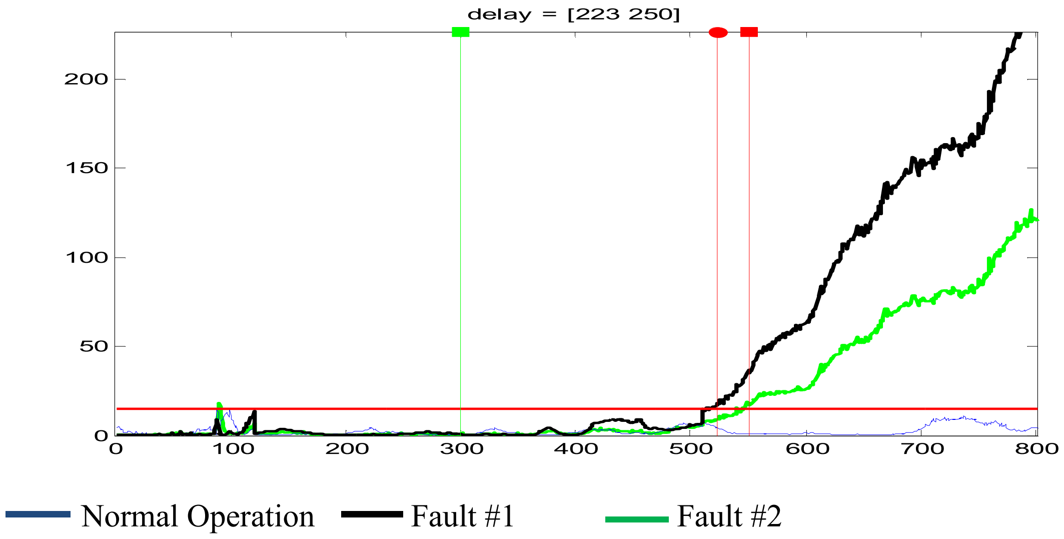

Figure 6.12 Detection of incipient faults 1 and 2 using Hotelling's T^2 statistics

Figure 6.13 illustrates the detection of an incipient fault (Fault # 2), the point of detection of the incipient faults and the detection delay time is indicated. For the case of this particular incipient fault the results indicated a trend of reduce detection delay time for fault initiated later in the process. For the other two faults simulated the detection delay time was fairly constant.

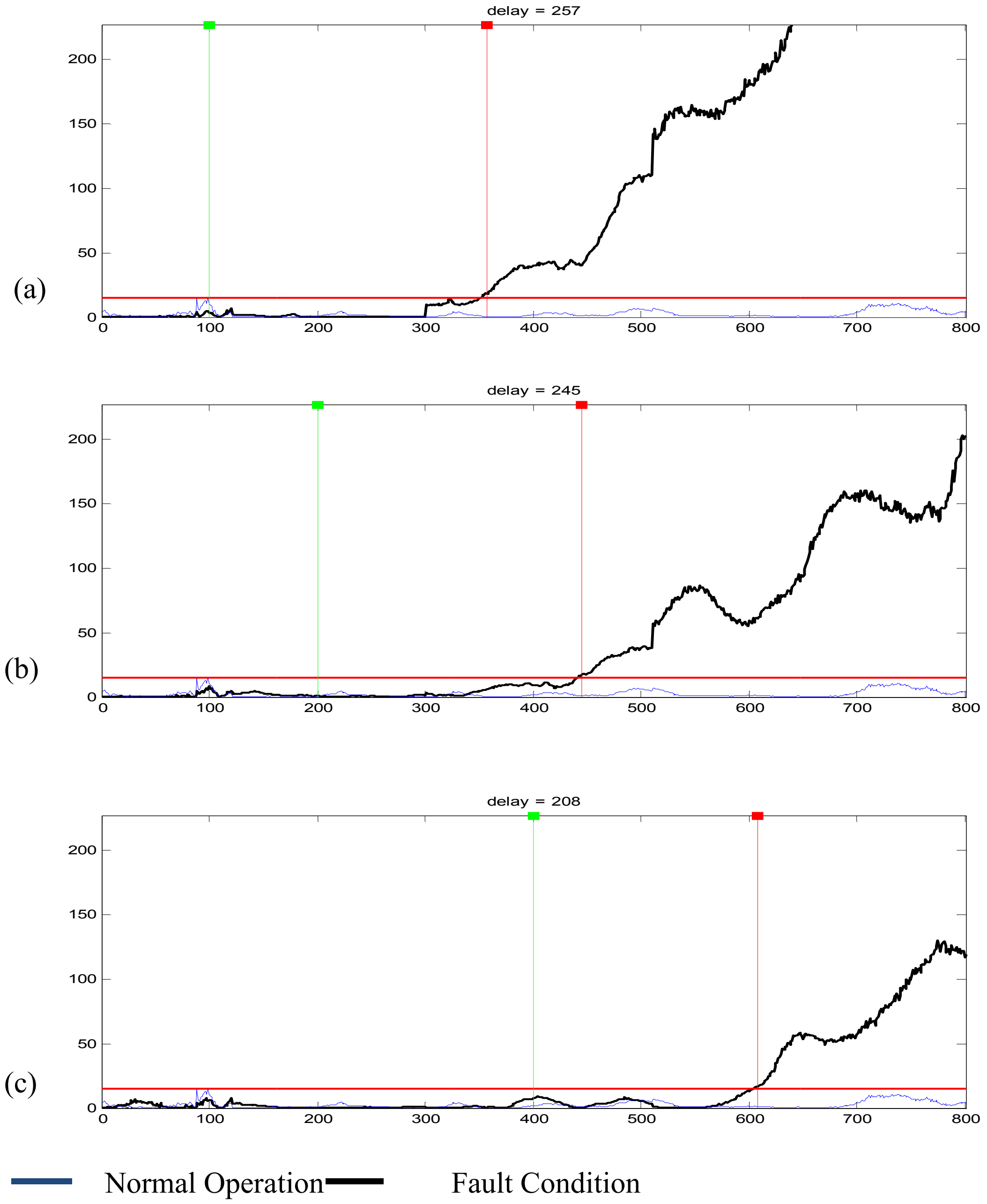

Figure 6.13 Detection of incipient Fault # 2 using T^2 statistics a) Fault initiated at t = 50h b) Fault initiated at t = 100h c) Fault initiated at t = 200h

6.5 Conclusion

The predictive capability of the PLS model in terms of quality variables proved to dramatically improved by combining the interval PLS approach with previously proposed data unfolding methods. This multi-way modelling approach combined with the proposed algorithm for identifying the optimal interval subdivision proved to produce significant reduction in the RMSE over the stand MPLS approach. The binary division algorithms offers an efficient alternative to employing a fix size interval selection approach to the implementation of an iPLS model. Fix-interval length iPLS approach would typically involve the use of a genetic algorithm to select a subset of the intervals that are best predictive of the quality variable. However, the binary algorithm demonstrates that optimal selection can significantly reduce the number of segments/intervals needed and thereby eliminating the need for employing a genetic algorithm.

The fault monitoring capabilities of the proposed process monitoring scheme did not provided as dramatic an improvement in comparison to previously reported methods but demonstrated that it was just as effective. If more simulated fault scenarios were supported by the simulator, perhaps a more clear distinction in the fault detection capabilities of the proposed scheme could be arrived at. Overall, both the Hotelling T^2 and *SPE* statistics seem to be capable of detecting both incipient and sudden faults arising at the differing points in the cultivation batch process, with the T^2 statistics proving slightly more reliable than the SPE statistics.

Chapter 7 : Conclusions and Suggestions for Further Works

7.1 Conclusions

Research efforts in the field of process performance monitoring have had significant impact on the utilisation of process measurement data gathered from plants. The reported applications have ranged from quality variable prediction, fault and disturbance detection, knowledge based fault diagnostic systems, and model based process control systems. Researchers have drawn upon statistical methods, mathematics, and design concepts from non-chemical engineering disciplines and adapted, investigate suitability, and conducted comparative study towards the goal of refining and improving their applicability to field of process performance monitoring. Chapters 2 and 3 reviewed some of these methods, the innovations and improvements have been contributed over the years by different researchers since the inception of multivariate statistical process controls.

This thesis also seeks to contribute to the efforts of refining and improving existing methods and suggest innovative solutions to expand the scope of applicability to more complex processes. Hence, the main aims and objectives of the thesis as were set out in Chapter 1.

The contribution of Chapter 4 sought to satisfy the first stated objective of subsection 1.2 in Chapter 1. A simplified CVA based state-space model design for the specific purpose of process monitoring was achieved by way of proposing the use of simpler state space representation more suitable for process monitoring specific applications and deriving a more efficiently estimation procedure for parameterization of state space matrices.

The CVA state space model was evaluated on the well-known Tennessee Eastman benchmark process. The fault detection performance showed that the performance capability of the state space model was maintained while achieving dramatic simplification of the set of stochastic estimation equations used to derive the reduce set of model parameters. A comparative study conducted by comparing published fault detection performance results of other statistical methods (CA, PCA, DPCA, and the traditionally CVA approach) for the same simulated faults on TE simulator, revealed that the proposed state space representation gave comparable, and in many cases better, fault detection performance than the traditional CVA state space modelling technique. Most notable is the detection of fault No. 15 in the Tennessee Eastman benchmark process and the significant reduction in detection delay time achieved for the more difficult to detect faults. The overall best performing monitoring statistics in terms of fault detection and detection delay time is the Hotelling's T^2 statistics of the output residuals T^2_{ey}.

The fault detection performance also faired comparably to that reported for the DICA and SSICA schemes (Odiowei and Cao 2010). They reported detection of faults # 3 and 9 a feat not previously accomplished to the author's best knowledge. The proposed CVA method, nevertheless, did fair better in terms of the percentage performance reliability for the faults detectable.

Chapter 5 explored two hybrid model approaches. One approach considered the merging of a mechanistic and data driven model based approach. The other investigated a hybrid implementation of two data based model a NN model and an OLS model. The hybrid mechanistic data based approaches were evaluated using a CSTR simulator while the hybrid data based model was evaluated using a ChemCad distillation column simulator.

In the case of the proposed mechanistic-data based hybrid scheme, a central difference to that of the traditional approach was related to the interface between the mechanistic model and the plant. The proposed scheme suggested using the controller output as injected inputs into the mechanistic model as oppose to implement the control loop and controller within the model.

Several hybrid variants were evaluated with all demonstrating improve detection performance over the pure mechanistic approach. It was demonstrated through select fault examples why the model uncertainty (model plant mismatches) can have negative impact on the fault detection capability via monitoring of the mechanistic model-plant residuals. The best performing hybrid model in relation to fault detection was the mechanistic – PLS1 based data based model HM3. The HM3 data based model was a one step ahead predictive model employing past output measurements to estimate the current outputs of the data based model.

Sixteen of the eighteen faults simulated on the CSTR were successfully detected, the valve sticking faults proved undetectable under steady state operation. The collection of detectable faults included incipient sensor fault drift error faults, the gradual failing of unit operations such as heat exchanger fouling and pump pressure lost. The impact of the sensor or unit operation fault was dependent upon whether the unit was incorporated within a control loop or not. Fault sensors or unit operations within the control or recycle loops could prove more troubling to isolate because of the inherent propagating effect of the loop.

Both the hybrid data based method proposed in Chapter 5 for the monitoring of the continuous distillation column and the multi-way interval PLS (MiPLS) model proposed in Chapter 6 for the monitoring of the batch penicillin process, employed an approach of developing multiple linear models to approximate and capture the nonlinearity of the process under monitor. The hybrid approach used OLS regression models to capture the variability in the process data measurements about different operating feed condition of the stream. The existing steady state condition of the distillation process was identified by applying a short-term moving average filter to the past values of the process variables. A NN model successfully provided a means of switching in the best fit OLS regression model to track and predict the process output variance based upon the current input variable variance.

The MiPLS model, on the other hand, exploited the fix time duration of the batch and derived linear PLS models that gave the best approximation over the specific interval of the batch. The optimal interval segmentations were identified by a proposed algorithm inspired by the polygon line segment algorithm proposed by Kegl et al. (1999) for constructing principal curves. The accuracy of the prediction of the process quality variables demonstrated significant improvement when the interval PLS derived using the optimal interval subdivision algorithm was combined with previously proposed data unfolding methods.

The proposed binary division algorithms offers an efficient alternative to employing a fix size interval selection approach to the implementation of an iPLS model. Fix-interval length iPLS approach would typically involve the use of a genetic algorithm to select a subset of the intervals that are best predictive of the quality variable. Employing the binary algorithm have facilitated the use of a far smaller set of define segments/intervals to implement the iPLS model thereby eliminating the need for employing a genetic algorithm.

Investigation into the detection of combine faults conducted in chapter 5 seem to reveal that a monitoring scheme ability to detect independent single fault conditions usually translates into being able to detect the existence of a multiple simultaneous fault scenario. The research analysis was limited two fault scenarios as such no conclusions or comment on multiple simultaneous faults beyond the two fault scenario can be made.

Building localized fault monitoring systems around specific unit operations or area of a plant may be more efficient that a plant-wide strategy. The impact of a fault tends to affect variables local to its vicinity first and may propagate outward, however, earliest detection would therefore best be facilitated via monitoring of those local variables. A distributed plant monitoring strategy as opposed to a centralized strategy would also better facilitate fault isolation and diagnostics.

7.2 Suggestions for Further Works

A significant amount of the analysis conducted in Chapter 5 was devoted to identify the best hybrid architecture in terms of mechanistic model – plant interface and the choice of past time delay feedback variables to serve as inputs to the hybrid system. As a consequence of such, a comprehensive evaluation of the available data based models to apply as compensation (error) model was not carried out. Future work could look into the applying non-linear PCA, NN model, alternate NLPLS implementation and CVA state space modelling to implement the compensation model for the proposed hybrid structure presented and analysed in Chapter 5. In particular, the proposed CVA state space model of Chapter 4 could be incorporated within the hybrid approaches to investigate whether such an implementation would offer any improvement or advantages in comparison to the implementations analysed in Chapter 5.

Future works could also consider developing an online training strategy for the hybrid data based model developed in Chapter 5 and used to the monitoring the distillation column. The similarity between the hybrid data based model and the MiPLS model used in Chapter 6 for batch process monitoring was pointed out in the previous subsection. It may be possible to adapt the procedure/algorithm in Chapter 6 which was used for automatically identifying the optimal subintervals and linear PLS models selection to facilitate the development of an online training method for the hybrid data based model proposed in Chapter 5.

Instead of the offline approach employed that deliberately establishes different nominal feed conditions and then injects pseudo random perturbations about the nominal conditions to generate simulation data to build the OLS regression models, an online approach would automatically identify when a new OLS model is needed to be developed or whether a previous OLS model could be applied. The algorithm in Chapter 6 could be essentially be adapted to carry out this role of identify when the current process state required the development of a new OLS model to maintain some specified minimum degree of estimation accuracy. The table of OLS model and vector of parameterization coefficients could then be updated automatically by the algorithm and the NN model train to map the new OLS coefficients to the short term steady state condition of the plant.

Originally, it was hoped to conduct online monitoring of an actual process using the hybrid mechanistic data driven based model proposed in Chapter 5. Doing so using commercially available dynamic chemical plant model software such as HYSYS and ChemCad are two software options readily available if the tradition mechanistic model plant interface is to be applied. Doing so for the case of the proposed mechanistic model plant interface would however require some adaptation of the software plant simulator to be able to accept external controller output signals to drive the plant actuators directly instead of implementing the controller and control loop within the simulator. In the case of HYSYS this could possibly be achieved by switching the controllers to manual model and using a spreadsheet to tie the manual output value of the controllers in the simulator to the actual controller output levels extracted from the plant SCADA system. In manual mode the controller output can be directly manipulated.

A final proposed area of future work is the use of variable specific lags/leads specification as opposed to specifying a fix lag/lead window size for all process variables employed by the dynamic model. Preliminary work and investigation into this design consideration, not documented in this thesis, does not seem to provide any significant improvement to the dynamic model developed. However, a more comprehensive investigation may confirm the assertion that the use of variable specific lag order may facilitate a more effective capturing of the dynamics of the process variables which may be characterized by different dynamics. One may want to consider the use of genetic algorithm (GA) to naturally evolve to an optimal or sub optimal variable lag order selection. This could be combined with the proposed CVA state space model of Chapter 5 to further improve on the model dimensionality reduction and one-step ahead prediction accuracy.

Appendix A

Introduction

The appendix provides a summary overview of some of the essential coding developed and used over the duration of my research to carry out model development, simulate and conduct fault analysis scenarios. Due to size constraints copying the codes directly into the appendix, as was done with the PLS algorithms at the end of section, would have made the report very bulky and the appendix not very reader friendly. Consequently, three charts are provided in the appendix to assist with navigating through some of the scripts/codes archived on the CD attached to the back of the inside cover of the booklet.

The charts graphically lay out the interlinking between the various scripts, identifying the main script and various subroutines/called functions employed by each script. The tier structure of the chart also seeks to indicate the function calling structure, that is, which scripts/functions serve as subroutines to which other functions.

CVA State Space Model Code

The chart shown in Figure A.1 outlines the code implementation used to conduct significant components of the analysis and results generated in chapter 4. The state space model implementation, in particular, was implemented using the script *CVASSModel.m* which calls upon three other subroutines as shown in the chart. The other subroutine were used to implement the monitoring statistics, evaluate fault detection points and carry out various data scaling and other pre-conditioning operation of the data set.

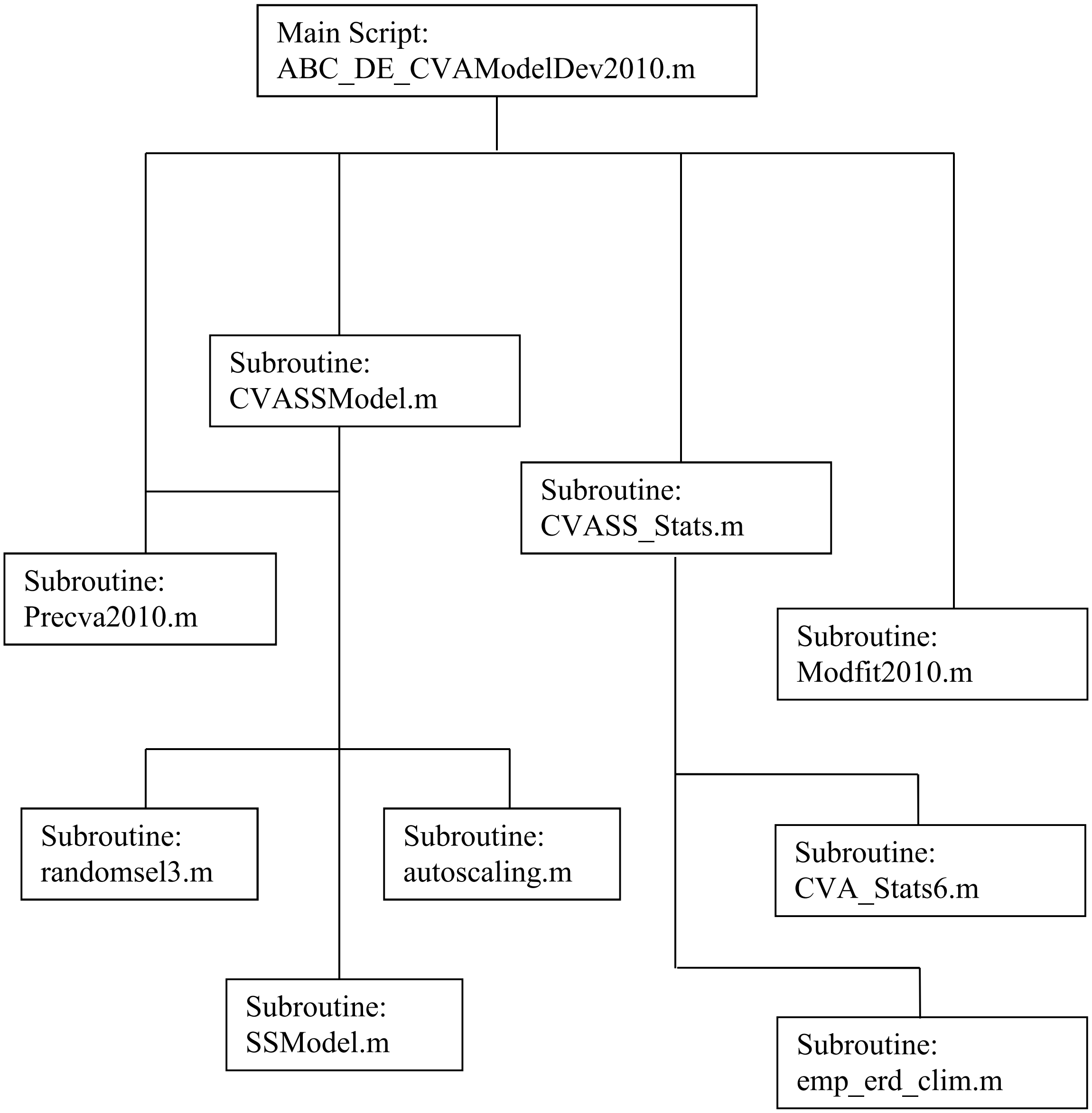

Figure A.1 Canonical variate analysis (CVA) state space script layout.

CSTR - Modelling and Mismatch Analysis – Chapter 5

The chart of Figure A.2 provides a listing of all files associated with the code development for the CSTR simulator and model-plant mismatch analysis discussed in chapter 5 of the thesis report. The *SignalExcitation.m* and *AddNoise_Faults.m* script was used to generate the pseudo random perturbations and noise or disturbance effects associated with select process variables.

The *PIcontrolblock.m* was used to implement the control structures. The *CSTRPlantmodel2.m* was to model the plant-model mismatch and in conjunction with the main-script, implement the various fault scenarios.

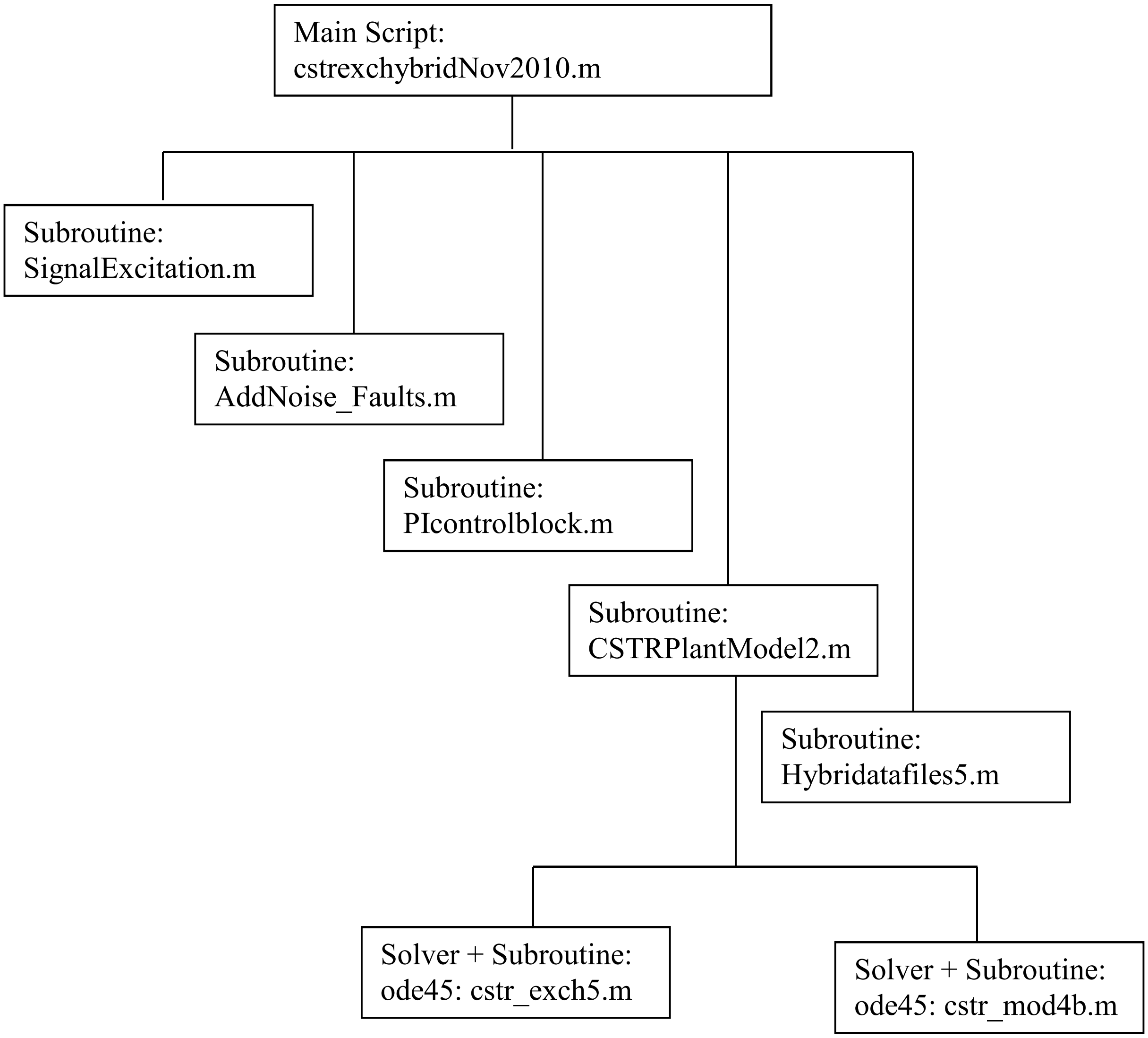

Figure A.2 CSTR plant-model mismatch coding chart

Binary Division Search Algorithm and PLS Algorithms

The chart of Figure A.3 shows the interlink between the matlab script files used to implement the binary division search algorithm proposed in chapter 6. The segment splitting algorithm can be adapted to incorporate any regression algorithm or subspace based algorithm for segment modelling: ordinary least squares OLS, partial least squares PLS, CVA state space modelling, etc. The loop iterations is implemented in the main script and terminates when the optimal sub-division splitting and models are derived. The splitsegment2.m script is essential to evaluating a particular subdivision selection and is an essential and permanent subroutine irregardless of the regression method employed for segment modelling.

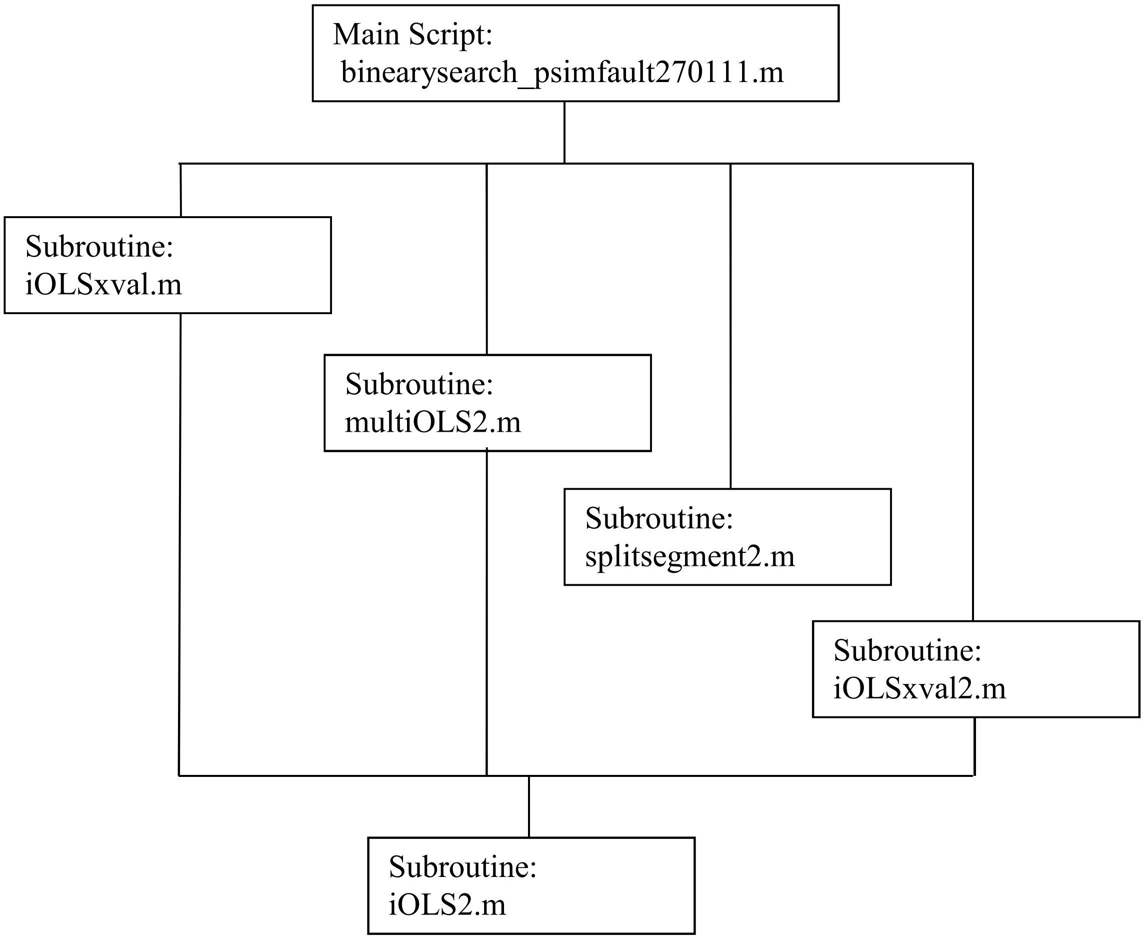

Figure A.3 Code Chart Outline of binary dividing segment length search algorithm

Partial Least Squares PLS Algorithm (Linear and Quadratic)

One of the scripts employed during my research for evaluating the linear and several quadratic PLS algorithms has been copied and inserted into this appendix (pg 184 to pg 190). The main function – *PLScode4.m* makes and internal call to PLSloop4.m which is an algorithm that implements and iterative loop. *PLSloop4.m* facilitates automatic selection of the number of latent variables to be used in model develop via cross-validation and the specification of a convergence tolerance at which termination of the iteration should terminate.

```
function [T1,T2,U,B,W1,W2,P1,P2,Q] = PLScode4(Y,X,opt,tol,maxiter,lv)
%X(n x m)
%Y(n x r)
% dim - number of latent variables
%
%opt = 1:linear PLS, 2:Quadratic PLS, 3:RB-NN, 4:NGA-QPLS, 5:
if isempty(tol) || tol == 0

    tol = 0.001;
end
%initialize
Ysize = size(Y);
Xsize = size(X);
n = Xsize(1);% number of data samples

nY = Ysize(2); % number or output variables
nX = Xsize(2); % number of predictor variables in X
%if lv > nX || isempty(lv)
%    lv = nX; % trap erroneous argument
%end
%
T1 = [];
T2 = [];
P1 = [];
P2 = [];
Q = [];
W1 = [];
W2 = [];
U = [];
B0 = [];
B1 = [];
B2 = [];
%

for j = 1:lv

    u = Y(:,1);% u(n x 1)
    %
    w1 = inv(u'*u)*X'*u; %u(nx1), w(mx1)
```

```
%normalize the weight vector

w1 = w1/sqrt(w1'*w1);

%calculate t

t1 = X*w1; % t(n x 1);

%first estimation of second order weights
w2 = w1;
t2 = t1;
switch opt
 case 1 %linear PLS

  % u = bo + t*b
     %replaces b
     b = inv(t1'*t1)*(t1'*u); % b1(1,1);

  case {2 3 4 5 6}
     dim = size(t1);
     I1 = ones(dim(1),1);
     Z = [I1, t1, t1.^2];
     b =  inv(Z'*Z)*(Z'*u);

end


conv = tol + 1;
iter = 1;

while conv > tol && iter <= maxiter

  [unew t1new t2new bnew w1new w2new q conv] = PLSloop4( X,Y,u, t1, t2,
  b, w1, w2, opt);

 iter = iter + 1;
 t1 = t1new;
 t2 = t2new;
 w1 = w1new;
 w2 = w2new;
 u = unew;
 b = bnew; %opt 1 to 3 replaces bnew in PLSloop3 while opt 4 optimizes it

end

%
%final calculation of u after convergence and final updating of w and b
%coefficients to give new t
switch opt

  case 1 %linear PLS

    up = b*t1; %T*B, B = [b1 b2 .. bn]
  case {2 3 4} %QPLS

    up = b(1) + b(2)*t1 + b(3)*t1.^2;

  case {5 6} %QPLS

    up = b(1) + b(2)*t1 + b(3)*t2.^2;
end

%final calculation of q and u
q = Y'*up*inv(up'*up);
q = q/sqrt(q'*q); % normalize q
u = Y*q;
%
% calculate update b vector with latest u and t scores
switch opt

  case 1 %linear PLS

    b = inv(t1'*t1)*(t1'*u); % b1(1,1);

  case {2 3 4} %QPLS
    dim = size(u);
    I1 = ones(dim(1),1);
    Z = [I1, t1, t1.^2];
    b =  inv(Z'*Z)*(Z'*u);

  case {5 6} %QPLS
    dim = size(u);
    I1 = ones(dim(1),1);
    Z = [I1, t1, t2.^2];
    b =  inv(Z'*Z)*(Z'*u);

end
%
   p1 = X'*t1*inv(t1'*t1); % p' = t'*X*inv(t'*t)
   p2 = X'*t2*inv(t2'*t2); % p' = t'*X*inv(t'*t)
%Residuals
if opt == 5 || opt == 6
    E = X - 0.5*(t1*p1' + t2*p2');
else
    E = X - t1*p1';
end
%
F = Y - u*q';
%
X = E;
Y = F;
%
T1 = [T1,t1];
T2 = [T2,t2];
P1 = [P1,p1];
P2 = [P2,p2];
U = [U,u];
```

```
    Q = [Q,q];
    W1 = [W1,w1];
    W2 = [W2,w2];
    %
    B0(j,j) = b(1,1);
    if opt ~= 1
        B1(j,j) = b(2,1);
        B2(j,j) = b(3,1);
    end
    B = [B0 B1 B2];
%
end



function [unew t1new t2new bnew w1new w2new q conv] = PLSloop4(X, Y, u, t1,
t2, b, w1, w2, opt)
%
% OLS to determine t

dim = size(u);

I1 = ones(dim(1),1);

switch opt

 case 1 %linear PLS

  % u = bo + t*b
     %replaces b
     b = inv(t1'*t1)*(t1'*u); % b1(1,1);
     bnew = b;
    % calculate Y projection

    up = t1*b;

  case {2 3}

     Z = [I1, t1, t1.^2];
     b =  inv(Z'*Z)*(Z'*u);
     bnew = b;
    % calculate Y projection

     up = Z*b;

  case 4
    % b is optimized in the iteration loop via passing
    % back into the function
     Z = [I1, t1, t1.^2];
     up = Z*b;

  case 5
    % b is optimized in the iteration loop via passing
    % back into the function
```

```
     Z = [I1, t1, t2.^2];
     up = Z*b;

  case 6
      Z = [I1, t1, t2.^2];
      b =  inv(Z'*Z)*(Z'*u);
      bnew = b;
      up = Z*b;

end

% calculate q not its transpose

  q = Y'*up*inv(up'*up); %q( r x 1)

%normalize q

q = q/sqrt(q'*q);

% calculate new u vector projection and check for convergence

 unew = Y*q;

%
 switch opt

  case 1 %linear PLS

   w1new = X'*unew*inv(unew'*unew);
   w2new = w1new;

  case 2 %nonlinear regression to give update of w

   dim = size(X);
   k = b(2)*I1 + 2*b(3)*t1; %(n x 1);
   for j = 1:dim(2)

     xx = X(:,j);
     z(:,j) = k.*xx;
   end

    Z = [z, I1, t1, t1.^2] ;
    %
    v = Z'*unew*inv(unew'*unew);
    v = v/sqrt(v'*v);
    s = Z*v;
    b = s'*unew*inv(s'*s);
    dw = b*v;

    w1new = w1 + dw(1:dim(2),1);
    w2new = w1new;

   case 3 %nonlinear regression to give update of w assume c is fixed
```

```
%using my approach
dim = size(X);
k = b(2)*I1 + 2*b(3)*t1; %(n x 1);
for j = 1:dim(2)

  xx = X(:,j);
  Zz(:,j) = k.*xx;
end
 %Z = [Z, I1, t, t.^2] ;
 delu = unew - u;
 %unew = Z*c; %one approaCH
 %delu = Z*c; %my approach, in which case b and w are updated
 dw = inv(Zz'*Zz)*Zz'*delu;
 %

 w1new = w1 + dw;
 w2new = w1new;
 % b = b + dwdc(dim(2)+1,dim(2)+3); %b + delb

case 4 %nonlinear regression to give update of w c
%using my way

dim = size(X);
k = b(2)*I1 + 2*b(3)*t1; %(n x 1);
for j = 1:dim(2)

  xx = X(:,j);
  z(:,j) = k.*xx;
end

 Z = [z, I1, t1, t1.^2] ;
 delu = unew - u;
 %unew = Z*c; %one approaCH
 %delu = Z*c; %my approach, in which case b and w are updated
 dwdb = inv(Z'*Z)*Z'*delu;
 %

 w1new = w1 + dwdb(1:dim(2),1);
 w2new = w1new;
 %b is optimized instead of recalculated and replaced
 bnew = b + dwdb(dim(2)+1:dim(2)+3,1); %b + delb

case 5 %nonlinear regression to give update of w c
%using my way

dim = size(X);
Z = b(2)*X;

k = 2*b(3)*t2; %(n x 1);
for j = 1:dim(2)

  xx = X(:,j);
  Z = [Z,k.*xx];
end
 Z = [Z, I1, t1, t2.^2] ;
```

```
    delu = unew - u;
    d2 = u.*u;
    R2 = diag(d2);
    R = inv(R2);
    %unew = Z*c; %one approaCH
    %delu = Z*c; %my approach, in which case b and w are updated
    dwdb = inv(Z'*R*Z)*Z'*R*delu;
    %

    w1new = w1 + dwdb(1:dim(2),1);
    w2new = w2 + dwdb((dim(2)+1):(2*dim(2)),1);
    %b is optimized instead of recalculated and replaced
    bnew = b + dwdb((2*dim(2)+1):(2*dim(2)+3),1); %b + delb

  case 6 %nonlinear regression to give update of w

   dim = size(X);
   Z = b(2)*X;

   k = 2*b(3)*t2; %(n x 1);
   for j = 1:dim(2)

     xx = X(:,j);
     Z = [Z,k.*xx];
   end
    %
    v = Z'*unew*inv(unew'*unew);
    v = v/sqrt(v'*v);
    s = Z*v;
    b = s'*unew*inv(s'*s);
    dwdb = b*v;

    w1new = w1 + dwdb(1:dim(2),1);
    w2new = w2 + dwdb((dim(2)+1):(2*dim(2)),1);
    %b is optimized instead of recalculated and replaced
    %bnew = b + dwdc((2*dim(2)+1):(2*dim(2)+3),1); %b + delb

end

% update t matrix
%normalize the weight vector

w1new = w1new/sqrt(w1new'*w1new);
w2new = w2new/sqrt(w2new'*w2new);
%calculate t

t1new = X*w1new; % t(n x 1);
t2new = X*w2new; % t(n x 1);
%check for convergence

delt1 = t1new - t1;
delt2 = t2new - t2;

conv = delt1'*delt1*inv(t1new'*t1new) + delt2'*delt2*inv(t2new'*t2new);
```

Appendix B

Introduction

The appendix provides a more detail explanation and the background theory associated with the orthogonal and oblique projection mathematics employed in the description of subspace system identification covered in chapter 3.

B.1 Orthogonal Projection

The orthogonal projection of the row space of A into the row space of B is defined as:

$$\boldsymbol{A}/\boldsymbol{B} = \boldsymbol{A}\boldsymbol{B}^T(\boldsymbol{B}\boldsymbol{B}^T)^{\dagger}\boldsymbol{B}$$

Where $(\bullet)^{\dagger}$ denotes the Moore-Penrose pseudo-inverse of the matrix $(\bullet)$.

The projection of the row space of $\boldsymbol{A}$ into the orthogonal complement of the row space of $\boldsymbol{B}$ is:

$$\boldsymbol{A}/\boldsymbol{B}^{\perp} = \boldsymbol{A} - \boldsymbol{A}/\boldsymbol{B}$$

Alternatively Eq. (B.1) maybe represent as:

$$\boldsymbol{A}/\boldsymbol{B} = \boldsymbol{A}\prod\nolimits_B$$

where $\prod_B$ denotes the operator that projects the row space of a matrix onto the row space of matrix $\boldsymbol{B}$:

$$\prod\nolimits_B = \boldsymbol{B}^T(\boldsymbol{B}\boldsymbol{B}^T)^{\dagger}\boldsymbol{B}$$

Likewise$\prod_{B^{\perp}}$ denotes the geometric operator that projects the row space of a matrix onto the orthogonal complex of the row space of $\boldsymbol{B}$:

$$\boldsymbol{A}/\boldsymbol{B}^{\perp} = \boldsymbol{A}\prod_{B^{\perp}}$$

where:

$$\prod_{B^{\perp}} = \boldsymbol{I}_B - \prod_B$$

and $\boldsymbol{I}_B$ is an identity matrix of the same dimension as $\boldsymbol{B}$.

The geometric interpretation of these orthogonal projections is depicted in Figure B.1. The combination of the projections $\prod_{B^{\perp}}$ and $\prod_B$ decomposes a matrix A into two matrices of which the row spaces are orthogonal:

$$\boldsymbol{A} = \boldsymbol{A}\prod_{B^{\perp}} + \boldsymbol{A}\prod_B$$

The decomposition may also be considered as the representation of the matrix A as linear combination of the rows of **B** and of the orthogonal complement of **B**:

$$\boldsymbol{A} = \boldsymbol{L}_{B^{\perp}}\boldsymbol{B}^{\perp} + \boldsymbol{L}_B\boldsymbol{B}$$

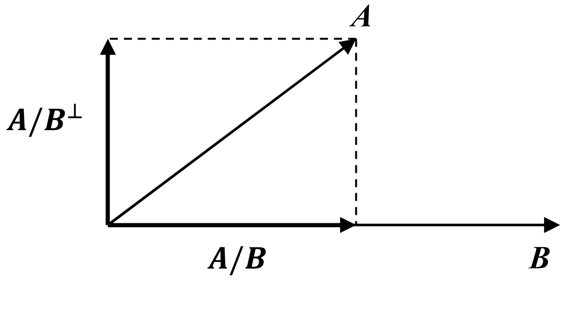
$\boldsymbol{A}$
$\boldsymbol{A}/\boldsymbol{B}^{\perp}$
$\boldsymbol{A}/\boldsymbol{B}$
$\boldsymbol{B}$

Figure B.1 Interpretation of the orthogonal projection in the *j*-dimensional space (*j* = 2 in this case).

B.2 Oblique Projection

The oblique projection of the row space of $\boldsymbol{A}$ along the row space of $\boldsymbol{B}$ into the row space of $\boldsymbol{C}$ is:

$$\boldsymbol{A}/_{\boldsymbol{B}}\boldsymbol{C} = (\boldsymbol{A}/\boldsymbol{B}^{\perp})(\boldsymbol{C}/\boldsymbol{B}^{\perp})^{\dagger}\boldsymbol{C}$$

Figure B.2 illustrates the geometric interpretation of the oblique projection which may be considered as the linear decomposition of the $\boldsymbol{A}$ unto the row spaces of two non-orthogonal matrices $\boldsymbol{B}$ and $\boldsymbol{C}$.

Properties of the orthogonal and oblique projections:

$$\boldsymbol{A}/\boldsymbol{A}^{\perp} = 0$$

.

$$\boldsymbol{A}/_{\boldsymbol{A}}\boldsymbol{C} = 0$$

$$\boldsymbol{C}/_{\boldsymbol{A}}\boldsymbol{C} = C$$

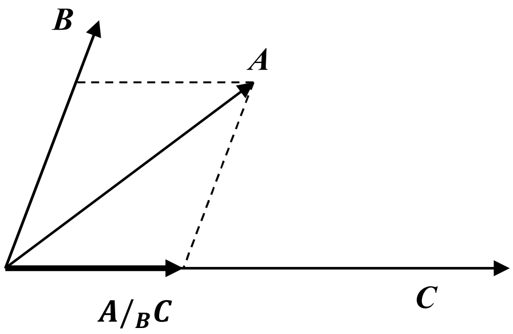

Figure B.2 Interpretation of the oblique projection in the j-dimensional space (*j* = 2 in this case).

References

Akaike, H.
1974a NEW LOOK AT STATISTICAL-MODEL IDENTIFICATION. Ieee Transactions on Automatic Control AC19(6):716-723.

Akaike, H.
1974b STOCHASTIC THEORY OF MINIMAL REALIZATION. Ieee Transactions on Automatic Control AC19(6):667-674.

Akaike, Hirotugu
1975 Markovian Representation of Stochastic Processes by Canonical Variables. Society of Industrial and Applied Mathematics - SIAM J Control 13(1):162-173.

Akaike, Hirotugu
1976 Canonical Correlation Analysis of Time Series and the Use of an Information Criterion. *In* Mathematics in Science and Engineering. K.M. Raman and G.L. Dimitri, eds. Pp. 27-96: Elsevier.

Baffi, G., E. B. Martin, and A. J. Morris
1999a Non-linear projection to latent structures revisited (the neural network PLS algorithm). Computers & Chemical Engineering 23(9):1293-1307.

Baffi, G., E. B. Martin, and A. J. Morris
1999b Non-linear projection to latent structures revisited: the quadratic PLS algorithm. Computers & Chemical Engineering 23(3):395-411.

Bajpai, R., and M. Reuss
1980 A mechanistic model for penicillin production. Journal of Chemical Technology and Biotechnology 30:330 - 344.

Birol, G., C. Undey, and A. Cinar
2002 A modular simulation package for fed-batch fermentation: penicillin production. Computers & Chemical Engineering 26:1553 - 1565.

Borin, A., and R. J. Poppi
2005 Application of mid infrared spectroscopy and iPLS for the quantification of contaminants in lubricating oil. Vibrational Spectroscopy 37(1):27-32.

Borjas, Santos D. M., and Claudio Garcia
2010 Subspace Identification using the integration of MOESP and N4SID methods applied to the Shell benchmark of a distillation column. *In* Proceedings of the 9th Brazilian Conference on Dynamics, Controls and their Applications Pp. 899 - 904. Serra Negra, Sao Paulo, Brazil.

Breiman, L., and J. H. Friedman
1997 Predicting multivariate responses in multiple linear regression. Journal of the Royal Statistical Society Series B-Methodological 59(1):3-37.

Brown, R. G., and P. Y. C. Hwang
1992 Introduction to Random Signals and Applied Kalman Filters: John Wiley and Sons, Inc.

Buhlmann, P.
1995 THE BLOCKWISE BOOTSTRAP FOR GENERAL EMPIRICAL PROCESSES OF STATIONARY-SEQUENCES. Stochastic Processes and Their Applications 58(2):247-265.

Candy, J. V., Bullock T. E., and Warren M. E.

1979 Invariant Description of the Stochastic Realization. Automatica 15:493-495.

Chen, J. H., and K. C. Liu

2002 On-line batch process monitoring using dynamic PCA and dynamic PLS models. Chemical Engineering Science 57(1):63-75.

Chen, Q. S., et al.

2008 Determination of total polyphenols content in green tea using FT-NIR spectroscopy and different PLS algorithms. Journal of Pharmaceutical and Biomedical Analysis 46(3):568-573.

Chen, Quansheng, Pei Jiang, and Jiewen Zhao

2010 Measurement of total flavone content in snow lotus (Saussurea involucrate) using near infrared spectroscopy combined with interval PLS and genetic algorithm. Spectrochim Acta A Mol Biomol Spectrosc 76(1):50-5.

Dejong, S.

1993 SIMPLS - AN ALTERNATIVE APPROACH TO PARTIAL LEAST-SQUARES REGRESSION. Chemometrics and Intelligent Laboratory Systems 18(3):251-263.

Detroja, K. P., R. D. Gudi, and S. C. Patwardhan

2007 Plant-wide detection and diagnosis using correspondence analysis. Control Engineering Practice 15(12):1468-1483.

DiCiccio, T. J., and B. Efron

1996 Bootstrap confidence intervals. Statistical Science 11(3):189-212.

Dong, D., and T. J. McAvoy

1996a Batch tracking via nonlinear principal component analysis. Aiche Journal 42(8):2199-2208.

Dong, D., and T. J. McAvoy

1996b Nonlinear principal component analysis - Based on principal curves and neural networks. Computers & Chemical Engineering 20(1):65-78.

Downs, J. J., and E. F. Vogel

1993 A PLANT-WIDE INDUSTRIAL-PROCESS CONTROL PROBLEM. Computers & Chemical Engineering 17(3):245-255.

Draper, Norman R., and Harry Smith

1998 Applied Regression Analysis: Wiley-Interscience.

Etezadi-Amoli, J., and R. P. McDonald

1983 A second generation nonlinear factor analysis. Psychometrika 48(3):315-342.

Ferrao, M. F., et al.

2011 Simultaneous determination of quality parameters of biodiesel/diesel blends using HATR-FTIR spectra and PLS, iPLS or siPLS regressions. Fuel 90(2):701-706.

Frank, I. E., and J. H. Friedman

1993 A STATISTICAL VIEW OF SOME CHEMOMETRICS REGRESSION TOOLS. Technometrics 35(2):109-135.

Garthwaite, P. H.

1994 AN INTERPRETATION OF PARTIAL LEAST-SQUARES. Journal of the American Statistical Association 89(425):122-127.

Geladi, Paul, and Bruce R. Kowalski

1986 Partial least-squares regression: a tutorial. Analytica Chimica Acta 185:1-17.

Gnanadesikan, R.

1977 Methods for Statistical Data Analysis of Multivariate Observations. New York: John Wiley and Son Inc.

Haber, R., and H. Unbenhauen

1990 Structure identification of non-linear dynamic systems- A survey on input-output approaches. Automatica 26(4):651-677.

Hannan, E. J., and B. G. Quinn

1979 DETERMINATION OF THE ORDER OF AN AUTOREGRESSION. Journal of the Royal Statistical Society Series B-Methodological 41(2):190-195.

Hastie, T., and W. Stuetzle

1989 PRINCIPAL CURVES. Journal of the American Statistical Association 84(406):502-516.

Healy, J.D.

1987 A note on multivariate CUSUM procedures. Technometrics 29:409 - 412.

Helland, I. S.

1988 ON THE STRUCTURE OF PARTIAL LEAST-SQUARES REGRESSION. Communications in Statistics-Simulation and Computation 17(2):581-607.

Hoskuldsson, A.

1992 QUADRATIC PLS REGRESSION. Journal of Chemometrics 6(6):307-334.

Höskuldsson, Agnar

1988 PLS regression methods. Journal of Chemometrics 2(3):211-228.

Hsieh, William

2001 Nonlinear Canonical Correlation Analysis of Tropical Pacific Climate Variability Using a Neural Network Approach. Journal of Climate 14(12): 2528-2539.

Hu, K. L., and J. Q. Yuan

2008 Statistical monitoring of fed-batch process using dynamic multiway neighborhood preserving embedding. Chemometrics and Intelligent Laboratory Systems 90(2):195-203.

Hurvich, C. M., R. Shumway, and C. L. Tsai

1990 IMPROVED ESTIMATORS OF KULLBACK-LEIBLER INFORMATION FOR AUTOREGRESSIVE MODEL SELECTION IN SMALL SAMPLES. Biometrika 77(4):709-719.

Jolliffe, I.T

2002 Principal component analysis. Aberdeen, UK: Springer-Varlag New York, Inc.

Juricek, B. C., W. E. Larimore, and D. E. Seborg

1999 Reduced-rank ARX and subspace system identification for process control. Dynamics & Control of Process Systems 1998, Volumes 1 and 2:247-252.

Juricek, B. C., D. E. Seborg, and W. E. Larimore

2005 Process control applications of subspace and regression-based identification and monitoring methods. ACC: Proceedings of the 2005 American Control Conference, Vols 1-7:2341-2346.

Kegl, B., et al.

1999 A polygonal line algorithm for constructing principal curves. *In* Advances in Neural Information Processing Systems 11. M.S. Kearns, S.A. Solla, and D.A. Cohn, eds. Pp. 501-507. Advances in Neural Information Processing Systems. Cambridge: M I T Press.

Kosanovich, K. A., et al.
1994 MULTIWAY PCA APPLIED TO AN INDUSTRIAL BATCH PROCESS. Proceedings of the 1994 American Control Conference, Vols 1-3:1294-1298.

Kresta, J. V., J. F. Macgregor, and T. E. Marlin
1991a MULTIVARIATE STATISTICAL MONITORING OF PROCESS OPERATING PERFORMANCE. Canadian Journal of Chemical Engineering 69(1):35-47.

Kresta, M., J. F. MacGregor, and T.E. Marlin
1991b Multivariate Statistical Monitoring of Process Operating Performance. Canadian Journal of Chemical Engineers 69:35 - 47.

Ku, Wenfu, Robert H. Storer, and Christos Georgakis
1995 Disturbance detection and isolation by dynamic principal component analysis. Chemiometrics and intelligent laboratory systems 30:179-196.

Lakshminarayanan, S., P. Mhatre, and R. Gudi
2001 Identification of bilinear models for chemical processes using canonical variate analysis. Industrial & Engineering Chemistry Research 40(20): 4415-4427

Lakshminarayanan, S., S. L. Shah, and K. Nandakumar
1997 Modeling and control of multivariable processes: Dynamic PLS approach. Aiche Journal 43(9):2307-2322.

Larimore, W. E.
1996 Statistical optimality and canonical variate analysis system identification. Signal Processing 52(2):131-144.

Larimore, Wallace E.
1983 System Identification, Reduced Order Filtering and Modelling via Canonical Variate Analysis. Proceedings from American Control Conference 2:445 - 451.

Larimore, Wallace E.
1990 Canonical Variate Analysis in Identification Filtering and Adaptive Control. Proceedings of the 28th Conference on Decision and Controls:596-604.

Lee, C., S. W. Choi, and I. B. Lee
2006 Variable reconstruction and sensor fault identification using canonical variate analysis. Journal of Process Control 16(7):747-761.

Lee, D. S., P. A. Vanrolleghem, and J. M. Park
2005 Parallel hybrid modeling methods for a full-scale cokes wastewater treatment plant. Journal of Biotechnology 115(3):317-328.

Lee, J. M., C. K. Yoo, and I. B. Lee
2004 Enhanced process monitoring of fed-batch penicillin cultivation using time-varying and multivariate statistical analysis. Journal of Biotechnology 110(2):119-136.

Li, B. B., E. B. Martin, and A. J. Morris
2001 Box-Tidwell transformation based partial least squares regression. Computers & Chemical Engineering 25(9-10):1219-1233.

Li, G., S. J. Qin, and D. H. Zhou
2010 Geometric properties of partial least squares for process monitoring. Automatica 46(1):204-210.

Li, T. H., H. Mei, and P. S. Gong
1999 Combining nonlinear PLS with the numeric genetic algorithm for QSAR. Chemometrics and Intelligent Laboratory Systems 45(1-2):177-184.

Li, W., et al.
2000 Recursive PCA for adaptive process monitoring. Journal of Process Control 10(5):471-486.

Liu, R. Y., and J. Tang
1996 Control charts for dependent and independent measurements based on bootstrap methods. Journal of the American Statistical Association 91(436):1694-1700.

Liu, Yu-ming, Jun Liang, and Ji-xin Qian
2004 The Application of Dynamic Principal Component Analysis to Enhance Chunk Monitoring of an Industrial Fluidized-Bed Reactor. Proceedings of the 5'h World Congress on Intelligent Control and Automation, Hangzhou, P.R China, 2004, pp. 1685 - 1688.

Lopes, J. A., et al.
2002 Multiblock PLS analysis of an industrial pharmaceutical process. Biotechnology and Bioengineering 80(4):419-427.

Lowry, C. A., W. H. Woodhall, and C. W. Champ
1991 A multivariate exponential weighted moving average control chart. Technometrics 34(1):46 - 53.

Lyman, P. R., and C. Georgakis
1995 Plant-Wide Control of the Tennessee Eastman Problem. Computers & Chemical Engineering 19(3):321-331.

MacGregor, J. F., et al.
1991 Multivariate statistical methods in process analysis and control. On-line sensors and data analysis. *In* Proceedings of the fourth international conference of chemical processes. Pp. 79 - 94. Padre Island, Texas.

MacGregor, J.F., and T. Kourti
1995 Statistical Process Control of Multivariate Processes. Control Engineering Practice 3(3):403 - 414

Malthouse, E. C., A. C. Tamhane, and R. S. H. Mah
1997 Nonlinear partial least squares. Computers & Chemical Engineering 21(8):875-890.

Malthouse, Edward Carl
1995 Nonlinear Partial Least Squares, Statistics Department, Northwestern University.

Martin, E. B., and A. J. Morris
1996 Non-parametric confidence bounds for process performance monitoring charts. Journal of Process Control 6(6):349-358.

Martin, E. B., A. J. Morris, and J. Zhang
1996 Process performance monitoring using multivariate statistical process control. Iee Proceedings-Control Theory and Applications 143(2):132-144.

McPherson, L., J. Morris, and E. Martin
2002 Super model-based techniques for batch performance monitoring. *In* European Symposium on Computer Aided Process Engineering - 12. J. Grievink and J. VanSchijndel, eds. Pp. 523-528. Computer-Aided Chemical Engineering. Amsterdam: Elsevier Science Bv.

McPherson, Lindsay
2007 Model-based Performance Monitroing of Batch Processes, Department of Chemical Engineering and Advanced Materials, University of Newcastle

Morris, A. J., and E. B. Martin

1998 Process performance monitoring and fault detection through multivariate statistical process control. Oxford: Pergamon Press Ltd.

Negiz, A., and A. Cinar

1997a Statistical Monitoring of Multivariable Dynamic Processes with State Space Models. AICHE 43(8):2002-2020.

Negiz, A., and A. Cinar

1997b Pls, balanced, and canonical variate realization techniques for identifying VARMA models in state space

Chemometrics and Intelligent Laboratory Systems 38(2):209-221.

Nomikos, P., and J. F. Macgregor

1994 MONITORING BATCH PROCESSES USING MULTIWAY PRINCIPAL COMPONENT ANALYSIS. Aiche Journal 40(8):1361-1375.

Nomikos, P., and J. F. MacGregor

1995 Multi-way partial least squares in monitoring batch processes. Chemometrics and Intelligent Laboratory Systems 30(1):97-108.

Odiowei, P. P., and Y. Cao

2010 State-space independent component analysis for nonlinear dynamic process monitoring. Chemometrics and Intelligent Laboratory Systems 103(1):59-65.

Oliveira, R.

2004 Combining first principles modelling and artificial neural networks: a general framework. Computers & Chemical Engineering 28(5):755-766.

Overschee, Peter Van, and Bart De Moor

1995 A Unifying Theorem for Three Subspace System Identification Algorithms. Automatica, Special issue on Trends in System Identifiction 31(12):1853 - 1864.

Overschee, Peter Van, and Bart De Moor

1996 Subspace identification for linear systems: Theory, implementation. applications. London: Kluwer Academic Publishers.

Peres, J., R. Oliveira, and S. F. de Azevedo

2001 Knowledge based modular networks for process modelling and control. Computers & Chemical Engineering 25(4-6):783-791.

Psichogios, D. C., and L. H. Ungar

1992 A HYBRID NEURAL NETWORK-1ST PRINCIPLES APPROACH TO PROCESS MODELING. Aiche Journal 38(10):1499-1511.

Qin, S. J., and T. J. McAvoy

1992 NONLINEAR PLS MODELING USING NEURAL NETWORKS. Computers & Chemical Engineering 16(4):379-391.

Qin, S. J., and T. J. McAvoy

1993 A DATA-BASED PROCESS MODELING APPROACH AND ITS APPLICATIONS. Dynamics and Control of Chemical Reactors, Distillation Columns and Batch Processes (Dycord Plus 92) 1993:93-98.

Qin, S. J., and T. J. McAvoy

1996 Nonlinear FIR modeling via a neural net PLS approach. Computers & Chemical Engineering 20(2):147-159.

Ricker, R. L.

1988 The Use of Biased Least-Squares Estimators for Parameters in Discrete-Time Pulse-Response Models. Industrial & Engineering Chemistry Research 27(2):343-350.

Russell, E. L., L. H. Chiang, and R. D. Braatz

2000 Fault detection in industrial processes using canonical variate analysis and dynamic principal component analysis. Chemometrics and Intelligent Laboratory Systems 51(1):81-93.

Schaper, C. D., et al.

1994 IDENTIFICATION OF CHEMICAL PROCESSES USING CANONICAL VARIATE ANALYSIS. Computers & Chemical Engineering 18(1):55-69.

Schwarz G.

1978 Estimating the dimension of a model. Annals of Statistics 6:461.

Silva, F. E. B., et al.

2009 Simultaneous determination of sulphamethoxazole and trimethoprim in powder mixtures by attenuated total reflection-Fourier transform infrared and multivariate calibration. Journal of Pharmaceutical and Biomedical Analysis 49(3):800-805.

Simoglou, A.

1999 Dynamic multivariate statistical process control using partial least squares and canonical variate analysis. Computers and Chemical Engineering:277 - 280.

Simoglou, A., E. Martin, and J. Morris

1999a A Comparison of Canonical Variate Analysis and Partial Least Squares for the Identification of Dynamic Processes. Proceedings from American Control Conference 2:832 - 837.

Simoglou, A., E. B. Martin, and A. J. Morris

1999b Dynamic multivariate statistical process control using partial least squares and canonical variate analysis. Computers & Chemical Engineering 23:S277-S280.

Simoglou, A., E. B. Martin, and A. J. Morris

2002 Statistical performance monitoring of dynamic multivariate processes using state space modelling. Computers & Chemical Engineering 26(6):909-920.

Van Overschee, P., and B. De Moor

1994 N4SID - SUBSPACE ALGORITHMS FOR THE IDENTIFICATION OF COMBINED DETERMINISTIC STOCHASTIC-SYSTEMS. Automatica 30(1):75-93.

Verhaegen, M.

1994 Identification of the deterministic part of MIMO state space models given in inovation from input-output data Automatica 30(1):61 - 74.

Viberg, M., et al.

1993 Performance of subspace based state space system identification methods. *In* Proceedings of the 12th IFAC Workd Congress. Pp. 369 - 372, Vol. 7. Sydney, Australia.

von Stosch, M., et al.

2011 A novel identification method for hybrid (N)PLS dynamical systems with application to bioprocesses. Expert Systems with Applications 38(9):10862-10874.

Wachs, A., and D. R. Lewin

1999 Process monitoring using model-based PCA.

Wangen, L. E., and B. R. Kowalski

1989 A multiblock partial least squares algorithm for investigating complex chemical systems. Journal of Chemometrics 3(1):3-20.

Welch, Greg, and Gary Bishop
2006 An Introduction to Kalman Filters. http://www.cs.unc.edu/~welch/kalman/kalmanIntro.html.

Willemain, T. R., and G. C. Runger
1996 Designing control charts using an empirical reference distribution. Journal of Quality Technology 28(1):31-38.

Wise, Barry M., and Neal B. Gallagher
1996 The process chemometrics approach to process monitoring and fault detection. Journal of Process Control 6(6):329-348.

Wold, S.
1992 NONLINEAR PARTIAL LEAST-SQUARES MODELING .2. SPLINE INNER RELATION. Chemometrics and Intelligent Laboratory Systems 14(1-3):71-84.

Wold, S., K. Esbensen, and P. Geladi
1987 PRINCIPAL COMPONENT ANALYSIS. Chemometrics and Intelligent Laboratory Systems 2(1-3):37-52.

Wold , S., et al.
1987 Multiway principal components and PLS-analysis. Journal of Chemometrics 1:41-56.

Wold, S., N. Kettanehwold, and B. Skagerberg
1989 NONLINEAR PLS MODELING. Chemometrics and Intelligent Laboratory Systems 7(1-2):53-65.

Yan, Xuefeng
2010 Hybrid artificial neural network based on BP-PLSR and its application in development of soft sensors. Chemometrics and Intelligent Laboratory Systems 103(2):152-159.

Yao, Y., and F. Gao
2008 Subspace identification for two-dimensional dynamic batch process statistical monitoring. Chemical Engineering Science 63(13):3411-3418.

Yue, H. H., and S. J. Qin
2001 Reconstruction-based fault identification using a combined index. Industrial & Engineering Chemistry Research 40(20):4403-4414.

Zhang, J.
2006 Improved on-line process fault diagnosis through information fusion in multiple neural networks. Computers & Chemical Engineering 30(3):558-571.

Zhang, J., E. B. Martin, and A. J. Morris
1996 Fault detection and diagnosis using multivariate statistical techniques. Chemical Engineering Research & Design 74(A1):89-96.

Zhao, S. J., J. Zhang, and Y. M. Xu
2006 Performance monitoring of processes with multiple operating modes through multiple PLS models. Journal of Process Control 16(7):763-772.